# Whey Protein Micro-Particles as Multifunctional Materials for Structure and Delivery

*By*

*Richard John Asa Moakes*


A thesis submitted to:
The University of Birmingham.
For the degree of
***Doctor of Engineering***

School of Chemical Engineering
College of Engineering and Physical Sciences
The University of Birmingham

April, 2018

# Abstract

Public awareness towards healthier lifestyles and obesity related illnesses has steadily increased over recent years. In response, the food industry has focused on healthier product formulations. Fluid gels, also known as sheared gels, comprising of micro-particles in suspension have been proposed as a promising candidate to replace high calorie fat components in food products; owing to their material characteristics closely mimicking those for oil droplets. This thesis studies the use of whey proteins as the prerequisite material for gelation; resulting in microgel suspensions via a shear-gel technology, to formulate multi-functional food ingredients.

This research uses a microstructural approach to show the underlying design principles behind the protein microgel suspensions, highlighting the ability to control subsequent material properties. This thesis demonstrates that primarily the particle microstructure was integral to the overall suspension rheology. It was observed that material response was not dependent on particle size, however, was greatly dictated by the processing parameters, highlighting different mechanisms to particle formation. Such mechanisms were closely correlated to gelation kinetics, where the rate of gelation either promoted or hindered weak inter-particle interactions post-processing.

Understanding the link between gelling kinetics and bulk rheology for thermally set systems was applied to prepare novel cold-set protein fluid gels, both in the presence and absence of a secondary dispersed phase. In these cases, varying concentrations of calcium salts were used to induce gels from denatured WPI under shear conditions.

Again, similar results were obtained, with systems prepared at higher gelling rates exhibiting lesser inter-particle bridges, shown by a reduction in G' values.

Composite systems formed of both oil and gel phases highlighted that the inherent placing of the emulsion droplets, whether it be within the gel particles or continuous medium, ultimately influenced material response. Thermally gelling WPI under shear led to the formation of a new microcapsule system, with the ability to structure the continuous phase at volume fractions, where particles are not closely packed. Leading to a system that mimicked that of a highly-concentrated emulsion, with as little as 5 % oil.

Finally, the micro composite systems termed "emulsion fluid gels" were studied for their delivery capabilities via an *in vitro* digestive system; independently modelling both gastric and intestinal environments. Release was expected to follow that of a simple emulsion, where proteolysis and stripping of the WPI results in droplet instability. However, the study here showed rapid proteolysis of the gel followed by gastro-stable droplets. Data suggested such stability and subsequent lack of release to be a function of the protein change during the thermal sol-gel transition; either forming a protective layer around the droplet or opening enzymatic cleavage sites for proteolysis. Arrangement of the protein at the interface was probed by changing the polarity of the oil droplet. This resulted in changes to the release profiles, consequently providing the potential for targeted delivery of lipophilic molecules/compounds.

Therefore, the formulation of WPI micro particles for their rheological enhancing and delivery capabilities has been studied, with a view to their potential application as multi-functional ingredients.

# Acknowledgments

I would like to express my thanks to my supervisor Prof. Ian Norton for crediting me with the opportunity to undertake this Eng.D; providing me with the chance to pursue a world of significant and exciting research. I would also like to thank Dr. Sullo for his support and guidance throughout the beginning of the project.

Within the University of Birmingham I would like to thank Dr. Richard Greenwood not only for his time and help with the Eng.D scheme, but friendship and memories cultivated within the program. Additionally, I would like to thank Kathleen Hynes for her amazing patience, and all the help and encouragement I have received from the support staff, John Hooper, Lynn Draper and Chris Dickinson.

I would like to show my gratitude to Kerry Group Plc, in particular Cal Flynn for making the project possible and EPSRC for funding.

Lastly, I would like to thank my family, friends and colleagues that have managed to both put up with me, and help me through my time at Birmingham. I will always remember the experiences I have accumulated alongside the many smiles and laughs we've had. Extra special thanks go to those who have given me that little push out of my comfort zone, allowing me to build and grow as a person.

***Thank you!***

# Contents

**Abstract** ... **ii**

**Acknowledgments** ... **iv**

**List of Figures** ... **x**

**List of Tables** ... **xxii**

**List of Equations** ... **xxiv**

**Nomenclature** ... **xxvi**

**Chapter 1. *Introduction*** ... **1**

**1.1. Background** ... **2**

**1.2. Industrial relevance** ... **6**

1.2.1. A brief background to Kerry Group Plc ... 6

1.2.2. Background case for the research ... 7

**1.3. Objectives** ... **8**

**1.4. Thesis layout** ... **8**

**1.5. Publications and presentations** ... **11**

**Chapter 2. *Literature Review*** ... **13**

**2.1. Whey protein** ... **14**

2.1.1. WPI production ... 15

2.1.2. Whey protein composition and structure ... 17

2.1.3. Uses of whey protein ... 22

**2.2. Material systems – structure/function relationships** ... **29**

2.2.1. Emulsion technologies ... 29

2.2.2. Emulsion rheology ..... 35
2.2.3. Emulsion functionality ..... 42
2.2.4. Microgel technologies ..... 45
**Chapter 3. *WPI Fluid Gels: The effects of Shear and Thermal History*** ..... **52**
**3.1. Introduction** ..... **53**
**3.2. Materials and Methods** ..... **53**
3.2.1. Materials ..... 53
3.2.2. Preparation of stock solutions ..... 53
3.2.3. Fluid gel preparation using a rheometer ..... 54
3.2.4. Static light scattering (SLS) ..... 56
3.2.5. Optical light microscopy ..... 56
3.2.6. Confocal laser scanning microscopy (CLSM) ..... 56
3.2.7. Rheological Methods ..... 57
**3.3. Results and Discussion** ..... **60**
3.3.1. Formulation of WPI Fluid Gels ..... 60
3.3.2. Fluid gel material properties ..... 75
**3.4. Conclusions** ..... **82**
**Chapter 4. *Cold-set particulate suspensions*** ..... **84**
**4.1. Introduction** ..... **85**
**4.2. Materials and Methods** ..... **85**
4.2.1. Materials ..... 85
4.2.2. Preparation WPI and WPI/Oil systems ..... 86
4.2.3. Rheological Analysis ..... 88
Experimental design for cold-set kinetics: ..... 88
4.2.4. Static light scattering (SLS) ..... 92

4.2.5. Zeta-potential determination ..... 92
4.2.6. Optical light microscopy ..... 93
**4.3. Results and Discussion ..... 94**
4.3.1. Cold-set gel kinetics: Quiescent systems ..... 94
4.3.2. Cold-set WPI suspensions: The effect of shear ..... 102
4.3.2. Cold-set WPI suspensions: Material response ..... 109
**4.4. Conclusions ..... 117**
**Chapter 5. *Whey Protein Emulsion Fluid Gels* ..... 119**
**5.1. Introduction ..... 120**
**5.2. Materials and Methods ..... 120**
5.2.1. Materials ..... 120
5.2.2. Preparation of oil filled fluid gels ..... 121
5.2.3. Static light scattering (SLS) ..... 123
5.2.4. Microscopy ..... 123
5.2.5. Rheological Analysis ..... 124
5.2.6. Encapsulation efficiency ..... 126
**5.3. Results and Discussion ..... 127**
5.3.1. Preparation of emulsion fluid gels (EmFG) ..... 127
5.3.2. EmFG material properties ..... 134
**5.4. Conclusions ..... 145**
**Chapter 6. *EmFG: In vitro digestion* ..... 146**
**6.1. Introduction ..... 147**
**6.2. Materials and Methods ..... 147**
6.2.1. Materials ..... 147
6.2.2. Preparation of EmFG particles ..... 148

6.2.3. Digestion and release ..... 149
6.2.4. Static light scattering (SLS) ..... 150
6.2.5. Microscopy ..... 151
6.2.6. Interfacial Tension Analysis ..... 151
6.2.7. Rheological Analysis ..... 151
**6.3. Results and Discussion ..... 152**
6.3.1. In vitro digestion of protein-oil composites ..... 152
6.3.2. Effect of oil polarity on emulsion failure (release) during digestion ..... 159
6.3.2. Effect of oil polarity on suspension properties ..... 164
**6.4. Conclusions ..... 166**
**Chapter 7. *Conclusions and Future Recommendations* ..... 168**
**7.1. Conclusions ..... 169**
**7.2. Future work ..... 174**
**Appendices ..... 180**
**Appendix. i ..... 181**
i.1. Rheometry ..... 181
i.2. Confocal microscopy ..... 185
i.3. Particle sizing (light scattering techniques) ..... 188
**Appendix. ii ..... 191**
ii.1. EmFG formulation design process ..... 191
ii.2. Summary of processing conditions ..... 198
ii.3. Coating thickness determination ..... 200
**Appendix. iii ..... 202**
iii.1. Initial digestion study and method design ..... 202
iii.2. Formulation effects on EmFG particles ..... 205

iii.3. Preliminary active release studies ..... 206

***References*** ..... **212**

# List of Figures

*Figure 1.1: Schematic representations for the microstructural design approach showing: (a) the commonly shown linear methodology (adapted from Norton and Norton (2010)), and (b) A dynamic microstructural design approach. ..... 3*

*Figure 2.1: Schematic taken from Smithers (2008) representing the increase in whey protein value as a function of scientific development between 1950 and 2000. .....14*

*Figure 2.2: Ribbon diagrams showing the 3-dimentional conformation for: (left) β-lactoglobulin (Brownlow et al., 1997), and (right) α-lactalbumin (Permyakov and Berliner, 2000).....19*

*Figure 2.3: Ribbon diagrams depicting dimeric association of β-Lg structures at a pH close to the isoelectric point (~pH 4.6-5.0) (Brownlow et al., 1997).....20*

*Figure 2.4: Electron micrographs of (left) WPI fibrils prepared via heat treatment at pH 2.0 (Loveday et al., 2010), and (right) globular WPI microstructure formed using heat denaturation at pH 5.0 (Bromley et al., 2006).....21*

*Figure 2.5: Milk-derived (whey protein and casein) hydrolysate functionality taken from Korhonen and Pihlanto (2006) .....28*

*Figure 2.6: Schematic representation of: (left) homogeneously dispersed emulsion, (middle) creamed emulsion, and (right) phase separated systems.....32*

*Figure 2.7: Resulting emulsion droplet size as a function of energy input for various fabrication methods: Rotating membrane (RME), High shear mixer (HSM), and Sonication (SON). Graph taken from Lloyd (2016). .....33*

*Figure 2.8: Schematic diagram of an adsorbed polymer exhibiting tail, loop and train conformations. Image taken from Stuart (1991). .....34*

*Figure 2.9: (Left) Typical viscosity (η) vs shear rate (γ) plot for emulsion systems with increasing droplet volume fraction (ϕ). (Right) Effect of droplet size on emulsion viscosity. Taken from Barnes (1994).*.....38

*Figure 2.10: G'/G" as a function of dispersed phase for simple oil in water emulsions. Taken from Tadros (1994).*.....39

*Figure 2.11: Frequency dependent depiction of a typical O/W emulsion as a function of dispersed phase volume. Taken from Mason et al. (1997) in Derkach (2009).*.....40

*Figure 2.12: MRI images showing cross-sections of a human abdomen, 40 minutes post ingestion of: A) an acid stable emulsion and B) acid unstable emulsion, showing the formation of a fat-rich layer over the aqueous phase. Images taken from Marciani et al. (2007).*.....43

*Figure 2.13: Gastric emptying as a function of emulsion stability (Marciani et al., 2007).*..44

*Figure 2.14: Thermograms obtained for κ-carrageenan fluid gels showing the change in enthalpy of melting between the fluid gel system and quiescent counterpart. Graph adapted from Garrec and Norton (2012).*.....47

*Figure 2.15: Viscosity flow profiles for particulate suspensions with increasing particle asymmetry. Inserts show representative images for each system (Wolf et al., 2001).*.....50

*Figure 2.16: Plot comparing the concentration dependency for classically sheared systems ((●) 0.75% agar, and (○) 1.75% agar) and spherical agar particles ((▼) 2% agar, and (△) 5% agar). Adapted from Adams et al. (2004).*.....51

*Figure 3.1: DSC trace obtained for WPI (10% (w/w)) primary solution showing convoluted peaks for both α-lactalbumin (smaller peak) and β-lactoglobulin (major peak). The grey dotted line indicates the intercept of the baseline used to determine the temperature of denaturation ($T_d$) for β-Lg.*.....55

*Figure 3.2: Water loss as a function of increasing centrifugal force for WPI suspensions prepared at 3 °Cmin$^{-1}$, (□) 200 s$^{-1}$ and (●) 800 s$^{-1}$ shear rates.*.....59

*Figure 3.3: Viscosity profiles for 10% (w/w) WPI solutions upon heating from 25 °C to 80 °C at 1 °Cmin$^{-1}$ followed by subsequent holding for 10 minutes. Apparent shear thickening with increasing processing rates is an artefact of secondary flow and shear banding within the vane geometry.....62*

*Figure 3.4: Diluted WPI fluid gel particles (1:4) viewed under confocal laser scanning microscopy: samples were excited at 405 nm using 40x magnification. Particles were prepared at 1 °Cmin$^{-1}$ at 200 s$^{-1}$ (a) and 800 s$^{-1}$ (b) (Scale bar shows 20 μm).....63*

*Figure 3.5: Flow profiles observed during sheared heating from 25 °C to 80 °C at (a) 3, (b) 5, and (c) 10 °Cmin$^{-1}$. (The dotted red line on (a) has been added as an example to highlight the linear region of the gelling profile used to obtain the rate of aggregation.) .....65*

*Figure 3.6: Rate of protein aggregation at varying shear rates as a function of the heating rate.....67*

*Figure 3.7: SLS size distributions obtained for WPI fluid gels prepared using varying shear rates (200 to 800 s$^{-1}$) at 1 °Cmin$^{-1}$ (a) and 10 °Cmin$^{-1}$ (b). Distributions are the average of 3 repeats, error bars have been shown for obtained $D_{4,3}$ values in Figure 3.8.....69*

*Figure 3.8: Mean particle size ($D_{4,3}$) as obtained by SLS for WPI fluid gels prepared at a range of heating rates (from 20°C to 80 °C), as a function of processing shear rate: 200 s$^{-1}$ (■), 400 s$^{-1}$ (●), 600 s$^{-1}$ (▲) and 800 s$^{-1}$ (◆). Particle time in the shear field was thus dependent on the heating rate applied. .....70*

*Figure 3.9: (a) Aspect ratio obtained for WPI particles prepared at various heating and shear rates: (●) 200 s$^{-1}$, (□) 400 s$^{-1}$, (◆) 600s$^{-1}$ and (△) 800 s$^{-1}$. Dotted line shows the average particle length to width ratio. (b) Typical images used to determine the aspect ratio, systems were prepared at 10 °Cmin$^{-1}$ at: (i) 200 s$^{-1}$ (x5 magnification), and (ii) 800 s$^{-1}$ (x10 magnification).....72*

*Figure 3.10: Relative change in viscosity obtained from fluid gel viscosity profiles. Fluid gels were prepared at varying heating rates (1 to 10 °Cmin$^{-1}$) as a function of shear rate 200 s$^{-1}$ (■), 400 s$^{-1}$ (●), 600 s$^{-1}$ (▲) and 800 s$^{-1}$ (◆).....74*

*Figure 3.11: (a) Amplitude, and (b) frequency sweeps for fluid gels $\phi_{FG}$90 prepared at 200 $s^{-1}$ (●,○) and 800 $s^{-1}$ (■,□), 10 °$Cmin^{-1}$. Closed markers denote G' and open, G". Amplitude sweeps were obtained at 1 Hz and frequency sweep at 0.05 % strain. Dashed lines show point at which the system begins to break down, deviating from the LVR. Plots show the average of three repeats.....76*

*Figure 3.12: Small deformation oscillatory data obtained for WPI fluid gels prepared at 200 $s^{-1}$ (●,○) and 800 $s^{-1}$ (■,□). Solid markers represent fluid gels formulated at 1 °$Cmin^{-1}$ and open 10 °$Cmin^{-1}$. Values of G' were obtained at 1 Hz.....77*

*Figure 3.13: Elastic moduli (G') plotted against volume fraction ($\phi_{FG}$) for fluid gel particles of similar size (ca. 30 $\mu$m). Particles were prepared at 400 $s^{-1}$ (1 °$Cmin^{-1}$) (●) and 600 $s^{-1}$ (5 °$Cmin^{-1}$) (○).....78*

*Figure 3.14: (a) Viscosity curves showing thixotropic behaviour for fluid gels prepared at 1 °$Cmin^{-1}$, 200 $s^{-1}$ (□,■), 400 $s^{-1}$ (○,●) and 600 $s^{-1}$ (△,▲) $\phi_{FG}$90. (Unfilled symbols denote ramp up and filled ramp down.). Data shows the average of three repeats. (b) Fluid gel viscosities at $\eta_{max}$ having been prepared using varying shear rates at 1 °$Cmin^{-1}$ (■) and 10 °$Cmin^{-1}$ (□).....79*

*Figure 3.15: (a) Flow curves for WPI fluid gels (prepared at 200 $s^{-1}$, 1 °$Cmin^{-1}$) sweep 1 (□,■) and sweep 2 (○,●). A five-minute recovery period was held between sweeps. (Open symbols denote increasing shear rates, filled denote decreasing shear rate.). Data shows the average of three repeats. (b) Thixotropic analysis for WPI fluid gels formulated at 1 °$Cmin^{-1}$ (●,○) and 10 °$Cmin^{-1}$ (■,□).....81*

*Figure 3.16: Size distributions obtained using SLS for WPI suspensions pre-thixotropy analysis (black line) and post-testing (grey line) for (a) particles prepared at 800 $s^{-1}$ and 10 °$Cmin^{-1}$, and (b) particles prepared at 200 $s^{-1}$ and 1 °$Cmin^{-1}$.....82*

*Figure 4.1: Schematic diagrams of a jacketed pin-stirrer (also known as a c unit). (a) shows unit dimensions in mm. (b) Sol/emulsion entry point has been highlighted (left) and salt injection port (right). The system is then sheared as a function of the retention time and pushed through the exit at the top.....87*

*Figure 4.2: Schematic diagrams of rheometer set-ups for diffusion of cross linker into the denatured WPI sol, whereby diffusion occurs: (a) across a membrane from the bottom-up, and (b) from a surrounding well (sides-in).....88*

*Figure 4.3: Flow profiles obtained for WPI (5 % (w/w)) systems undergoing dynamic cold-set gelation at 50 $s^{-1}$ through the addition of $CaCl_2$ via: (a) diffusion through dialysis tubing, and (b) diffusion form a well surrounding the geometry. Data presented shows only a single run, as the method was not adopted for the study.....89*

*Figure 4.4: Flow profiles obtained for cold-set WPI systems (25 mM $CaCl_2$, WPI 5% (w/w)) undergoing gelation with a preparation shear field of (●) 50 $s^{-1}$, (■) 100 $s^{-1}$ and (▲) 200 $s^{-1}$.....90*

*Figure 4.5: Zeta-potential measurements obtained via titration method from pH 12 to pH 2 using NaOH and HCl: (○) indicate zeta potential (left axis) and (●) show mean particle sizes.....93*

*Figure 4.6: Single frequency (1Hz, 0.5 % strain) spectra obtained for WPI systems undergoing cold set gelation with increasing $Ca^{2+}$ concentrations: (●) 10 mM, (▽) 25 mM, (■) 40 mM, (○) 50 mM, and (▲) 100 mM.....95*

*Figure 4.7: Relationship between the change in gel strength at $t_e$ (1800 s), as described by the storage modulus ($\Delta G'$), as a function of the salt ($CaCl_2$) added. Equation of the line* $y = 3171\text{-e-}0.06x4.2$, *was used to give the parameters in Equation 4.1.....96*

*Figure 4.8: Mechanical spectra obtained for WPI/Oil systems undergoing gelation with the addition of (a) 25 mM and (b) 50 mM $CaCl_2$: (●) 0 % (v/v), (▽) 10 % (v/v), (■) 20 % (v/v), (◇) 30 % (v/v), and (▲) 40 % (v/v). (i) shows the evolution of G' over time and (ii) shows the relative term of the same data, where G' for the oil fractions have been normalised by G' for no oil systems ($G'_{\phi=0}$). Inserts show the gelled systems at time, $t_e$..... 100*

*Figure 4.9: Static light scattering particle size distributions for WPI systems immediately diluted on exiting the pin stirrer set to a rotation speed of 1000 rpm (closed markers) and 2000 rpm (open markers): (●/○) 25 mM, (■/□) 40 mM and (▲/△) 50 mM $Ca^{2+}$..... 102*

*Figure 4.10: Schematic representations showing the microstructures of WPI cold-set micro-particles. (a) Regular network, where a well-ordered structure exposes binding sites for further aggregation. (b) Less ordered structure due to more rapid aggregation of the WPI globules, sterically burying binding sites within the gel network slowing further aggregation steps.* ..... *103*

*Figure 4.11: Mean particle sizes ($D_{4,3}$) obtained from static light scattering distributions for WPI systems 48 hrs post production: pin stirrer set to 1000 rpm (closed markers) and 2000 rpm (open markers) rotation speed.* ..... *104*

*Figure 4.12: Particle size distributions for: (a) Pre-emulsions before gelation, (b) cold-set emulsion-WPI systems after 48 hrs (25 mM), (c) Cold-set emulsion-WPI systems after 48 hrs (50 mM), and (d) Average particle sizes ($D_{4,3}$) obtained 48 hrs post production using static light scattering distributions for: WPI/Oil systems prepared at to 1,000 rpm rotation speed and 25 mM (closed markers) and 50 mM (open markers).* ..... *105*

*Figure 4.13: Optical micrograph depicting a typical, diluted cold-set WPI/Oil system (5 % (w/v) WPI, 10 % (v/v) oil, 50 mM $CaCl_2$) post dispersion, highlighting a protein particle, un-trapped oil droplets and an oil droplet that has become trapped within the protein particle. Scale bar represents 100 microns.* ..... *108*

*Figure 4.14: (a) Strain sweeps (1 Hz, 20 °C) for WPI systems taken 48 hrs post production, as a function of $Ca^{2+}$ salt addition and shear applied during gelation. Symbols represent (■,□) 25 mM, and (▲,△) 50mM $CaCl_2$; closed markers denote systems processed at 1000 rpm and open 2000 rpm mixing speeds. (b) Equivalent stress vs G' plots obtained for WPI systems crosslinked with 25 and 50 mM $CaCl_2$ at 1000 rpm processing speed only (● - 25 mM and ○ - 50 mM $CaCl_2$). (Dashed lines are for guiding the eye, highlighting the point of at which the system is no longer within the LVR)* ..... *109*

*Figure 4.15: Mechanical spectrum obtained for a 50 mM $Ca^{2+}$, 40% (v/v) WPI/Oil system, prepared using 1000 rpm stirrer speed. (Closed markers denote G' and open G''). (Data obtained at 0.5% strain, 20 °C)* ..... *111*

*Figure 4.16: Storage modulus (at 1 Hz, 20 °C) plotted against oil fraction for (a) 25 mM $Ca^{2+}$ and (b) 50 mM $Ca^{2+}$ WPI/Oil systems prepared using 1000 rpm stirrer speed. Closed markers denote G' at $t_0$ (immediately post-production) and open G' at 48 hrs post-production. * Data point removed as an outlier..... 113*

*Figure 4.17: Amplitude sweeps (1Hz, 20 °C) for: (a) 25 mM $Ca^{2+}$ and (b) 50 mM $Ca^{2+}$ WPI/Oil systems prepared using 1000 rpm stirrer speed. Mechanical spectra were obtained 48 hrs post production. Symbols represent (●) 0% oil, (○) 10% oil, (▼) 20% oil, (△) 30% oil, and (■) 40% oil fractions (v/v) (note the change in y-axis scale). * mechanical data for 25 mM Ca2+, 10%, proposed in Figure 4.16a as an outlier..... 115*

*Figure 4.18: Schematic of the contact sites between: (a) two protein particles, highlighting the long region of interaction, and (b) protein particles separated with oil droplets, showing much smaller contact zones. The contact area between can be directly linked to the degree of interactions that can occur between the species. ..... 116*

*Figure 5.1: Optical micrograph highlighting (A) an uncoated oil droplet and (B) a coated oil droplet (EmFG particle)..... 127*

*Figure 5.2: Oil droplet entrapment efficiencies for: (a) EmFG systems prepared with increasing WPI concentrations ranging between 5 and 30% (w/w) at a fixed $\phi_{oil}$ of 10% (v/v), and (b) EmFG systems prepared with increasing $\phi_{oil}$ between 5 and 20% (v/v) with a fixed WPI concentration of 15% (w/w). ..... 128*

*Figure 5.3: CLSM micrographs of EmFG particles. Gel phase has been stained using Rhodamine B (excitation wavelength: 532 nm, emission wavelength: 560-600 nm) and oil phase either negatively stained or stained using Nile red (excitation wavelength: 488 nm, emission wavelength: 690-700 nm). (a) 3D stack showing topographical detail of the EmFG particles, (b) cross section depicting stained gel layer surrounding a negatively stained oil core, and (c) stained cross section showing protein shell (blue) and oil core (red). Scale bars represent 25 μm (a and b) and 50 μm (c). ..... 130*

*Figure 5.4: Particle size distributions for: (a) EmFG prepared with a range of WPI concentrations between 5 and 30% (w/w) with a fixed $\phi_{oil}$ of 10% (v/v), and (b) EmFG*

*prepared with a range of $\phi_{oil}$ from 5 to 20% (v/v) with a fixed WPI content of 20% (w/w).* ..... *132*

*Figure 5.5: Optical micrographs of a 30% (w/w) WPI system, highlighting highly dispersed emulsion droplets with large aggregated protein particles in the back ground. Scale bar represents 50 μm.* ..... *133*

*Figure 5.6: (a) Frequency sweeps at 1 Pa stress, 25 °C, obtained for EmFG prepared using 20% (w/w) WPI and (●,○) no oil, (■,□) 5% (v/v) oil, (▼,▽) 10% (v/v) oil, (◆,◇) 15% (v/v) oil, and (▲,△) 20% (v/v) oil. Open markers represent the storage moduli (G') and closed show loss moduli (G''). (b) Storage modulus at 1 Hz verses normalised particle phase volume for systems with, (●) no oil - 20% (w/w) shear/heat treated WPI, and 20% (w/w) WPI EmFG containing: (■) 5% (v/v) oil, (▼) 10% (v/v) oil, (◆) 15% (v/v) oil, and (▲) 20% (v/v) oil. Volume fractions were normalised using the maximum random packing fraction for hard spheres, 0.64. Dashed line represents maximum packing faction for hard spheres.* ..... *135*

*Figure 5.7: Stress sweeps obtained at 1 Hz (25 °C) for EmFG prepared with 20% (w/w) WPI and: (a) 5% (v/v) oil, (b) 10% (v/v) oil, (c) 15% (v/v) oil, and (d) 20% (v/v) oil. Dashed vertical line is a guide for eye, to show shear stress at the point of solid to liquid crossover.* ..... *138*

*Figure 5.8: Stress required to induce a crossover to liquid-like behaviour, determined using stress sweeps as the point at which the storage modulus (G') crosses the loss modulus (G'') for EmFG systems prepared using 20% (w/w) WPI and oil fractions between 5 and 20% (v/v).* ..... *139*

*Figure 5.9: Viscosity profiles obtained for 20% (w/w) WPI EmFG containing: (a) 5% (v/v) oil, (b) 10% (v/v) oil, (c) 15% (v/v) oil, and (d) 20% (v/v) oil. Closed markers represent sweep 1 and open, sweep 2.* ..... *140*

*Figure 5.10: Thixotropic analysis obtained as the area between the viscosity profiles for 20% (w/w) WPI EmFG with increasing oil phase volumes from 5 to 20% (v/v) ((●) denote thixotropic analysis for sweep 1 and (○) denotes values for sweep 2).* ..... *141*

*Figure 5.11: Size distributions obtained using SLS for EmFG suspensions pre-thixotropy analysis (black line) and post-testing (grey line) for: (a) particles prepared at 10% (v/v) oil and 20% (w/v) WPI..... 142*

*Figure 5.12: Storage modulus as a function of time for EmFG systems (◆) 5% (v/v) oil, (□) 10% (v/v) oil, (△) 15% (v/v) oil, and (●) 20% (v/v) oil. All EmFG underwent a rejuvenation process of 10 $s^{-1}$ for 10 s before measuring G' at 1 Hz and 1 Pa stress for 30 minutes..... 144*

*Figure 6.1: Release profiles for: (a) gastric and (b) intestinal digestion of a simple WPI stabilised emulsion (○) and high oleic sunflower oil microgel composites (●)...... 153*

*Figure 6.2: Composite droplet size distributions as a function of digestion time (gastric conditions) and optical micrographs depicting typical images for composites undergoing digestion at time (a) 0 hours, (b) 1 hour and (c) 6 hours. Scale bars represent 100 μm.... 155*

*Figure 6.3: Micrographs showing proteolysis of the gel layer under a gastric (4:1 digester to sample ratio) environment: (a) 1 min, (b) 2 mins, (c) 3 mins, (d) 4 mins and (e) 5 mins. Scale bar shows 100 μm..... 157*

*Figure 6.4: Schematic showing the evolution of a secondary interfacial layer, resulting in the blockage of enzymatic cleavage sites. Proteins adapted from Wilde et al. (2004) ..... 159*

*Figure 6.5: Interfacial tension measurements showing decreasing tension for water and (▼) paraffin oil, (△) silicone oil, and (●) high oleic oil systems. Additionally, measurements for each oil system in the presence of WPI have been shown: (◆) paraffin oil, (◇) silicone oil, and (■) high oleic oil, overlapping ca. 14 $mNm^{-1}$. Data shows the average of 3 repeats, with error bars showing the 95% confidence interval (error bars are hidden by the data points, apart from paraffin only)..... 160*

*Figure 6.6: Optical micrographs presenting typical images for (a) silicone oil EmFG and (b) paraffin oil EmFG. ..... 161*

*Figure 6.7: Particle size distributions for: (●) silicone oil, (▽) paraffin oil, and (■) sunflower oil EmFG systems. The surface weighted mean ($D_{[3,2]}$) for each system has been presented in top right of the plot.* ..... *161*

*Figure 6.8: Release plots for the gastric digestion of: (a) silicone, (b) paraffin oil and intestinal digestion (c) silicone, (d) paraffin oil micro-composites.* ***Note changes in y-axis scale.*** ..... *162*

*Figure 6.9: Frequency sweeps obtained (1 Pa stress) for microgel composites prepared using (●/○) high oleic oil, (▼/▽) silicone oil and (■/□) paraffin oil as the oil substrate. Closed markers denote G' and open G".* ..... *164*

*Figure 6.10: Stress sweeps obtained at 1Hz for microgel composites prepared with (●) high oleic oil, (▼) silicone oil and (■) paraffin oil. Dashed lines are to guide the eye, highlighting the end of the LVR.* ..... *166*

*Figure 8.1: Schematic representations of: (a) cone and plate, (b) parallel plates, and (c) couette measuring systems: where $\Gamma$ is the torque (Nm), u is the displacement, $\theta$ is the angle of the cone, h is the height at a given radius, r (m), and L is the length (m).* ..... *183*

*Figure 8.2: Schematic representation of a confocal microscope setup.* ..... *186*

*Figure 8.3: Rhodamine B, showing its highly-conjugated ring structure.* ..... *188*

*Figure 8.4: Schematic of a static light scattering (SLS) setup.* ..... *189*

*Figure 8.5: Micrographs showing initial EmFG particles prepared at 3 °Cmin$^{-1}$ (pH 6.4): (a) and (b) show the same image at different focus heights and (c) shows a typical image taken from the same slide, but different area. Scale bar represents 50 μm.* ..... *192*

*Figure 8.6: EmFG suspension prepared at pH 6.4, 0.5 °Cmin$^{-1}$, showing a change in microstructure from smaller to larger protein aggregates. Scale bar represents 50 μm..* *193*

*Figure 8.7: Representative optical micrographs obtained for EmFG systems prepared using (a) $Fe^{2+}$ (0.5 M), (b) $K^{+}$ (1 M) and (c) $Ca^{2+}$ (0.5M) salts. Scale bar represents 50 μm.* ..... *195*

*Figure 8.8: Typical image of WPI EmFG capsules having been prepared at pH 4.6 and 0.5 °Cmin$^{-1}$. Scale bar represents 50 μm. Also presented in Chapter 5, Figure 5.1..... 196*

*Figure 8.9: Entrapment efficiency as a function of emulsion ageing time (0 and 48 hrs).. 197*

*Figure 8.10: WPI-Oil composites entrapment as a function of the preparation at pH4.6. Prepared at 0.5 °Cmin$^{-1}$ with varying mixing rates: 250, 450 and 800 rpm stirrer speed. 198*

*Figure 8.11: Determination of coating thickness using a light scattering technique; (a) shows typical size distribution for emulsions both pre- and post-processing, highlighting a shift to higher particle sizes with gelation (system shown here is prepared using 0.5 M $CaCl_2$). (b) shows half the shift observed from the distributions, as a function of the cation type and concentration (□) $Ca^{2+}$ and (●) $K^+$..... 201*

*Figure 8.12: Oil release under intestinal conditions for simple WPI emulsion systems. Images show stirred systems at (a) t=0, (b) t=24 hrs and (c) t=24 hrs after separation (static conditions). Images a and b have had the contrast enhanced to highlight the change in colour due to the reduction of droplet number scattering the light (less white more yellow)..... 202*

*Figure 8.13: Intestinal digestion of EmFG after a 10 min static resting period: (a) 0 hrs, (b) 20 hrs and (c) 44 hrs digestion time. Dotted red lines show phase separated (released) oil. Total oil content within the system was 10 mL. ..... 203*

*Figure 8.14: Oil release under intestinal conditions over 48hrs. No error bars are present due to data showing a single experiment. ..... 204*

*Figure 8.15: (●) Gastric and (○) intestinal release plots (n=1) for WPI EmFG having undergone the primary emulsification stage stabilised using NaCas..... 206*

*Figure 8.16: (a) UV/Vis spectra obtained for β-carotene in hexane at concentrations of: (●) 1 mM, (○) 2 mM, (◆) 4 mM, (△) 6 mM, (■) 8 mM and (□) 10 mM. (b) Calibration curve taken at 450 nm, equation of the line is y=125.72x-0.0027. ..... 207*

*Figure 8.17: β-Carotene release plots for: (●) gastric conditions, (○) intestinal conditions, and (▼) intestinal conditions in the presence of bile salts (0.5% (w/v)) (error bars masked by points).....208*

*Figure 8.18: Plot showing the decrease in interfacial tension for water/oil systems with β-carotene (closed) and without β-carotene (open). No protein present.....210*

*Figure 8.19: Fluorescein release profile (n=1), obtained using a dialysis technique and conductivity measurements in water. Inserts show the change in water-colour over the dissolution period.....211*

# List of Tables

*Table 2.1: Whey protein fractions and basic primary structure properties (Etzel, 2004, Madureira et al., 2007).....18*

*Table 2.2: Table highlighting some of the uses of whey proteins across food research.....23*

*Table 4.1: Table showing gelation onset times for WPI systems undergoing gelation with increasing additions of salt. Table also shows storage moduli at the point of gelation ($t_o$) and at the end of the test ($t_e$ – 1800 s).....97*

*Table 4.2: Parameters obtained from applying the power law model (Equation 4.2), describing the rate of gelation occurring in the WPI systems with the addition of salt.....98*

*Table 4.3: Parameters obtained from applying the power law model (Eq. 4.1), describing the effect of oil fraction on the rate of gelation for WPI systems with the addition of 25 mM and 50 mM $CaCl_2$.....99*

*Table 4.4: Table of stresses to apparent yielding, as determined as the point at which the storage and loss moduli no longer behave linearly. Obtained for WPI/Oil suspensions prepared at 1000 rpm with increasing oil fractions from 10 to 40% (v/v), as a function of cross-linking concentration. Values shown are taken from the data obtained for Figure 4.18 as the stress measured at the point of exiting the LVR.....114*

*Table 8.1: Table of shear stress and strain equations for common rheological geometries: where $\Gamma$ is the torque (Nm), u is the displacement, $\theta$ is the angle of the cone, h is the height at a given radius, r (m), and L is the length (m).....183*

*Table 8.2: Table of salts and corresponding concentrations used within EmFG formulation studies.....194*

*Table 8.3: Summary table highlighting the various parameters changed in the development of EmFG systems. (+) shows increased entrapment and (-) decreased. "*" denotes systems that were prepared in the same way.* ..... *199*

*Table 8.4: Table summarising the processing parameters and values used to prepare the final EmFG systems.* ..... *200*

# List of Equations

*Equation 2.2: Stokes' equation describing the velocity of separation ($v_s$) as a function of the droplet radius (r), density of the continuous ($\rho_c$) and dispersed phases ($\rho_d$), viscosity of the continuous phase ($\eta_c$) and gravity (g).* ..... *30*

*Equation 2.3: Einstein equation showing relative viscosity ($\eta_r$) (the ratio of the overall viscosity ($\eta$) to the viscosity of the solvent ($\eta_s$)) for infinitely dilute dispersions, $\phi < 0.01$, where Einstein's coefficient, "a", is a constant (2.5 for spheres).* ..... *36*

*Equation 2.4: Extended Einstein equation compensating for finite changes in dispersed phase, where a, b, c etc. are constants.* ..... *37*

*Equation 2.5: Krieger-Dougherty model for hard sphere suspensions.* ..... *37*

*Equation 3.1: Fluid gel particle volume fraction as a function of both the volume of water removed during centrifugation, and syneretic effects of the gelled particles.* ..... *58*

*Equation 3.2: Degree of aggregation, expressed as the change in viscosity of the suspension.* ..... *66*

*Equation 3.3: Rate of aggregation, derived from the change in viscosity (equation 3.2) with respect to time.* ..... *66*

*Equation 3.4: Empirical model expressing the number of primary particles (N) within an aggregate as a function of the gelation rate and time, (Berli et al., 1999).* ..... *67*

*Equation 3.5: Relative change in viscosity for WPI solutions undergoing gelation within a sheared environment.* ..... *73*

*Equation 4.1: Relationship between $Ca^{2+}$ concentration (mM) and storage modulus.* ..... *96*

*Equation 4.2: Power function applied to gelling curves (Figure 4.6) for calculating the gelation rate coefficient, $k_c$, and the order of reaction, n, where* x *is the concentration of calcium added*.....97

*Equation 4.3: Adapted equation based on an original model for the aggregation of soy protein by Berli et al. (1999), showing free volume as the limiting factor for particle growth: where $D_a$ is the degree of aggregation within in the final particle, k is a rate constant, t are given times, and $\phi$ is the packing fraction of oil droplets.*..... 107

*Equation 5.1: Determination of the volume occupied by the particles within the EmFG systems using a reduced water method*..... 125

*Equation 5.2: Entrapment efficiency, calculated by taking the ratio of uncoated droplets ($N_{fo}$) to gelled droplets ($N_{em}$)*..... 126

*Equation 5.3: Krieger-Dougherty model for hard sphere suspensions*..... 136

# Nomenclature

| | |
|---|---|
| $D_{4,3}$ | Volume Weighted Mean |
| DLS | Dynamic Light Scattering |
| EmFG | Emulsion Fluid Gel |
| FG | Fluid Gel |
| G' | Elastic or Storage Modulus |
| G'' | Viscous or Loss Modulus |
| IFT | Interfacial Tension |
| α-Lac | α-Lactalbumin |
| β-Lg | β-Lactoglobulin |
| LVR | Linear Viscoelastic Region |
| O/W | Oil in Water |
| pI | Isoelectric point |
| SLS | Static Light Scattering |
| W/O | Water in Oil |
| WPI | Whey Protein Isolate |
| WPC | Whey Protein Concentrate |
| $d\alpha$ | Change in Aggregation |
| $\phi_{FG}$ | Fluid Gel Particle Volume Fraction |
| $\phi_{max}$ | Maximum Packing Fraction |
| $\eta$ | Viscosity |
| $[\eta]$ | Intrinsic Viscosity |

# Chapter 1. *Introduction*

## 1.1. Background

The role that fats play within food with respect to texture and physical properties are vital for consumer satisfaction (Norton and Norton, 2010). This, however, has led to a high concentration of fat in routine diets, promoting a high risk of obesity and other health related diseases (Norton et al., 2007). Recent global studies on adult obesity showed that in 2014 around 2.0 billion men and women exceeded a BMI of 25 upwards, predicted to have increased to about 2.7 billion by 2025 ("World-Obesity-Day", 2015). More concerning statistics have recognised that within the European region, noncommunicable diseases (not caused by infection or transmittable) such as malnutrition (including micronutrient deficiencies and obesity resulting in cardiovascular, diabetes, cancer and respiratory problems), account for 77 % of the total disease, yielding close to 86 % of patients with premature mortality (WHO, 2015). This can be combatted by reducing the calorific content of food products. However, unfortunately in many cases removing the fat component in a food system has a negative effect on its intrinsic properties: structure, mouth feel and palatability *etc*. In response, microstructural engineering has been used to formulate systems to give controlled material properties (Norton et al., 2015), which can be used to replicate the structural responses the consumer is accustomed to, without the calorific content.

The microstructural design approach is commonly represented as a linear progression (Figure 1.1a), whereby a process and ingredients are linked forming a microstructure which dictates the material properties needed for consumer response/requirement (Norton and Norton, 2010, Norton et al., 2015). Figure 1.1b

shows a three-step representation of this approach, highlighting three key areas: components, processing and material properties.

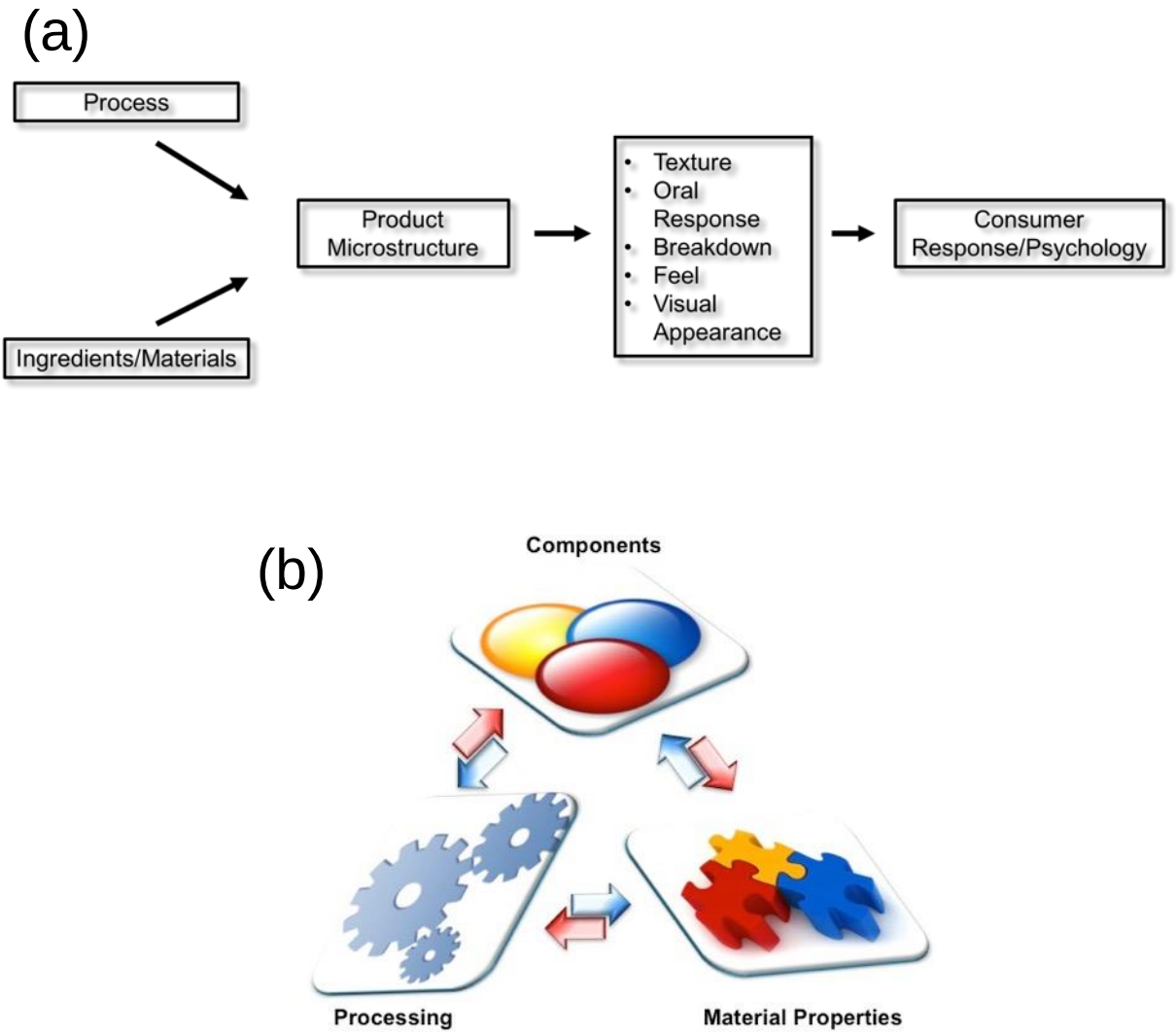


*Figure 1.1: Schematic representations for the microstructural design approach showing: (a) the commonly shown linear methodology (adapted from Norton and Norton (2010)), and (b) A dynamic microstructural design approach.*

On a simple level of understanding this alludes to a more dynamic approach, whereby knowledge within two of the segments allows a better prediction over the third. For example, in industry, where the processing equipment is commonly fixed (due to large

costs involved in the installation of new processes) the final material properties can be manipulated by changing the starting materials *etc*. However, this becomes more complicated for complex systems (Fischer and Windhab, 2011).

Although presented slightly differently both approaches ultimately result in the same outcome, effectively posing the option to reverse engineer products; working backwards from a defined set of properties (material responses/a process/ingredients) and manipulating the other two parameters to achieve them. One example arising from this approach are fluid gels; as controlling the processing (shear applied) and formulation (gelling material and cross-linker), microstructures have been engineered to give properties characteristic of oil/emulsions, forming discreet particles that weakly-interact. These have found promising application within the food industry, being applied to structure fluids as fat mimetics (Fernández Farrés et al., 2014, Sullo et al., 2014). The use of particulate gel suspensions, with particles sizes within the micron-scale, have received increasing interest in recent years, for their textural role as fat mimetics; replicating high fat products, for example mayonnaise, where the rheology of the full fat counterpart was replicated by replacing the majority of the oil content with spherical agar particles (Norton and Norton, 2010). Additionally, the presence of small, soft and smooth particles lowers the friction between oral surfaces providing enhanced fat perception (Fernández Farrés et al., 2013, Garrec, 2013).

An essential feature regarding their application is the intrinsic rheological properties of fluid gels, since they behave in a solid-like fashion at rest, but flow above a critical value of applied stress (Norton et al., 1999). These rheological properties can be finely controlled to meet requirements for desired applications by varying the composition (e.g. polysaccharide, protein), cross-link density (e.g. salt, concentration),

particle size and/or degree of particle-particle interactions (Adams et al., 2004, Altmann et al., 2004, Norton and Frith, 2001, Norton et al., 2006b, Norton et al., 1999, Wolf et al., 2001). Both particle size and degree of interactions are directly related to the processing conditions used in production (Garrec and Norton, 2012, Gabriele et al., 2009).

Fluid gels are formed when a separation process is applied to a biopolymer system undergoing its sol-gel transition (Norton et al., 1999). Amongst all the existing methods for the preparation of gel particles (e.g. breakdown of quiescently formed gels, emulsion route or biopolymer mixtures), shear induced fluid gels are typically more attractive due to relatively easy modulation and careful control of resulting properties, by varying two parameters: Shear and thermal history. Whereas, particles produced via a phase separation route followed by gelation (e.g. emulsion route) require additional steps; due to the transfer of produced particles into an aqueous phase, lowering efficiency.

Fat replacers based on biopolymer particles with controlled size and shape are already commercially available. *Simplesse*® (CP Kelco) is a system of microparticulated, denatured whey protein spheres between 0.1 to 3 μm in diameter; owing to their size and morphology, the protein particles are able to replicate organoleptic mouth feel. The protein particles are formed using a rapid heating process (up to 120 °C) over a short period of time to denature the whey protein. Reducing the pH of the system below the isoelectric point increases electrostatic repulsion, aided by aggregate blocking agents (i.e. lecithin) and high shear, leading to an incomplete aggregation process that results in discrete particles (Singer et al., 1988).

Owing to their nutritional value and thermo-irreversible nature many proteins, in particular milk proteins such as whey, pose as excellent candidates for the preparation

of multi-functional ingredients, as both nutrition delivery and fat reducing agents within food. Having said this, there is little literature based on the production of fluid gels using dairy proteins as the gelling agent. Furthermore, an understanding of the role that the shear-gel process has on the resulting structuring and delivery properties has also not been investigated. This would directly result in a rheology modifier with the ability to both transport and act as a protecting vessel for nutraceuticals.

## 1.2. Industrial relevance

As previously highlighted the use of fluid gels as a food ingredient shows great promise, however, without being incorporated into the ingredients industry will remain an used technology. As such, this doctorate of engineering was conducted alongside Kerry Group Plc in order to further knowledge in the field of fluid gels, and provide a route to potential commercialisation.

### *1.2.1. A brief background to Kerry Group Plc*

Kerry started in the early 1970's primarily as a dairy industry, trading under the name of Kerry Co-operative Creameries Ltd, the smallest of Ireland's six agricultural Co-operatives. By the time Kerry moved to become a public limited company in 1985, sales had increased from €29 million to €268 million, however the capital required for such a rate of growth presented a challenge. As a result, company organisation and structure had to be changed, leading to the emergence of Kerry Group plc, the first steps on the way to becoming an Irish multinational. The takeover of Beatreme in 1988 put Kerry Group on the path to become a global ingredients corporation, maturing into the

company it is today, with operations based over 23 countries globally. Currently Kerry Group plc has grown to sales in the region of €6.1 billion annually, stretching mainly across the dairy, ingredients and consumer goods portfolios (Kerry, 2015).

### *1.2.2. Background case for the research*

The increased pace of life within modern day society has motivated the need for fast and convenient food products, which in many cases has compromised their nutritional values. A more apparent awareness to the impact this is having upon daily health has sparked a drive towards more functional foods, demanding greater innovation from ingredients industries; more particularly within the Kerry Corporation, their nutrition and pharma sectors. As such, to remain a leader within the field of ingredients, innovation of new and novel technologies are necessary.

Having been established in the use of proteins for functional ingredients, Kerry are looking to grow their portfolio in this sector, innovating their uses into new technologies. In addition, from a nutritional aspect, proteins play a vital role within a healthy balanced diet. Furthermore, per gram they contain just under half the total calories within fats. For these reasons proteins pose a solid choice as the starting material for fat replacement systems.

In conjunction with consumer demand, the use of proteins as a multifunctional ingredient; not only acting as a rheological modifier, but as a nutritional enhancer, encapsulant for delivery, taste masking and/or protection, increases product value. As such, the work detailed within this thesis falls inline with Kerrys' mission statement "to be a world leader in taste and nutrition serving the food, beverage and pharmaceutical industries, and a leading supplier of added value brands…" providing novel alternatives

to fat components in food, with the ability to retain and deliver key nutritional compounds associated with a healthy diet.

## 1.3. Objectives

Having identified a lack of knowledge within key areas of proteins in the field of fluid gels, the aims of this thesis are to:

- Investigate the effects of processing on the bulk suspension material characteristics, arising from the resulting particle intrinsic properties.
- Utilise the knowledge base derived from processing fluid gel particles to formulate a system capable of both the structuring of liquids and delivery key vitamins/minerals typically lost throughout the fat reduction process.
- Understand the behaviour of the delivery agent once eaten: within digestive conditions.

## 1.4. Thesis layout

The layout of this thesis has moved away from the traditional structure, whereby all the materials and methods for all the results chapters are collated into one single place. As such, the results chapters read more like individual research papers, with methods specific to the work conducted in the results/discussion. Additionally, a brief introduction and paragraph in the conclusions are used to highlight the progression of the work. The aim of this design was to focus on main outcomes of each chapter, dividing the work up into individual segments, with supporting data (formulation design

and short further studies) allocated to the appendix. Thus, the layout of this thesis will be as follows:

The following chapter, Chapter 2, will contain a literature review assessing recent and relevant work within the fields of whey proteins and their uses, emulsions and fluid gels, connected with the research presented in this thesis.

The results chapters starting with Chapter 3, the first published chapter, discusses the effects of processing (shear and thermal history) on the resulting intrinsic properties of WPI gel particles. It looks at changes in particle size and morphology influenced by the kinetics of protein aggregation, detailing a qualitative model for particle formation. The chapter then proceeds to study material characteristics of the gel suspensions, reporting elastic behaviour as a function of particle volume fraction. This highlights the link between processing conditions and resulting interactions when particles are in close enough proximity.

Chapter 4 focuses on the preparation of particulate gel systems via a cold-set route to gelation. The research presented in this section first uses heat to denature the protein, that later become cross-linked using ion bridging. The chapter starts by looking at controlling gelling kinetics through varying salt concentrations and the addition of oil as a filler matrix. Particulate systems were then formed by applying the cross-linking agent within a shear environment. Particle size and suspension properties were studied, looking at using gelling kinetics to explain observed behaviours.

Chapter 5, the second of the published chapters, presents the preparation of composite particles, showing their material response to increasing levels of oil entrapped. It discusses the balance between protein concentration and oil fraction undergoing the gel/shear process and its effect on entrapment efficiency. It continues

detailing particle morphology and size, showing the core-shell structure adopted during gelation. Finally, the chapter moves on to discuss the material response as a function of oil fraction. Further, a description into suspensions acting as a soft glass, with particles becoming locally frozen "in-cage" is proposed. This leads to yielding and thinning behaviours under shear.

The last of the results chapters investigates the *in vitro* digestion of the EmFG particles prepared in Chapter 5: under both gastric and intestinal conditions. Initial results show no release was facilitated from the particles. Hot-stage microscopy was used to monitor proteolysis of the WPI shell, showing rapid break down over the first 5 minutes of digestion, however droplets remained stable for the rest of the experiment. Interfacial properties were probed by changing the hydrophobicity of the dispersed phase. This led to emulsion failure under gastric conditions. As such a model for emulsion stability has been proposed. Lastly, mechanical testing was used to further probe changes in the gel microstructure, with suspension rheology changing as a function of substrate polarity.

The thesis then concludes by summarising the key findings within each chapter, describing the research as a whole and presenting recommended work to take the research further (Chapter 7). Lastly, an Appendix is then placed at the end (Chapter 8) containing supplementary data, not presented within the results pages. A list has then been collated, containing all the sources of information used within the preparation of the thesis (Chapter 9).

## 1.5. Publications and presentations

**First author:**

- Moakes, R. J. A., Sullo, A., & Norton, I. T. (2015). Preparation and characterisation of whey protein fluid gels: The effects of shear and thermal history. *Food Hydrocolloids, 45*(0), 227-235. (Chapter 3)

- Moakes, R. J. A., Sullo, A., & Norton, I. T. (2015). Preparation and rheological properties of whey protein emulsion fluid gels. *RSC Advances, 5*(75), 60786-60795. (Chapter 5)

**Second author:**

- Fernández Farrés, I., Moakes, R. J. A., & Norton, I. T. (2014). Designing biopolymer fluid gels: A microstructural approach. *Food Hydrocolloids, 42, Part 3*(0), 362-372.

**Conferences attended:**

- *UK-Ireland Food Business Innovation* Summit, Dublin 2013.
- *2nd UK Hydrocolloids Symposium,* Birmingham 2015.

**Oral presentations (speaker underlined):**

- Moakes, R. J. A., Sullo, A., Norton, I. T., Whey Protein Shear Gels: Structure and Function. *18th Gums and Stabilisers for the Food Industry*, Wrexham 2015.
- Moakes, R. J. A., Sullo, A., Norton, I. T., Rheological Properties of Novel Whey Protein Emulsion Fluid Gels, *7th International Symposium on Food Rheology and Structure*, Zurich 2015 **(Proceedings published, could not attend).**

- Moakes, R. J. A., Norton, I. T., Whey Protein Micro-Composties for Functional Delivery, *3rd International Food Structures, Digestions and Health Conference,* New Zealand 2015.

In each publication, where the author of this thesis (Richard J. A. Moakes) is the 1st author of the paper, the research has been: conceived, designed/undertaken and written by the author. The subsequent named authors are academic supervisors who have aided by proof reading, approving the manuscripts, and/or providing the facilities to carry out the research.

# Chapter 2. *Literature Review*

## 2.1. Whey protein

With the drive for increased sustainability and value-added products across all industries, the incorporation of "waste" streams into usable products is gaining interest. In 2015, globally over 285 million tons of milk were produced, with close to half the total originating from within the EU. Furthermore, over 150 million tonnes of whey was produced in 2005 following a gradual increase over the previous 10 years (Smithers, 2008). This results in a large amount of waste, as a consequential by-product to the cheese and yoghurt production processes. Previously discarded as fertilisers or into waste systems such as rivers or municipal services, whey presents an industrial problem (Smithers, 2008). Therefore, the incorporation of the proteins into new products is both economically and nutritiously advantageous, adding value to the waste stream as shown in Figure 2.1, and promoting green sustainability within the industry.

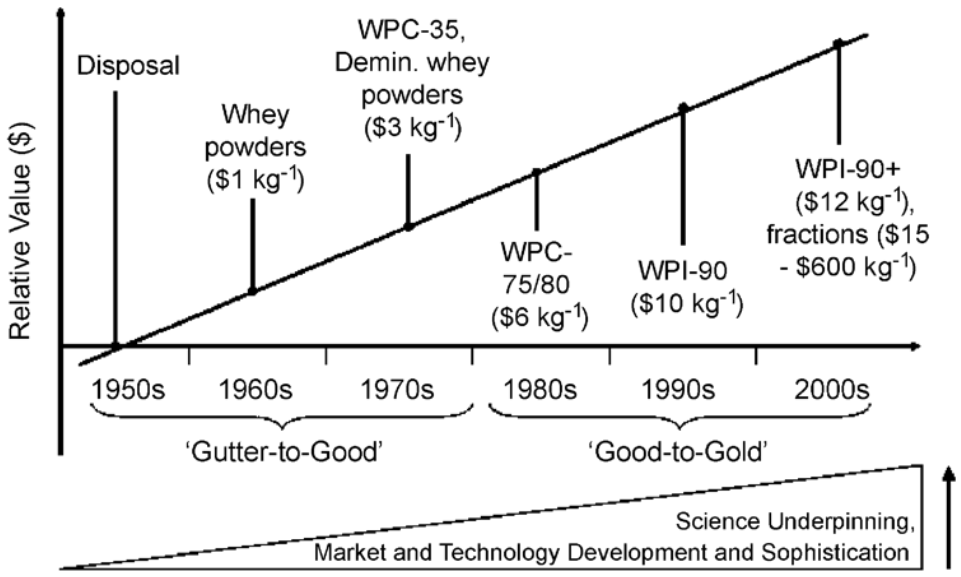


*Figure 2.1: Schematic taken from Smithers (2008) representing the increase in whey protein value as a function of scientific development between 1950 and 2000.*

### *2.1.1. WPI production*

As previously stated, whey is a by-product of the cheese making process. Historically, the production of cheese was used as a preservation method, using bacteria to ferment milk into a solid with a much longer shelf life. The composition of milk is dynamic, changing as a function of many variables: breed of cow, diet, season *etc.,* however, typically is formed of fat, lactose, minerals, water and protein (~32 g/L) (Haug et al., 2007). The conversion of lactose to lactic acid during fermentation reduces the pH, and caseins precipitate through the addition of rennet (enzyme). At this point the coagulated caseins (also known as curds) are separated from the whey (80% caseins, 20% whey) and further processed into cheese. This leaves a large quantity of whey, including salt whey, which due to its high salinity results in it becoming underutilised with high disposal costs (Kapoor and Metzger, 2004).

In recent years, interest surrounding whey from both an industrial and academic background has prompted numerous methods for both the isolation and concentration of the waste stream, forming whey protein concentrates (WPC) and isolates (WPI). For this review, separation methods have been split into academic and industrial techniques. Academic techniques are generally based on precipitation, where, typically due to their complexity, low cost efficiency and poor selectivity they are not implemented into large-scale production. Whereas, for higher throughput within industrial separation, whey proteins are typically isolated using filtration processes (Tovar et al., 2012).

#### *2.1.1.1. Lab-scale whey protein extraction*

Precipitation of the protein at a bench-scale predominantly relies on the aggregation of native proteins. Generally, this can be achieved through either manipulation of the solvent properties, pH and salt concentrations, which result in a change of the surface charges, or through heat denaturation and dewatering of the biopolymer. In many cases, especially within food applications the addition of salt or acids/bases are unfavourable. Additionally, denaturation of the protein at this stage can lead to loss of bioavailability, which again is unfavourable within the final product (Cheang and Zydney, 2003). Coacervation/complexation of proteins to a carrier polymer has also been shown as an extraction technique. However also present draw backs, as the multi-step procedures result in poor yields. Thus, chromatography techniques including high performance liquid (HPLC), size exclusion (SEC) and gel permeation (GPC) gain more use in isolating the proteins (Tovar et al., 2012, Morr and Ha, 1993). Although the isolation of pure proteins is achieved, the techniques are slow, providing small quantities over reasonable timeframes. A higher yielding method to concentrate the protein via a foaming technique (Shea et al., 2009), whereby proteins are separated by adsorption to the water/air interface, becoming removed and dried to leave powders, is again a promising technique to use, as there are no use of chemicals. Additionally, proteins remain stable increasing their bioavailability thereafter. In the same way, freeze drying also presents itself as a clean candidate for the retrieval of the proteins, however both methods present issues when scaling-up, with low cost effectiveness.

#### *2.1.1.2. Industrial-scale whey protein extraction*

In practice, at a commercial scale, WPCs and WPIs as products are typically derived using membrane separation processes. These include: ultrafiltration, reverse osmosis and diafiltration, resulting in concentrations ranging from 30 to ca. 80 %. To reach higher concentrations, in the case of whey protein isolates, gel filtration and ionic selection processes such as ion-exchange chromatography are employed (Tovar et al., 2012, Etzel, 2004). In each case proteins traverse across a barrier (membrane) via an applied driving force, either concentration gradient or charge density. This can therefore be applied as a continuous process, resulting in high throughputs and pure samples. In addition, systems do not have to undergo changes in acidity or become exposed to high temperatures, allowing the protein to retain much of their native structures.

### *2.1.2. Whey protein composition and structure*

Naturally, whey contains the macronutrients needed for healthy growth during the infantile stages, thus contains many different fractions including: β-lactoglobulin (β-Lg), α-lactalbumin (α-Lac), bovine serum albumin (BSA), lactoferrin and numerous immunoglobulins (fraction concentrations have been presented in Table 2.1). As seen from Table 2.1 the two major proteins, β-Lg and α-Lac, contribute to ~80 % of whey, of which *ca.* 70 % is lactoglobulin and 30 % lactalbumin. It is for this reason that many of the mechanisms and material properties for systems incorporating whey proteins, are modelled upon the dominant

*Table 2.1: Whey protein fractions and basic primary structure properties (Etzel, 2004, Madureira et al., 2007)*

| Protein | Concentration ($gL^{-1}$) | Molecular weight (kDa) | Number of amino acid residues |
|---|---|---|---|
| β-Lactoglobulin | 3.2 | 18,277 | 162 |
| α-Lactalbumin | 1.2 | 14,175 | 123 |
| Bovine Serum Albumin | 0.4 | 66,267 | 582 |
| Immunoglobulins | 0.7 | 25,000 - 70,000 | - |
| Lactoferrin | 0.1 | 80,000 | 700 |

protein, β-Lg. Therefore, this review focuses primarily on the structure of β-Lg.

#### *2.1.2.1. β-Lactoglobulin and α-lactalbumin structures*

In nature proteins are found within organisms acting across a wide range of biological roles. Some of their functions closely linked to health and nutrition are: repair/maintenance, hormones to regulate homeostasis, enzymes, within the immune system, nutrient transport and as an energy supply. The macronutrient functionality is dictated by the structure of the polymer chain. Proteins, also known as polypeptides, are complex polymer chains, however, unlike typical polymers they do not consist of regularly repeating units. Instead, the polymer backbone is generated from a combination of twenty-one small organic compounds known as amino acids. Macrostructure thus becomes a function of the residue combinations, number density and addition of prosthetic groups (non-amino compounds *e.g.* lipids, sugars, mineral *etc.*) conjugated within the peptide, to give the protein sub-structures: primary, secondary, tertiary and quaternary (Nelson et al., 2008).

The primary structure, as previously alluded to, relates to the amino residue sequence along the polymer backbone. Amino acid sequencing and spacing results in the formation of localised sub-structures commonly referred to as the protein secondary structure. The secondary sub-units amass shape in the form of helices and sheets (as seen in Figure 2.2). The morphologies of such structures are dependent on a combination of the translational movements within the covalent linkages across the backbone, and number of hydrogen bonding donor/acceptor groups; leading to helical arrangements to provide the lowest conformational energies (Pauling et al., 1951, Donohue, 1953). In a similar way, β-sheets are formed through lateral bonding of the peptide chains, with the backbone aligning in parallel, anti-parallel or mixed arrangements.

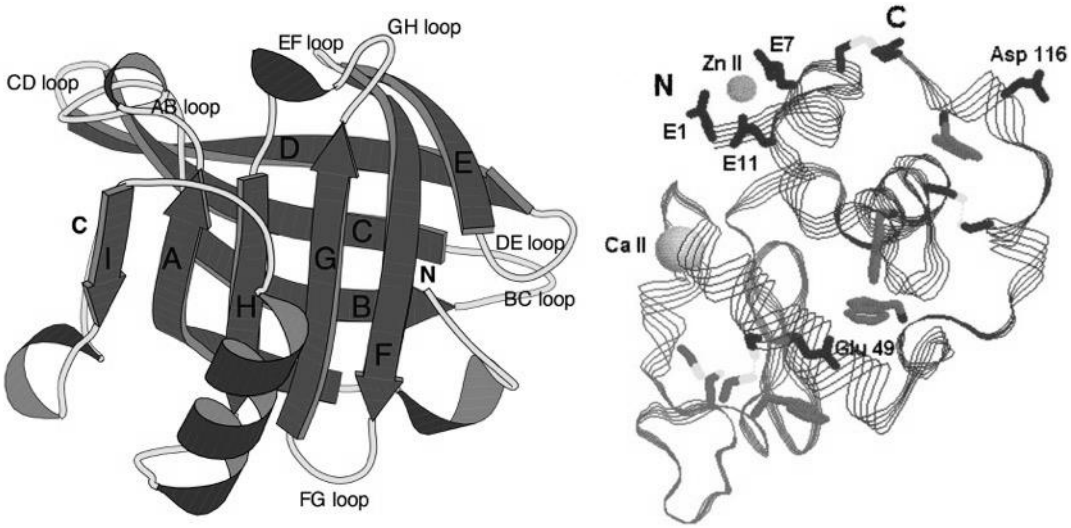


*Figure 2.2: Ribbon diagrams showing the 3-dimentional conformation for: (left) β-lactoglobulin (Brownlow et al., 1997), and (right) α-lactalbumin (Permyakov and Berliner, 2000).*

Once two or more sub-structures are present, their arrangement in space is called the tertiary structure. The tertiary structures for both β-Lg and α-Lac have been shown in Figure 2.2 *left* and *right* respectively. The biological importance of α-Lac within the synthesis of lactose has long been known (Brew et al., 1968). Although the folding dynamics within the α-Lac structure are a little unusual (Bu et al., 2001), the helical motifs facilitate domains for ion binding, for use both catalytically and within nutrient transport, as well as providing resistance to denaturation (Permyakov and Berliner, 2000). On the other hand, the primary role of β-Lg has been largely debated, with its use remaining unclear. However, the many β-sheet motifs found within its core structure, similar in nature to lipocalycins and retinol-binding proteins, have led to suggest its application within fatty acid transportation within digestion (Pérez and Calvo, 1995, Brownlow et al., 1997). More recently studies have also suggested their role within immuno and metabolic regulation (Madureira et al., 2007).

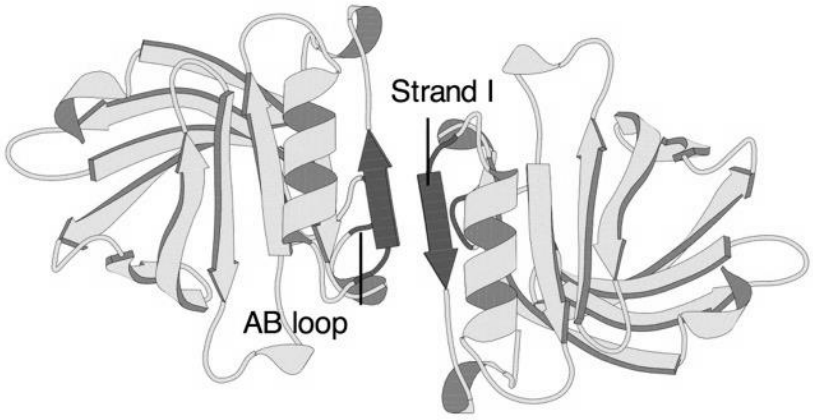


*Figure 2.3: Ribbon diagrams depicting dimeric association of β-Lg structures at a pH close to the isoelectric point (~pH 4.6-5.0) (Brownlow et al., 1997).*

The arrangement of the sub-units within the secondary structure, allows β-Lg to crystallise into multiple lattices, including several pH dependant conformational states. This affects the quaternary structure of the protein, adopting a dimeric form within environments around the isoelectric point (shown in Figure 2.3) through hydrogen association along strand I, and a monomeric form at acidities both above and below. The change in quaternary conformation has a direct effect on the nature and the accessibility of the buried sites, generally referred to as non-polar or lipophilic regions. In turn, this affects the morphology of the resulting protein, with larger proteins generally adopting a globular structure, burying the non-polar residues and/or β-sheets (generally recognised as lipophilic structures) within the centre of the macrostructure (Chothia, 1976).

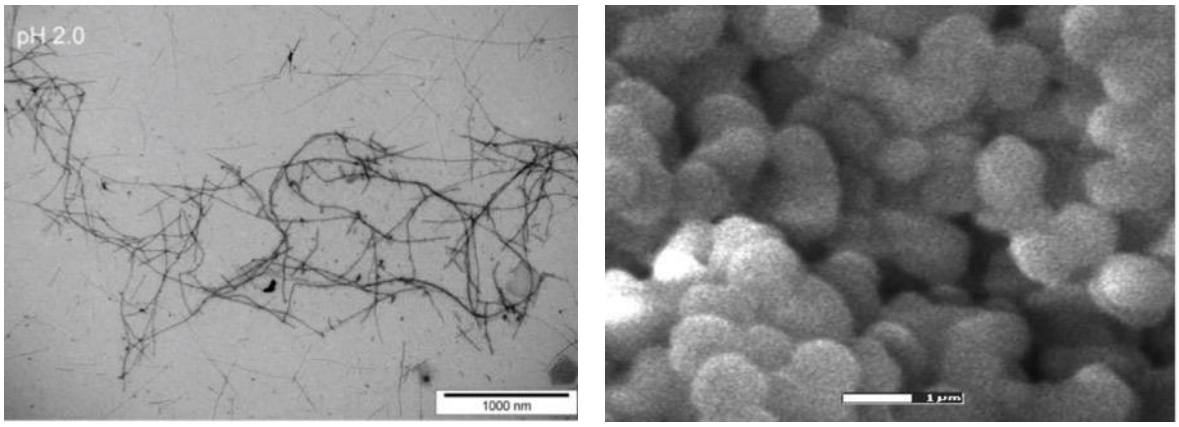


*Figure 2.4: Electron micrographs of (left) WPI fibrils prepared via heat treatment at pH 2.0 (Loveday et al., 2010), and (right) globular WPI microstructure formed using heat denaturation at pH 5.0 (Bromley et al., 2006).*

The change in quaternary structure can be seen for β-Lg, with thermal denaturation leading to hydrophobic aggregation into spherical globules at native pH

(Figure 2.4 (*right*)) (Bromley et al., 2006). pH modulated dissociation of the dimeric structure into monomeric units, thus results in strand-like association (Loveday et al., 2010, Loveday et al., 2012), forming rigid or flexible fibrils at low or high pH respectively (Figure 2.4 (*left*)). Here the aggregation is based on a "trimming" mechanism proposed for hen egg fibrils (Mishra et al., 2007), where the resultant singular peptide units are able to open during denaturation, and stack (Loveday et al., 2012).

### *2.1.3. Uses of whey protein*

The drive towards functional foods is ever demanding, with the increasing pace of life and need for quick and accessible consumable products. In a review article focused on functional foods for their inherent nutritional properties (Norton et al., 2015), it was highlighted that high protein foods are advantageous not only for their ability to structure products, but for their multi-applicable biological attributes: increased satiety effects, growth and tissue repair, essential amino acids and supplemented amino acids. The incorporation of such macronutrients, in particular whey proteins, into products needs careful thought in regard to both their nutritional value and resulting material structure, factoring in textural/sensory characteristics into the end product.

Alongside its various biological properties as a macronutrient, whey also plays a vital role within food structures for water binding, viscosity modification, emulsification and as a bulking agent *etc*. Owing to their diversity, whey proteins provide preferred alternatives to synthetic additives, or biopolymers with little calorific value; just 4 kcal g-

$^{1}$ as opposed to 9 kcal $g^{-1}$ in fats. As such, they have found applications spread across a wide field, shown in Table 2.2.

*Table 2.2: Table highlighting some of the uses of whey proteins across food research.*

| **Application** | ***Example*** | **Reference** |
|---|---|---|
| Food additives | In yoghurt | *Onsekizoglu and Gunasekaran (2016)*<br>*Buldo et al. (2016)*<br>*Picot and Lacroix (2004)* |
| | In meats | *El-Magoli et al. (1996)*<br>*Peña-Ramos and Xiong (2003)*<br>*Andrés et al. (2008)* |
| | In beverages | *Singh et al. (2015)*<br>*Sinha et al. (2007)*<br>*Schmitt et al. (2011)* |
| Particulate suspensions | Microgels | *Dissanayake et al. (2010)*<br>*Singer et al. (1988)* |
| | High density gels | *Sağlam et al. (2011)*<br>*Dickinson (2016)* |
| Stabilisation | Foaming | *Foegeding et al. (2006)*<br>*Lazidis et al. (2016)* |
| Emulsification | Functionality | *Murray and Ettelaie (2004)*<br>*Dickinson (2001)*<br>*Gunasekaran et al. (2007)* |
| Delivery medium | Gel encapsulant | *Liang et al. (2010)*<br>*López-Rubio and Lagaron (2012)* |
| | *Complexes structures* | *Livney (2010)*<br>*Ron et al. (2010)*<br>*Zimet and Livney (2009)* |
| Hydrolysates | Nutraceuticals | *Brandelli et al. (2015)*<br>*Corrêa et al. (2014)*<br>*Ha and Zemel (2003)*<br>*McIntosh et al. (1998)*<br>*Madureira et al. (2007)* |

#### *2.1.3.1. Whey protein in food structures*

Foods undergo many processing stages both in production, and once bought by the consumer. Typically, within meat products much of the original structure can be lost during thermal processing (cooking), through loss of both fat and water components. One way to prevent this loss is through the incorporation of additives, which reinforce the product during thermal treatment. The use of whey as modifier both structurally and texturally aimed to control these sensory attributes (El-Magoli et al., 1996). Incorporation of WPC's into cooked meat products managed to retain much of the original structure post thermal processing. This was achieved through a reduction in product shrinkage, where the protein forms a network or scaffold throughout the fibrous meat matrix. The work, even though promising for retaining structure in the form of volume, neglected to probe the toughness of the food, as in many cases, gelled proteins have resulted in "rubbery" sensations (Norton et al., 2015). Later studies by Andrés et al. (2008) however, found that although the protein played an important role in the reduction of shrinkage, it had negligible effect on system elasticity, contrary to concerns highlighted regarding sensory.

Biologically proteins are important, with their functionality dictated through their inherent structures. Secondary and subsequent tertiary structures provide proteins with the intrinsic properties required for the stabilisation of phase-separated systems; where both hydrophilic and hydrophobic regions exposed during partial denaturation, allow adsorption to an interface, lowering the interfacial tension between the phases (Dickinson, 2001, Damodaran, 2005). As such, proteins are extensively used in the stabilisation of emulsions and aerated systems, spanning from alcoholic beverages to solid food foams. Typically egg white proteins have been incorporated into systems,

stabilising air cells in cake batters and meringues amongst many others. However, more recently dairy proteins have received much attention. Historically, tailoring of the interfacial elasticity has been achieved by controlling the conformation and interactions of proteins and particles via the addition of salts or changes in pH *etc.* (Damodaran, 2005, Murray, 2007, Murray and Ettelaie, 2004). However, newer research incorporating whey protein micro-particles, stabilised foams using a mechanistic approach that bound the continuous phase through increasing lamella viscosity. The result of which slowed drainage, directly correlating to increased half-lives (Lazidis et al., 2016).

The formation of whey protein micro particles within fat replacement is also gaining attention. The formation of dense protein gel particulates not only provide suspensions with controlled material response needed to build structure within foods (Sağlam et al., 2011, Sağlam et al., 2012), but also results in "hard" particles shown to lower the friction coefficients between surfaces, previously interpreted to give the "oily" perception needed for fat mimetics (Garrec, 2013). Similarly, micro-sized gel particles have been commercially presented as *Simplesse*®. Again, their small spherical morphology providing the organoleptic properties needed within creamers and fat replacers (Singer et al., 1988). Although intrinsic suspension properties such as size, particle shape, and elastic behaviour between droplets have been mimicked, the taste in comparison to the original full fat product is still lacking. This impacts the overall consumer perception of the product, inherently producing a boundary towards uptake into everyday products. Therefore, incorporating a small amount fat into the hydrocolloid based mimetics has demonstrated a potential delivery system for the

"fatty" flavour the palette is accustomed to, whilst retaining a high degree of lipid reduction (Hamilton and Norton, 2016).

Similar oil in multi-phase water systems ($O/W_1/W_2$) use supramolecular chemistry to electrostatically bond proteins and biopolymer, internally trapping emulsion droplets within a water based micro-composite (Chung et al., 2013, Matalanis and McClements, 2013, Zhang et al., 2015). Again, this showed a promising step towards fat reduction (Chung et al., 2013). Even so, protein-polysaccharide complexes have gained greater interest as edible Pickering particles, for the stabilisation of emulsions (Guzey and McClements, 2006). Pickering stabilisation works on a mechanism where solid, hard particles sit on interface between the two immiscible fluids (Dickinson, 2010, Yang et al., 2017). The relatively large contact zone arising between particle and fluid results in the large energy requirement for adsorption onto the interface. Thus, once the energy is removed the particle becomes restricted to the interface needing a significant activation energy to remove it again. As such, true Pickering stabilised droplets are very stable by sterically preventing coalescence (Vignati et al., 2003, Neirynck et al., 2004, Benichou et al., 2007). Although promising, the nature of electrostatic binding restricts the use of such systems to very narrow pH and ionic environments, where both polymers have significantly opposite zeta potentials. As such conjugates, a similar concept to complexes, where the biopolymers have been chemically bonded - typically via heating (Maillard reaction or dry heating (Akhtar and Dickinson, 2003, Zhu et al., 2008)), are resistant to changes in pH. Again, the particulates increase droplet stability with the added benefit that the thicker interfacial barrier proposes a control mechanism for nutraceutical delivery (Benichou et al., 2007). Thus, a multiphase delivery system is presented, whereby active compounds can be delivered within: the hydrophobic core

(Benichou et al., 2007), by direct complexation with polymers (Zimet and Livney, 2009, Livney, 2010, Kurukji et al., 2016), or a combination of the two.

As previously shown, whey proteins are versatile within foods with their various structures: gels, microgels, complexes/conjugates, Pickering particles, and emulsifiers. Their numerous applications therefore typically guide such systems towards functional delivery, as encapsulants and protectors (McClements, 2015). For example, the entrapment of actives with complexes significantly reduces the degradation of unstable molecules, whilst retaining optical transparency as a function of the nano-scale particulates (Ron et al., 2010). This makes them ideal for nutrient fortification within beverages. Furthermore, delivery of vital minerals within solid/semi-solid products is achieved through the inclusion of gelling salts into gel matrices (Remondetto et al., 2004, Onsekizoglu and Gunasekaran, 2016). The microstructure (globular or filamentous) at this point plays a decisive role in regards to nutrient release; as release/gel breakdown can be directly correlated to the degree of hydrogel swelling (Gunasekaran et al., 2007, Gunasekaran et al., 2006).

#### *2.1.3.2 Whey protein uses in nutraceuticals and delivery*

The use of whey to transport nutrients and actives is commonly shown (Livney, 2010, McClements, 2015, Onsekizoglu and Gunasekaran, 2016, Picot and Lacroix, 2004, Ron et al., 2010, Zimet and Livney, 2009); however, application of the proteins themselves as the bioactives is often overlooked. Protein hydrolysates, short chained peptides, are commonly used within sports nutrition as their small nature allows for rapid uptake by the body (Manninen, 2004). Such amino acid sequences are present in

everyday products, remaining buried within the parent protein sequence until enzymatically cleaved and released upon digestion (Korhonen and Pihlanto, 2003).

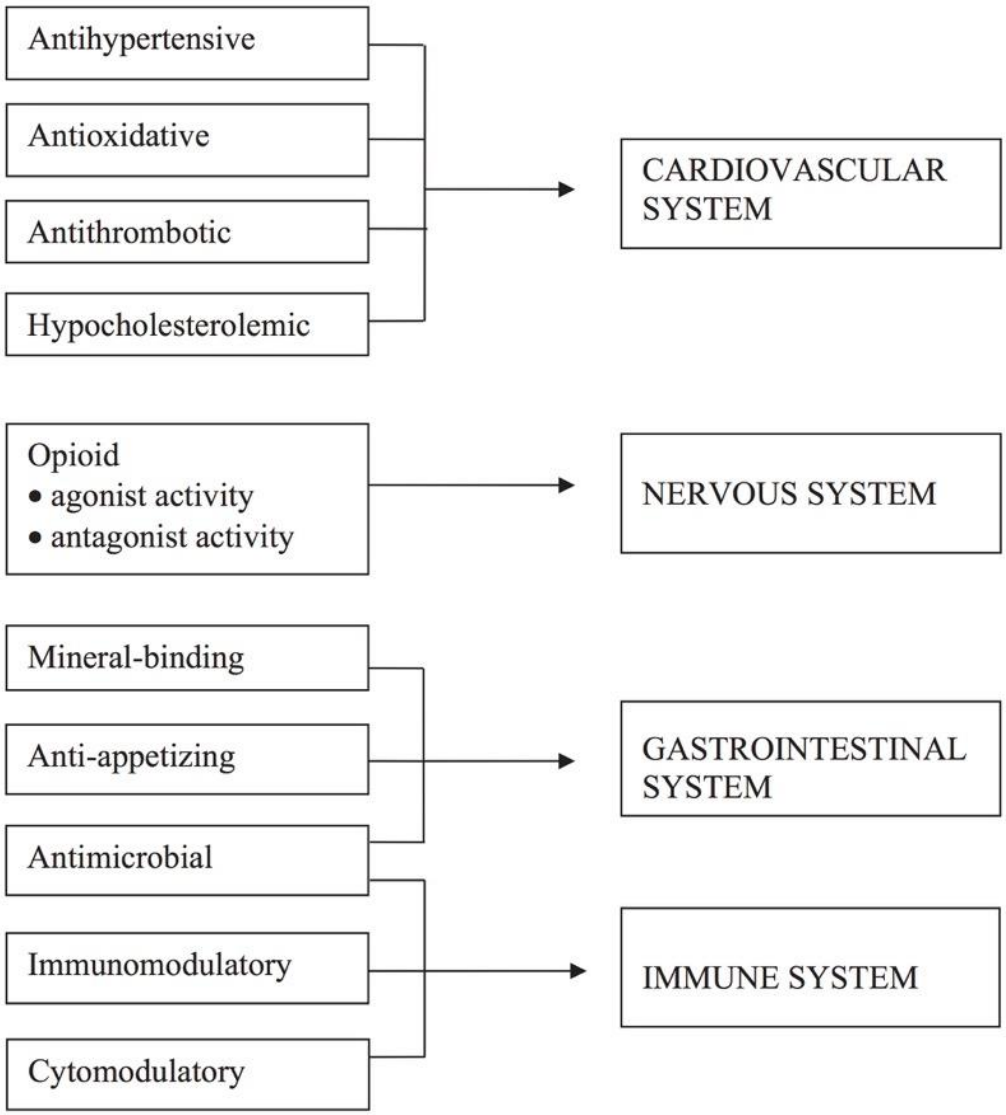


*Figure 2.5: Milk-derived (whey protein and casein) hydrolysate functionality taken from Korhonen and Pihlanto (2006)*

The physiological role of these peptides has become increasing acknowledged over the years, clinically shown to affect the major bodily systems: nervous, immune,

cardiovascular and digestive systems (Figure 2.5) (Korhonen and Pihlanto, 2006). Hydrolysis of the major whey proteins yields certain biologically active sequences related to opioid activity (pain relief), ACE-inhibitory commonly used in the reduction of hypertension (Pihlanto-Leppälä, 2000) and dietary regulation (Luhovyy et al., 2007, Ricci-Cabello et al., 2012). Unfortunately, many of the required concentrations to produce foods with the desired efficacy for enhanced health claims, lead to bitter in mouth experiences (Liu et al., 2014), tarnishing the final product. Therefore, careful consideration in regards to product formulation is needed. Engineering carrier systems to mask hydrolysate taste in therefore required, in order to enhance palatability.

## 2.2. Material systems – structure/function relationships

The previous section highlighted the use of whey within both food and delivery systems. However, the way such systems react to external factors including storage, cooking and digestion is yet to be explored. The structure-function relationship has long been known, with material properties *e.g.* stability (including shelf-life), textural, and breakdown pathways *etc*., remaining closely controlled by the products structure/microstructure. This section therefore aims to review the literature regarding the formation of such systems, showing the link between microstructure and material properties for the main systems explored in this thesis: emulsions, and microgels.

### *2.2.1. Emulsion technologies*

Many modern-day food systems have focused on using fats, in the form of emulsions to build structure. Typically defined as, “a colloidal dispersion of two or more

immiscible fluids," emulsions are generally categorised into two main systems: oil in water (O/W) *e.g.* milk, and water in oil (W/O) *e.g.* spreads. These mixtures however pose many challenges for food scientists, as they are inherently unstable systems. It is therefore important to fully understand such dispersions, to manipulate them towards desired material responses.

#### *2.2.1.1. Emulsion formation and theory*

Emulsions are relatively simple systems to prepare, for instance one can add oil to water and with mechanical disruption, shaking/stirring, form droplets. However, maintaining the emulsion over time can be reasonably complex. This is due to emulsion formation being a kinetically, as opposed to a thermodynamically driven process. The laws of thermodynamics state that a system will always tend to its lowest energy state. Thus, for a system of two immiscible fluids, this will be discreet layers with the smallest possible interface. Therefore, to form droplets, their formation process must occur on a shorter time-scale in comparison to relapsing back to its two separated layers. Kinetics in such systems can therefore be dictated by a number of factors, including but not limiting to: fluid interfacial tension, density, viscosity and droplet size/distribution (Binks, 1998). The effects of the last three are shown using the Stokes' law (Equation 2.1):

$$v_s = \frac{2r^2(\rho_c - \rho_d)g}{9\eta_c}$$

*Equation 2.1: Stokes' equation describing the velocity of separation ($v_s$) as a function of the droplet radius (r), density of the continuous ($\rho_c$) and dispersed phases ($\rho_d$), viscosity of the continuous phase ($\eta_c$) and gravity (g).*

From the Stokes' equation it is possible to see the impact of flow/drag, physically preventing the droplets from coming into close proximity, once dispersed. Typically, longer emulsion stability can be sought by: increasing the viscosity of the continuous medium – reducing the diffusivity of the droplets, reducing droplet size, or, by more closely matching the two fluid densities. Alternatively, chemical modification to the fluid-fluid interface can be employed as a means to enhanced stability. In these cases, a reduction between the interfacial tension of the components is required. This is achieved by either by reducing the difference in fluid hydrophilic/hydrophobic ratio, or more commonly through the addition of an emulsifier/surfactant, the energetics of the system can be lowered prolonging emulsion stability (Walstra, 1993).

"Instability" within emulsion science is commonly used interchangeably for both the migration of droplets from a homogeneous dispersion to highly concentrated domains, and recombining of droplets into two separated layers. Here the two have been separated, with the former describing a reversible system of creamed, sedimented or flocculated droplets that remain discreet, whereas the latter inferring complete separation, Figure 2.6. In the second case, two resolved layers are generally promoted through Ostwald ripening and/or coalescence of the individual particles. In brief, the mechanisms that drive the two separation phenomena are as follows. Ostwald ripening or coarsening, occurs when the dispersed phase contains a distribution of particle sizes. Due to the unfavourable energetics of small droplets, arising from a large surface area to volume ratio with high Laplace pressures, droplets dissolve, subsequently diffusing into their larger more energetically neighbours (Voorhees, 1985). On the other hand, coalescence is driven by droplets coming into close contact. When this occurs the volume of continuous phase separating the droplets is significantly reduced, forming a

thin film. As droplets are forced into closer and closer proximity film thinning occurs, eventually resulting in film rupture. At this point the dispersed phases come into direct contact, merging to form one, larger entity (Kabalnov, 2007). It is important to differentiate between the two subsets when describing both food and delivery systems as dispersion of a creamed system, for example is easily achieved, whereas phase separation leads to negative changes in structural, textural, perceived and delivery attributes.

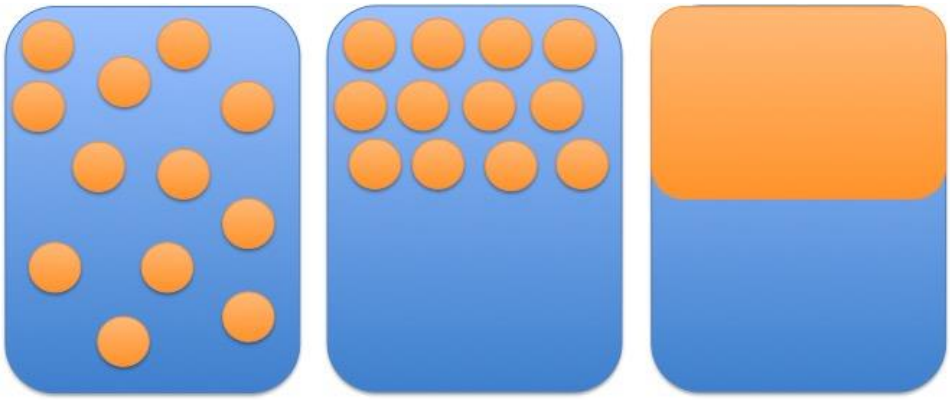

*Figure 2.6: Schematic representation of: (left) homogeneously dispersed emulsion, (middle) creamed emulsion, and (right) phase separated systems.*

#### *2.2.1.2. Controlling droplet size*

Emulsion droplet size is controlled as a function of two competing kinetic mechanisms: droplet break-up and re-coalescence. Therefore, where re-coalescence occurs on a shorter time-scale than mechanical disruption, the resulting droplets remain large, and vice versa for longer re-coalescence rates. Typically, droplet breakdown is increased through a larger degree of mechanical shear, focusing on top-down development of droplets. Commonly, emulsions have been formed using high shear

processes such as high-pressure homogenisation. However more recently, newer technologies such as sonication are being employed in order to increase droplet homogeneity, and lower energy consumption (O'Sullivan and Norton, 2016).

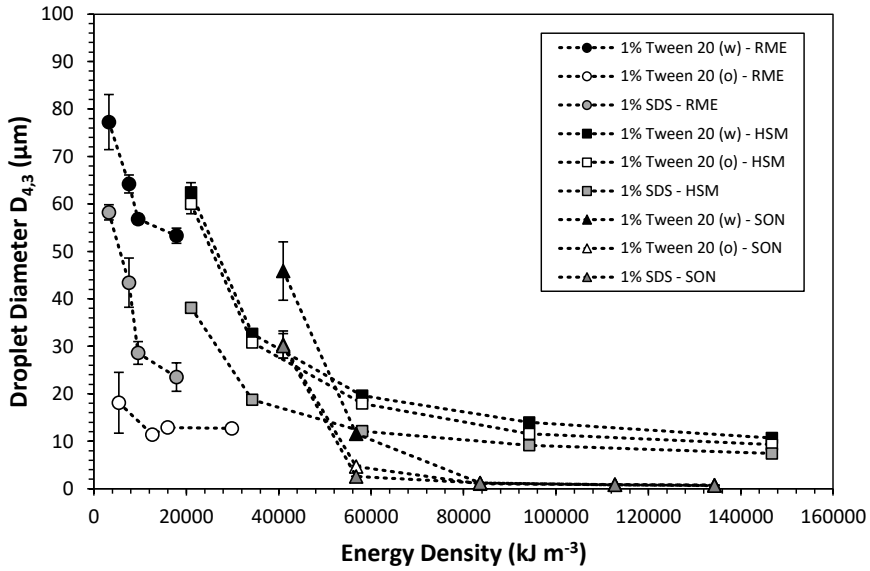


*Figure 2.7: Resulting emulsion droplet size as a function of energy input for various fabrication methods: Rotating membrane (RME), High shear mixer (HSM), and Sonication (SON). Graph taken from Lloyd (2016).*

In terms of energetics, droplet size reduction can be described as a decay (Lloyd, 2016), reaching a minimum size irrespective of processing (see Figure 2.7). In these cases, energy transfer to the dispersed phase becomes limited, resulting in low efficiencies, as the energy becomes increasingly lost to the surroundings (as heat, noise, eddies etc). In response, a bottom-up approach, whereby emulsion droplets are grown through a membrane can been employed. This technique facilitates increased control over the microstructure by manipulating the membrane pore size, material, detachment

speed and flux, again leading to increasing droplet homogeneity whilst reducing energy consumption (Lloyd, 2016).

In reality, both emulsion stability and to an extent droplet size, are generally controlled through the use of emulsifiers or surfactants. Emulsifiers are molecules that sit on an interface, lowering the tension between the two species. Such molecules are amphipathic, consisting of a hydrophilic head and aliphatic tail, allowing it to reside in both phases. In addition to lowering the system tension, emulsifiers provide a barrier between droplets, sterically hindering coalescence (Walstra, 1993).

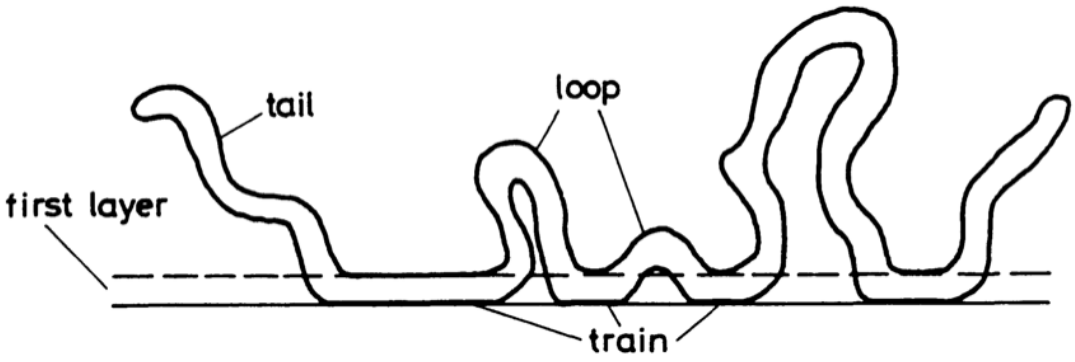


*Figure 2.8: Schematic diagram of an adsorbed polymer exhibiting tail, loop and train conformations. Image taken from Stuart (1991).*

Proteins provide ideal structures, due to changes in hydrophobicity/hydrophilicity along their polymer backbones. Initially, proteins in an aqueous environment adopt an energetically favourable confirmation, *i.e.* the hydrophobic regions are typically encompassed within the core, with the hydrophilic segments on the outer surface. On reaching an oil interface the shifting protein dynamics cause unravelling of the structure, allowing the protein to adsorb to the interface (Sethuraman et al., 2004). This results in varying adsorption patterns dependent on the

protein backbone. Such conformations are described as the tail, loops and train models (shown in Figure 2.8) (Stuart, 1991, Horne and Leaver, 1995). These mechanisms of stabilisation (reduction in interfacial tension and steric effects) evidently lead to an overall reduction in droplet size, as re-coalescence becomes prevented during fabrication. Droplet size is thus a function of the emulsifier mass transport from the surrounding continuous phase to the interface, (Lloyd, 2016, Walstra, 1993, Dickinson, 1998, Lee and Norton, 2013).

### *2.2.2. Emulsion rheology*

Many of the emulsion intrinsic characteristics including size, volume fraction, emulsifier and chemical properties, are what primarily govern its functionality and use. Many food systems are complex with multiple components that all interact, resulting in a final product with well-defined perceptual attributes. Even so, a simple oil in water model shows many of these complexities, where a combination of the continuous phase, nature of the droplets and droplet-droplet interactions results in a multitude of different material and delivery properties (Barnes, 1994).

In many cases where emulsions have been used within food structuring, the focus is placed upon its non-linear rheology - viscosity and flow behaviour. As such, emulsion rheology has been well documented (Barnes, 1994, Derkach, 2009, Stokes et al., 2013). For the purpose of this review a simple oil in water system is regarded, in order to better understand behaviour as a function of the dispersed phase microstructure.

#### *2.2.2.1. Effects of phase volume*

Primarily, emulsion rheology is governed by the total volume occupied by the dispersed phase (Pal and Rhodes, 1989, Tadros, 1994). The effect of volume fraction ($\phi$) on viscosity can be sub-divided into three main areas: infinitely diluted systems, concentrated systems and a meso-stage in-between. Typically, infinitely dilute systems, where $\phi < 0.01$, can be modelled using the Einstein equation (Equation 2.2).

$$\eta_r = \frac{\eta}{\eta_s} = 1 + a\phi$$

*Equation 2.2: Einstein equation showing relative viscosity ($\eta_r$) (the ratio of the overall viscosity ($\eta$) to the viscosity of the solvent ($\eta_s$)) for infinitely dilute dispersions, $\phi < 0.01$, where Einstein's coefficient, "a", is a constant (2.5 for spheres).*

Here the ratio between overall viscosity ($\eta$) and the viscosity of the solvent ($\eta_s$) (also known as the relative viscosity ($\eta_r$)) is shown as a function of the volume fraction ($\phi$) and the Einstein coefficient ($a$). In these cases, $\phi$ has little effect on flow behaviour resulting in Newtonian flow, where relative viscosity changes are linearly proportional to the ratio of dispersed to continuous phase. The meso-stage, up to $\phi < 0.64$ initially retains a Newtonian behaviour, becoming increasingly pseudo-plastic as systems become more highly packed (see Figure 2.9 *(Left)*). As such, increasing the dispersed phase results in non-linear changes in viscosity. Thus, finite systems can no longer be simply modelled using the Einstein equation, needing multiple components to better predict viscosity (Equation 2.3) (Schuster, 1996).

$$\eta_r = 1 + a\phi + b\phi^2 + c\phi^3 + \ ....$$

*Equation 2.3: Extended Einstein equation compensating for finite changes in dispersed phase, where a, b, c etc. are constants.*

Highly concentrated emulsions ($\phi$ > 0.64, for randomly close packed monodisperse spheres) exhibit apparent yielding and strong shear thinning behaviours, characteristic of plastic systems. Such properties arise through the close packing of droplets, sterically confining movement, resulting in "flocculated-like" systems that become broken down within the shear flow. Within this regime viscosity becomes a function of the droplet packing, generally expressed as the ratio between maximum packing fraction ($\phi_{max}$) and volume occupied by the dispersed phase (see Equation 2.4).

$$\eta_r = \eta_c \left(1 - \frac{\phi}{\phi_{max}}\right)^{-[\eta]\phi_{max}}$$

*Equation 2.4: Krieger-Dougherty model for hard sphere suspensions.*

Where $\eta_r$ is the relative viscosity, $\eta_c$ is the viscosity of the continuous phase, [$\eta$] is the intrinsic viscosity, $\phi$ is the volume fraction taken up by the spheres and $\phi_{max}$ is the maximum packing fraction.

#### *2.2.2.2. Effects of droplet size*

The effect of droplet size on bulk rheology has seen some contention within the literature. In principle a reduction in droplet size should not initially change the system viscosity (Barnes, 1994). However, experimental data presented by Pal (1996) showed

significant differences in viscosity for both course and fine emulsions. Such observations are better argued as an artefact to the change in size distribution, and not actual droplet size itself. This generally results in better packing, which translated into terms of viscosity, becomes less viscous (Barnes, 1994). However, reducing particle size to a sub-micron scale results in a dispersed phase that is more susceptible to fluctuations in Brownian motion and osmotic pressures, forming hydrodynamic interactions between suspended particles (Brady, 1993). At this point, colloidal effects are much more prominent, forming systems that increasingly resist flow as droplet size is reduced. Therefore, flow behaviour gives the illusion of increasing viscosity, situated within the higher end of the shear thinning region; as actually flow profiles are being shifted to higher shear rates, whilst retaining constant limiting viscosities (max and min), Figure 2.9 *(Right*) (Barnes, 1994).

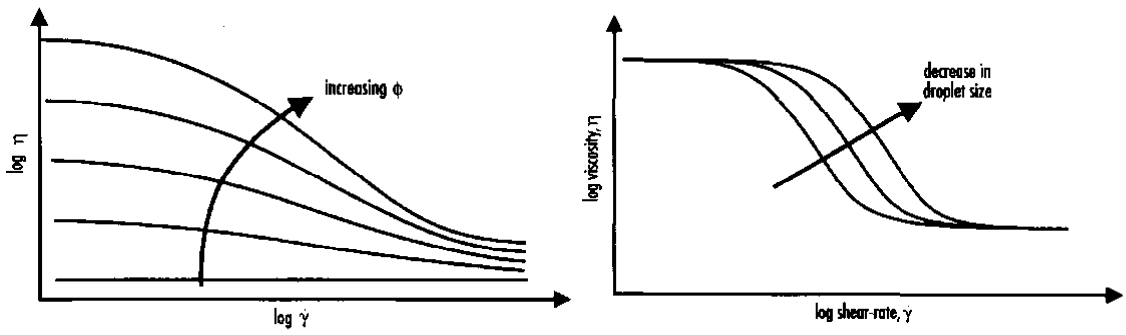


*Figure 2.9: (Left) Typical viscosity (η) vs shear rate (γ̇ ) plot for emulsion systems with increasing droplet volume fraction (ϕ). (Right) Effect of droplet size on emulsion viscosity. Taken from Barnes (1994).*

### *2.2.2.3. Emulsion viscoelasticity*

Linear properties (frequency dependent moduli (G'/G'')) typically indicate the magnitude of elastic (G') components, with the ability to store energy, and viscous (G'') components, which transfer energy to the surroundings. It is fair to assume that all dispersed systems display a degree of viscoelasticity, due to interactions between their various components (Barnes, 2000). As such, increasing the amount of dispersed phase will result in an increase in elasticity, similarly to that already shown for non-linear behaviours (Barnes, 1994). Again, emulsions with a low oil content are primarily viscously dominated, with viscoelastic properties controlled primarily by the continuous phase. Increasing the oil fraction results in dispersions with a greater elastic component, until a cross over point is observed ($\phi_c$) (Figure 2.10).

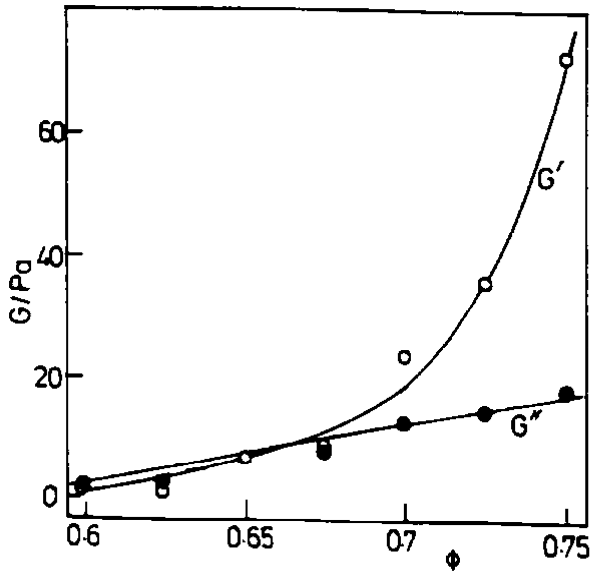


*Figure 2.10: G'/G'' as a function of dispersed phase for simple oil in water emulsions. Taken from Tadros (1994).*

At this point, manifestation of a predominantly elastic network arises through the overlapping of adsorbed interfacial layers; as steric confinement forces droplets into contact with each other (Tadros, 1994). Subsequently, systems present a pseudo-solid behaviour that becomes increasingly more solid-like at higher packing fractions (Figure 2.11) (Mason et al., 1995, Mason et al., 1996).

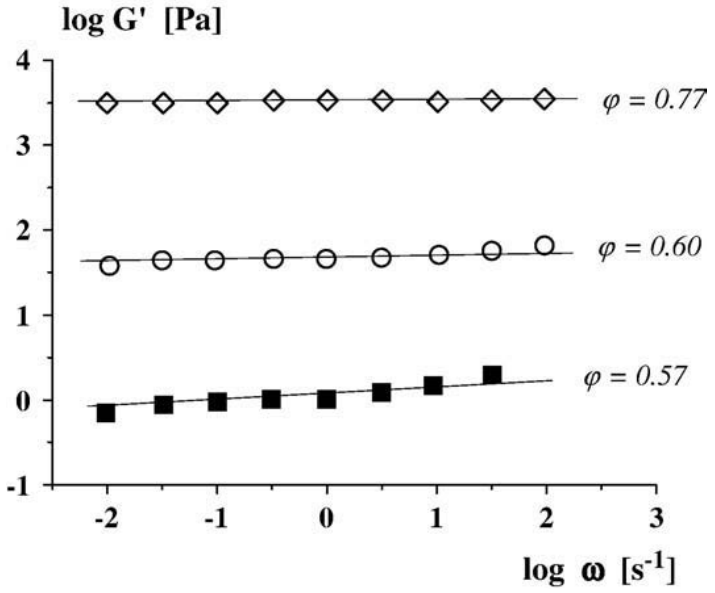


*Figure 2.11: Frequency dependent depiction of a typical O/W emulsion as a function of dispersed phase volume. Taken from Mason et al. (1997) in Derkach (2009).*

The effect of droplet size will invariably play a role in the viscoelastic response, as a function of interacting surface area once $\phi_c$ has been reached (Malkin et al., 2004); provided sufficient emulsifier is present to cover any change in effective surface area (Pal, 1996, Pal and Rhodes, 1989, Tadros, 1994). Therefore, choice of interacting species (polymer/molecule) at the interface can be used to manipulate rheological response. Thus selection of the polyelectrolyte (Dickinson et al., 1993), thickness (Prestidge and

Tadros, 1988), and flexibility of the interface (Dickinson, 1998, Murray, 2002) can be tailored to fabricate emulsion characteristics ranging all the way from low viscosity liquids, through to gel-like networks.

Structuring is commonly found through careful application of polyelectrolyte and environmental control (ion concentration and pH) (van Aken et al., 2011). The role of zeta-potential ($\zeta$) hugely impacts particulate or polymer structures within colloidal systems; where aggregation or dispersity is the result of net surface charges, inducing short range inter-particle interactions through attractive or repulsive forces. As a result, emulsion systems have been shown to exhibit rheologies (viscosities and elasticities) that greatly differ, on the scale of several orders in magnitude (Dickinson et al., 1993). Once again, the chemical composition of proteins make them ideal materials for such concepts, as the many functional groups housed within their residue chains provide tailorable charges across a range of pH.

Alongside their polyelectrolytic effects, their ability to adopt changing conformations when encountering an interface (MacRitchie, 1978) generates elastic interfaces with varying thicknesses (Murray, 2002). As an example, for milk proteins - on adsorption of β-lactoglobulin at an interface, much of its native globular structure is retained, resulting in the formation of a thin monolayer that acts like deformable particles. Further loss of the tertiary structure, as a function of numerous variables including time, heat, pH *etc.,* converts the monolayer into a two-dimensional gel-like structure, with viscoelastic characteristics (Dickinson, 2001). Conversely, the highly-disordered structure of β-casein promotes loops and tails, sterically creating a much thicker interfacial layer. However lack of inter-protein bonds greatly reduces its interfacial viscoelasticity (Dickinson, 1998).

### *2.2.3. Emulsion functionality*

The importance of emulsion structure becomes more apparent when regarding their potential applications. More and more emulsion systems are becoming incorporated into foods, being used for roles such as fat reduction, satiety, and delivery. The way in which these roles are achieved is through careful engineering of the microstructures to formulate scientifically designed functionalities.

#### *2.2.3.1. Emulsion design in fat reduction*

The first step into reducing the solid lipid content of a product would be to replace it with a non-calorific component, water, resulting in a water in oil emulsion (Norton and Norton, 2010). Here, fat reduction becomes a function of the percentage of dispersed water. Typically, low fat spreads are representative of such systems with water droplets becoming immobilised within a solid fat/polymer matrix. The functionality of spreads is mainly governed through three main areas: Appearance, spreading properties, and organoleptic perception; where a common feature across all three areas is droplet concentration and size (Norton et al., 2006a). The effects of increasing droplet concentration, unlike fluid systems (*e.g.* mayonnaise where bulk rheology is governed by close packing of droplets), has a negative effect on material hardness. Here the dispersed droplets act as filler matrices, where softer droplets effectively weaken the network (Dickinson and Chen, 1999, Oliver et al., 2015), producing a more pliable material. Droplet concentration also plays a role in product taste, whereby the potential for salt release is a function of the droplet number density. Furthermore, in the case of salt release from within such matrices, release is governed

by phase inversion during mastication; interestingly, relying on poor stability of the emulsion within the oral cavity, allowing the water droplets to coalesce (Norton et al., 2006a).

#### *2.2.3.2. Emulsions for satiety*

The link between the rate of gastric emptying and appetite suppressive hormone release has long been established (Santangelo et al., 1998). The progressive chain of thought is therefore to manipulate this biological system, in an attempt to regulate calorie intake. One means of undertaking this is via engineering of "smart" interfaces, presenting emulsions with triggered structural responses within the GI tract (Lundin et al., 2008, Golding and Wooster, 2010, Golding et al., 2011).

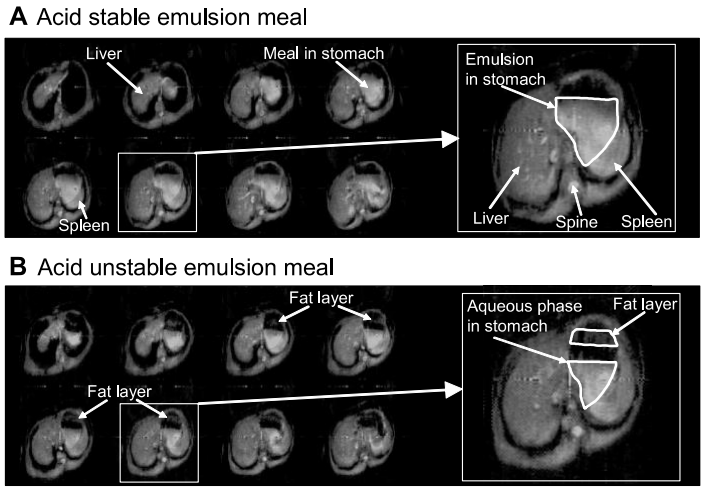


*Figure 2.12: MRI images showing cross-sections of a human abdomen, 40 minutes post ingestion of: A) an acid stable emulsion and B) acid unstable emulsion, showing the formation of a fat-rich layer over the aqueous phase. Images taken from Marciani et al. (2007).*

As such, the engineering of emulsions with interfaces that: 1) fail, leading to droplet coalescence or, 2) flocculate under acidic conditions, resulting in intra-gastric layering of droplets, as shown in Figure 2.12. The underlying biological reaction to this phenomenon is heightened levels of cholecystokinin (CCK) within the blood plasma, inducing satiation (Foltz et al., 2009). Consequently, in separating the multiple components into lipid rich and poor states, the aqueous phase inevitably contains much fewer calories. As such, based on caloric density, the hypothesis would be that emptying occurs on a much quicker time scale (Kalogeris et al., 1983). This was supported by work in both humans (Marciani et al., 2007, Marciani et al., 2006) and rats (Friedman et al., 1996), where emulsion instability led to rapid initial emptying, slowing upon reaching the high calorie lipid phase, shown in Figure 2.13.

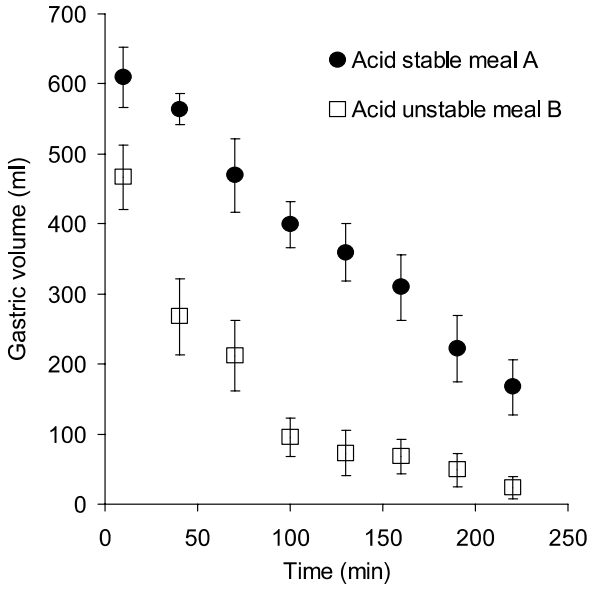


*Figure 2.13: Gastric emptying as a function of emulsion stability (Marciani et al., 2007).*

More recent attempts to control food flow through the GI tract have obscured detection of the oil droplets through augmentation of the interface. This was achieved *in vitro*, through thermal complexation of β-lactoglobulin and methylated nanocrystalline cellulose at body temperature. Subsequently, proteolysis was prevented hindering release of the oil (Scheuble et al., 2014). Therefore, resultant uptake of the oil becomes slowed, allowing the emulsion to transition further into the intestine. This can then promote satiation through the ileal brake. Although, the data presented is promising *in vitro*, further work using much closer *in vivo* models is needed to fully demonstrate the systems' potential.

### *2.2.4. Microgel technologies*

Hydrocolloids have extensively been applied as rheological modifiers within the food industry for many years, however, more recent developments in microstructural engineering have shown microgels as potential candidates within fat reduction (Norton and Norton, 2010). From a sensory science aspect, mimicking the perceived characteristics of lipid components in consumables is challenging; with the need to replicate individual droplet, droplet-droplet and bulk system properties. Such characteristics have been tackled using the microstructural design approach, through careful control over the underlying formation mechanisms and chemistries (Fernández Farrés et al., 2013, Fernández Farrés and Norton, 2014, Gabriele et al., 2009, Gabriele et al., 2010, Garrec et al., 2013, Garrec and Norton, 2012, Norton et al., 2006b, Norton et al., 1999).

#### *2.2.4.1. Microgel formation*

Typically, microgels are formed via an entrapment process, localising a gelling system to areas of high and low polymer concentrations. Thus, gelled particles become dispersed within a secondary continuous phase. This review will mainly focus on discreet individual particles dispersed within a non-gelling medium, however, it is not the case for all microgel systems; where regions of high polymer concentrations are immobilised within a secondary gel phase (Nishinari et al., 2000, Norton and Frith, 2001, Van Den Berg et al., 2009, Wolf et al., 2000, Norton et al., 2006b). Particulate gels are generally formed via two separating routes: chemical or mechanical separation.

Chemical separation techniques rely on the chemistries of the components to promote phase separation. Emulsions provide an excellent environment to form microgel particles; using a water in oil emulsion, the aqueous phase can be gelled, separated, and redispersed in a solvent (generally water) (Sağlam et al., 2011, Adams et al., 2004). Production of particles in this way provides several advantages, as both particle size and shape can be carefully controlled (Norton et al., 2006b). However, separation of the particles from the oil can hinder large scale production within food products. To this end, particulate microgel suspensions produced by a simple shearing method are more favourable.

Shear gels, often referred to as fluid gels, are formed via the application of mechanical shear as a polymer is forced through its sol-gel transition. The first proposal for the formation and stability of such systems by Norton et al. (1999) suggested a nucleation and growth process, where particles grew until an equilibrium was reached between size and shear regime. Shifts in system equilibrium were suggested to be controlled through two major routes: polymer concentration and magnitude of

separation. More recent studies have built on such proposals, highlighting gelation kinetics as the driving force behind both particle size and morphology (Gabriele et al., 2009). Where aggregation kinetics are fast, rapid formation of helices and subsequent junction sites lead to the formation of large anisotropic particles, as larger gels become broken down by the shear flow. A reduction in gelling kinetics leads to thermodynamically stable micro-spheres, where shear disruption prevents helical formation at the surface, resulting in particulates with hair-like structures (Garrec and Norton, 2012, Garrec et al., 2013).

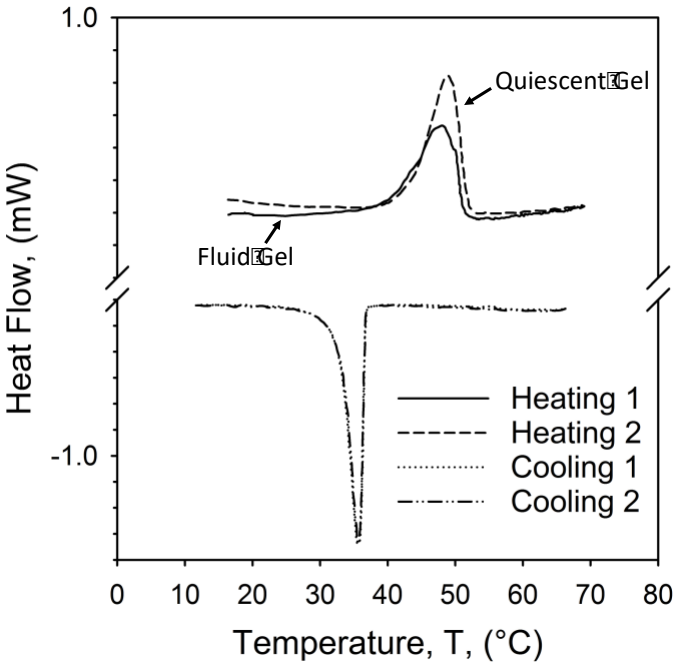


*Figure 2.14: Thermograms obtained for κ-carrageenan fluid gels showing the change in enthalpy of melting between the fluid gel system and quiescent counterpart. Graph adapted from Garrec and Norton (2012).*

Besides obstruction to helical formation at the particle interface, kinetics plays an important role within particle intrinsic properties (*i.e.* network density). Typically, as a

result of weak interfacial tensions between the two phases (gelled and un-gelled) and particle peripheries experiencing greater shear forces, a gradient from high to low polymer density is observed across the particles (Fernández Farrés et al., 2014). These observations have been investigated via calorimetry, whereby significant changes in melting enthalpies were observed for fluid gels and their quiescent counterparts (see Figure 2.14) (Garrec and Norton, 2012). Although it is reasonable to expect such differences, where molecular interactions have been inhibited by the shearing process, these observations are more closely correlated to gelling rates; where polymers with faster kinetics did not show such discrepancies (Fernández Farrés et al., 2014, Norton et al., 1986, Norton et al., 1999).

#### *2.2.4.2. Controlling fluid gel behaviour*

To better understand fluid gel design principles and resulting material characteristics, the interplay between processing parameters and formulation have been extensively studied; (Fernández Farrés et al., 2013, Fernández Farrés and Norton, 2014, Gabriele et al., 2009, Garrec et al., 2013, Garrec and Norton, 2012, Hamilton and Norton, 2016, Norton et al., 1999). Typically, fluid gels show weakly dependent viscoelastic responses to frequency, falling between a strong gel and weakly converging polymer network (Garrec and Norton, 2012). It has been argued that these behaviours arise through the overlapping of "hairy" un-gelled polymer chains at the particle interfaces, where the number of interactions can be controlled through the applied shear and cooling rate during gelation; directly manipulating the elastic modulus of the systems. The effects of shear, however, had little effect on material viscosity, with all systems

exhibiting similar flow curves (Gabriele et al., 2009). Here, equivalence across systems is likely to have arisen due to close packing of the gel particles. Thus, suspensions act like highly concentrated emulsions with viscosities independent of the dispersed phase, but characterised on the micro-scale (packing, size-distribution and inter-particle interactions) as particles "squeeze" past each other (Núñez et al., 1996). In this case, the viscosity is driven more by particle deformability and morphology than the degree of interactions between them.

Work undertaken by Wolf et al. (2001) also studying the effects of particle morphology on the system rheology has been shown in Figure 2.15. Here, flow profiles for deformed particles were compared to those obtained for spherical particles, exhibiting increasing viscosities as a function of the particle length. It was found that as particles moved away from being spherical in nature, the rheology more closely followed those for long polymer chains, whereby large hydrodynamic volumes led to enhanced viscosities. Unfortunately, particle shape/morphology in many polysaccharide systems is not trivial to obtain, as the refractive indices of the gel and continuous phase are often too close. This has called for more interpretive means of analysis. As such rheology has been used to measure the intrinsic viscosity of a system if infinitely dilute. The intrinsic viscosity can be related to dispersed polymers molecular weight and radius of gyration (Mendichi et al., 2003). Thus, an indication towards particle shape can be obtained. Using this technique Garrec et al. (2013) provided data supporting the "hairy-sphere" inference, showing carrageenan fluid gel particles to be deformable with linear polymer-like tendencies.

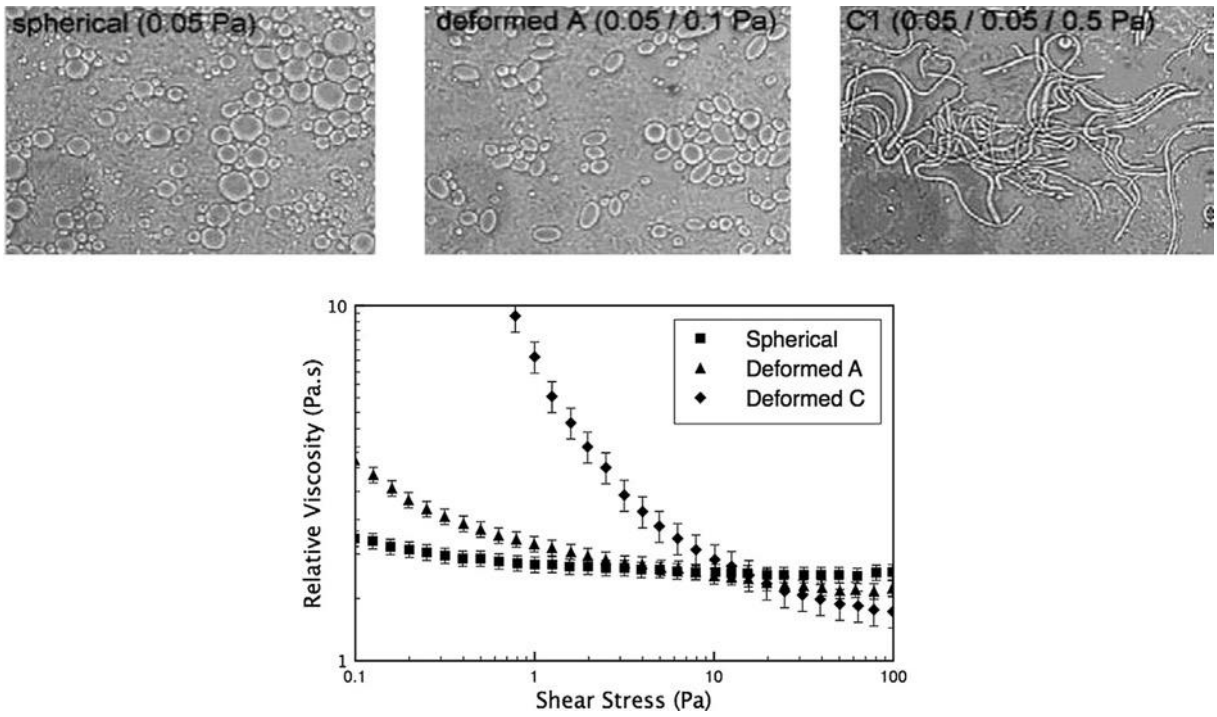


*Figure 2.15: Viscosity flow profiles for particulate suspensions with increasing particle asymmetry. Inserts show representative images for each system (Wolf et al., 2001).*

Interactions between particles as a function of both the shape and volume fraction (volume occupied by the particles) has additionally been shown by Adams et al. (2004). It was found that sheared particles expanded across a much larger volume, as a function of their anisotropy, allowing elastic responses at much lower volume factions in comparison to the spherical particles (Figure 2.16). Again, sheared systems more closely resembled polymer suspensions, whereas, for the spherical particles close packing needed to be achieved before a bulk elastic network was demonstrated. In this case elasticity was better demonstrated as a function of the contact zones between spheres through application of the Hertz' model.

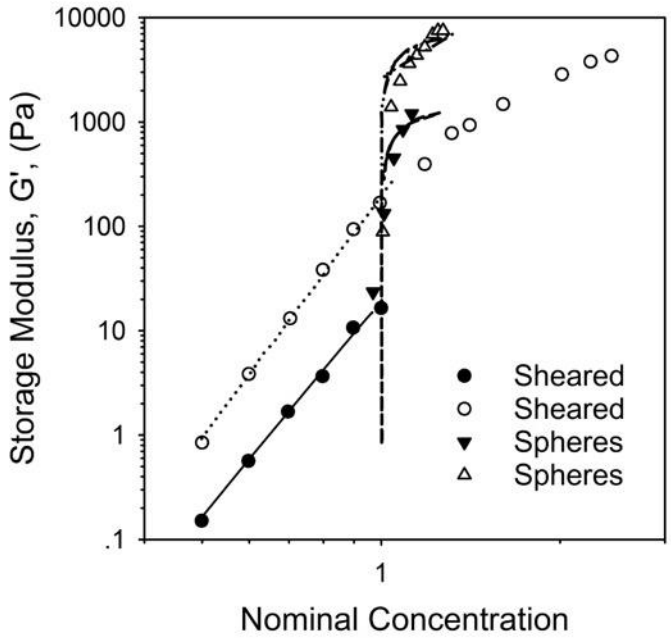


*Figure 2.16: Plot comparing the concentration dependency for classically sheared systems ((●) 0.75% agar, and (○) 1.75% agar) and spherical agar particles ((▼) 2% agar, and (△) 5% agar). Adapted from Adams et al. (2004).*

In effect, the controllable weak solid-like network, which flows upon shearing, provides fluid gels with a huge potential for oil replacement in food products (Norton and Norton, 2010). It is for this reason that the work carried out hence forth looks at replicating such systems, using WPI as the gelling material, in order to increase the nutritional value and functionality of the product.

# Chapter 3. *WPI Fluid Gels: The effects of Shear and Thermal History*

*Adapted from (Moakes et al., 2015a)*


***Synopsis***

Fluid gels were prepared via heat-induced gelation of a 10% (w/w) protein solution under controlled temperature and shear. Physical properties of the resulting gel particles (e.g. size and particle-particle interactions) were found to be dependent on the combination of shear and thermal history. Discrete large aggregates (>120 μm) were obtained at low shear, with aggregate size decreasing (<40 μm) at higher shear. Such microstructural changes in the particles led to the control of the suspension rheology. All suspensions showed a marked shear thinning behaviour associated with particle break-up which was observed to be more apparent for larger aggregates, originally made at low shear. The viscoelastic properties of the particulate systems, once in intimate contact (e.g. high volume fractions) resembled a pseudo solid material. In addition, it was shown that at a given volume fraction, the elasticity of the suspension varied dependant on their original processing conditions, owing to the degree of particle-particle interactions. A qualitative model has therefore been presented for the formation of particles by which the rheology is determined.

## 3.1. Introduction

From an application point of view, coupled with the highly controllable rheological properties, thermal stability and formulation simplicity are equally important within industry: owing to many potential thermal processes and cost effectiveness within product production. This chapter therefore investigates the formation of thermally stable whey protein aggregates by applying shear to whey protein systems undergoing a sol to gel transition. The research uses whey protein isolate (WPI), owing to its thermal denaturation and subsequent irreversible gelation, as a potential candidate for the preparation of fluid gels without additives. Therefore, the production of WPI fluid gels at native pH are investigated, with emphasis to the effect of shear and thermal history on particle intrinsic properties, and their corresponding rheological properties thereafter.

## 3.2. Materials and Methods

### *3.2.1. Materials*

Whey protein isolate (WPI) (WPI, W994, S-493391) was obtained from Kerry Ingredients (Listowel, Ireland). The composition of the WPI as stated by the supplier was 91.0 % protein, moisture 4.0 %, fat 1.0 %, ash 3.5 % and lactose 0.5 %. Mineral content of the WPI was: Ca – 0.50, P – 0.65, Na – 0.10, K – 0.15, Mg – 0.02 and Cl - 0.02 %.

### *3.2.2. Preparation of stock solutions*

Whey protein stock solutions of 10% (w/w) were prepared by dispersing WPI powder in deionised water. Sodium Azide (0.02% (w/w)) was added to the solution to

prevent bacterial growth. Solutions were then stirred for two hours at ambient temperature until completely dispersed and stored at 5 °C until usage (pH remained unadjusted ca. pH 6.4).

### *3.2.3. Fluid gel preparation using a rheometer*

A Malvern Kinexus Pro, stress controlled rheometer (Malvern Instruments Ltd, UK) equipped with a couette measuring system, cup diameter 27 mm and vane diameter 25 mm was used to prepare all WPI fluid gels. The vane geometry, although faced with concerns regarding non-uniform shear between paddles, and proneness to secondary flow regimes (Barnes and Nguyen, 2001, Barnes and Carnali, 1990), was chosen for its ability to manufacture relatively large sample volumes for further testing (ca. 40 ml in comparison to several ml in a cone and plate) and closeness to the industrial method of fluid gel production (pin stirrer). Aliquots of WPI solution were transferred using a syringe to the rheometer cup, set to a temperature of 25 °C. The geometry was then lowered and sample temperature left to equilibrate for 2 minutes before shear-heating profiles were undertaken. Heating profiles starting at 25 °C and increasing to 80 °C with a 10-minute holding period were conducted at various heating rates (1, 3, 5 and 10 °Cmin$^{-1}$), under steady shear (200, 400, 600 and 800 s$^{-1}$), before quiescent cooling at 3 °Cmin$^{-1}$ to 20 °C. In all experiments, a thermal cover was placed over the system to aid the prevention of water loss. Samples were then removed from the geometry and stored at 5 °C for 24 hours before being prepared into known volume fractions for further testing (as described in section 3.2.7). Each sample was prepared in triplicate with apparent viscosity profiles showing the average of at least three repeats (error shows the 95% confidence interval).

### *3.2.3.1. Identification of upper thermal limits*

Upper thermal limits were defined using differential scanning calorimetry (Figure 3.1). Thermograms showed typical heating traces for WPI, with a prominent exotherm centred around ~73 °C, and shoulder at lower temperatures pertaining to the denaturation of β-Lg (β-lactoglobulin) and α-Lac (α-lactalbumin) respectively (Fitzsimons et al., 2007). 80 °C was therefore significantly above the WPI denaturation temperature ($T_d$) (obtained using the same method as (Stading and Hermansson, 1990); whereby $T_d$ was found by deconvolution of the exotherms, followed by extrapolation to the baseline*)..*

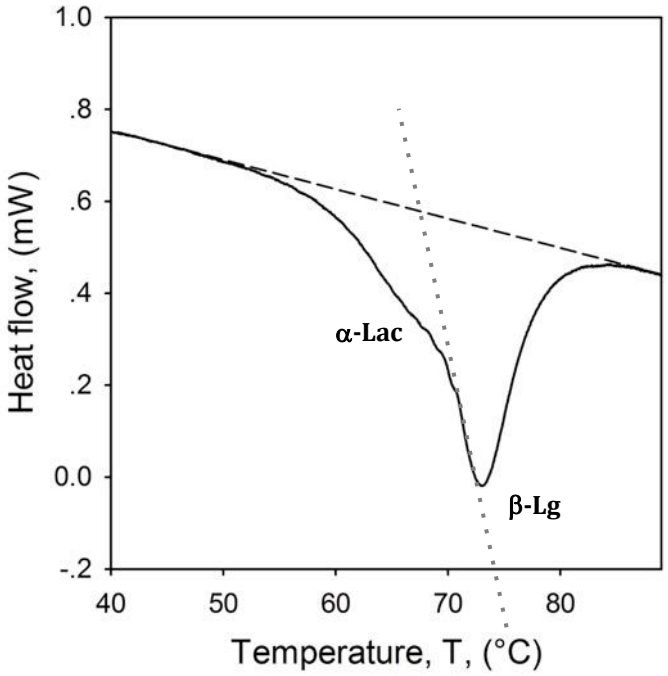


*Figure 3.1: DSC trace obtained for WPI (10% (w/w)) primary solution showing convoluted peaks for both α-lactalbumin (smaller peak) and β-lactoglobulin (major peak). The grey dotted line indicates the intercept of the baseline used to determine the temperature of denaturation ($T_d$) for β-Lg.*

### *3.2.4. Static light scattering (SLS)*

Particle size distributions were determined using static light scattering. A Malvern Mastersizer MS2000 (Malvern Instruments Ltd, UK) attached to a Hydro SM manual small volume sample dispersion unit was used to obtain both surface and volume weighted means, $d_{3,2}$ and $d_{4,3}$ respectively. Particle sizes were calculated based on the Mie theory as such particles are assumed to be monodisperse homogenous spheres. Samples were prepared by diluting gel particles in distilled water to avoid multiple scattering and pre-defined software refractive indices (RI) for the water and protein were used: 1.33 and 1.6 respectively. Average distributions based on 3 runs were then taken in triplicate. (For further theory see Appendix i)

### *3.2.5. Optical light microscopy*

An optical light microscope, Brunel SP300-fl (Brunel Microscopes Ltd, UK) fitted with an SLR camera (Canon EOS Rebel XS, DS126 191) was used to image fluid gel particles with objective lenses up to 40x magnification (5x, 10x, 20x and 40x). Slides were prepared by firstly diluting fluid gel samples (1:4), then adding one drop onto a microscope slide (VWR, UK) and covered with a cover slip (Thickness No.1, VWR, UK).

### *3.2.6. Confocal laser scanning microscopy (CLSM)*

Confocal laser scanning microscopy (CLSM) samples were prepared in the same manner as outlined in section 3.2.5. Self-fluorescing properties of whey protein were used in order to prevent any changes in the microstructure that could be induced through staining, or covalent tagging of the molecules. A Leica TCS-SPE confocal microscope (Leica Microsystems Ltd, UK) fitted with an argon laser was used for all

CLSM analysis. Protein particles were excited at 405 nm and detected at 450-500 nm. Stacked images were obtained using 0.5 μm spacing through the gel particles under 40x and 60x magnification; Immersion oil (56822, Sigma-Aldrich, UK) was used to bridge the gap between coverslip and objective lens. Images were again processed using a software package (ImageJ) to extract 3D images and enhance the contrast. (For further description see Appendix i)

### *3.2.7. Rheological Methods*

A protein content of 9 % was calculated for gel particles based on limited denaturation (90% of the initial protein having become denatured at the temperature and heating times applied during processing - in correspondence with data presented by Croguennec et al. (2004)). However, material response for fluid gels arises through the volume occupied by the particles; thus, for all rheological testing, samples were prepared in volume fractions ($\phi_{FG}$) from 55 to 90 % on a gel particle basis. All fluid gel samples were analysed at 25 °C and subjected to pre-shear (10 $s^{-1}$ for 10 s) to ensure consistent loading conditions. (For further theory see Appendix i)

#### *3.2.7.1. Preparation of volume fractions*

Volume fractions were determined using a similar method first proposed by Garrec et al. (2013), shown in Equation 3.1:

$$\phi_{FG} = \varphi_{FG} + [(1 - \varphi_{QG}) - \varphi_{syn}]$$

*Equation 3.1: Fluid gel particle volume fraction as a function of both the volume of water removed during centrifugation, and syneretic effects of the gelled particles.*

Where $\phi_{FG}$ is the volume occupied by the fluid gel particles, $\varphi_{FG}$ relates to the ratio of solid component remaining post-centrifugation, $\varphi_{QG}$ is the solid component for a quiescent gel and $\varphi_{syn}$ is fraction of water lost through syneresis. Data obtained for WPI systems highlighted syneretic effects to be negligible, thus volume fraction calculations were based on the ratio of initial mass to remaining mass post-centrifugation (assuming 1 g of water to occupy 1 mL volume). The free water was removed from the system using centrifugation, Sigma 3K30 (Sigma Laborzentrifugen GmbH, Germany). Relative centrifugal force (RCF) and duration was determined experimentally as the point at which continued water loss ceased for all fluid gels. Figure 3.2 shows water loss as a function of increasing centrifugal force. Samples were first placed in the centrifuge for 10 mins, supernatant removed and measured. Samples were re-centrifuged increasing the force applied incrementally. Thus, water was removed until a plateau was obtained.

Post centrifugation at 10,000 g the supernatant was removed, this was then termed 100 % volume fraction; assuming water only remained within the gelled entities, as particles become packed/compressed during centrifugation. Gel particles were then diluted with deionised water to give desired $\phi_{FG}$. In each case fresh deionised water was used to re-suspend the particles, removing any ungelled protein and additional ions found within the WPI powder. Suspensions were further stored at 5 °C for 24 hours before testing.

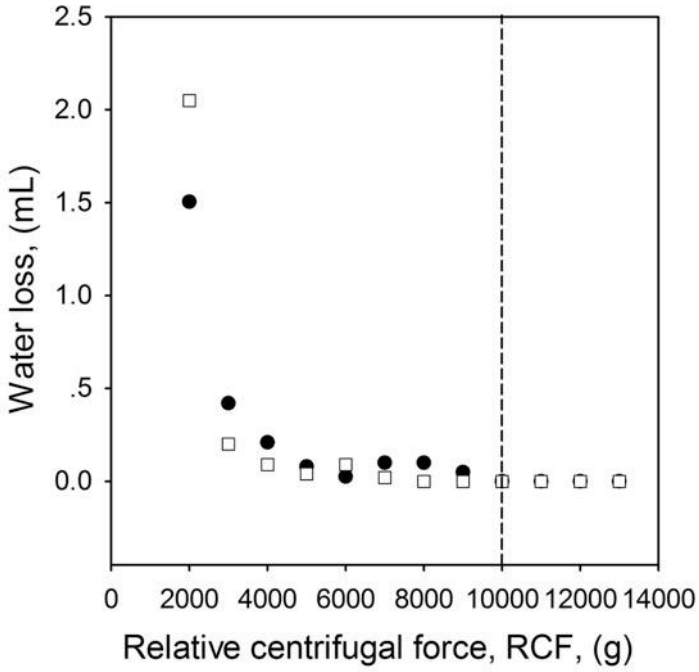


*Figure 3.2: Water loss as a function of increasing centrifugal force for WPI suspensions prepared at 3 °Cmin$^{-1}$, (□) 200 s$^{-1}$ and (●) 800 s$^{-1}$ shear rates.*

#### *3.2.7.2. Dynamic oscillatory measurements*

Frequency sweeps were conducted with a serrated 25 mm parallel plate and serrated bottom plate using a 1 mm gap. All frequency sweeps were obtained in controlled strain mode between 0.1 and 10 Hz. A frequency range of 2 logarithmic decades was applied to probe particle interactions at lower frequency ranges, within the limitations of the instrument and chosen geometry. Strains were determined by amplitude sweeps and were set to within the linear viscoelastic region (LVR) for all samples tested (<1% strain).

#### *3.2.7.3. Viscosity measurements*

Thixotropic studies were undertaken using the same measuring system as described in section 3.2.7.2. Fluid gel samples with $\phi_{FG}$= 90% were subjected to increasing shear rates from 0.01 to 800 $s^{-1}$, before decreasing the shear rate (800 to 0.01 $s^{-1}$) in a time dependent fashion (5 min ramps). This method was then repeated using a five-minute recovery period in between sweeps.

## 3.3. Results and Discussion

### *3.3.1. Formulation of WPI Fluid Gels*

#### *3.3.1.1. Effects of shear rate on the degree of aggregation*

Viscometry was used to study the formation of 10% (w/w) whey protein fluid gels at native pH (~6.4). Figure 3.1 shows the changes in apparent viscosity for WPI solutions at different shear rates (200 to 800 $s^{-1}$) whilst the temperature was increased from 25 to 80 °C at 1 °C$min^{-1}$, and subsequently held for 10 minutes. On heating, the system's apparent viscosity slowly decreases until a critical temperature is reached, above which, a rapid increase in the viscosity is observed. The viscosity increases in two-steps, similarly to polysaccharide (κ-carrageenan) fluid gels (Gabriele et al., 2009), where the mechanism for particle formation was of nucleation and growth. Growth of the initial nuclei has previously been reported to occur through one of two mechanisms: enrichment from the surrounding un-gelled polymer, or particle-particle aggregation as two nuclei come together (coalesce) (Gabriele et al., 2009, Garrec and Norton, 2012). The formation of WPI gel particles can also be explained on the same grounds. Heat induced gelation of whey proteins is a multi-step mechanism, primarily led with the

unfolding of the native structure (Bauer et al., 1998, Cairoli et al., 1994, Hoffmann et al., 1996, Sawyer, 1968).

The WPI gel structure is mainly formed through the polymerisation of β-lactoglobulin, WPI's major protein constituent, which initially partially denatures whilst retaining its dimeric form. With further restructuring to the secondary structure, intermolecular β-sheets provide points of association leading to the formation of oligomers with higher molecular mass (Lefèvre and Subirade, 2000), accompanied by an observed change in turbidity in accordance with Walkenstrom et al. (1998). These then act as nuclei - small particulates with accessible points of association, allowing further growth via enrichment from the surrounding unfolded protein, until a primary particle is formed. At this initial stage, the number and volume fraction of initial particles are mainly responsible for the increase (onset) in viscosity (Mudgal et al., 2011b). As the onset of increasing viscosity appears constant across all fluid gels prepared, it is suggested that the number and size of the initial particles remains unaffected by the shear at this point in the process (Figure 3.3). This is in agreement with current protein denaturation/aggregation knowledge, as the formation of the initial clusters occurs over a very short time scale - seconds (Morris et al., 2009).

As the growth process continues the number of primary particles within the system rises until particle-particle aggregation becomes dominant. This leads to the formation of larger aggregates with increased phase volume. As a result, the viscosity of the system increases as expected for highly flocculated suspensions (Barnes, 1994, Buscall et al., 1987, Goodwin and Reynolds, 1998, Chung et al., 2014). Correspondingly, the viscosity change throughout the sol-gel transition decreases with increasing shear rates from 200 to 800 $s^{-1}$, as shown in Figure 3.3, as particle-particle aggregation

becomes increasingly hindered. A degree of apparent shear thickening, when comparing flow profiles for systems prepared at higher shear rates can also be seen. Such observations are not expected within the polymer concentrations studied, and are best described as an artefact of the vane geometry; previously reported to exhibit secondary flow and shear banding for non-Newtonian fluids (Barnes and Carnali, 1990, Wang et al., 2011, Sherwood, 2008). For this reason, final viscosities have not been used. Instead the relative change in viscosity has been studied to show increases in viscosity as a function of gelation (see later in Figure 3.10).

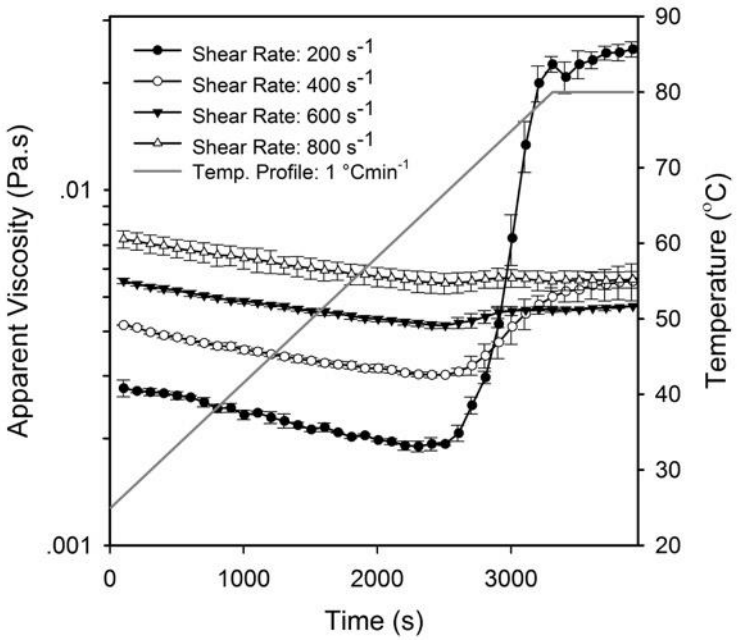


*Figure 3.3: Viscosity profiles for 10% (w/w) WPI solutions upon heating from 25 °C to 80 °C at 1 °Cmin$^{-1}$ followed by subsequent holding for 10 minutes. Apparent shear thickening with increasing processing rates is an artefact of secondary flow and shear banding within the vane geometry.*

WPI aggregation was also investigated using confocal laser scanning microscopy, with particles shown in Figure 3.4.

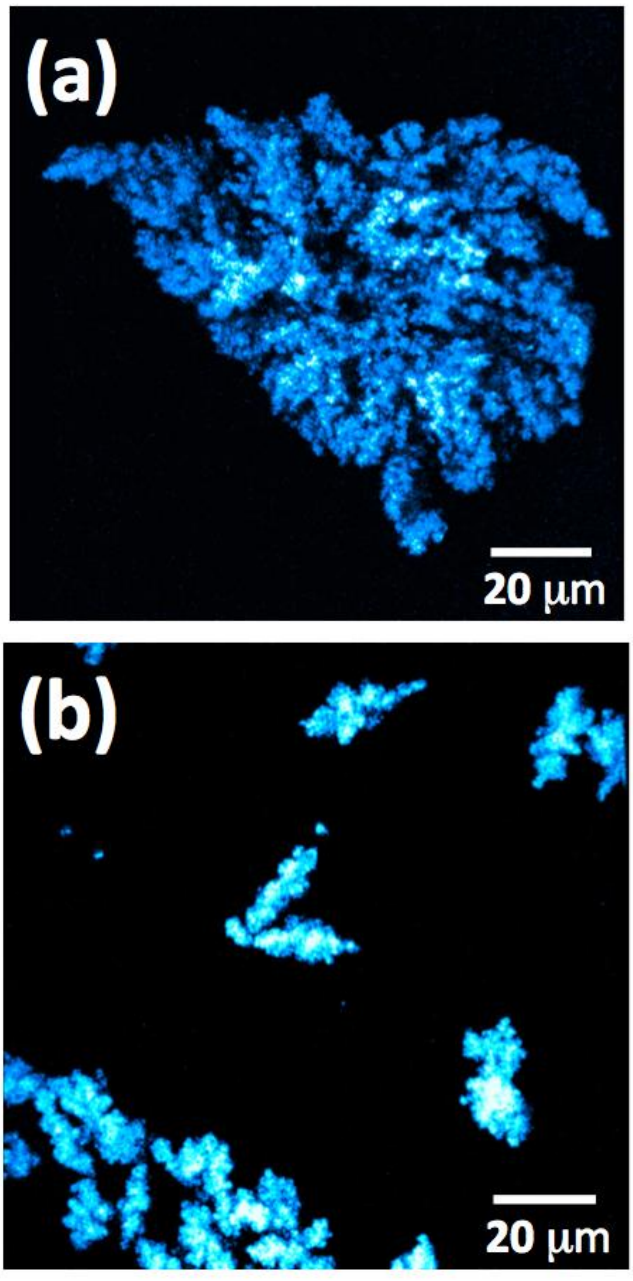


*Figure 3.4: Diluted WPI fluid gel particles (1:4) viewed under confocal laser scanning microscopy: samples were excited at 405 nm using 40x magnification. Particles were prepared at 1 °Cmin$^{-1}$ at 200 s$^{-1}$ (a) and 800 s$^{-1}$ (b) (Scale bar shows 20 µm).*

Fluid gels particles prepared at 200 $s^{-1}$ were primarily large and highly aggregated (Figure 3.4a), seeming to have formed through interconnected particles, forming a three-dimensional network as previously described. However, by increasing the shear rate to 800 $s^{-1}$ whilst undergoing the sol-gel transition, it was observed that applied separation was sufficient to prevent any secondary aggregation, restricting the final aggregates to the size of the primary particles (Figure 3.4b). Reinforcing the hypothesis that growth occurs via the bonding of primary particles to form larger aggregates that grow to a size dictated by the applied shear field.

#### *3.3.1.2. Effects of heating rate*

The effect of applied heating rate on the production of WPI fluid gels is shown in Figures 3.5 and 3.6. Here the apparent viscosity profiles of 10% (w/w) WPI solutions were measured on heating to 80 °C at 3, 5 and 10 °$Cmin^{-1}$ (Figure 3.5). The obtained data revealed that as the heating rate increased the overall viscosities of the systems increased when compared to those prepared at 1 °$Cmin^{-1}$. The increase in heating rate leads to more rapid aggregation of the protein forming larger particles (Figure 3.7), thus increasing the effective volume of the final aggregates and consequently the viscosity of the suspensions (Genovese, 2012). Above the critical gelling concentration nucleation is no longer the rate-limiting step for aggregation. Thus, larger aggregates can rapidly form resulting in higher viscosities (Mudgal et al., 2009, Mudgal et al., 2011b, Walkenstrom et al., 1998). Following this point, the change in viscosity as a function of time, at a constant heating rate, can be viewed as linearly proportional to the degree of aggregation occurring within the process; assuming change in viscosity arsing through shear

thinning as the particles grow are negligible. Such linearity has been highlighted using a dotted line in Figure 3.5a, starting after the initial onset and finishing prior to plateauing at the end of the gelation process.

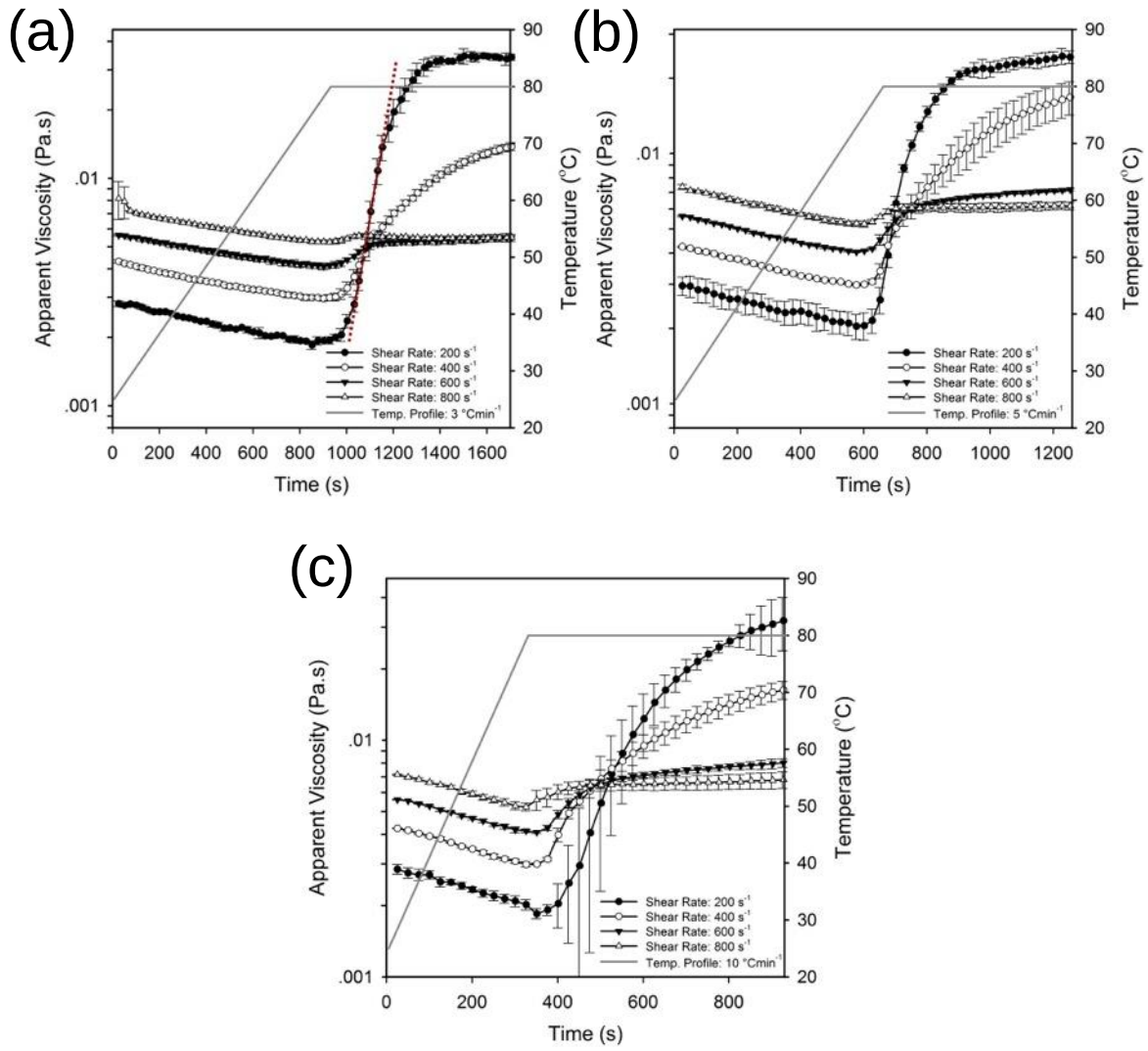


*Figure 3.5: Flow profiles observed during sheared heating from 25 °C to 80 °C at (a) 3, (b) 5, and (c) 10 °Cmin$^{-1}$. (The dotted red line on (a) has been added as an example to highlight the linear region of the gelling profile used to obtain the rate of aggregation.)*

Therefore, the relative change in viscosity has been used to calculate the degree of aggregation ($d\alpha$) (Equation 3.2), and the magnitude of change in respect to time used to

show the rate of aggregation (Equation 3.3) shown in Figure 3.6. The rate of aggregation ($d\alpha/dt$), was calculated as:

$$d\alpha = \frac{\eta_i - \eta_{i-1}}{\eta_{int}}$$

*Equation 3.2: Degree of aggregation, expressed as the change in viscosity of the suspension.*

$$Rate\ of\ Aggregation = \left(\frac{d\alpha}{dt}\right)_i$$

*Equation 3.3: Rate of aggregation, derived from the change in viscosity (equation 3.2) with respect to time.*

where $\eta_i$ and $\eta_{i-1}$ are the viscosity at time $t_i$ and $t_{i-1}$ respectively, and $\eta_{int}$ is the initial viscosity. Corresponding values of $t_i$ and $t_{i-1}$ were determined from the linear region of the viscosity profile, after the onset of gelation had been reached. It was observed that the rate of aggregation was dependent on both the shear rate and the heating rate applied to the system. Figure 3.6 clearly shows that increasing the shear rate during the sol-gel transition, slows the rate at which aggregates form across all heating rates studied; as the imposed shear hinders the denatured protein from coming into contact and bonding.

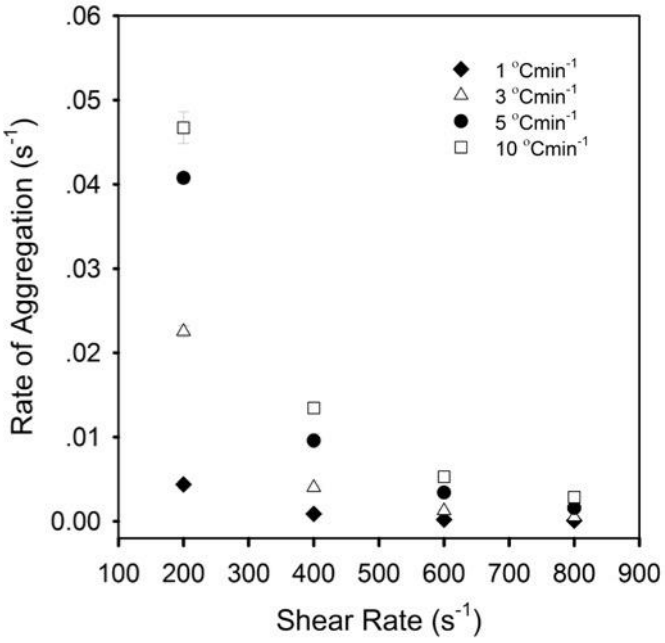


*Figure 3.6: Rate of protein aggregation at varying shear rates as a function of the heating rate.*

On the other hand, as the heating rate increases, the rate of aggregation increases (Figure 3.6) owing to the temperature dependence of aggregate growth being purely kinetic (Le Bon et al., 1999). Therefore, the number of primary particles that interact to form an aggregate is also expected to increase following an equation originally proposed by Berli et al. (1999) (Equation 3.4):

$$N = 1 + k(t - t_0)$$

*Equation 3.4: Empirical model expressing the number of primary particles (N) within an aggregate as a function of the gelation rate and time, (Berli et al., 1999).*

Where N is the number of primary particles, $t_0$ is the initial time at which $N$=1, and $k$ is the aggregation rate constant. Hence, as "$k$" increases, due to higher heating rates, the

number of primary particles coming together also increases, resulting in the formation of larger aggregates. This explains the difference in viscosity profiles observed between solutions heated at 10 °Cmin$^{-1}$ and those heated at 1 °Cmin$^{-1}$. However, as suggested by Gabriele et al. (2009), increasing the applied heating rate would decrease the processing time, as a consequence the system experiences the given shear for less time, decreasing the likelihood that larger aggregates become subsequently broken down within the shear regime.

#### *3.3.1.3. Qualitative model for particle formation*

Size distributions for WPI gel particles made at varying shear regimes and maximum/minimum heating rates (1 and 10 °Cmin$^{-1}$) are shown in Figure 3.7a and 3.7b respectively. It was observed that fluid gels produced in this manner were mono-modal, with the exception of samples prepared at the lowest shear rate, where a small shoulder can be observed. Such mono-modal distributions across the majority of the samples infers a consistent degree of shear was obtained throughout the system. This suggests that at higher shear rates, particles were not sequestered to dead spots within the vane geometry, a previous concern to using this set up. However, the presence of a shoulder at lower shear rates may be due to large aggregates becoming trapped in the proximity of the vane geometry during processing, thus avoiding the shear field (Figure 3.7a). As the shear rate increased the distributions shifted towards lower particle sizes, as growth during the gelation process becomes increasingly limited by the imposed shear. Distributions for particles prepared at 10 °Cmin$^{-1}$ have been shown in Figure 3.7b.

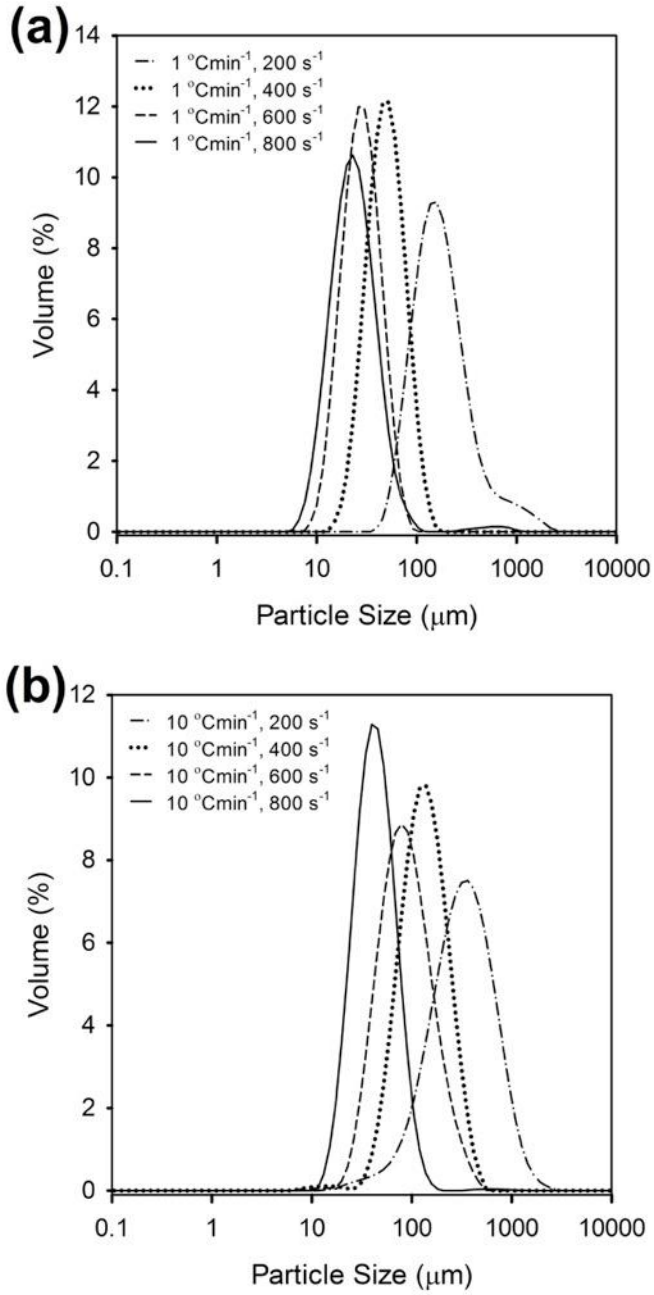


*Figure 3.7: SLS size distributions obtained for WPI fluid gels prepared using varying shear rates (200 to 800 $s^{-1}$) at 1 °$Cmin^{-1}$ (a) and 10 °$Cmin^{-1}$ (b). Distributions are the average of 3 repeats, error bars have been shown for obtained $D_{4,3}$ values in Figure 3.8.*

Again, mono-modal peaks were observed; however, aggregates produced at higher heating rates were larger in size as predicted by Equation 3.4. Mean sizes for all WPI

fluid gel particles obtained at varying shear and thermal histories are shown in Figure 3.8.

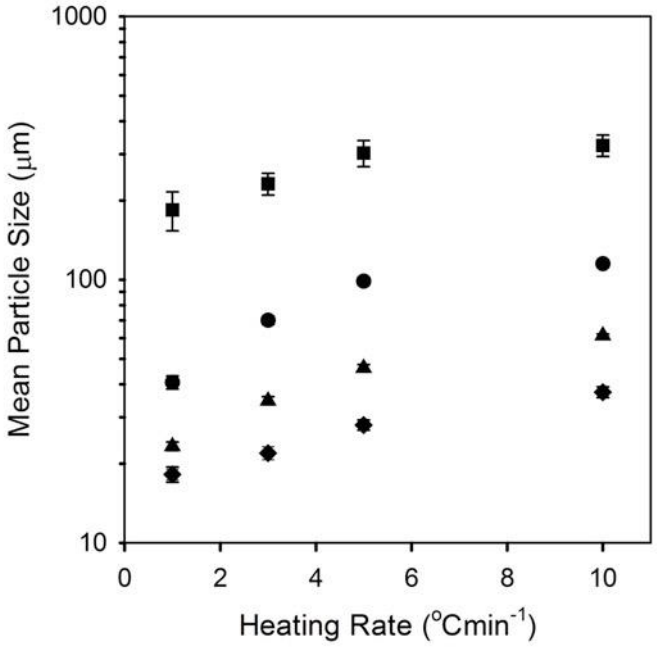


*Figure 3.8: Mean particle size ($D_{4,3}$) as obtained by SLS for WPI fluid gels prepared at a range of heating rates (from 20°C to 80 °C), as a function of processing shear rate: 200 $s^{-1}$ (■), 400 $s^{-1}$ (●), 600 $s^{-1}$ (▲) and 800 $s^{-1}$ (◆). Particle time in the shear field was thus dependent on the heating rate applied.*

The data obtained showed a relationship between the size of the WPI particles and shear rate employed during the processing; with increasing shear forming smaller aggregates. Particle size also shifted towards higher values as the heating rate increased, for all applied shear rates, as earlier ascribed to faster aggregation kinetics, resulting in an increase in particle-particle aggregation. To this end, it can be seen that particle size, and thus the degree of aggregation, is dictated by both the shear exerted, and heating rate applied to the system. Therefore, showing that the rate of aggregation is a function

of both shear and heating rate, and should be accounted for when considering "*k*" (Equation 3.4).

The reduction in particle size as a function of applied shear rate is highly dependent on the heating rate adopted in the formation process; shown by particles made at 1 °Cmin$^{-1}$ becoming further reduced in size than those prepared at 10 °Cmin$^{-1}$ when compared at the same shear rate. This is clear evidence for a change in the aggregate formation mechanism. It is suggested that in the initial stages of aggregate formation, relatively weak hydrophobic interactions hold the primary particles together. At this point the shear-induced aggregate breakdown is more effective than in the latter stages of formation, where particles become more firmly structured through covalent bonding (Mudgal et al., 2011a). Therefore, when energy is applied to the system at a faster rate (higher heating rates), aggregates are more rapidly formed that quickly become resistant to shear breakdown. Thus, it is proposed that at 10 °Cmin$^{-1}$ aggregates are formed within the shear field, whereas at 1 °Cmin$^{-1}$ initial larger aggregates are formed, becoming subsequently broken down, to result in smaller final sizes.

Particle morphology was also studied as a function of both processing parameters: Shear rate and thermal history. Length to width measurements were obtained from micrographs using an imaging package (imageJ) and plotted in Figure 3.9. The aspect ratio was observed to be independent of heating rate for most systems, except suspensions prepared at 200 s$^{-1}$, where an increase in the overall length of the particles occurred. A higher length to width ratio for particle growth primarily occurs within the shear regime, as a function of the elongational flow exerted within the rheometer. Even though small changes in particle morphology were observed,

differences were not significant. As such, particles were assumed to be the average aspect ratio across all systems, when considered rheologically.

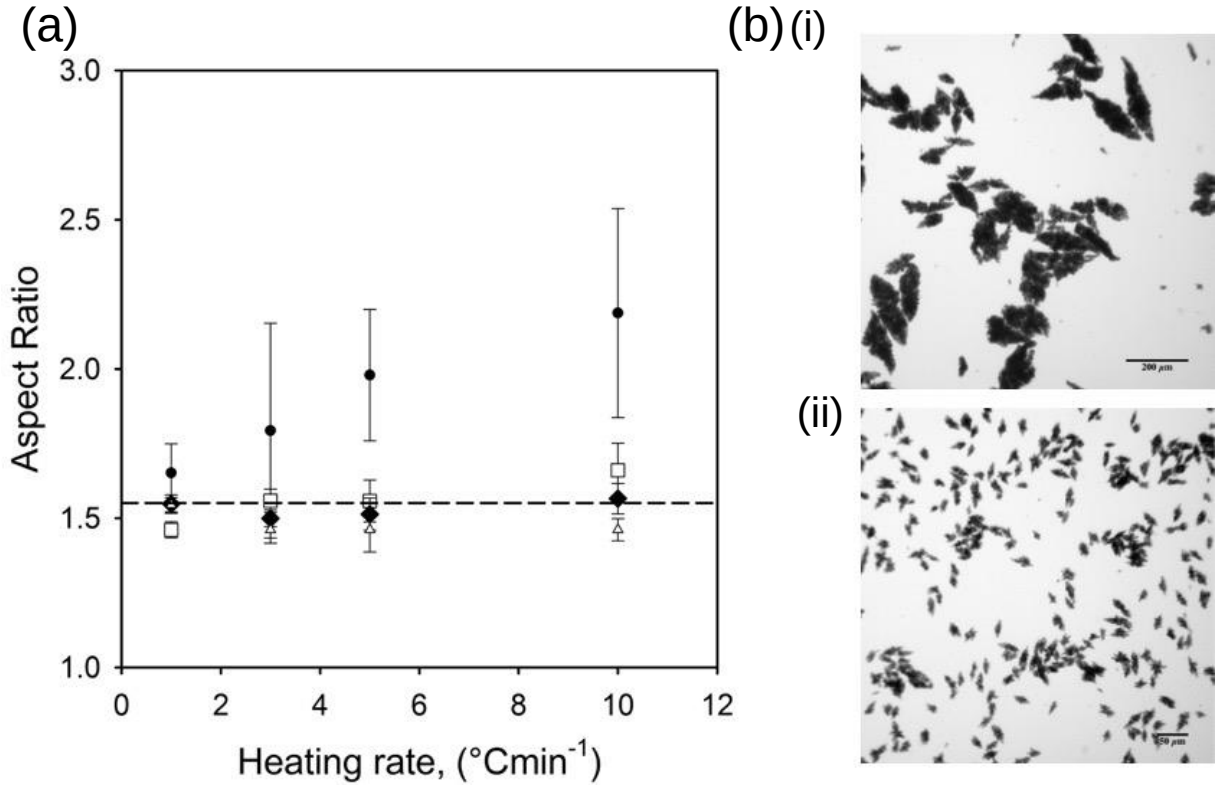


*Figure 3.9: (a) Aspect ratio obtained for WPI particles prepared at various heating and shear rates: (●) 200 $s^{-1}$, (□) 400 $s^{-1}$, (◆) 600$s^{-1}$ and (△) 800 $s^{-1}$. Dotted line shows the average particle length to width ratio. (b) Typical images used to determine the aspect ratio, systems were prepared at 10 °Cmin$^{-1}$ at: (i) 200 $s^{-1}$ (x5 magnification), and (ii) 800 $s^{-1}$ (x10 magnification).*

Assuming constant particle shape across all systems, deviations in viscosity are likely to arise as a function of the aggregation. This is in agreement with data published for highly aggregated suspensions (Barnes, 1994, Genovese, 2012, Goodwin and Reynolds, 1998). Figure 3.10 shows the change in relative system viscosity across all shear and thermal histories calculated using Equation 3.5.

$$\Delta\eta = \frac{\eta_{final} - \eta_{initial}}{\eta_{initial}}$$

*Equation 3.5: Relative change in viscosity for WPI solutions undergoing gelation within a sheared environment.*

Where $\eta_{final}$ is the final viscosity post-gelation and $\eta_{initial}$ is the viscosity at the onset of gelation.

Neglecting effects posed by the anisotropic morphology of the particles and subsequent orientation in flow, changes in the shear field result in the limitation of aggregation within the dispersed phase. Following the general dependence of viscosity on the dispersed phase volume fraction (Krieger and Dougherty, 1959), the viscosity of an aggregated suspension is assumed to be based primarily on the effective volume of the disperse phase, thus depending on the degree of aggregation (Barnes, 2000, Genovese, 2012). As explained earlier the effective volume fraction depends on the mechanism of aggregation leading to the number of aggregates per resulting particle. This can be clearly seen in Figure 3.10 for suspensions prepared at 400, 600 and 800 $s^{-1}$, where the change in system viscosity mirrors the increase in particle size (Figure 3.8). On the other hand, suspensions prepared at 200 $s^{-1}$ exhibit similar viscosity changes (over all heating rates), despite the large difference in particle size. The result in plateaued viscosities are suggested that for such large aggregates the effective volume fraction is equal to the maximum packing fraction (highly concentrated regime), where flow is not only characterised by size, but also by particles moving, ‘‘squeezing’’, past each other. The bulk viscosity thus becomes a function of particle deformability and packing similarly to the behaviour of highly ‘‘packed’’ emulsions (Barnes, 1994, Núñez et al., 1996). From this it is reasonable to assume that the deformability of the aggregate is

a function of its size. As such, particles exhibit changes in density associated with phenomena observed for fractal geometries within colloidal aggregates, following cluster-cluster aggregation (Li and Ganczarczyk, 1989, Meakin, 1983, Schaefer et al., 1984). Therefore, larger more aggregated particles exhibit decreased densities becoming more deformable than the smaller more rigid particles formed at higher shear rates. This in turn would explain the constant viscosity observed for fluid gels made at 200 $s^{-1}$. From the above results, it is concluded that aggregation of self-similar primary particles to form large aggregates represents the mechanism for WPI fluid gels. Further building on the last statement, aggregate formation through this process can either occur within the shear field, or as gel formation and subsequent breakdown.

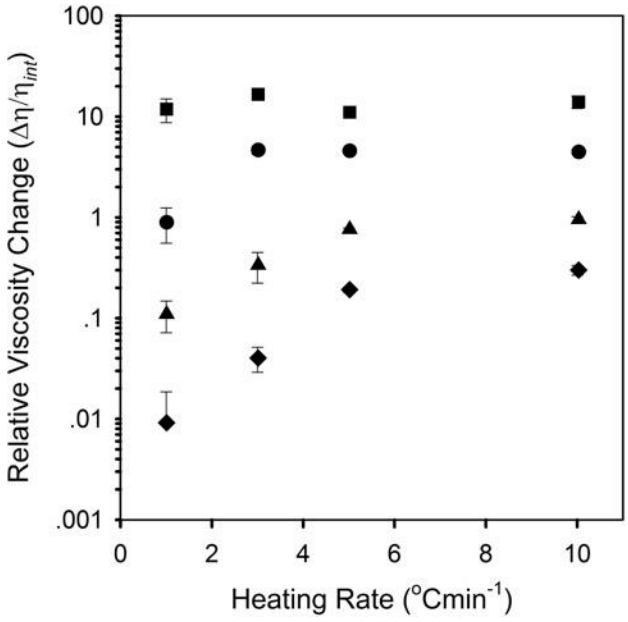


*Figure 3.10: Relative change in viscosity obtained from fluid gel viscosity profiles. Fluid gels were prepared at varying heating rates (1 to 10 °Cmin$^{-1}$) as a function of shear rate 200 s$^{-1}$ (■), 400 s$^{-1}$ (●), 600 s$^{-1}$ (▲) and 800 s$^{-1}$ (◆).*

### *3.3.2. Fluid gel material properties*

#### *3.3.2.1. Small deformation rheology of fluid gels*

To further probe particle mechanical properties, WPI fluid gels were characterised under small deformation rheology. Figure 3.11b shows frequency sweeps obtained for fluid gels prepared at different shear rates at a given volume fraction ($\phi_{FG}$) of 90 % The mechanical spectra for both gels is typical of an interconnected structure where elastic modulus (G') dominates the viscous component (G'') as described by Ross-Murphy (1994); whereby both moduli are only slightly dependant on frequency (over the range investigated), previously reported for κ-carrageenan fluid gels (Garrec and Norton, 2012). Figure 3.10a shows amplitude sweeps for the same fluid gel systems. The linear viscoelastic region extends to a critical strain (shown by the dashed lines in Figure 3.10a) above which the material begins to flow (Garrec et al., 2013). The critical strain required to initiate flow decreased as the shear rate used in the preparation of the fluid gels increased *i.e.* particles became smaller. Although WPI fluid gels made at lower shear rates are characterised by a higher degree of aggregation, the ability of the aggregates to deform may also play a role at such a high strain. Large aggregates with a more open network structure are expected to be softer, as such will deform under applied shear before any flow is induced. Deformation of soft particles could lead to a larger contact area and greater friction (Yoon et al., 2005), in turn increasing their maximum strain within the linear viscoelastic region. Once flowing, particles produced at lower shear rates showed a lower dependence on strain implying greater inter-particle structuring (Garrec et al., 2013).

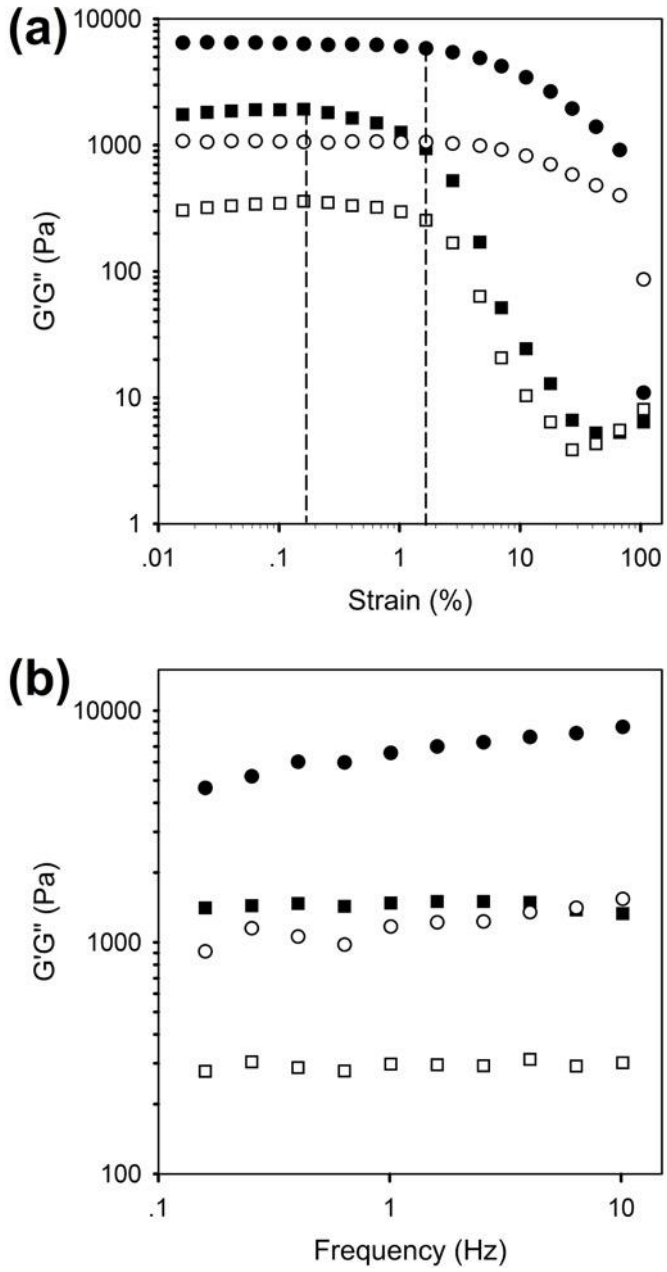


*Figure 3.11: (a) Amplitude, and (b) frequency sweeps for fluid gels $\phi_{FG}$90 prepared at 200 $s^{-1}$ (●,○) and 800 $s^{-1}$ (■,□), 10 °C$min^{-1}$. Closed markers denote G' and open, G". Amplitude sweeps were obtained at 1 Hz and frequency sweep at 0.05 % strain. Dashed lines show point at which the system begins to break down, deviating from the LVR. Plots show the average of three repeats.*

Figure 3.12 highlights the correlation of elastic modulus (G') to particle phase volume ($\phi_{FG}$). Elasticity arises through the close packing of particles above a critical

phase volume, 0.55. Figure 3.12 clearly shows that the elasticity of the suspensions is a function of both the shear and heating rates used in the formation process. Fluid gels made at 10 °Cmin$^{-1}$ exhibit higher elastic moduli than those prepared at 1 °Cmin$^{-1}$, since higher heating rates favour particle-particle interactions. On the other hand, shear induced breakdown will limit the extent of particle-particle interactions, which explains the lower storage modulus for particles made at 800 s$^{-1}$.

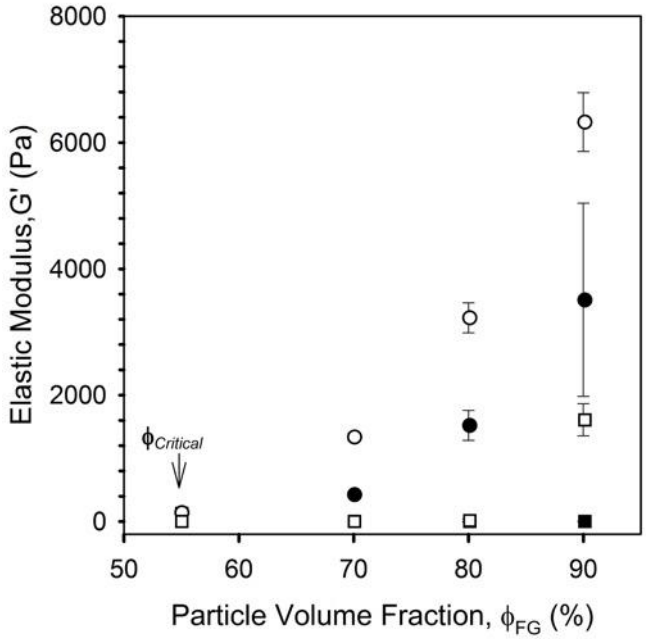


*Figure 3.12: Small deformation oscillatory data obtained for WPI fluid gels prepared at 200 s$^{-1}$ (●,○) and 800 s$^{-1}$ (■,□). Solid markers represent fluid gels formulated at 1 °Cmin$^{-1}$ and open 10 °Cmin$^{-1}$. Values of G' were obtained at 1 Hz.*

Although suspension elasticity arises primarily through interactions between particles, the effect of aggregate size, encompassing particle deformability and packing, should also be considered (Barnes, 1994). To this end, the extent of interactions between aggregates by comparing fluid gels of similar particle size was further studied

(Figure 3.13). Although particles were of similar size (*ca.* 30 μm) it was observed that the two showed different elastic moduli, over a range of volume fractions. Again, elasticity was predominantly dictated by the level of shear applied during the formation process with fluid gels prepared at 400 $s^{-1}$ having a higher elastic modulus than those made at 600 $s^{-1}$. This indicates that aggregates formed where particle growth is limited to a greater extent by shear, results in a reduction in inter-particle interactions; most-likely as a result of the previously defined mechanism, where rapid formation of a gel, due to a higher heating rate becomes broken down, resulting in a surface with fewer sites for further interactions.

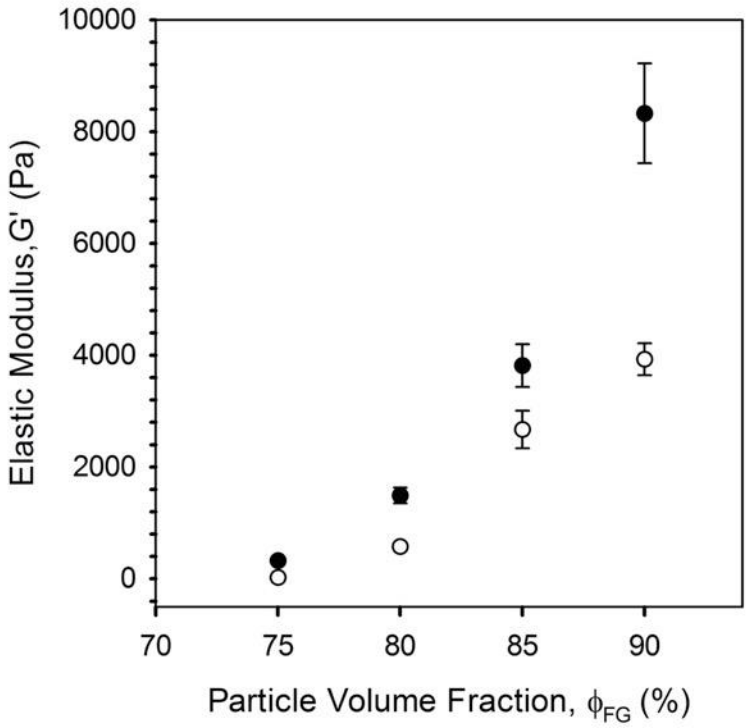


*Figure 3.13: Elastic moduli (G') plotted against volume fraction ($\phi_{FG}$) for fluid gel particles of similar size (ca. 30 μm). Particles were prepared at 400 $s^{-1}$ (1 °C$min^{-1}$) (●) and 600 $s^{-1}$ (5 °C$min^{-1}$) (○).*

### *3.3.2.2. Fluid gel flow behaviour*

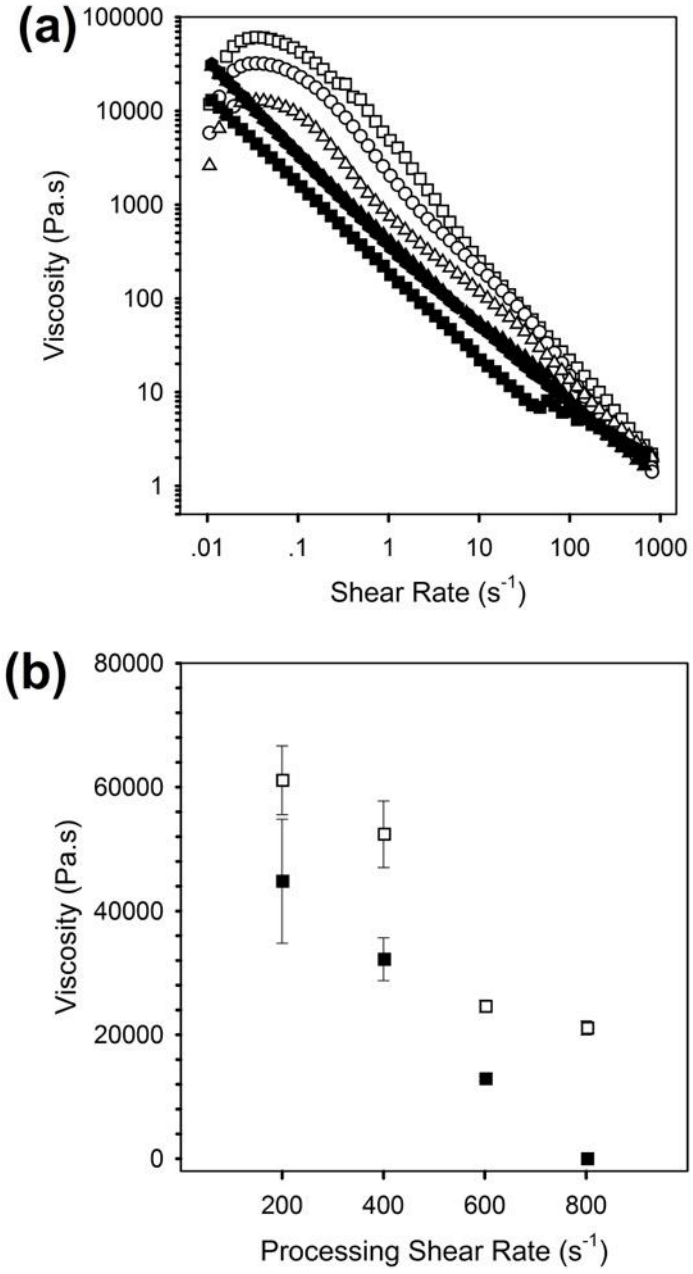


*Figure 3.14: (a) Viscosity curves showing thixotropic behaviour for fluid gels prepared at 1 °Cmin$^{-1}$, 200 s$^{-1}$ (□,■), 400 s$^{-1}$ (○,●) and 600 s$^{-1}$ (△,▲) $\phi_{FG}$90. (Unfilled symbols denote ramp up and filled ramp down.). Data shows the average of three repeats. (b) Fluid gel viscosities at $\eta_{max}$ having been prepared using varying shear rates at 1 °Cmin$^{-1}$ (■) and 10 °Cmin$^{-1}$ (□).*

Flow behaviours of WPI shear gels formed at 1 °Cmin$^{-1}$ are shown in Figure 3.14a. Again, a comparison is made across suspensions with the same phase volume (90 %). Fluid gels exhibit characteristic shear thinning behaviour typical of highly aggregated suspensions (Berli and Quemada, 2000, Quemada, 1998). At low shear rates, systems show an apparent increase in viscosity until a maximum, $\eta_{max}$, is reached; ascribed to stress overshoot during start up (Ravindranath and Wang, 2008, Boukany et al., 2009), increasing as a function of the processing parameters. It was observed that smaller aggregates had lower viscosities than larger aggregates prepared at lower shear rates. This clearly demonstrates that for the same degree of space filling, the more aggregated particles produce a higher viscosity. Values at $\eta_{max}$ (0.03 s$^{-1}$ for all samples) for WPI fluid gels prepared at different shear and heating rates are compared in Figure 3.14b. Increasing the shear rate during production led to a decrease in the suspension viscosity at both heating rates, again due to the lower degree of particle-particle interactions (Figure 3.14b).

With increasing shear rate the viscosity decreases, following shear-thinning behaviour. The non-linearity in the systems is either due to alignment of suspended particles in the direction of flow or to the breakdown of the aggregates (Quemada, 1998). For this reason, sample data is presented for both the upward and downward sweeps. The presence of hysteresis revealed a thixotropic behaviour arising from aggregate breakdown that led to an overall change in the phase volume; as such the viscosity decreases. Additionally, at higher shear rates abruption in the data set is observed within the decreasing sweep. It is suggested that such discrepancies arise through stress tensor at high shear rates, as the particle mass causes momentum transport, resulting in particle-velocity perturbation and collision as the energy is

removed (Savage and Jeffrey, 2006). A second sweep separated by a five-minute recovery period was used to explore the reduction in viscosity with shear. After the recovery time, it was observed that the second sweep followed a similar profile to the decrease in shear observed in the first sweep, shown in Figure 3.15a.

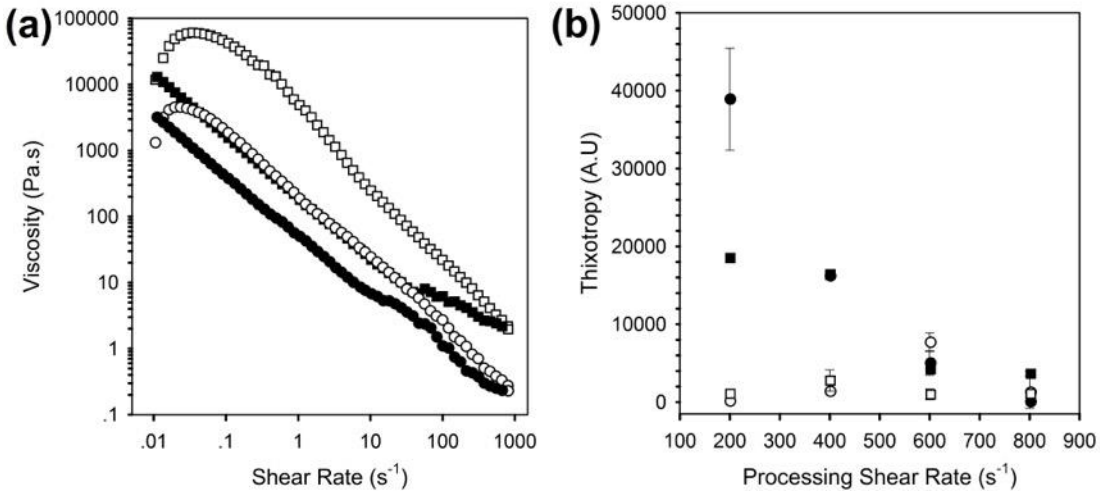


*Figure 3.15: (a) Flow curves for WPI fluid gels (prepared at 200 $s^{-1}$, 1 °C$min^{-1}$) sweep 1 (□,■) and sweep 2 (○,●). A five-minute recovery period was held between sweeps. (Open symbols denote increasing shear rates, filled denote decreasing shear rate.). Data shows the average of three repeats. (b) Thixotropic analysis for WPI fluid gels formulated at 1 °C$min^{-1}$ (●,○) and 10 °C$min^{-1}$ (■,□).*

This suggested that no recovery of the system occurred within this time frame, inferring that the lowering in viscosity observed in the first sweep was caused by permanent damage to the aggregates: this was confirmed by SLS data that showed a shift in the mean size ($D_{4,3}$) from 262 **±13** to 212 **±12** μm (Figure 3.16b). The degree of thixotropy (calculated as the area within the hysteresis loop) was compared across all fluid gels for different processing conditions: heating and shear rates (Figure 3.15b).

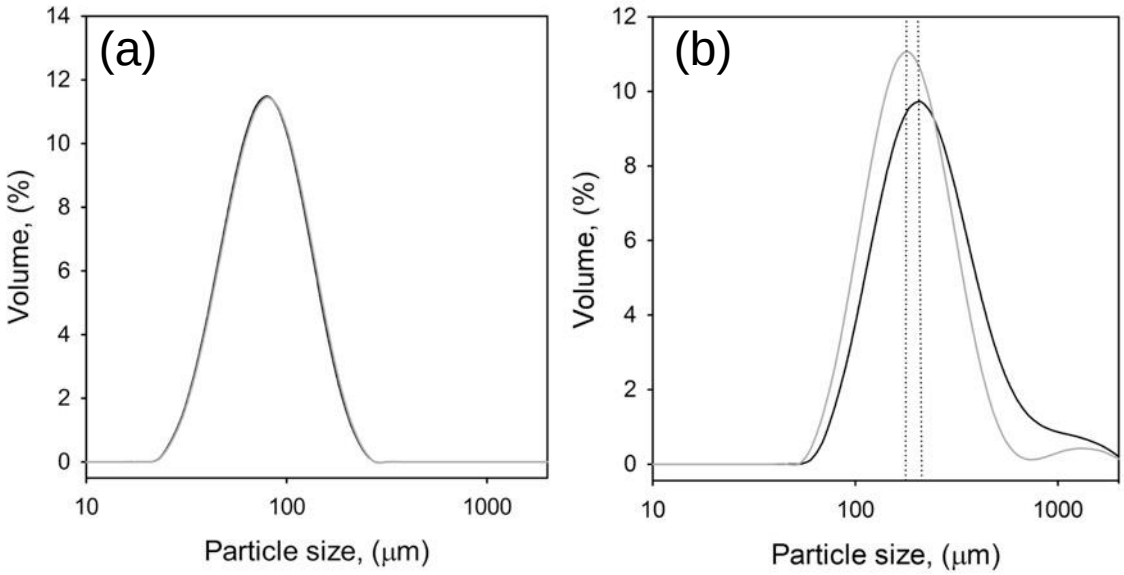


*Figure 3.16: Size distributions obtained using SLS for WPI suspensions pre-thixotropy analysis (black line) and post-testing (grey line) for (a) particles prepared at 800 $s^{-1}$ and 10 °C$min^{-1}$, and (b) particles prepared at 200 $s^{-1}$ and 1 °C$min^{-1}$.*

The evaluation of the hysteresis area revealed that the structural breakdown occurs mainly during the first ramp and is more apparent for fluid gels made at low shear rates (200 $s^{-1}$). This infers that larger aggregates are more easily disrupted in comparison to smaller ones, most-likely due to a fractal nature, where the lower density of the larger aggregates increases the probability of inherent weak spots.

## 3.4. Conclusions

This study presents the formation of micro gel particles prepared in the absence of additives. The data shown has been used to build a qualitative model for the formation of WPI gel particles, and used to describe their subsequent rheological properties. The model proposed is primarily based on the general understanding of particle growth and the aggregation process. Firstly, unfolded proteins interact to form

primary particles. In the second stage these primary particles move into contact with each other becoming weakly bound by relatively weak forces. Ultimately, the particles become more firmly bound as result of covalent bonding, i.e. disulphide bonds, forming secondary aggregates/final particles. It is in this second stage that structural organisation can be controlled through manipulating the rate of aggregation. Fast heating rates promote particles that interact quickly becoming rapidly resistant to shear, as such large aggregates are produced. On the other hand, low heating rates or increasing shear rates lower the rate of aggregation, slowing the strengthening stage, causing particles to be more affected by the flow. Consequently, smaller aggregates or even single resulting particles are produced. Trends in bulk rheology were described through the model proposed for particle formation, resulting in highly tuneable suspensions. Thus, systems show promise within the food industry as low fat, thermally stable ingredients with the ability to build structure within final products.

Although the particles presented within this chapter are thermally stable, owing to their irreversibly denatured structures, their processing still requires a heating step. This may be unfavourable in many food products. For this reason, the formation of particulate suspensions under the influence of shear, by means of cold-set gelation, needs to be studied (Chapter 4.). It was shown within this chapter that kinetics played an important role on the particle intrinsic properties. Therefore, careful control over the gelation rates were studied, with a view to controlling bulk suspension characteristics.

# Chapter 4. *Cold-set particulate suspensions*

***Synopsis***

Gelation kinetics for WPI and WPI/oil systems were studied using varying concentrations of calcium chloride ($CaCl_2$). Rates of aggregation were determined for quiescent systems and used to explain material properties post shearing during gelation. An ageing effect was observed for systems post-production due to a secondary aggregation step, resulting in large aggregates ranging from ca. 150 to ~550 μm. Final particle size was correlated to the $Ca^{2+}$ ion concentration, with a larger extent of aggregation with increasing salt content. Aggregate size had little effect on material response, however. Systems prepared with 50 mM CaCl2 lowered bulk elasticity when compared to the 25 mM systems. Viscoelastic behaviours for mixed WPI/oil systems have been suggested to arise through close packing of the dispersed phases (WPI and oil droplets). This results from an effective phase volume increase, accompanying gelation; where WPI aggregates structure the continuous phase. As such, the rheology exhibited characteristics typical of concentrated emulsions. A mechanistic approach to particle formation was proposed, with an aim to explain resulting material properties.

## 4.1. Introduction

Thermal stability plays a key role within food formulations, with many food components undergoing chemical or physical transitions when heated. However in many cases, especially within protein systems, a heating step is required to induce the needed structuring (Hillier et al., 1980, Stading and Hermansson, 1990). For many refrigerated products such heating is unfavourable, therefore newer routes to build structure are needed. One proposed method is cold-set gelation. Here, proteins are first denatured at a pH where electrostatic repulsive forces prevent the polymers from aggregating (Barbut and Foegeding, 1993). Aggregation can then be achieved at reduced temperatures (room temperature instead of 80 °C) through salt bridging. The previous chapter focused on thermally produced WPI suspensions, showing a close correlation between suspension rheology and formation kinetics. Therefore, this research looks to control gelation kinetics under a cold-set mechanism, in order to formulate particulate suspensions with controllable intrinsic properties. These results would lead to a potential rheological modifier, with applications throughout thermally sensitive products.

## 4.2. Materials and Methods

### *4.2.1. Materials*

Whey protein isolate (WPI) was obtained from Kerry Ingredients, Listowel, Ireland (WPI, W994, S-493391) and used without further purification. WPI composition as stated by the supplier was 91.0 % protein, moisture 4.0 %, fat 1.0 %, ash 3.5 % and lactose 0.5 %. Mineral content of the WPI was: Ca – 0.50, P – 0.65, Na – 0.10, K – 0.15, Mg

– 0.02 and Cl - 0.02 %. High oleic oil (from sunflower) was obtained from Cargill (Cargill Inc., BE). Sodium azide, sodium hydroxide and calcium chloride were purchased from Sigma-Aldrich (Sigma-Aldrich, UK).

### *4.2.2. Preparation WPI and WPI/Oil systems*

#### *4.2.2.1. Preparation of WPI stock solutions*

Whey protein stock solutions (5.36% (w/w)) were prepared by dispersing WPI in deionised water. An anti-microbial, sodium azide (0.02% (w/w)) was added to all solutions to enhance storage times. Solutions were stirred overnight at ambient conditions until completely hydrated, pH adjusted to 8.0 using NaOH (5 M) and heated at 85 °C for 15 minutes. Solutions were then rapidly cooled using an ice bath and stored at 5 °C until further usage.

#### *4.2.2.2. Preparation of emulsions*

Oil in water emulsions were prepared by the addition of high oleic sunflower oil to WPI stock solution (oil fractions ranging from 10 to 40% (v/v)). Systems were subsequently mixed in a high shear mixer (Silverson, SL2T) at 4,000 rpm for 10 minutes.

#### *4.2.2.3. Gelation of WPI and WPI/Oil systems under shear*

A jacketed pin stirrer (unit dimensions shown in Figure 4.1a) was used to process WPI solutions and emulsions undergoing gelation. WPI, emulsion and salt solutions were pumped into the mixing chamber at a rate resulting in a 10 minute residence time at either 1,000 or 2,000 rpm mixing speeds (shaft speed). Where the oil

fraction was increased, salt concentrations were modified to retain the same molar ratio resulting in final concentrations of 5 % (w/w) WPI and 25, 40 and 50 mM $CaCl_2$.

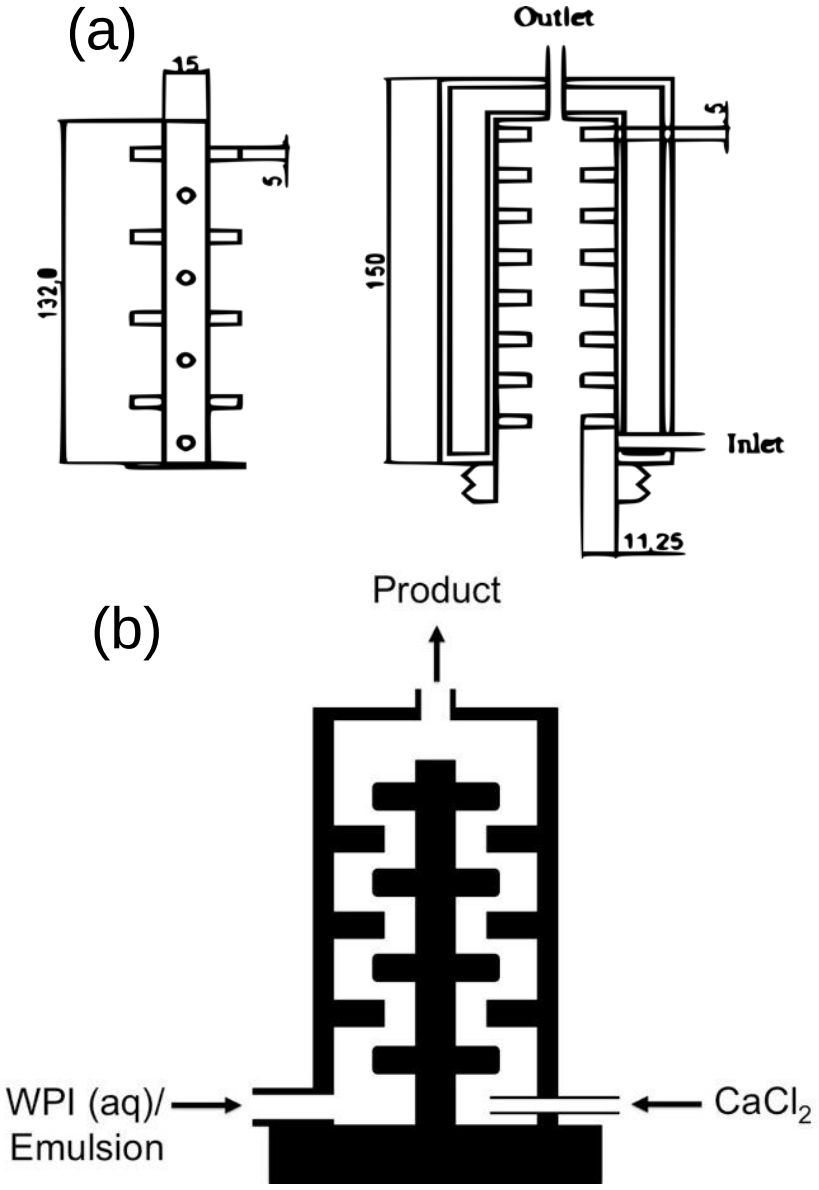


*Figure 4.1: Schematic diagrams of a jacketed pin-stirrer (also known as a c unit). (a) shows unit dimensions in mm. (b) Sol/emulsion entry point has been highlighted (left) and salt injection port (right). The system is then sheared as a function of the retention time and pushed through the exit at the top.*

### *4.2.3. Rheological Analysis*

#### *4.2.3.2. Gelling Kinetics*

**Experimental design for cold-set kinetics**:

Initially a dynamic approach to study the rate of gelation was undertaken in a similar fashion to Fernández Farrés and Norton (2014); whereby a rheometer was used to apply shear and measure the evolution of viscosity. Here however, as a pH change could not result in the release of crosslinking ions (shown by Fernández Farrés *et al.*), several diffusion techniques were tested.

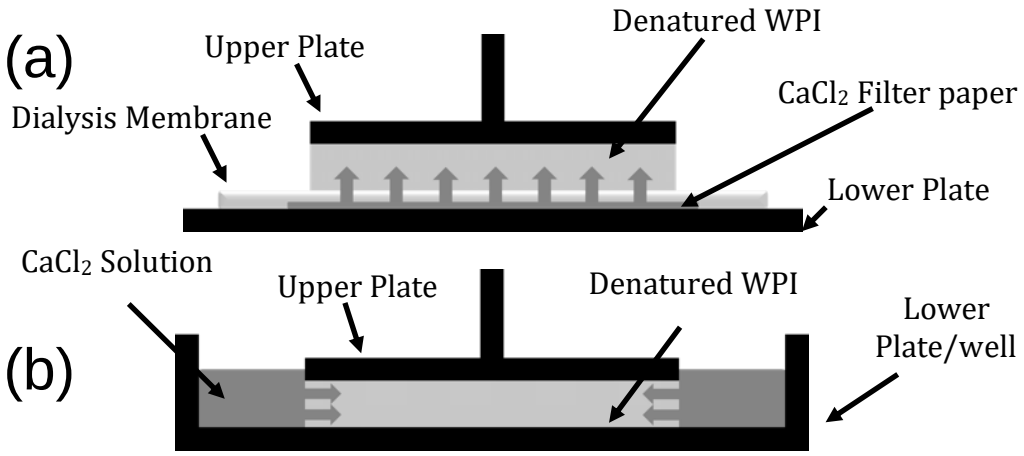


*Figure 4.2: Schematic diagrams of rheometer set-ups for diffusion of cross linker into the denatured WPI sol, whereby diffusion occurs: (a) across a membrane from the bottom-up, and (b) from a surrounding well (sides-in).*

In the first instance, diffusion of $Ca^{2+}$ through a membrane was studied. In this instance filter paper was completely saturated with calcium chloride solution, and placed on the rheometer lower plate. Dialysis membrane was used to cover the filter paper and WPI solution placed on top (in contact with the upper geometry) (see Figure 4.2a). The second method, shown in Figure 4.2b, involved the addition of $CaCl_2$ solution

into a well surrounding the geometry's gap. Thus, changing the diffusion of ions from diffusing vertically to horizontally through the WPI.

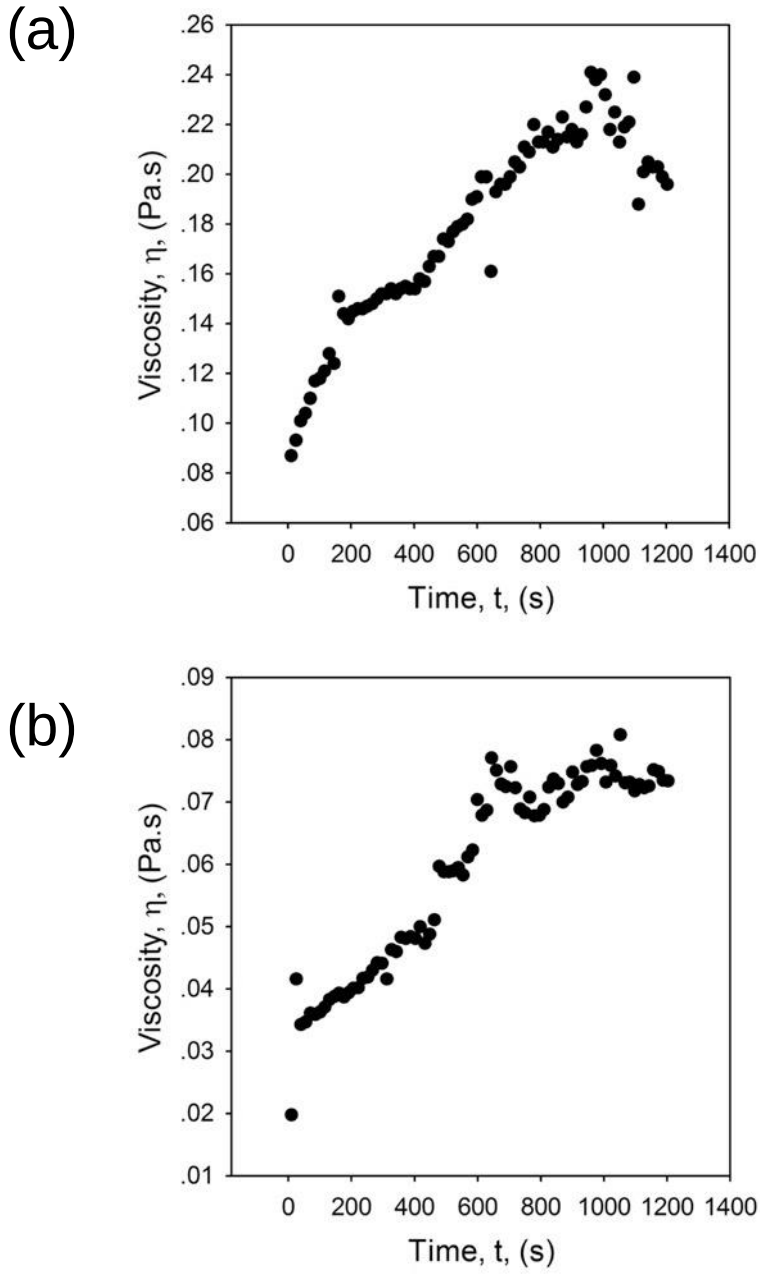


*Figure 4.3: Flow profiles obtained for WPI (5 % (w/w)) systems undergoing dynamic cold-set gelation at 50 $s^{-1}$ through the addition of $CaCl_2$ via: (a) diffusion through dialysis tubing, and (b) diffusion form a well surrounding the geometry. Data presented shows only a single run, as the method was not adopted for the study.*

Figure 4.3 shows the flow profiles obtained for both systems (diffusion vertically and horizontally). Both gelation profiles showed an increase in viscosity as a function of time, resulting from the formation of flocculated networks. However, noise within the gelling curve, most likely as a result of heterogeneous gelation, prevented the gelling rates from being obtained. (Figure 4.3 shows a single run, thus no error bars presented) Increased homogeneity was therefore sought by briefly mixing the calcium salt into the formulation before sample addition into the rheometer. This led to smoothing of the profiles, shown in Figure 4.4. However, inconsistency between samples still prevented kinetics to be calculated.

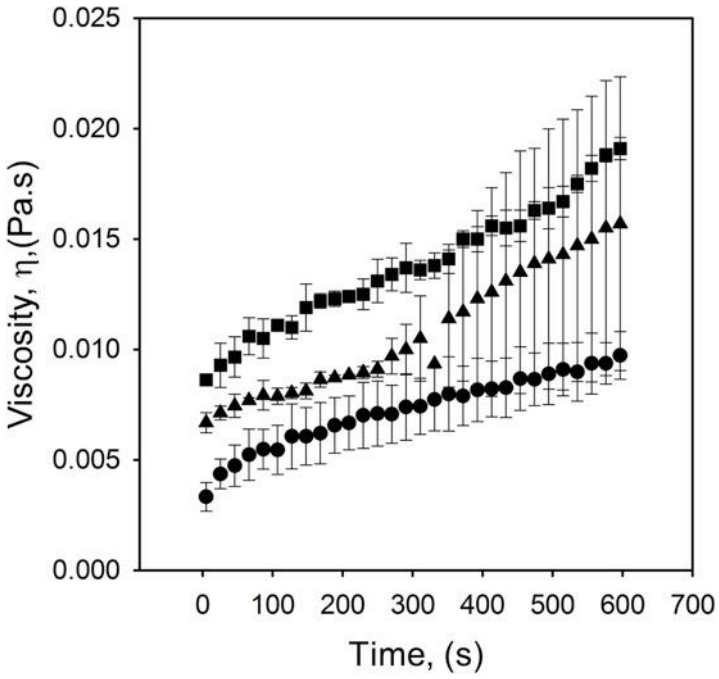


*Figure 4.4: Flow profiles obtained for cold-set WPI systems (25 mM $CaCl_2$, WPI 5% (w/w)) undergoing gelation with a preparation shear field of (●) 50 $s^{-1}$, (■) 100 $s^{-1}$ and (▲) 200 $s^{-1}$.*

It was therefore decided to calculate kinetics from equivalent quiescent gels (formulations of the system remained the same, however shear was not applied), using an oscillatory technique (data presented later in the results section, Figures 4.6 and 4.8).

#### *4.2.3.1. Dynamic oscillatory measurements*

Gelling curves were obtained using a serrated parallel plate setup (25 mm) 1 mm gap height at 20 °C. WPI and emulsion systems were first mixed with $CaCl_2$ (cross-linking agent) and then placed in the rheometer. A single frequency experiment was run at 1 Hz, 0.5 % strain for 30 minutes whilst recording the evolution of the storage and loss moduli (G' and G'' respectively). (For further detail see Appendix i)

#### *4.2.3.2. Dynamic oscillatory measurements*

Testing was conducted both immediately and 48 hours post-processing using a Bohlin Gemini HR Nano stress-controlled Rheometer (Malvern Instruments Ltd, UK). After 48 hours samples were placed on a vortex shaker for 10 seconds before conducting analysis at 20 °C using a 40 mm parallel plate setup, 1 mm gap height. (For further theory see Appendix i)

**Amplitude sweeps:**

Amplitude sweeps were conducted at 1 Hz using controlled strain, ranging between 0.1 and 100 %.

**Frequency Sweeps:**

Frequency sweeps were obtained between 0.1 and 10 Hz at controlled strain. The strain was determined by amplitude sweeps as detailed above, using a deformation within the linear viscoelastic region (LVR) for all systems tested.

### *4.2.4. Static light scattering (SLS)*

A MS2000 Mastersizer with attached Hydro SM manual small volume dispersion unit (Malvern Instruments Ltd, UK) was used to obtain size distributions. Distributions are the average of three repeats. Particle sizes were calculated based upon the Mie theory, thus particles were assumed to be monodisperse, homogenous spheres. Samples were prepared by diluting gel particles in distilled water to avoid multiple scattering and pre-defined software refractive indices (RI) for the water and protein were used: 1.33 and 1.6 respectively. Additionally, in the binary systems containing protein and oil, the refractive index of the gel was used, 1.6, following initial experiments that did not identify significant changes in distributions when analysed using either the refractive index of the oil or protein. (For further theory see Appendix i)

### *4.2.5. Zeta-potential determination*

The zeta-potential (ζ-potential) of WPI as a function of pH was investigated using electrophoretic mobility, via a dynamic light scattering (DLS) technique with a Zetasizer Nano Series ZS (Malvern Instruments, UK). Zeta-potential measurements were carried out on protein concentrations of 0.1% (w/w), in a capillary cell designed for electrokinetic measurements. Zeta-potential measurements are reported as the average

of three repeat measurements, with error showing the 95% confidence interval, Figure 4.5.

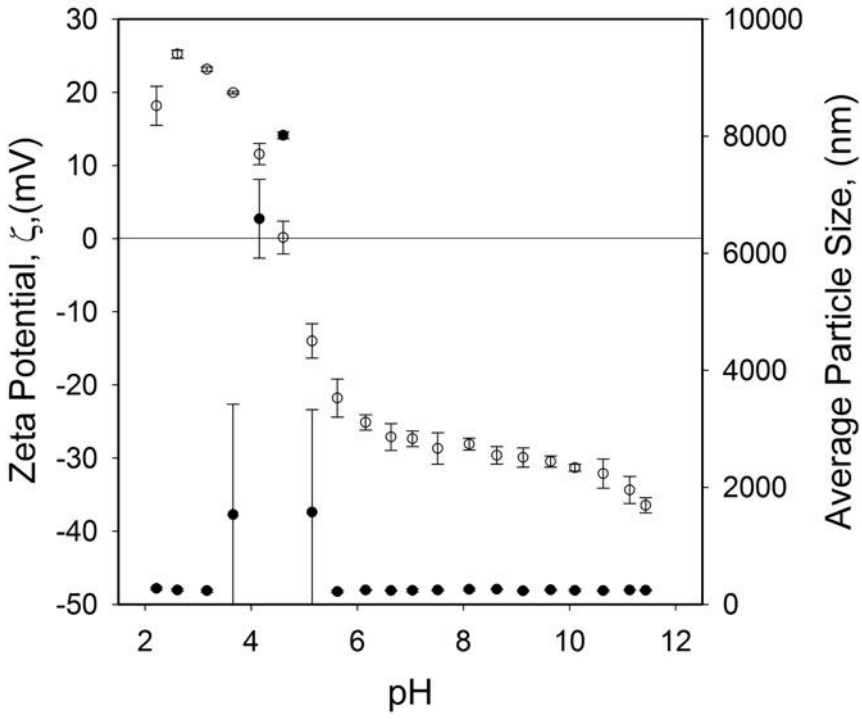


*Figure 4.5: Zeta-potential measurements obtained via titration method from pH 12 to pH 2 using NaOH and HCl: (○) indicate zeta potential (left axis) and (●) show mean particle sizes.*

### *4.2.6. Optical light microscopy*

Samples visualised immediately post-processing were firstly diluted on exiting the pin stirrer to avoid any further aggregation; otherwise systems were placed on a vortex shaker for 10 seconds before being diluted. A Brunel SP300-fl (Brunel Microscopes Ltd, UK) optical light microscope fitted with an SLR camera (Cannon EOS Rebel XS, DS126 191) at 20x and 40x optical magnification was used to image the

particles. Slides were prepared by addition of 50 μL of sample to a microscope slide (VWR, UK) and covered with a coverslip (Thickness no.1, VWR, UK).

## 4.3. Results and Discussion

### *4.3.1. Cold-set gel kinetics: Quiescent systems*

#### *4.3.1.1. Salt concentration dependence*

The negative zeta-potential of the protein at basic conditions (pH 8.0, Figure 4.5) prevented spontaneous aggregation of the polymers during heating. However, pH induced conformational change from dimeric to monomeric, coupled with thermal pre-treatment results in the exposure of sulphydryl and carboxyl groups (Bhattacharjee et al., 2005, Sawyer, 1968, Bolder et al., 2007), which are highly susceptible to ion cross-linking (Barbut and Foegeding, 1993, Hongsprabhas and Barbut, 1996, Hongsprabhas and Barbut, 1997b, Hongsprabhas and Barbut, 1997a, Hongsprabhas et al., 1999). This basis was used to force the WPI solutions through a sol-gel transition; whereby charge screening through the addition of salt led to subsequent bridging and aggregation. The gelation process was monitored using small deformation rheology, presented in Figure 4.6; change in storage modulus as a function of time for WPI systems with varying concentrations of cross-linker ($Ca^{2+}$).

The addition of 10 mM $Ca^{2+}$ resulted in no change in G' over the 30 mins tested, even though previous studies have shown similar systems to form a gel network (Barbut and Foegeding, 1993). The differences shown here are believed to be a function of the shorter pre-treatment (Ni et al., 2015, Hongsprabhas and Barbut, 1996, Hongsprabhas and Barbut, 1997a), and are likely to arise from a lower degree of protein unfolding

(Bolder et al., 2007). However, such systems were still accompanied by a change in turbidity, suggesting the formation of small particulates, insufficient in number to form the continuous 3-dimensional network (Ako et al., 2010, Nicolai, 2016).

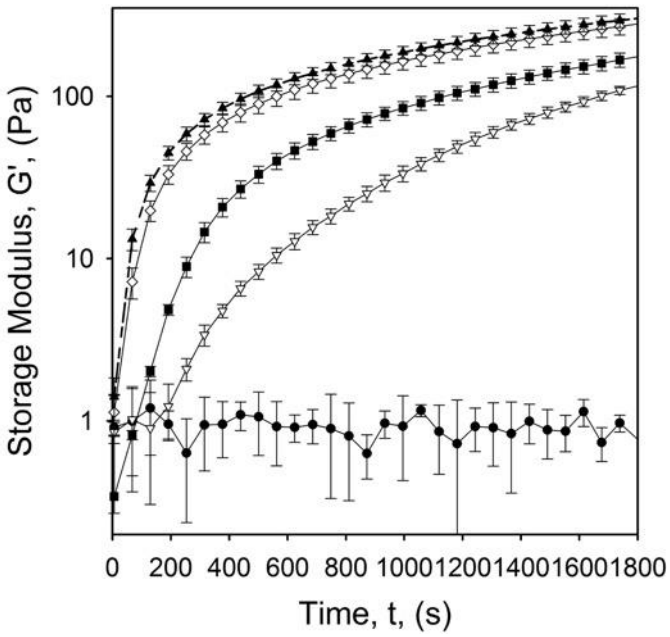


*Figure 4.6: Single frequency (1Hz, 0.5 % strain) spectra obtained for WPI systems undergoing cold set gelation with increasing $Ca^{2+}$ concentrations: (●) 10 mM, (▽) 25 mM, (■) 40 mM, (○) 50 mM, and (▲) 100 mM.*

Further increasing the salt concentration resulted in the formation of self-supporting gel networks, with storage moduli (G') after 1800 s ($t_e$) dependent on concentration (Table 4.1). Such observations have been well documented for quiescent gels (Bryant and McClements, 2000, Brodkorb et al., 2016, Hongsprabhas and Barbut, 1997a), as a consequence to changes in the ionic environment; where an increase in electrostatic shielding, and degree of ion bridges between polymer chains form stronger networks. The effect of cation concentration on the change in storage modulus over the

30 minutes studied was derived using a concentration vs G' plot (Figure 4.7) similarly to Fernández Farrés and Norton (2014) and Gabriele et al. (2009). The correlation between ΔG' (change in storage modulus) at $t_e$ (1800 s) and cation concentration has been shown for the cold-set quiescent systems (Equation 4.1):

$$\Delta G' = 317(1 - e^{-0.06[Ca^{2+}]})^{4.2}$$

*Equation 4.1: Relationship between $Ca^{2+}$ concentration (mM) and storage modulus.*

Furthermore, Table 4.1 highlighted an inverse relationship between gelation onset time ($t_0$) and increasing $Ca^{2+}$, previously reported for cold set gels (Hongsprabhas et al., 1999, Marangoni et al., 2000).

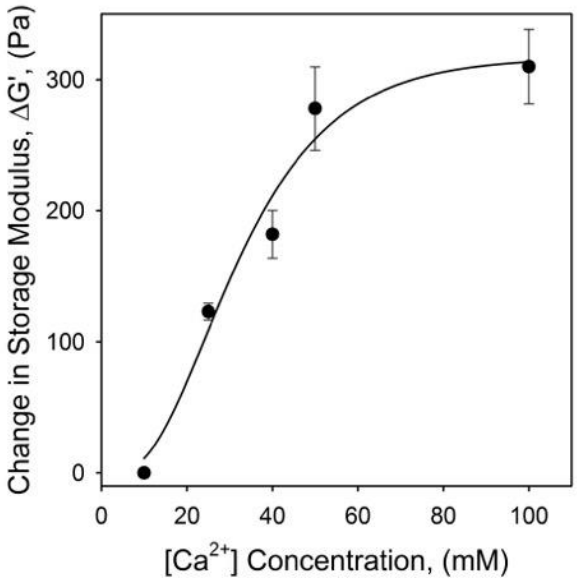


Figure 4.7: Relationship between the change in gel strength at $t_e$ (1800 s), as described by the storage modulus (ΔG'), as a function of the salt ($CaCl_2$) added. Equation of the line $y = 317\left(1 - e^{-0.06[x]}\right)^{4.2}$, was used to give the parameters in Equation 4.1.

*Table 4.1: Table showing gelation onset times for WPI systems undergoing gelation with increasing additions of salt. Table also shows storage moduli at the point of gelation ($t_o$) and at the end of the test ($t_e$ – 1800 s).*

| $Ca^{2+}$ conc. | Onset | | Test End | |
|---|---|---|---|---|
| ($x$) | $t_o$ (s) | G' (Pa) | $t_e$ (s) | G' (Pa) |
| 10 mM | **N/a** | | | |
| 25 mM | 154 | 0.84 **±0.6** | 1800 | 116.45 **±6.4** |
| 40 mM | 86 | 0.86 **±0.4** | 1800 | 175.70 **±18.1** |
| 50 mM | 18 | 1.19 **±0.4** | 1800 | 279.52 **±31.8** |
| 100 mM | 8 | 1.41 **±0.4** | 1800 | 303.37 **±28.4** |

The kinetics were further probed by modelling gelling curves as a power function, calculating the gradients (gelation rate coefficient), $k_c$, and reaction orders, $n$ (Equation 4.2):

$$y(x) = k_c x^n$$

*Equation 4.2: Power function applied to gelling curves (Figure 4.6) for calculating the gelation rate coefficient, $k_c$, and the order of reaction, n, where x is the concentration of calcium added.*

Parameters for $k_c$ and $n$ have been tabulated in Table 4.2. It was observed that increasing the salt concentration led to an increase in the gelation rate coefficient ($k_c$); corresponding with the shift in $t_0$. Similar observations showing faster kinetics as a function of salt concentration have previously been reported (Marangoni et al., 2000); where the increased degree of electron shielding provides a route to overcoming the energy barrier needed for spontaneous aggregation, resulting in the more rapid formation of protein structural units, "flocs" (Bryant and McClements, 2000, Kuhn et al.,

2010, Bryant and McClements, 1998, Foegeding et al., 2002, Hongsprabhas and Barbut, 1997b, Totosaus et al., 2002).

*Table 4.2: Parameters obtained from applying the power law model (Equation 4.2), describing the rate of gelation occurring in the WPI systems with the addition of salt.*

| $Ca^{2+}$ conc. ($x$) | $k_c$ | $n$ | $R^2$ |
|---|---|---|---|
| 10 mM | **N/a** | | |
| 25 mM | 2.0 x$10^{-5}$**±1.4x$10^{-5}$** | 2.08**±0.066** | 1.00 |
| 40 mM | 0.01**±0.0002** | 1.29**±0.007** | 0.998 |
| 50 mM | 0.34**±0.06** | 0.90**±0.013** | 0.999 |
| 100 mM | 0.64**±0.06** | 0.82**±0.013** | 0.999 |

A change in reaction order from secondary to first with increasing salt concentration (from 25 to 40 mM) can be observed through the order coefficients ($n$) (Table 4.2). Similar work previously published by Hongsprabhas et al. (1999) showed a transition in rate constants for cold-set WPI gels with increasing salt concentrations. It was proposed that the balance between charge screening and crosslinking ($Ca^{2+}$ bridging), result in the observed change in reaction order; where at low salt concentrations competition between the two mechanisms occurs. It is suggested in this study that the same two phenomena are observed. At low concentrations, gelation is controlled by two steps: the first, dispersion and formation of the localised salt concentrations which provide enough screening between the negatively charged proteins to come into close proximity, followed by arrangement of the polymer and the formation of an ionic bridge. However, as the salt concentration is increased (> 40 mM), the time required for charge dispersion becomes negligible, as sufficient salt in present to inhibit the repulsion between protein throughout the system, shifting the rate limiting

step towards the secondary crosslinking stage, causing a transition to first order kinetics.

#### *4.3.1.2. Oil fraction dependence*

The effect of an included oil phase on cold-set WPI gelation is presented in Table 4.3 and Figure 4.8.

*Table 4.3: Parameters obtained from applying the power law model (Eq. 4.1), describing the effect of oil fraction on the rate of gelation for WPI systems with the addition of 25 mM and 50 mM $CaCl_2$.*

| Oil Frac. ($x$) | 25 mM $Ca^{2+}$ | | | 50 mM $Ca^{2+}$ | | |
|---|---|---|---|---|---|---|
| | $k_c$ | $n$ | $R^2$ | $k_c$ | $n$ | $R^2$ |
| 10 % | $1.3 \times 10^{-5} \pm 2.2 \times 10^{-5}$ | $2.27 \pm 0.16$ | 0.99 | $0.092 \pm 0.045$ | $1.04 \pm 0.06$ | 0.98 |
| 20 % | $1.0 \times 10^{-5} \pm 2.7 \times 10^{-5}$ | $2.37 \pm 0.30$ | 0.99 | $0.27 \pm 0.28$ | $0.93 \pm 0.11$ | 0.99 |
| 30 % | $9.8 \times 10^{-6} \pm 4.4 \times 10^{-5}$ | $2.36 \pm 0.35$ | 0.99 | $0.39 \pm 0.95$ | $0.88 \pm 0.19$ | 0.99 |
| 40 % | $5.1 \times 10^{-8} \pm 1.3 \times 10^{-4}$ | $3.12 \pm 1.36$ | 0.99 | $0.52 \pm 0.53$ | $0.88 \pm 0.10$ | 0.99 |

Here the $Ca^{2+}$ molar ratio was kept constant at either 25 mM (Figure 4.8a) or 50 mM (Figure 4.8b). Gelling curves obtained for 25 mM systems showed irregular gelation with a large variation between repeats. Such poor reproducibility has been reflected in values obtained for $k_c$ and $n$ where no significant change is observed across all oil fractions. These observations are likely due to creaming of the emulsion droplets (visually observed - shown in the insert to Figure 4.8aii), as a result of slow aggregation kinetics, leading to regions of high and low oil concentrations and subsequently inhomogeneous gels.

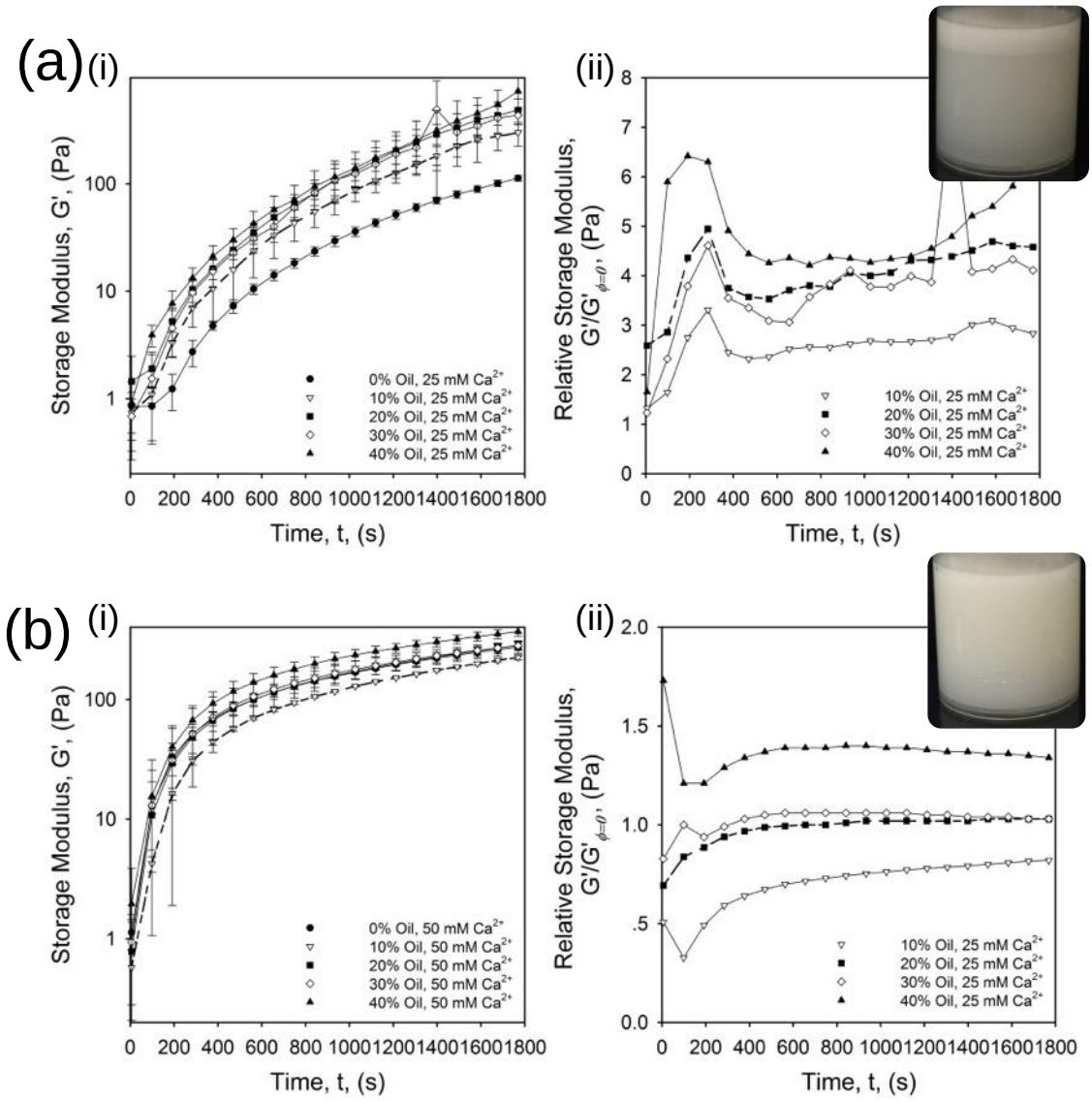


*Figure 4.8: Mechanical spectra obtained for WPI/Oil systems undergoing gelation with the addition of (a) 25 mM and (b) 50 mM $CaCl_2$: (●) 0 % (v/v), (▽) 10 % (v/v), (■) 20 % (v/v), (◇) 30 % (v/v), and (▲) 40 % (v/v). (i) shows the evolution of G' over time and (ii) shows the relative term of the same data, where G' for the oil fractions have been normalised by G' for no oil systems ($G'_{\phi=0}$). Inserts show the gelled systems at time, $t_e$.*

Gels formed using 50 mM, however, did not cream (as shown by the insert to Figure 4.8bii), with the oil becoming trapped due to rapid formation of a gelled network; as shown by the increase in $k_c$ values obtained for 50 mM systems. Therefore, gelling

profiles obtained for these systems exhibited greater reproducibility, with discrete errors.

An overall increase in gel strength was observed at $t_e$ when increasing the oil fraction from 10 to 40 %, with the two intermediate fractions resulting in the same storage moduli. Initial weakening (decrease in G') of the gel system was observed with the addition of 10 % oil (shown in Figure 4.8bii, where relative G' values ($G'_{\phi=10}/G'_{\phi=0\,oil}$) are less than 1). Here droplets appear to act as inactive fillers (Dickinson and Chen, 1999, Geremias-Andrade et al., 2016), whereby interactions between the two phases (oil and gel) are postulated to be hindered though their surface chemistries; arising from protein denaturation and adsorption to the oil interface, sterically preventing the arrangement needed for ion bridging between WPI fractal aggregates and oil droplets during gelation (Hongsprabhas et al., 1999). Further increasing the volume fraction of the dispersed phase to 40 % had the opposite effect on gel modulus, strengthening the matrix; highlighting a change in structural mechanism. It is believed that in this case, although oil droplets still do not interact with the surrounding matrix, as previously hypothesised, a more compacted gel network is formed whereby a larger degree of volume is occupied by the oil (Sok Line et al., 2005, Mao et al., 2014). Intermediate oil fractions with the same moduli are therefore argued to show a transition between the two mechanisms, where disruption of the network becomes compensated for with increasing system density.

### *4.3.2. Cold-set WPI suspensions: The effect of shear*

#### *4.3.2.1. Particle size analysis*

Cold-set WPI microgel systems were prepared through the addition of the $Ca^{2+}$ to denatured WPI within a shear environment. Size distributions were obtained by immediately diluting the microgel systems on exiting the pin-stirrer to prevent any further secondary aggregation (Figure 4.9).

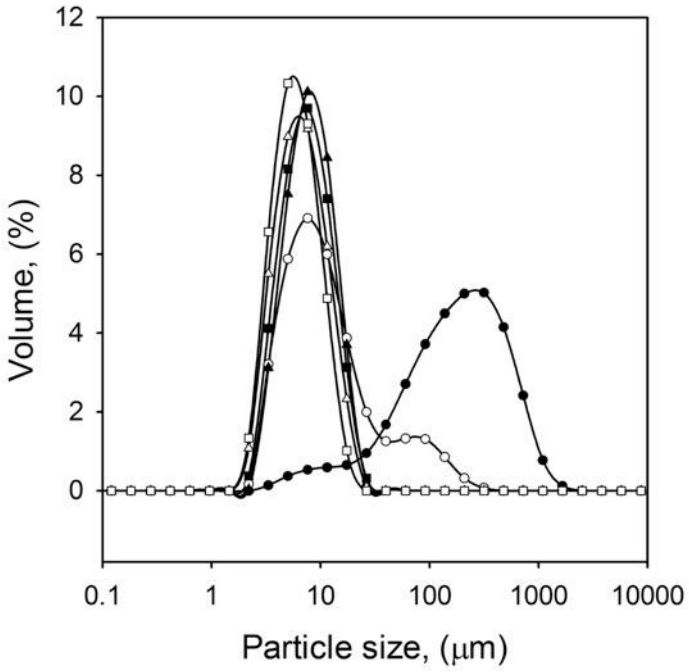


*Figure 4.9: Static light scattering particle size distributions for WPI systems immediately diluted on exiting the pin stirrer set to a rotation speed of 1000 rpm (closed markers) and 2000 rpm (open markers): (●/○) 25 mM, (■/□) 40 mM and (▲/△) 50 mM $Ca^{2+}$.*

It was observed that both salt concentration and applied shear had little effect on the resulting particle size, with distributions showing good agreement with each other, centred over 8 μm. For the lowest salt concentration (25 mM), bimodal distributions were observed; the original peak again centred at ~8 μm and a second peak at higher

particle sizes (~100 μm and ~500 μm for systems prepared at 2000 rpm and 1000 rpm respectively). This was explained by aggregation of the protein within the exit tube on a time scale dictated by its length. It is argued that aggregation at this point shows an inverse relationship to the gelation kinetics previously described. In this case, where the residence time within the mixing chamber remained constant for all systems, more rapid particle formation resulted in them being exerted to longer timescales within the shear regime. As such, where gelation has occurred at a faster rate, large particulates form, becoming broken down within the shear flow, as previously reported for sheared microgel systems, slowing further structuring (Moakes et al., 2015a, Fernández Farrés et al., 2013). Additionally, faster aggregation results in less ordered structures (Hongsprabhas et al., 1999, Taylor and Fryer, 1994), potentially burying linkage sites within the particle (Alting et al., 2002); this has been shown via schematic diagram, Figure 4.10.

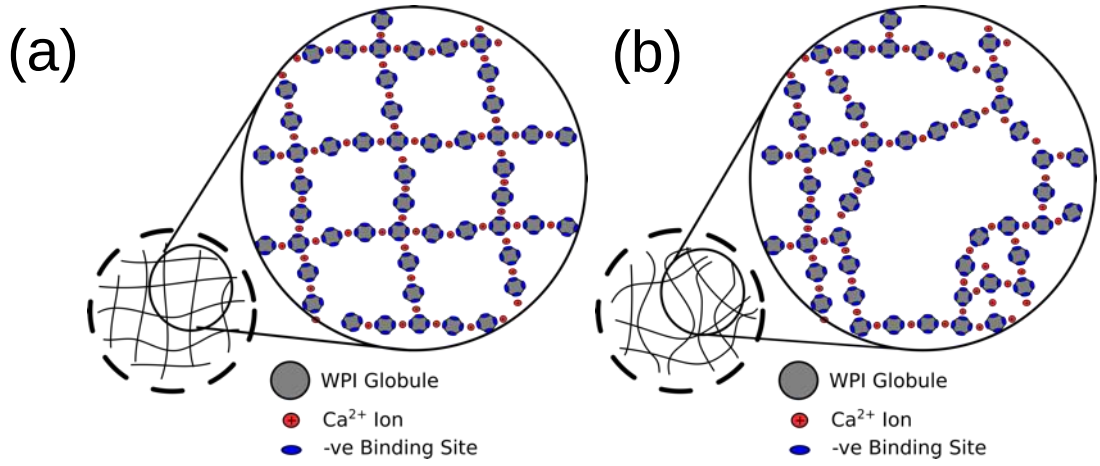


*Figure 4.10: Schematic representations showing the microstructures of WPI cold-set micro-particles. (a) Regular network, where a well-ordered structure exposes binding sites for further aggregation. (b) Less ordered structure due to more rapid aggregation of the WPI globules, sterically burying binding sites within the gel network slowing further aggregation steps.*

Post-shear effects were investigated through particle size analysis after a 48 hr storage period. Systems were first agitated to remove any weak particle-particle interactions as detailed by Garrec et al. (2013), and mean sizes (shown in Figure 4.11) obtained from particle size distributions (Figure 4.12).

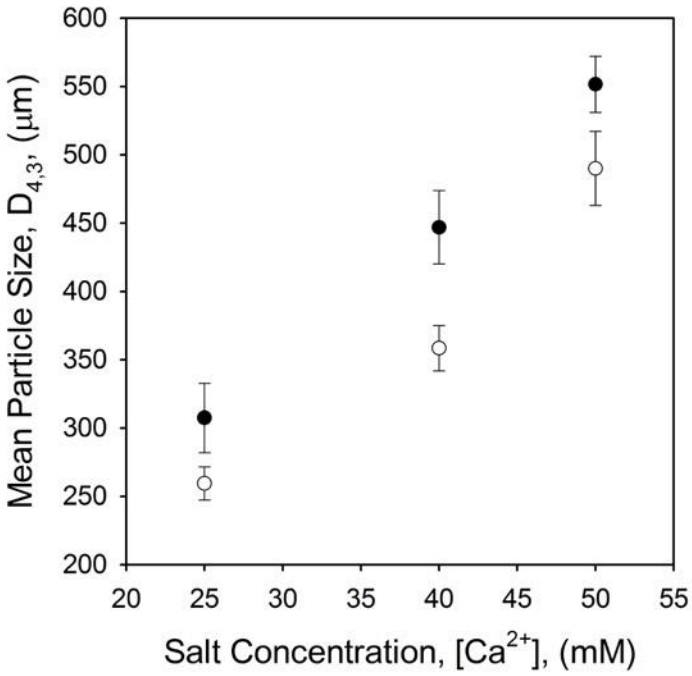


*Figure 4.11: Mean particle sizes ($D_{4,3}$) obtained from static light scattering distributions for WPI systems 48 hrs post production: pin stirrer set to 1000 rpm (closed markers) and 2000 rpm (open markers) rotation speed.*

Ageing effects were observed through particle growth across all systems; where a secondary aggregation step, aggregation of the primary aggregates shown in Figure 4.9, resulted in large aggregates termed "final particles". A clear dependency on $Ca^{2+}$ can be seen for particles prepared at both stirrer rates, highlighting a strong linear correlation to larger particle sizes as the concentration increased. Additionally, where a larger extent of shear was applied during processing comparable particle sizes post-ageing

were lower. Such observations are argued to arise from the degree of unbound salt post-shearing.

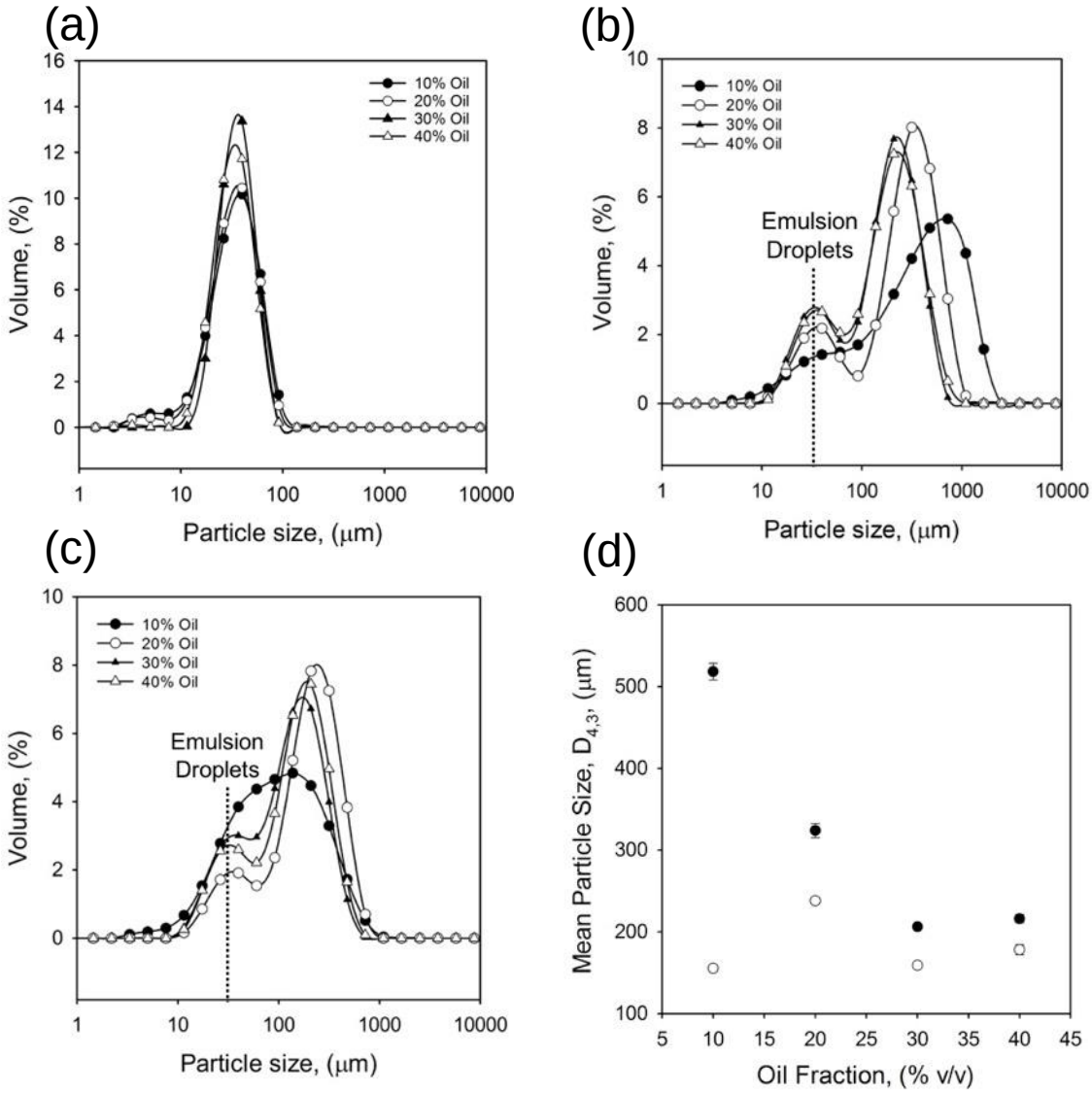


*Figure 4.12: Particle size distributions for: (a) Pre-emulsions before gelation, (b) cold-set emulsion-WPI systems after 48 hrs (25 mM), (c) Cold-set emulsion-WPI systems after 48 hrs (50 mM), and (d) Average particle sizes ($D_{4,3}$) obtained 48 hrs post production using static light scattering distributions for: WPI/Oil systems prepared at to 1,000 rpm rotation speed and 25 mM (closed markers) and 50 mM (open markers).*

Particle growth within the processing unit was previously shown to be the same across all systems (Figure 4.9), to this extent it is assumed that the same concentration of $Ca^{2+}$ becomes bound within the particles in each system. Therefore, surplus cross-linker post-shear, as a function of the initial concentration, gives rise to the varying degrees of secondary aggregation. Similar secondary aggregation of primary particles has already been shown for heat set WPI gel particles (Chapter 3), where final particles were comprised of clustered primary aggregates, formed in the initial stages of heat denaturation and aggregation (Moakes et al., 2015a). Here, the size of the particles were shown to be a function of the number of primary aggregates forming each final particle, described empirically by Berli et al. (1999) (Equation 3.4 (Chapter 3)). In this work presented here, the final particle sizes can be modelled in the same way, where particles are grown from clusters of primary aggregates formed within the shear field (Figure 4.9). Resulting sizes become a function of the salt content, $k \propto [Ca^{2+}]$, for systems having undergone shear at a given, singular rate.

Figure 4.12 shows particle size distributions for WPI cold set gels as a function of oil volume. Size distributions for pre-emulsions prepared prior to the gelation step, highlight no changes in droplet size as a function of the oil, with all distributions centred over 30 μm (Figure 4.12a). The same peaks are observed in both sets of distributions for cold-set systems (both prepared at 25 and 50 mM $Ca^{2+}$), centred again *ca.* 30 μm, however, additional secondary peaks at large particle sizes are observed, relating to the formation of primarily gelled particles (Figure 4.12b and c, 25 and 50 mM respectively). For systems prepared using 25 mM $Ca^{2+}$, a clear shift in particle size as a function of the oil content can be seen, Figure 4.12d. It is argued that as the oil fraction increases, the larger degree of space filling results in confinement of the aqueous phase, restricting

growth of the particles throughout the secondary aggregation step. Thus, the average particle size becomes reduced, plateauing at around 30%, shown in Figure 4.12d. Therefore, particles formed through steric confinement at higher volume fractions can no longer simply be described by the previously presented equation for particle growth (Equation 3.4, Chapter 3), needing a term to describe the non-gelling volume within the system. Equation 4.4 builds on the original model proposed by Berli et al. (1999) factoring in the degree of free space within a phase separated system. Hence particles can grow to a limit determined by confinement of the oil droplets. As such, particle size ($D_a$) at any given time, *t*, becomes a function of the aggregation rate, however the extent of aggregation becomes limited by the extent of oil packing ($\phi$).

$$D_a = \phi - (1 + k(t - t_0))^{-\frac{\phi}{\phi_{max}}}$$

*Equation 4.3: Adapted equation based on an original model for the aggregation of soy protein by Berli et al. (1999), showing free volume as the limiting factor for particle growth: where $D_a$ is the degree of aggregation within in the final particle, k is a rate constant, t are given times, and $\phi$ is the packing fraction of oil droplets.*

#### *4.3.2.1. Microscopy*

Figure 4.13 shows a typical micrograph for cold-set WPI/oil systems having undergone sheared-gelation, stored (48 hrs) and agitated. Micrographs complimented turbidity changes, showing the presence of a globular gel structure. A high degree of anisotropy can also be seen for the particles, with irregular morphologies and large size distributions typical of sheared systems; similarly observed for thermally set WPI particles (Moakes et al., 2015a). Additionally, images visually depicted low levels of oil

entrapment across all systems, with few droplets becoming trapped within the gelled matrices. Again, such observations correspond to the proposed routes for particle formation: where droplets remain in the continuous phase by either providing breakage points during the agitation step, or by resulting in a separated system whereby the droplets confine the growth.

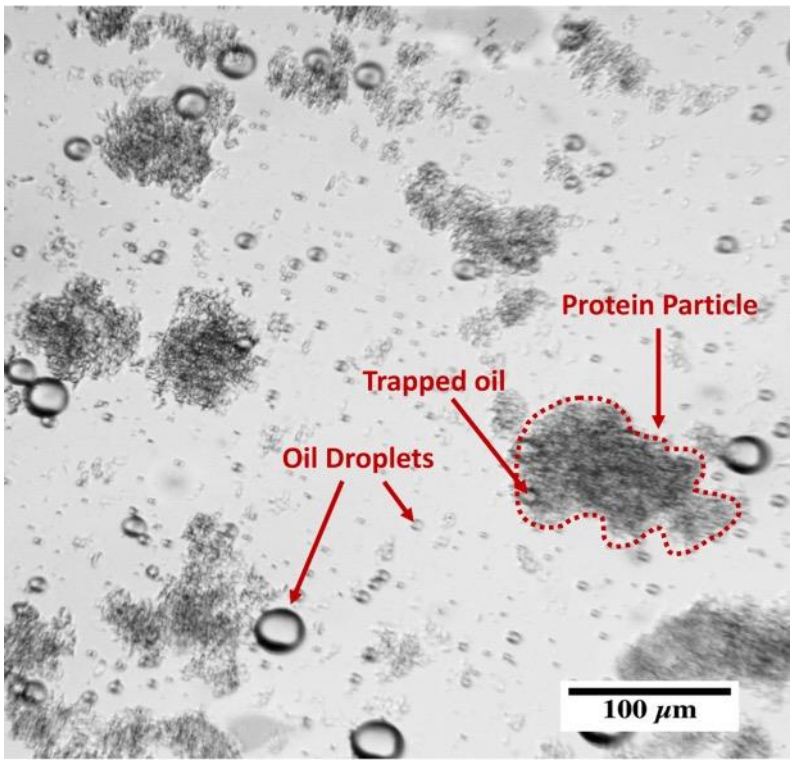


*Figure 4.13: Optical micrograph depicting a typical, diluted cold-set WPI/Oil system (5 % (w/v) WPI, 10 % (v/v) oil, 50 mM $CaCl_2$) post dispersion, highlighting a protein particle, un-trapped oil droplets and an oil droplet that has become trapped within the protein particle. Scale bar represents 100 microns.*

### *4.3.2. Cold-set WPI suspensions: Material response*

#### *4.3.2.1. Effect of $Ca^{2+}$ salt concentration*

Amplitude sweeps for 25 and 50 mM $CaCl_2$ crosslinked systems without oil (Figure 4.14) show mechanical spectra where storage moduli within the LVR were independent of shear during production. However, the effects of $Ca^{2+}$ concentration were much more apparent.

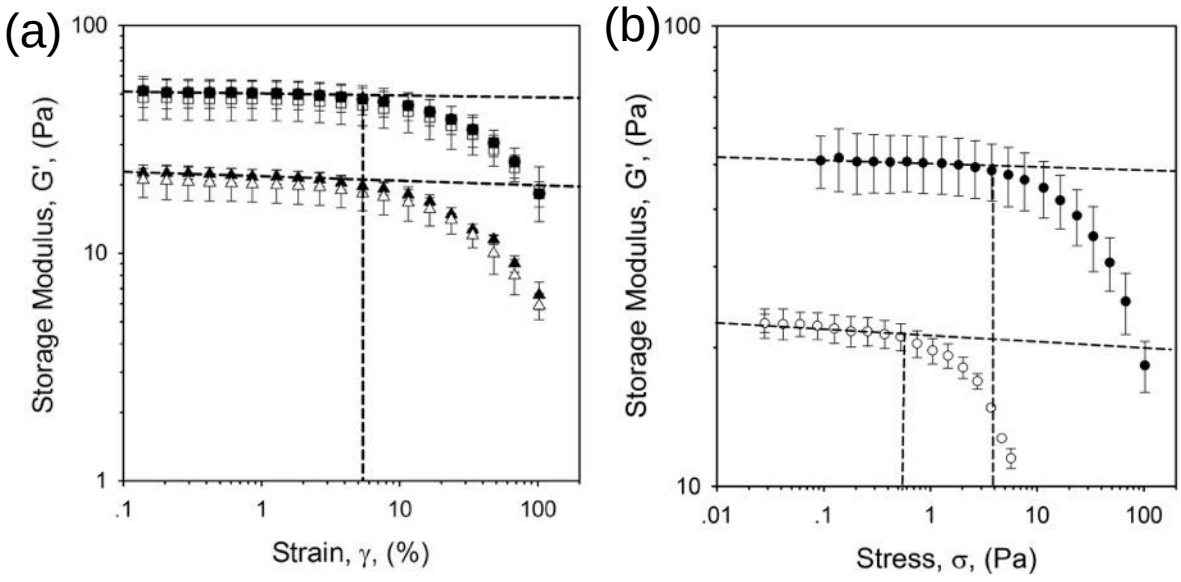


*Figure 4.14: (a) Strain sweeps (1 Hz, 20 °C) for WPI systems taken 48 hrs post production, as a function of $Ca^{2+}$ salt addition and shear applied during gelation. Symbols represent (■,□) 25 mM, and (▲,△) 50mM $CaCl_2$; closed markers denote systems processed at 1000 rpm and open 2000 rpm mixing speeds. (b) Equivalent stress vs G' plots obtained for WPI systems crosslinked with 25 and 50 mM $CaCl_2$ at 1000 rpm processing speed only (● - 25 mM and ○ - 50 mM $CaCl_2$). (Dashed lines are for guiding the eye, highlighting the point of at which the system is no longer within the LVR)*

Here, particles prepared using lower cross-linker concentrations resulted in a greater storage modulus, presenting an inverse trend to previously published cold-set

polysaccharide microgels (Fernández Farrés and Norton, 2014). Additionally, G' values obtained for sheared systems had an inverse correlation (higher $Ca^{2+}$ concentrations reduced G') when compared to their quiescent counterparts (data shown previously in Table 4.1). Again this was not expected with data previously published by Adams et al. (2004) for microgel suspensions; which indicated that increasing the concentration of cross-linker strengthened the particles, resulting in a greater bulk modulus. Therefore, the lower storage moduli observed within this study are suggested to be governed by the gelation kinetics. The extent and strength of crosslinks become reduced with more rapid aggregation (Alting et al., 2002), as a result of a more closed microstructure as previously described (Hongsprabhas et al., 1999).

The point at which the system begins to breakdown, and is no longer within the LVR (denoted here as apparent yielding behaviour) has been shown in Figure 4.14. Amplitude sweeps were used to further probed the degree and nature of the interactions between particles. Strains to "yield" (Figure 4.14a) remained constant across all systems, where the deformation required to break particle-particle interactions did not change. However, when comparing the stress to "yield", obtained for the same sweeps, a clear difference can be seen (Figure 4.14b). This infers that a greater force is required to break the inter-particle interactions. Again, this is argued to be a function of the gelling rates, leading to a greater degree of interaction sites buried within the particle at higher $Ca^{2+}$ concentrations. Similar dependencies once "yielded" (rate of G' reduction) suggests a similarity between systems; where particle interactions and/or deformability are of the same length-scale (Garrec et al., 2013).

#### *4.3.2.2. Effect of emulsion volume*

Frequency sweeps obtained for all systems, both with and without the addition of oil, resulted in spectra with increasing G' as a function of frequency (a representative mechanical spectrum has been shown in Figure 4.15). Such observations have been previously reported for typical microgel suspensions and fluid gels.

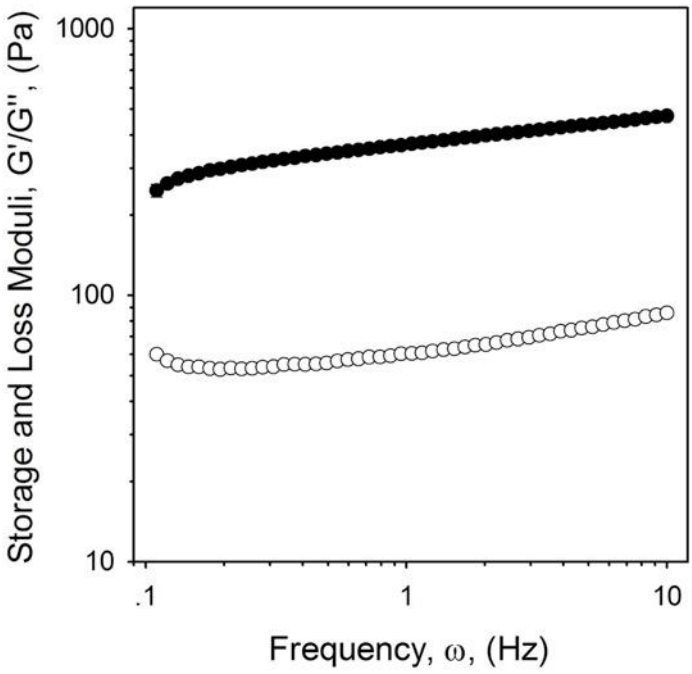


*Figure 4.15: Mechanical spectrum obtained for a 50 mM $Ca^{2+}$, 40% (v/v) WPI/Oil system, prepared using 1000 rpm stirrer speed. (Closed markers denote G' and open G''). (Data obtained at 0.5% strain, 20 °C)*

These inherent properties arise from the prevention of a continuous gel network during gelation, leading to discrete particles with the ability to create highly flocculated systems. As such, the materials frequency dependence (weak through to strong gels) is primarily governed through a large effective phase volume and degree of inter-particle interactions. This results in gel-like materials where G' dominates G'' (Fernández Farrés

et al., 2013, Fernández Farrés and Norton, 2014, Gabriele et al., 2009, Garrec and Norton, 2012, Moakes et al., 2015a, Moakes et al., 2015b, Adams et al., 2004).

Changes in G' (at 1 Hz) were compared as a function of oil at both salt concentrations studied, directly after processing ($t_0$) and after storage ($t_{48hrs}$). Figure 4.16 shows positive correlations between G' and oil fractions for all systems measured immediately post-shearing and storage. The data for 25 mM, 10% oil at 48hrs has been omitted within this figure (highlighted in Figure 4.16a) statistically as an outlier – more than three times the standard deviation the linear trend between points. However, the data has been presented in Figure 4.17a for the readers knowledge. In all cases the gelling polymer to volume, and salt to polymer ratio were kept constant, thus changes in the resulting rheological properties are described as a function of the oil content. Plots for both 25 mM and 50 mM oil/WPI systems showed similar lines of best fit, as a function of the oil volume. It is proposed that suspension rheology in these cases were primarily driven through close packing of the oil droplets, which arises from an effective volume increase as the continuous phase becomes trapped during the formation of WPI particles. Greater consequential crowding promoted interactions between both neighbouring protein and oil particulates (Ye and Taylor, 2009, Sok Line et al., 2005). Therefore, pseudo-solid behaviour is exhibited, G' dependencies following similar correlations to those for typically concentrated emulsions; where particles and droplets come into close proximity and for an elastic network throughout the (Otsubo and Prud'homme, 1994, Derkach, 2009).

Figure 4.16a again shows the effect of ageing previously seen with SLS, through a shift in material response to higher G' values over time; as a function of particle growth.

However, such changes in suspension moduli were not observed at 50 mM (Figure 4.16b).

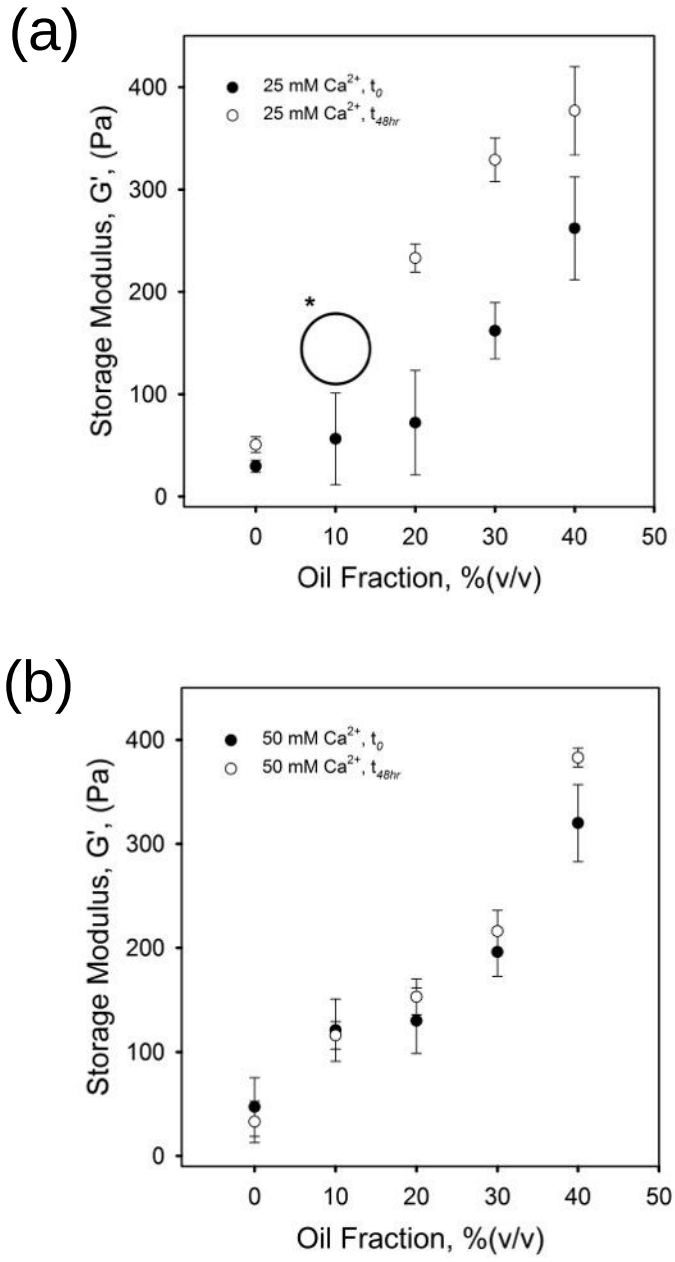


*Figure 4.16: Storage modulus (at 1 Hz, 20 °C) plotted against oil fraction for (a) 25 mM $Ca^{2+}$ and (b) 50 mM $Ca^{2+}$ WPI/Oil systems prepared using 1000 rpm stirrer speed. Closed markers denote G' at $t_0$ (immediately post-production) and open G' at 48 hrs post-production.* ***** *Data point removed as an outlier.*

Ageing dependency on ionic environment is once again argued to be a consequence of the gelation kinetics, where faster rates result in a greater extent of structuring within the shear environment, and subsequently fewer sites for inter-particle interactions thereafter (previously discussed).

Oil/WPI systems apparent "yielding", determined as the point at which the system no longer behaves in a linear fashion, was investigated again through strain dependence on the elastic modulus. It was observed that on increasing deformation, breakdown of the weakly flocculated macrostructure (interactions between particle-droplet and particle-particle) occurs, shown by a decrease in storage moduli. Comparable results were obtained for both salt-set systems, depicted in Figure 4.17a and b (25 and 50 mM respectively). It was observed that, in systems with incorporated oil, increasing the oil fraction had an effect on the length of the LVR across both systems, elongating the strain to failure (also seen through increasing stress to "yield": Table 4.4).

*Table 4.4: Table of stresses to apparent yielding, as determined as the point at which the storage and loss moduli no longer behave linearly. Obtained for WPI/Oil suspensions prepared at 1000 rpm with increasing oil fractions from 10 to 40% (v/v), as a function of cross-linking concentration. Values shown are taken from the data obtained for Figure 4.18 as the stress measured at the point of exiting the LVR.*

| Salt Conc. | "Yield" stress ($\tau_y$) at given oil fractions (Pa) | | | | | | | |
|---|---|---|---|---|---|---|---|---|
| | 10 % | | 20 % | | 30 % | | 40 % | |
| 25 mM | - | | 25.3 | **±1.44** | 38.23 | **±2.15** | 41.95 | **±7.12** |
| 50 mM | 6.07 | **±1.30** | 8.94 | **±1.49** | 13.83 | **±2.01** | 34.77 | **±1.26** |

Such an observation infers a more elastic network, with increasing oil creating a stronger, more deformable structure between the gelled particles (Mason et al., 1995).

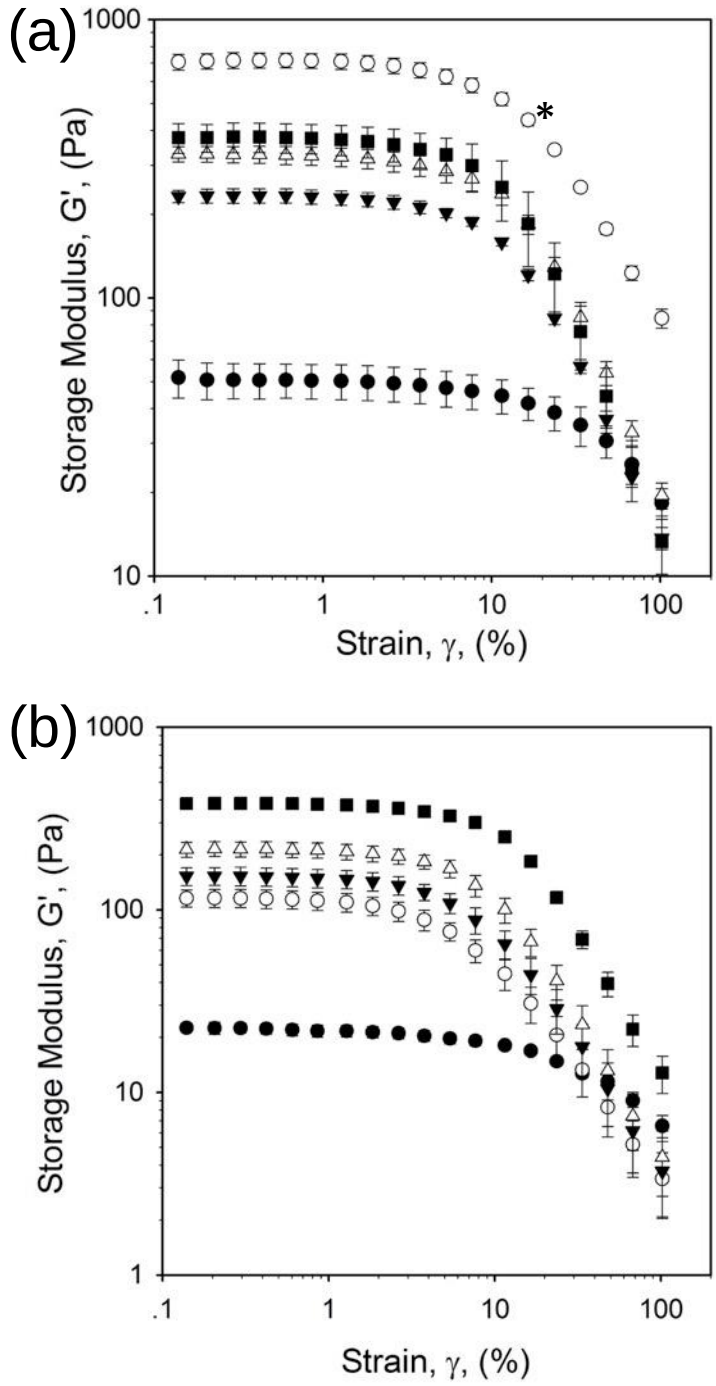


*Figure 4.17: Amplitude sweeps (1Hz, 20 °C) for: (a) 25 mM $Ca^{2+}$ and (b) 50 mM $Ca^{2+}$ WPI/Oil systems prepared using 1000 rpm stirrer speed. Mechanical spectra were obtained 48 hrs post production. Symbols represent (●) 0% oil, (○) 10% oil, (▼) 20% oil, (△) 30% oil, and (■) 40% oil fractions (v/v) (note the change in y-axis scale). * mechanical data for 25 mM Ca2+, 10%, proposed in Figure 4.16a as an outlier.*

At higher strains, once having "yielded", oil systems showed similar dependencies on strain, with the magnitude of loss in G' being superimposable. However, this was not true for systems without oil, where a much more shallow gradient is seen. These differences in strain dependency post-"yielding" are argued to arise from the spherical shape of the oil droplets in comparison to the irregular asymmetric morphology of the protein particles. Therefore, the oil droplets sitting between the particles provide much smaller contact zones for interactions to occur, visually represented by a schematic in Figure 4.18. Therefore, a more abrupt reduction in inter-particle/droplet interactions occurs, preventing the anisotropic particles being in contact over a much longer length scale (Norton et al., 2006b).

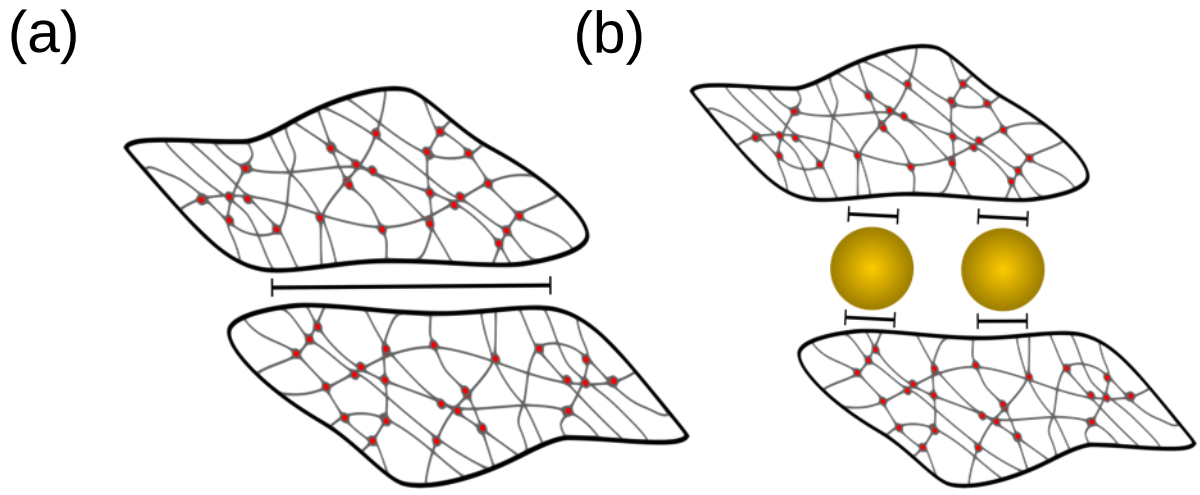


*Figure 4.18: Schematic of the contact sites between: (a) two protein particles, highlighting the long region of interaction, and (b) protein particles separated with oil droplets, showing much smaller contact zones. The contact area between can be directly linked to the degree of interactions that can occur between the species.*

## 4.4. Conclusions

This study has revealed that gelling kinetics for quiescent WPI cold-set gels can be modulated through both the concentration of $Ca^{2+}$ added and volume fraction of oil within the system. A mechanistic shift was proposed for systems prepared at low $CaCl_2$ concentrations, where aggregation was governed by ionic dispersion followed by arrangement and bridging of the polymer, to gelation kinetics more closely following rates governed solely by arrangement and bridging at higher concentrations. The kinetics were compared to particle intrinsic properties, prepared using a shearing method. Particle sizes immediately after processing were close to 8 μm irrespective of shear or cross-linker concentration, suggesting the applied shear was too great to allow further aggregation within the pin-stirrer. As such, the small aggregates were termed primary particles. Re-evaluating particle size 48 hrs post-production showed a secondary aggregation step where primary particles interacted to form secondary larger aggregates, with sizes dependant on both salt and oil concentrations. Suspension rheology was probed through small and large deformation oscillatory measurements. The elastic response showed a good correlation to gelling kinetics obtained for comparable quiescent gels. As such it was proposed that increased rates of aggregation led to the formation of particles with less interaction sites, similarly to previously reported thermally set particles. In summary, it was shown that controllable systems could be prepared via a cold-set method, presenting a potential candidate for rheological modification in thermally sensitive products.

Even though systems showed promise as thermo-sensitive structuring agents, optical micrographs highlighted low levels of oil entrapment. As such, their use as taste-masking agents or selective delivery is compromised. Therefore, a thermally set

technique was studied, in order to prepare microcapsules (oil cores with protein shells) with the intention to deliver actives in fortified or nutraceutical products. Thus, the following chapter (Chapter 5) looks at the formation of WPI/oil micro-capsules with particular focus on their ability to create structure.

# Chapter 5. *Whey Protein Emulsion Fluid Gels*

*Adapted from (Moakes et al., 2015b)*

***Synopsis***

A shear-gel approach was used to coat an O/W emulsion with a whey protein shell (see image below) for application as a multifunctional device; to deliver compounds, whilst acting as a rheological modifier. Micro-particles were prepared through shear flow during the sol-gel transition of a WPI/oil mixture, preventing the formation of a continuous WPI-oil network. The result was discrete spherical particles, with sizes in the micron scale (~25 μm). Through careful control over both the oil and WPI components, encapsulation efficiencies of up to 99 % were obtained. Subsequent rheological properties highlighted elastic behaviour (G') dependent on oil content; where higher oil fractions increased the effective phase volume of the particles. The result was packing fractions that exceeded those for hard spheres (>0.64), leading to pseudo-solid characteristics at rest, apparent yield stresses and thixotropic behaviour under shear. As such, particles prepared in this way had the potential to deliver lipophilic compounds, whilst retaining the ability to build structure.

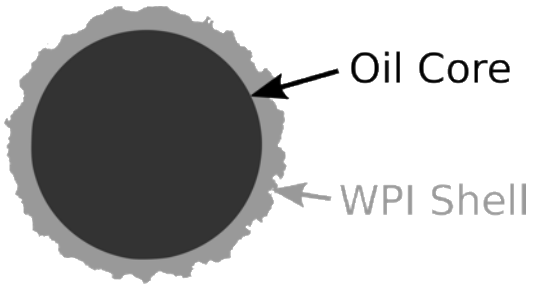

## 5.1. Introduction

The chapter combines the key findings from chapter 3 with emulsion technology in order to form microcapsules that interact to structure fluids. The research builds on work presenting $O/W_1/W_2$ filled hydrogel systems, by applying a "shear gel approach" to promote interactions between resulting particles. As such, it surpasses current surfactant or Pickering stabilised emulsions by gelling a continuous WPI layer around an oil core. The applied technique results in elastic suspensions, whereby the particles become trapped, suspended in an aqueous phase. The micro-particles thus offer the capacity to act as a multifunctional composite, for both controlled rheological applications and pose the potential to encapsulate poorly soluble molecules. The work focuses on whey protein isolate (WPI) as the coating material owing to its thermo-denaturation and subsequent hydrophobic aggregation, forming a gel layer around the surface of an oil substrate. Shear separation will then be applied to prevent complete gelation, promoting particle-particle interactions. Therefore, the preparation of emulsion fluid gels (suspension of microgel particles comprising of an oil core) has been investigated, with particular attention to the resulting rheological properties.

## 5.2. Materials and Methods

### *5.2.1. Materials*

Whey protein isolate (WPI) was obtained from Kerry Ingredients, Listowel, Ireland (WPI, W994, S-493391) and used without further purification. WPI composition as stated by the supplier was 91.0 % protein, moisture 4.0 %, fat 1.0 %, ash 3.5 % and lactose 0.5 %. Mineral content of the WPI was: Ca – 0.50, P – 0.65, Na – 0.10, K – 0.15, Mg

– 0.02 and Cl - 0.02 %. High oleic sunflower oil was obtained from Cargill (Cargill Inc., BE). Sodium azide, hydrochloric acid, silicon oil, Nile Red and Rhodamine B were purchased from Sigma-Aldrich (Sigma-Aldrich, UK).

### *5.2.2. Preparation of oil filled fluid gels*

Emulsion fluid gels (EmFG) were prepared by gelling a system of whey protein isolate and oil under imposed shear. As such, WPI solutions were first produced and used to stabilise emulsion droplets. Following this process, the proteins were thermally forced through their sol-gel transition, under stirred conditions, to result in a dispersion of WPI-oil micro-particles. The following method describes a detailed protocol, used to prepare the systems used throughout this chapter. However, details retaining to the formulation development process, leading to the system studied here, have been collated in Appendix ii; as to give further details on why certain process were incorporated.

#### *5.2.2.1. Preparation of WPI stock solutions*

Whey protein stock solutions (5 to 30% (w/w) on a protein basis) were prepared by dispersing WPI in deionised water. An anti-microbial, sodium azide (0.02% (w/w)) was added to all solutions to enhance storage times. Solutions were stirred overnight at ambient conditions until completely hydrated and stored at 5 °C until further usage. For the preparation of stained samples Rhodamine B (0.015 mM) was added to stain the protein. Stained samples were kept covered to prevent photo bleaching.

#### *5.2.2.2. Preparation of emulsions*

Oil in water emulsions were prepared by the addition of high oleic sunflower oil to WPI primary solutions prepared in section 5.2.2.1., so that total volumes resulted in oil fractions ranging from 5 to 20% (v/v). The mixtures were subsequently mixed in a high shear mixer (Silverson, SL2T) at 4000 rpm for 10 minutes, to result in emulsion systems. The pH was adjusted to pH 4.6 with concentrated hydrochloric acid (12 M) and aged for 48 hours, increasing the surface hydrophobicity (for further information see Appendix ii), before gelling under shear. Stained EmFG were prepared with the addition of Nile Red (0.015 mM) to the oil phase and kept covered to prevent photo bleaching.

#### *5.2.2.3. Preparation of oil filled fluid gels*

A jacketed vessel and overhead stirrer equipped with pitched blade impeller was used to prepare all WPI EmFG. Aliquots of emulsion were added to a jacketed vessel set to 50 °C, controlled through a circulating water bath. Shear was applied through the stirrer and impeller at 450 rpm. Once thermal equilibrium was obtained (Ca. 10 minutes), emulsions were heated at a rate of 0.5 °C$min^{-1}$ to 80 °C: 80 °C was used following calorimetry data previously presented in Chapter 3, as the point at which gelation had completed. Suspensions were subsequently decanted and left to cool quiescently under ambient conditions. Cooled EmFG were further stored at 5 °C for seven days until rheometrically tested. In all experiments, a cover was applied to minimise water loss. When staining, the system was covered in aluminium foil to avoid fluorescence quenching.

### *5.2.3. Static light scattering (SLS)*

A MS2000 Mastersizer with attached Hydro SM manual small volume dispersion unit (Malvern Instruments Ltd, UK) was used to obtain size distributions. Distributions show the average of three repeats. Particle sizes were calculated based upon the Mie theory, thus particles were assumed to be monodisperse, homogenous spheres. Samples were prepared by diluting gel particles in distilled water to avoid multiple scattering and pre-defined software refractive indices (RI) for the water and protein were used: 1.33 and 1.6 respectively. Due to the protein-oil composition of the particles the refractive index of the gel was used, similarly to Chapter 4, following initial experiments that did not identify significant changes in distributions when analysed using either the refractive index of the oil or protein. (For further theory see Appendix i)

### *5.2.4. Microscopy*

#### *5.2.4.1. Optical light microscopy*

Samples were prepared by first diluting the EmFG in deionised water (7.5 % (v/v)). A Brunel SP300-fl (Brunel Microscopes Ltd, UK) optical light microscope fitted with an SLR camera (Cannon EOS Rebel XS, DS126 191) at 20 and 40x optical magnification was used to image the particles. Slides were prepared by addition of 50 μL of sample to a microscope slide (VWR, UK) and covered with a coverslip (Thickness no.1, VWR, UK).

#### *5.2.4.2. Confocal Laser scanning microscopy (CLSM)*

Stained samples prepared with both Rhodamine B and Nile Red were imaged using concave microscope slides (60 μL), with a coverslip sealed using super glue. Fluorescence free, UV transparent immersion oil (Sigma-Aldrich, UK) was used to bridge the gap between coverslip and objective lens (40x magnification). A Leica TCS-SPE confocal microscope (Leica Microsystems Ltd, UK) fitted with an argon laser was used for all CLSM analysis. Rhodamine B stained protein was excited at 532 nm and detected at 560-600 nm, and Nile Red was excited at 488 nm and detected at 680-700 nm respectively. 3-dimensional images were obtained using 0.5 μm slices throughout. Further image processing was undertaken using an image software package (ImageJ). (For further theory see Appendix i)

### *5.2.5. Rheological Analysis*

Rheometry was conducted using a Bohlin Gemini HR Nano stress-controlled Rheometer (Malvern Instruments Ltd, UK) equipped with serrated parallel plate (25 mm diameter) at 1 mm gap height (greater than 10x average particle size). Experiments were undertaken at 25 °C using silicon oil to prevent any evaporation of the continuous phase. The sample was allowed to equilibrate for 15 mins prior to testing, allowing for consistent loading conditions. Particle phase volumes were obtained using a method outlined in Chapter 3; whereby aliquots of a given volume were centrifuged, water phase separated and volumes obtained. Phase volumes were calculated as followed (Equation 5.1):

$$Particle\ Phase\ Volume = 1 - \left(\frac{Volume\ of\ Water\ Removed}{Total\ Initial\ Volume}\right)$$

*Equation 5.1: Determination of the volume occupied by the particles within the EmFG systems using a reduced water method.*

#### *5.2.5.1. Determination of solid to liquid behaviour*

Liquid-like behaviour was determined as the stress required to cause a transition from storage modulus (G') to loss modulus (G'') dominance; the G'/G'' cross over point on a stress controlled amplitude sweep. Amplitude sweeps were conducted at 1 Hz from 0.1 to 400 Pa at 25 °C.

#### *5.2.5.2. Dynamic oscillatory measurements*

Frequency sweeps were obtained between 0.1 and 10 Hz (25 °C), using controlled stress. The stress was determined by amplitude sweeps as a value within the linear viscoelastic region (LVR) for all EmFG tested. For samples containing no oil a, couette, double gap geometry was used: as the large surface area allowed lower values of G' to be probed in the lower viscosity fluids.

#### *5.2.5.3. Viscosity measurements*

Viscosity measurements were undertaken between 0.1 and 400 $s^{-1}$ (25 °C). Shear sweep time was set to 10 minutes (ramp ascending and descending). Two consecutive sweeps were run with the second commencing immediately after the first having been completed.

#### *5.2.5.4. Recovery analysis*

EmFG recovery was probed at 25 °C by primarily rejuvenating the system. A pre-shear (10 $s^{-1}$ for 10 s) was applied to the system and subsequent change in storage modulus (G') recorded over the following 30 min. G' was obtained at 1Hz and 1 Pa.

### *5.2.6. Encapsulation efficiency*

Optical microscopy was used to analyse oil droplet entrapment for each system. Micrographs of the raw emulsion were obtained and emulsion droplets in each image manually counted to give an average droplet count ($N_{em}$). In each case images were taken at two focal planes to visualise droplets with a lower density, which migrate to the top of the microscope side. Thus, $N_{em}$ was determined over 24 micrographs that make a set of 12 images (3 inter-samples images, 4 intra-sample images). Values for uncoated emulsion droplets ($N_{fo}$) in the final EmFG systems were then obtained in the same manner. Uncoated droplets were determined by eye, as droplets without a textural layer over them. An example of both a coated and uncoated droplet has been shown in Figure 5.1. The ratio of the two was used to calculate the percentage of encapsulated high oleic sunflower oil, as shown in Equation 5.2:

$$\%_{Encapsulated} = \left(1 - \frac{N_{fo}}{N_{em}}\right) \times 100$$

*Equation 5.2: Entrapment efficiency, calculated by taking the ratio of uncoated droplets ($N_{fo}$) to gelled droplets ($N_{em}$).*

Encapsulation was averaged over 12 sets of micrographs, with error calculated as the 95 % confidence interval.

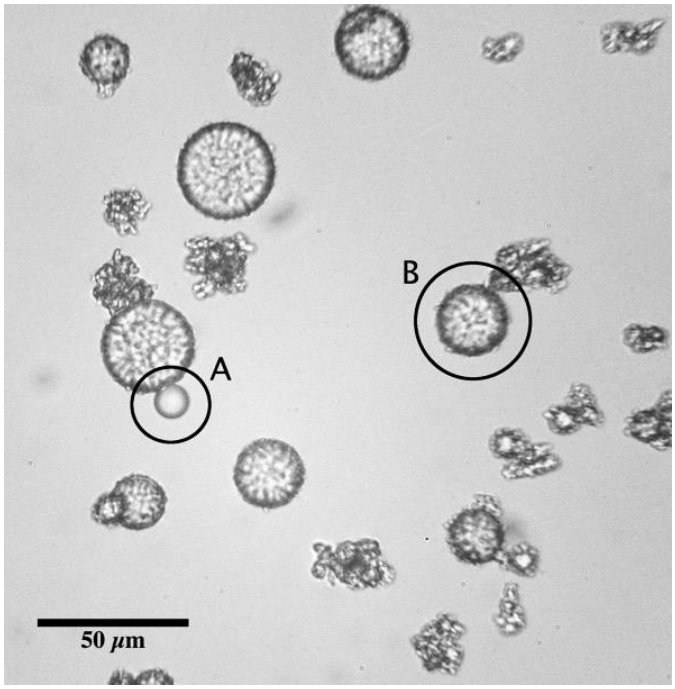


*Figure 5.1: Optical micrograph highlighting (A) an uncoated oil droplet and (B) a coated oil droplet (EmFG particle).*

## 5.3. Results and Discussion

### *5.3.1. Preparation of emulsion fluid gels (EmFG)*

An O/W system where the excess WPI emulsifier exceeded the critical gelling concentration (Stading and Hermansson, 1990) (> 1% (w/w)), was subjected to heat treatment under shear conditions. The shear flow exerted on the system during the sol-gel transition prevented the formation of a continuous gel network, resulting in single discrete particles/encapsulates.

#### *5.3.1.1. Entrapment efficiency*

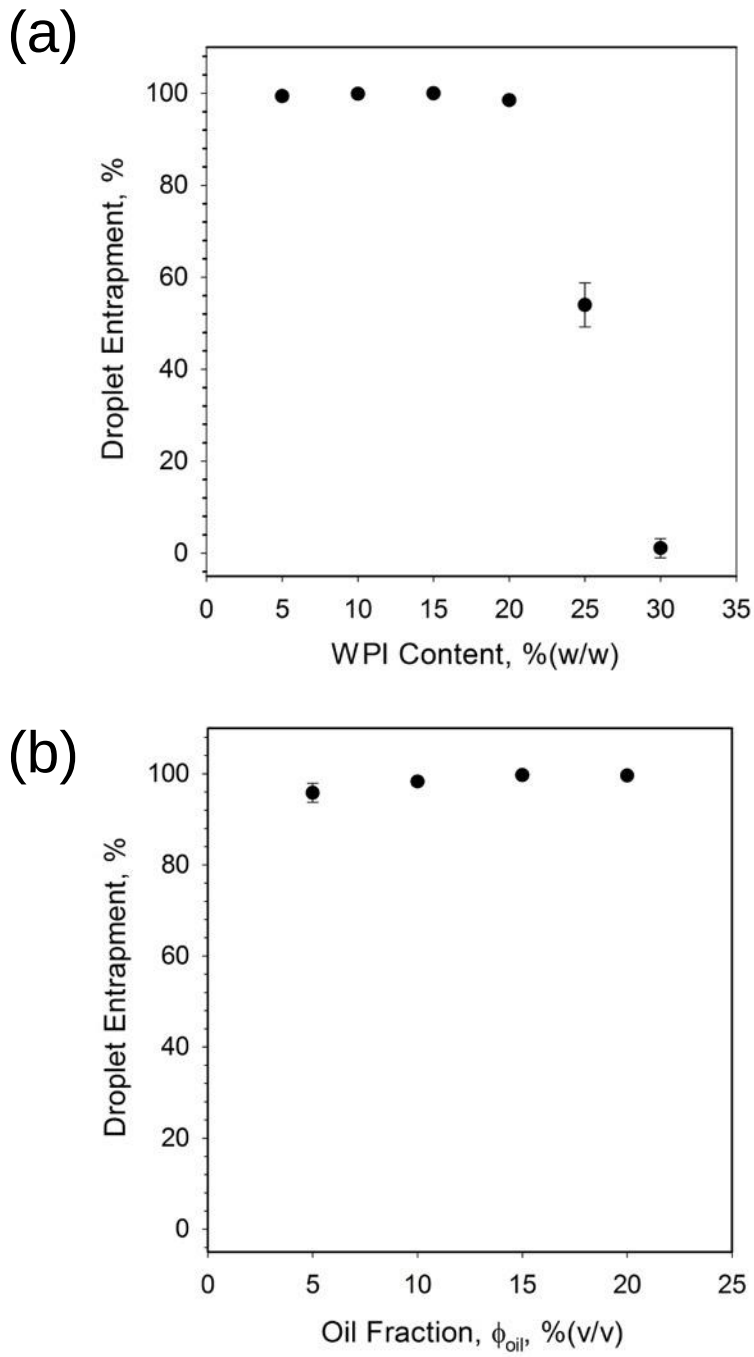


*Figure 5.2: Oil droplet entrapment efficiencies for: (a) EmFG systems prepared with increasing WPI concentrations ranging between 5 and 30% (w/w) at a fixed $\phi_{oil}$ of 10% (v/v), and (b) EmFG systems prepared with increasing $\phi_{oil}$ between 5 and 20% (v/v) with a fixed WPI concentration of 15% (w/w).*

Figure 5.2 shows the entrapment efficiencies for systems with both: (a) increasing WPI concentration, and (b) high oleic sunflower oil phase volume, $\phi_{oil}$. It was observed that high levels of entrapment, ~99 %, were achieved in systems with lower WPI concentrations, however, as the WPI exceeded 20% (w/w), entrapment decreased. It is argued that the degree of encapsulation is closely correlated to the flow behaviour of the system during the sol-gel transition. It has previously been reported by Hermansson (1975) and Walkenstrom et al. (1998) that around the isoelectric point of WPI (ca. pH 5) a transition from Newtonian to pseudo-plastic flow occurs in unheated systems containing 20% (w/w) whey protein; with yield stresses observed on further concentrated solutions. Such changes in the system viscosity would retard or prevent the diffusion of denatured protein to the oil/water interface due to a reduction in mobility and increased collisions with other denatured polymer chains. In turn, both increased formation of WPI aggregates without included oil and free emulsion droplets were observed in the final suspensions.

Increasing the phase volume of the sunflower oil from 5 to 20% whilst retaining a standard WPI concentration (15% (w/w)) however, had little effect on the emulsion entrapment, yielding droplet entrapment in excess of 95%. Here, the increase in oil was not sufficient to raise the viscosity of the system, and hinder polymer diffusion. However, at low oil fractions increasing the WPI concentration from 5 to 15% (w/w) caused an observed transition from suspension creaming to sedimentation, inferring a net change in particle density, most likely as a result of a change in shell thickness.

### *5.3.1.2. Particle morphology*

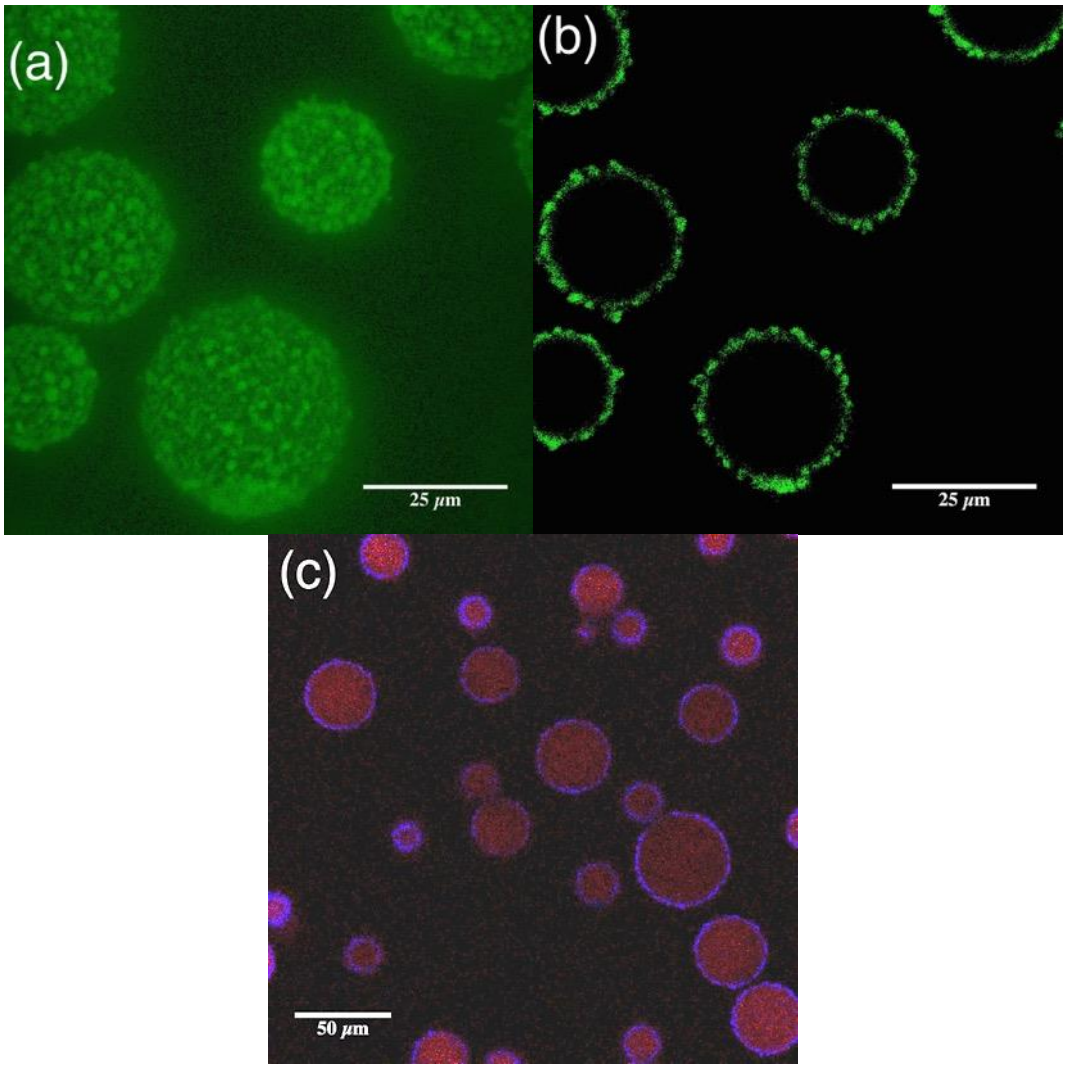


*Figure 5.3: CLSM micrographs of EmFG particles. Gel phase has been stained using Rhodamine B (excitation wavelength: 532 nm, emission wavelength: 560-600 nm) and oil phase either negatively stained or stained using Nile red (excitation wavelength: 488 nm, emission wavelength: 690-700 nm). (a) 3D stack showing topographical detail of the EmFG particles, (b) cross section depicting stained gel layer surrounding a negatively stained oil core, and (c) stained cross section showing protein shell (blue) and oil core (red). Scale bars represent 25 μm (a and b) and 50 μm (c).*

Particle morphology was studied using confocal laser scanning microscopy (CLSM). Previous work regarding the formation of WPI microgel particles through the

application of shear (chapter 3), show irregular shaped particles, characterised by a large length to width ratio. However, the incorporation of oil in to the system resulted in particles with a defined spherical morphology, as shown in Figure 5.3. Imaging the EmFG particles at 0.5 μm intervals (z-stack) gave enhanced topographical detail (Figure 5.3a), allowing the coating to be observed. A non-uniform shell with much greater thickness than expected for purely emulsified droplets was shown, identifying the presence of a gel layer. Additionally, cross-sections were obtained using CLSM, which again show shell thickness and non-uniformity, but also through negative staining and dying, oil reservoirs in the centre of the particles (Figures 5.3b and 5.3c respectfully).

The mechanism for particle formation is thought to be based upon the oil acting as a substrate for shell growth. Growth occurs through enrichment from the surrounding un-gelled biopolymer. Primarily led by the β-lactoglobulin, heat induced denaturation of the native structure causes hydrophobic regions to become exposed (Hoffmann et al., 1996, Sawyer, 1968). Hydrophobic interactions then dominate the gelation process causing diffusion of the denatured polymer and protein nuclei (small agglomerates of denatured WPI) to adsorb to the already protein coated droplets (oil/water interface). Shear imposed upon the system then restricts particle-particle aggregation, preventing a continuous network from forming. As a result, particles grow to an extent permitted by the shear flow, however, are primarily dictated by the size of the emulsion droplets.

#### *5.3.1.3. EmFG particle size distributions*

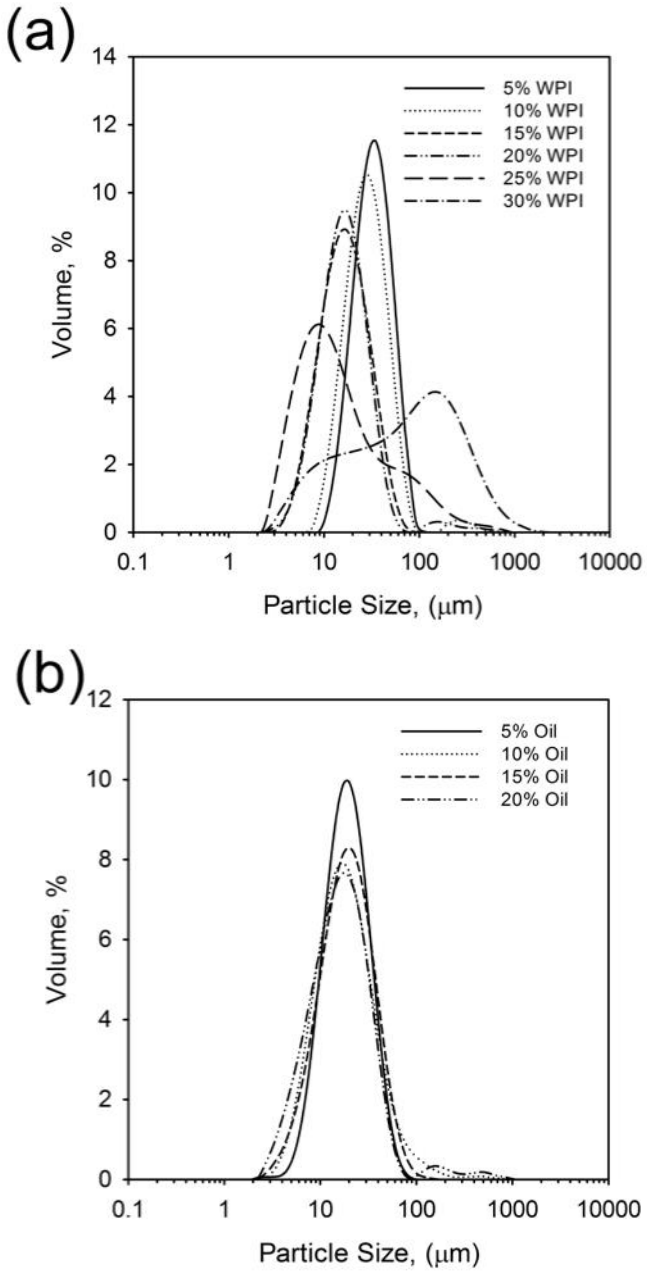


*Figure 5.4: Particle size distributions for: (a) EmFG prepared with a range of WPI concentrations between 5 and 30% (w/w) with a fixed $\phi_{oil}$ of 10% (v/v), and (b) EmFG prepared with a range of $\phi_{oil}$ from 5 to 20% (v/v) with a fixed WPI content of 20% (w/w).*

Particle size distributions for all EmFG systems are shown in Figure 5.4. It is clear from Figure 5.4a that increasing WPI concentration, up to 25% (w/w), results in a shift towards smaller particle sizes. Particles are primarily a function of the emulsion droplet size, thus such observations would be expected as increasing the emulsifier concentration causes the formation of smaller droplets (McClements, 2005, Walstra, 1993). However, by further increasing the protein concentration up to 30% (w/w), the formation of a bimodal system centred at ~9 μm, with a second peak at much higher particle sizes (~200 μm) was observed.

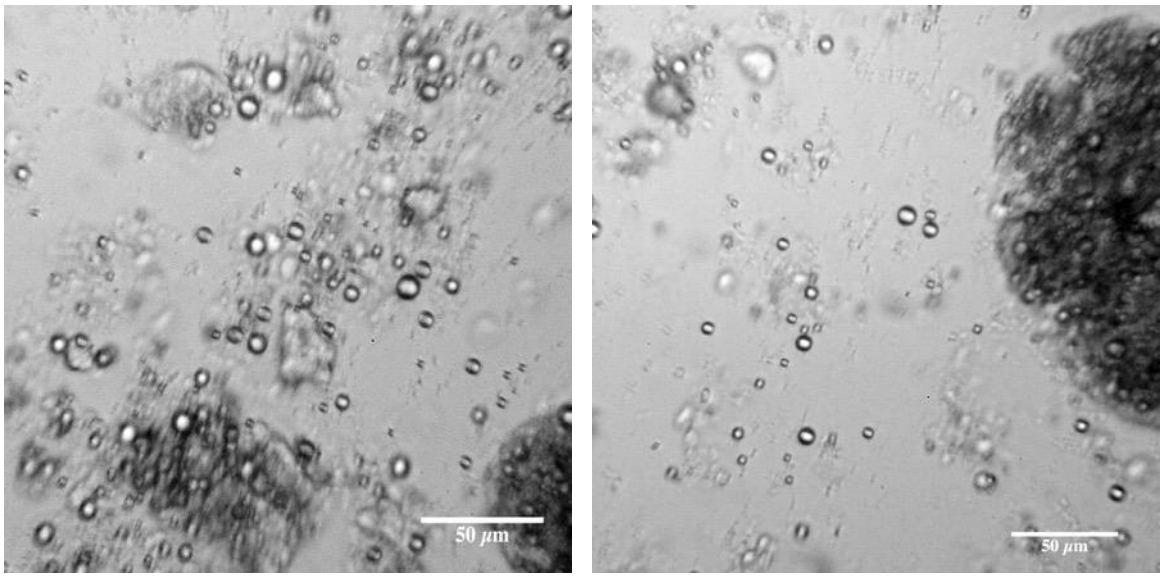


*Figure 5.5: Optical micrographs of a 30% (w/w) WPI system, highlighting highly dispersed emulsion droplets with large aggregated protein particles in the back ground. Scale bar represents 50 μm.*

The shift from monomodal to bimodal is due to the formation of gelled particles where no oil has been entrapped as observed via microscopy (Figure 5.5). As previously

described, the change in system flow results in aggregated protein, as diffusion of the denatured polymer becomes restricted, causing a transition from protein-oil to protein-protein interactions. The extent of such a transition is thus reflected by the change in peak intensity observed in systems with 20 to 30% (w/w) WPI. Figure 5.4b shows little effect on the resulting particle size as a function of oil fraction, as a result of consistent emulsifier concentrations and unrestricted diffusion of biopolymer to the substrate interface. Thus, all distributions are centred around 25-30 μm complimenting sizes observed via microscopy (Figures 5.1 and 5.3).

### *5.3.2. EmFG material properties*

#### *5.3.2.1. Small deformation oscillation testing*

To further understand and characterise the EmFG physico-mechanical properties, small deformation rheology was carried out. Figure 5.6a shows frequency sweeps obtained for EmFG systems prepared with varying oil fractions from 0 to 20% (v/v). Systems containing no oil displayed typical liquid-like behaviour where both moduli were dependent on frequency and G'' is higher than G' throughout the measured frequency range (Ross-Murphy, 1994). The addition of oil caused a transition in rheological behaviour to pseudo-solid where G' is higher than G'', with both moduli becoming further independent to frequency as a function of the oil. Here particle proximity is such that inter-particle interactions arise as observed for WPI microgel particles (Moakes et al., 2015a), however, as the shear and thermal history exerted was consistent across all systems, it is argued that system elasticity becomes a function of

the oil content; where increasing oil fractions increase the effective phase volumes of the particles, as shown in Figure 5.6b.

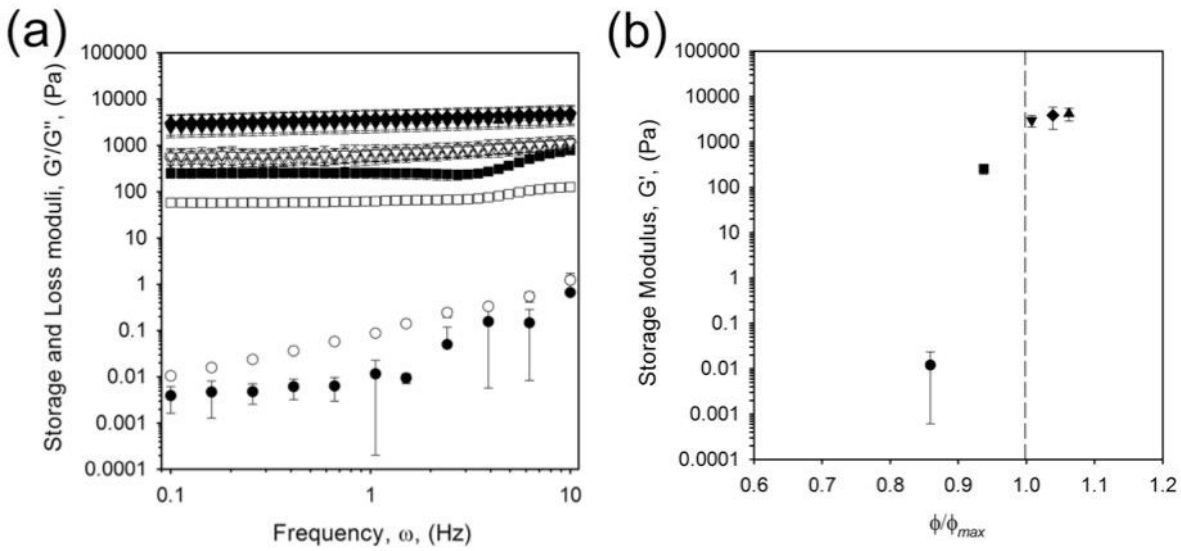


*Figure 5.6: (a) Frequency sweeps at 1 Pa stress, 25 °C, obtained for EmFG prepared using 20% (w/w) WPI and (●,○) no oil, (■,□) 5% (v/v) oil, (▼,▽) 10% (v/v) oil, (◆,◇) 15% (v/v) oil, and (▲,△) 20% (v/v) oil. Open markers represent the storage moduli (G') and closed show loss moduli (G"). (b) Storage modulus at 1 Hz verses normalised particle phase volume for systems with, (●) no oil - 20% (w/w) shear/heat treated WPI, and 20% (w/w) WPI EmFG containing: (■) 5% (v/v) oil, (▼) 10% (v/v) oil, (◆) 15% (v/v) oil, and (▲) 20% (v/v) oil. Volume fractions were normalised using the maximum random packing fraction for hard spheres, 0.64. Dashed line represents maximum packing faction for hard spheres.*

Particle intrinsic properties (hardness) and resulting mechanism through which system elasticity arises was probed by comparing the results obtained to the Krieger-Dougherty (KD); a model used to describe hard sphere rheology. The KD model is used to describe the relationship between relative viscosity ($\eta_{rel}$) and particle phase volume for hard sphere suspensions (Krieger and Dougherty, 1959), Equation 5.3.

$$\eta_{rel} = \left(1 - \frac{\phi}{\phi_{max}}\right)^{-[\eta]\phi_{max}}$$

*Equation 5.3: Krieger-Dougherty model for hard sphere suspensions.*

The equation relates the ratio between the phase volume of the suspension, $\phi$, to the maximum random packing fraction for monodisperse hard spheres (0.64), $\phi_{max}$, as a function of the intrinsic viscosity, $[\eta]$. Although presented for viscosity and not elasticity, what is clear from Equation 5.3 is that as the viscosity asymptotes the maximum packing fraction does not exceed 0.64 (maximum packing). As such, systems presented in Figure 5.6b, do not fit typical hard sphere models.

Similar observations have been reported for agar microgel suspensions presented by Adams et al. (2004), where above a critical volume fraction, $\phi_c$, an elastic response was observed, becoming insensitive to increasing phase volumes above $\phi_{max}$. It was explained that above $\phi_c$, elasticity was a function of the modulus arising from the soft, deformable particles. However, the plateauing effect was unexplained, suggested as an artefact of the phase volume calculation. EmFG are therefore also assumed to act as soft spheres. It is suggested that the deformable oil core and elastic whey protein shell allows for the EmFG particle deformation when highly concentrated, reaching phase volumes that exceed those expected for rigid spheres. At such high phase volumes a jamming phenomenon is observed, thus particle rheology mainly represents a function of the shell (Koumakis et al., 2012). Hence above a volume fraction of 0.64 particles are packed to an extent that system elasticity is close to those shown for filled quiescent gels (Chen et al., 2000), hence frequency sweeps show gel-like behaviour (Figure 5.6a).

EmFG prepared using 5% (v/v) oil showed marked storage moduli even though $\phi_{max}$ had not been reached. Here, an elastic response is observed not through the jamming of particles, but assumed to arise from interactions between the EmFG particles, resulting in steric confinement. Between $\phi_c$ and $\phi_{max}$ it is argued that EmFG act as a soft-glass where particles become trapped allowing localised motion but not long range diffusion, similarly to results published by Koumakis et al. (2012) and Le Grand (2008). Therefore, the EmFG can be categorised into three regimes; dispersed particles below $\phi_c$ (5% oil), glassy between $\phi_c$ and $\phi_{max}$, and jammed above $\phi_{max}$ (10% oil).

#### *5.3.2.2. Material solid to liquid behaviour*

The effect of oil fraction on material response was further probed through the use of stress sweeps. Figure 5.7 shows the data obtained for EmFG with increasing oil content (from (a) to (d)). The stress sweeps indicate that at a critical stress the network started to break down. Further increase of the stress led to a transition at which point the loss modulus dominated the storage (shown by the dashed line). At this point a change in material response occurs, where the system no longer resembles a pseudo-solid, but is much more fluid-like.

For systems described previously as glassy ($>\phi_c$ and $<\phi_{max}$), where particles have become trapped through inter-particle interactions, the linear viscoelastic region (LVR) was observed to be much shorter than those for jammed systems. This can be seen more clearly from the crossover point in Figure 5.8, where stress values needed to induce liquid-like behaviour have been shown as a function of oil content: values obtained from stress sweeps shown in Figure 5.7. Again, a similar correlation can be seen when

compared to data obtained for frequency sweeps; where a plateau is reached for oil fractions above 10% (v/v). Again, such observations can be interpreted through the deformability and jamming of the particles.

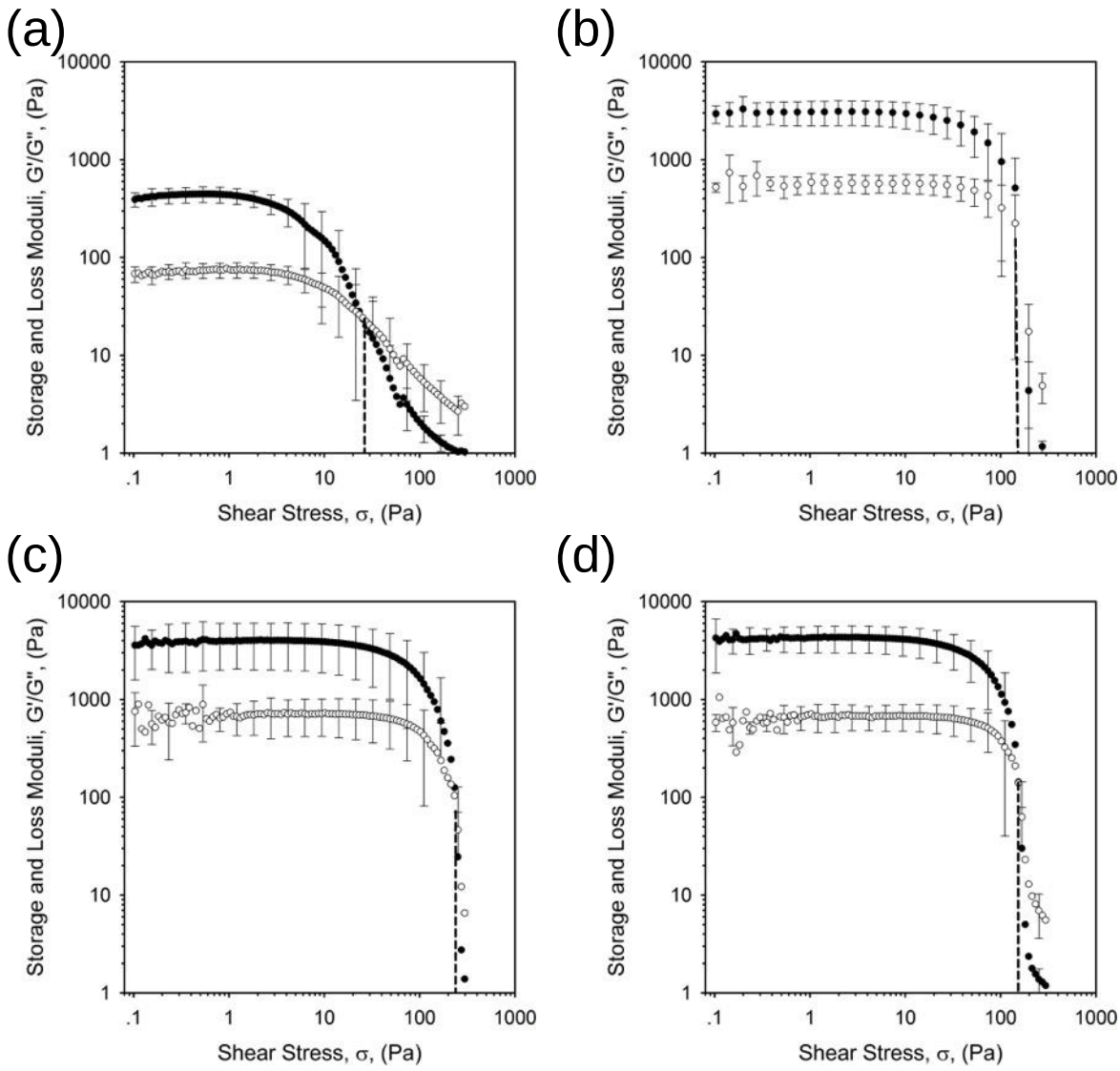


*Figure 5.7: Stress sweeps obtained at 1 Hz (25 °C) for EmFG prepared with 20% (w/w) WPI and: (a) 5% (v/v) oil, (b) 10% (v/v) oil, (c) 15% (v/v) oil, and (d) 20% (v/v) oil. Dashed vertical line is a guide for eye, to show shear stress at the point of solid to liquid crossover.*

Where particles have become deformed and compressed, a larger stress is needed to induce flow due to an increased number of particle-particle interactions as observed for κ-carrageenan fluid gels (Garrec et al., 2013). However, where particles are not jammed but sterically trapped (5% (v/v) system), fewer interactions between particles need to be broken to induce flow (Le Grand, 2008). Therefore, similarity between the particle surfaces, produces systems where the transition from solid to liquid-like behaviour is determined by the packing density.

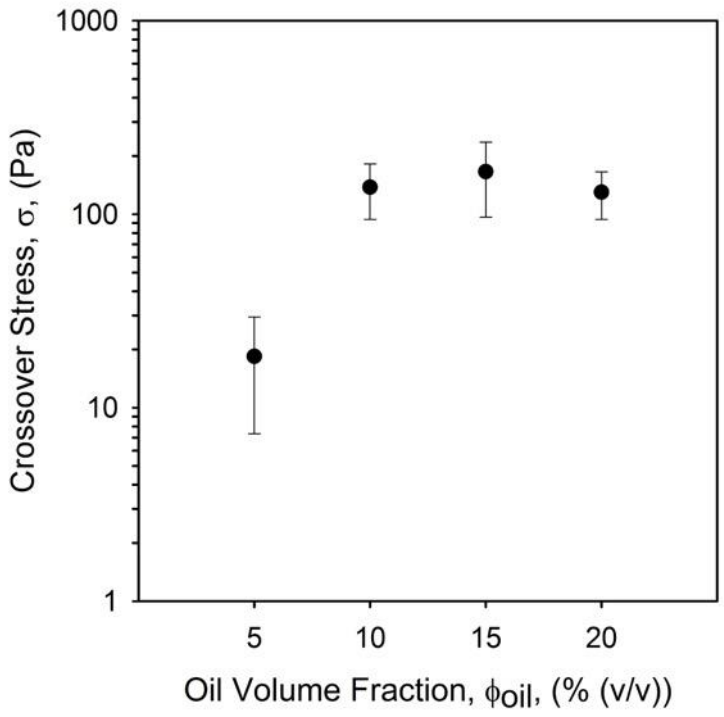


*Figure 5.8: Stress required to induce a crossover to liquid-like behaviour, determined using stress sweeps as the point at which the storage modulus (G') crosses the loss modulus (G") for EmFG systems prepared using 20% (w/w) WPI and oil fractions between 5 and 20% (v/v).*

#### *5.3.2.3. Suspension flow behaviour*

System flow behaviours for all WPI EmFG were studied and presented in Figure 5.9.

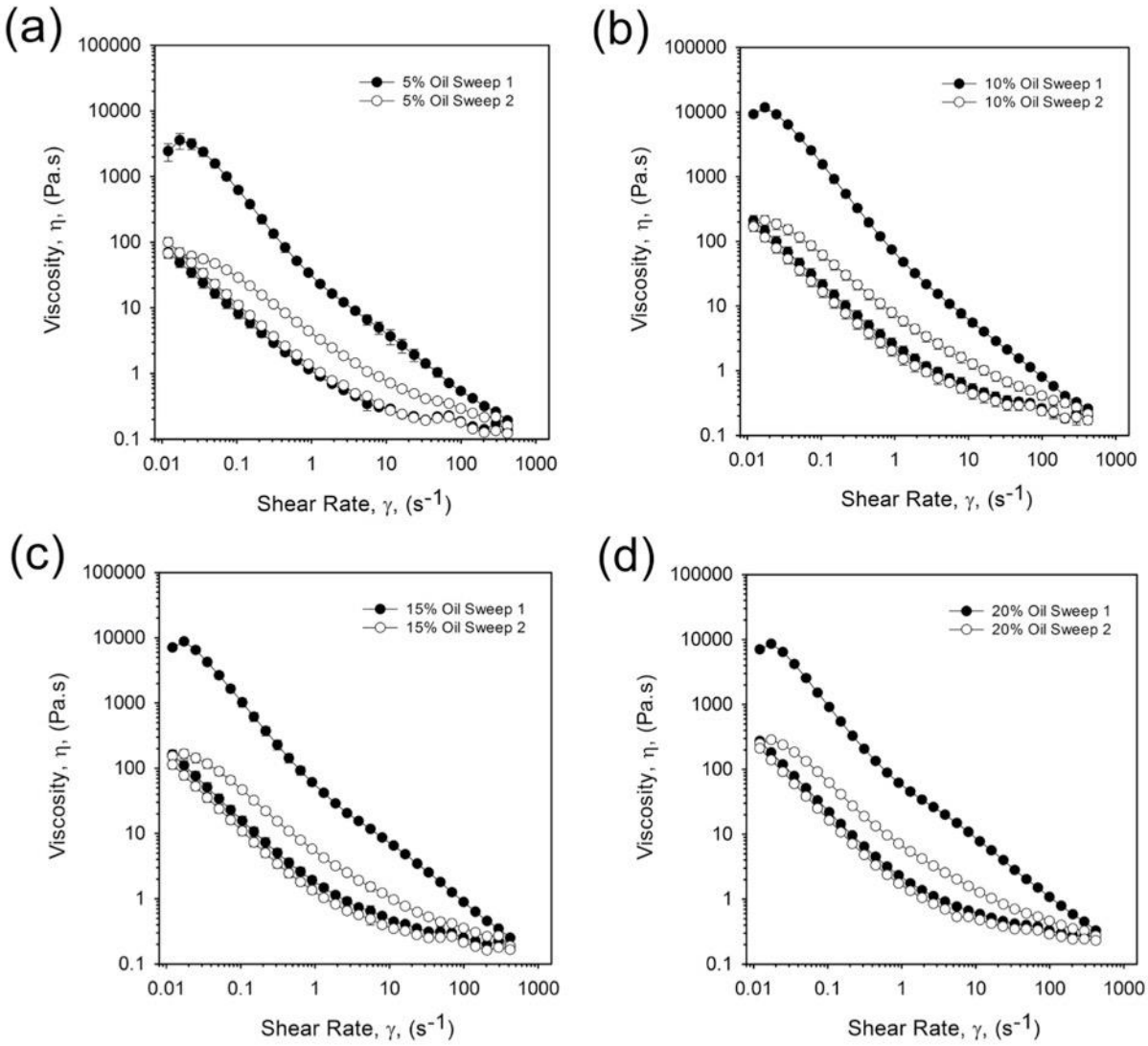


*Figure 5.9: Viscosity profiles obtained for 20% (w/w) WPI EmFG containing: (a) 5% (v/v) oil, (b) 10% (v/v) oil, (c) 15% (v/v) oil, and (d) 20% (v/v) oil. Closed markers represent sweep 1 and open, sweep 2.*

EmFG showed marked shear thinning behaviours typical of highly flocculated suspensions (Quemada, 1998). At very low shear rates (~0.01 $s^{-1}$) an apparent shear thickening can be observed as an artefact to stress overshoot (Ravindranath and Wang, 2008, Boukany et al., 2009). Continued increase in the applied strain resulted in thinning of the suspensions. The observed thinning is due to the heterogeneous flow across the shear rates applied, as a result of the break down to the weakly flocculated network (Quemada, 1998). Thus, a degree of inter-particle interactions are suggested, where initially a interacting network across the sample volume becomes broken down into smaller flocs, and eventually single particles.

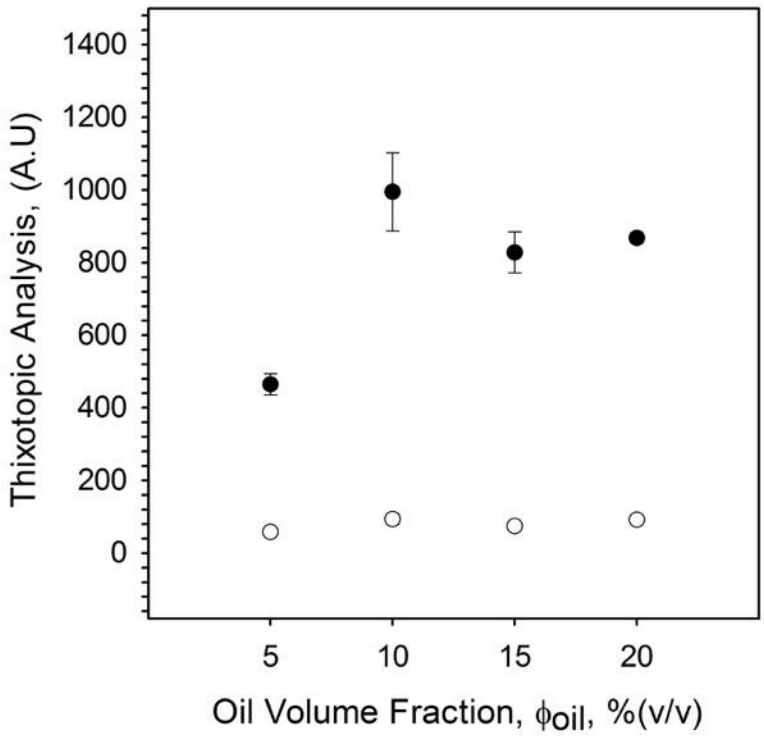


*Figure 5.10: Thixotropic analysis obtained as the area between the viscosity profiles for 20% (w/w) WPI EmFG with increasing oil phase volumes from 5 to 20% (v/v) ((●) denote thixotropic analysis for sweep 1 and (○) denotes values for sweep 2).*

To analyse this further, data has been presented for the ramp up, down and additionally a second sweep taken immediately after the first. The presence of hysteresis highlighted a thixotropic nature arising through the breakdown of floccs, as seen in Figure 5.10. The plot shows a similar correlation as previously observed for yield stresses and frequency sweeps whereby the more highly packed systems (10 to 20% (v/v) oil) have a greater hysteresis. This indicates that jammed systems have a much higher degree of inter-particle interactions as a result of greater packing density. Below the maximum packing fraction a lower degree of thixotropy is observed, as expected, as non-deformed particles present a smaller surface area for inter-particle interactions to occur.

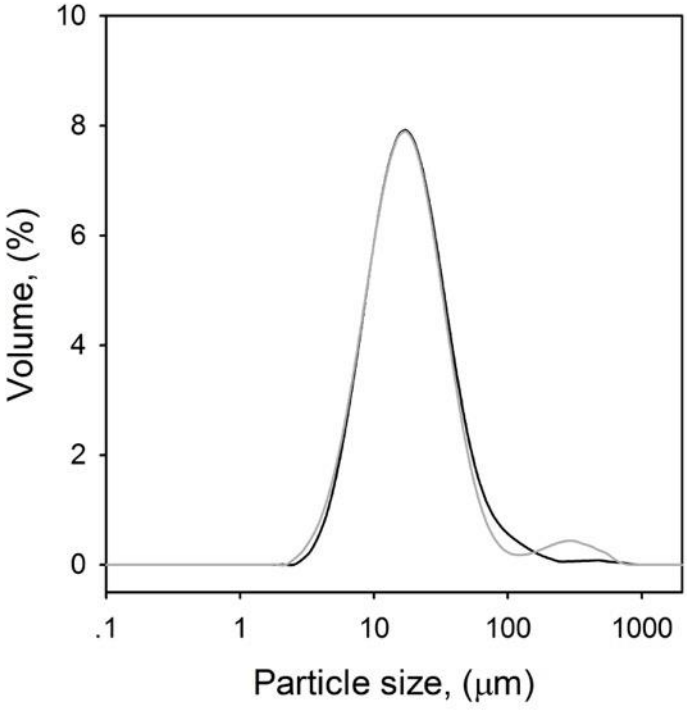


*Figure 5.11: Size distributions obtained using SLS for EmFG suspensions pre-thixotropy analysis (black line) and post-testing (grey line) for: (a) particles prepared at 10% (v/v) oil and 20% (w/v) WPI.*

The data presented for the second sweep showed a similar thixotropic behaviour for all systems, irrespective of oil content, where bridging between particles have been temporarily broken. This is supported by a combination of microscopy and light scattering techniques, which showed that the applied shear was insufficient to break the single particles; with the same particle size distributions observed pre- and post-shear sweeps Figure 5.11. Therefore, it is argued that the shear applied throughout the first sweep disrupts the network to an extent that the originally flocculated networks become broken down to discrete particles. This is followed by restructuring, but on a time scale that is much slower than the break down.

#### *5.3.2.4. Material recovery*

The recovery was further probed using oscillatory rheology. Primarily the system underwent rejuvenation, whereby the flocculated structure is broken down at a shear rate found within the shear-thinning region for all systems (10 $s^{-1}$ for 10 s). The structuring was then observed through the storage modulus (G') over the subsequent 30 minutes, Figure 5.12. The recovery curves show an exponential process, initially rapid, followed by a more gradual increase in elastic modulus as the number of available interactions between particles becomes fewer; modelled as a power function, $n$=0.45**±0.7** (power index obtained by fitting to curves in Figure 5.12). The same power law dependency observed across all systems can be argued as the same recovery mechanism being observed *i.e*. initially there is rapid formation of a large number of small flocs, as the flocs grow in size the change in G' slows as fewer larger particles are available to bridge. Recovery was independent of oil fraction at volume fractions greater

than 0.64, with the extent and rate of recovery suggested as a function of the similarity between particle surfaces. For systems <0.64, G' values were lower by a factor of 10; as is observed from the frequency sweep data, again due to less bridging where non-deformed particles present a smaller contact area to interact. As such, the hysteresis observed through dynamic shear experiments is suggested to arise not through the rupturing of the gelled structure, but from the break-down of reversible bridging between the particles.

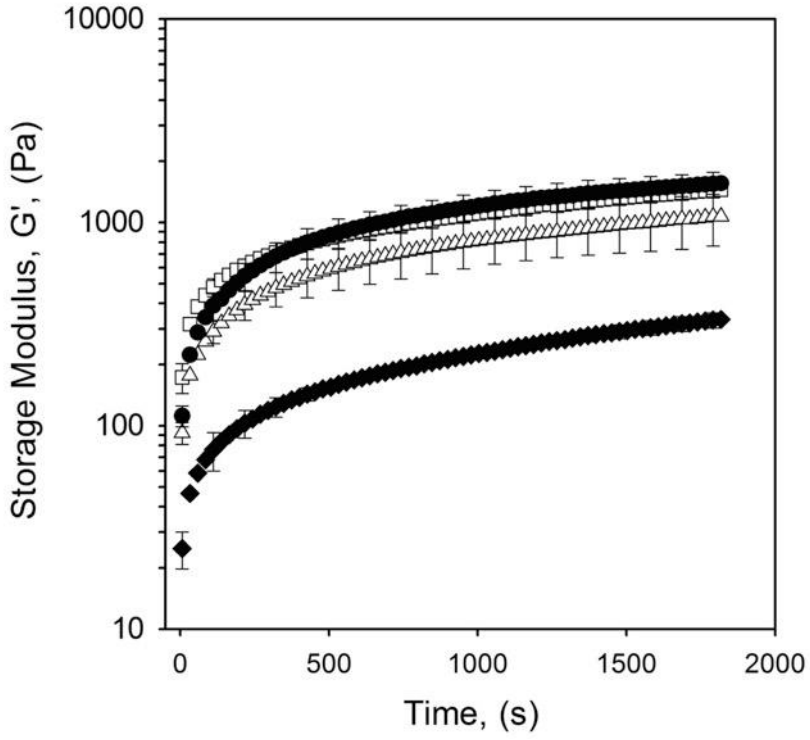


*Figure 5.12: Storage modulus as a function of time for EmFG systems (◆) 5% (v/v) oil, (□) 10% (v/v) oil, (△) 15% (v/v) oil, and (●) 20% (v/v) oil. All EmFG underwent a rejuvenation process of 10 $s^{-1}$ for 10 s before measuring G' at 1 Hz and 1 Pa stress for 30 minutes.*

## 5.4. Conclusions

This study has shown that oil droplets can be incorporated into a WPI gel layer by applying a shear-gel technique. Entrapment efficiency was observed to be dependent on the protein concentration, as a function of the viscosity and flow behaviours, reaching up to 99 % of oil droplets becoming coated. Small deformation rheology was used to characterise the suspensions, which showed pseudo-solid like behaviour at rest, however, by applying increasing shear force to the system, the suspensions could be made to flow. Suspension rheology highlighted a significant dependence on the oil fraction, with the addition of oil increased the effective phase volume of the particles, resulting in an increase in particle contact. Increasing the oil content to around 10% (v/v) led to packing fractions that exceeded those for hard spheres. As such, particle properties have been expressed as soft and deformable. Flow behaviours of the suspensions were indicative of highly flocculated systems; where reversible shear thinning was observed through break down and restructuring of weak inter-particle bridges.

In summary, this study has shown the preparation of systems with both high levels of oil entrapment and rheologies indicative of solid-like products. As such, it highlights the application of such systems as fortified food ingredients, for low fat replacements; as the oil core also provides a route to deliver the key fat-soluble compounds typically lost in the reduced fat products. To further probe EmFGs as a potential delivery vehicle in fortified products, understanding the breakdown of the gelled shell in essential to understand the release mechanism. Therefore, the following chapter looks at an *in vitro* simulation for the digestion of the microcapsules.

# Chapter 6. *EmFG: In vitro digestion*


***Synopsis***

Emulsion fluid gel's (EmFG) intrinsic ability to deliver potential lipophilic compounds was studied using an *in vitro* system, focusing on EmFG digestion. The hypothesised mechanism for release *in vivo* was emulsion failure, driven by enzymatic proteolysis of the gel leading to instability of the droplets. To this end, system stability was studied under digestive conditions in the absence of actives. The micro-composites showed poor release under both environments, *ca.* 3% (vol) (sunflower oil), closely related to the degree of oil remaining un-trapped during the processing stages (Chapter 5). Gel digestion and droplet coalescence was investigated using a combination of microscopy and particle sizing techniques; showing rapid proteolysis of the shell, with emulsion droplets remaining stable thereafter. A mechanism was proposed for droplet stability; where the formation of a secondary interfacial protein layer, formed during the sol-gel transition, provided enzymatic protection through steric effects. The suggested mechanism was further probed via forcing a change in protein conformation at the substrate interface, by varying oil polarities. Such changes facilitated release under gastric environments, however, droplets remained stable to intestinal digestion, again suggesting that digestion was controlled by the interfacial intrinsic properties (protein adsorption). Finally, a mechanical approach was used to analyse microstructural changes, where the suspension's ability to structure was dependant on the oil used; increasing polarity resulted in lower storage moduli. Weakening of the inter-particle network again highlighted a change in the formation of the gel surrounding the oil. It is therefore suggested that understanding protein properties at the EmFG core interface, can allow control over particle digestibility, providing a means of tailoring particle properties for targeted delivery in fortified products.

## 6.1. Introduction

Enhanced functionality within products is an ever-growing market ("Functional-Foods", 2016). In addition, the reduction of fat within foods consequently results in a decrease in the lipid soluble components needed for a healthy diet. The ability to deliver such compounds, or essential lipids *etc.* to the body is therefore key. However, many of these ingredients such as omega-3 oils, hydrolysates and fat-soluble compounds have adverse effects within the GI route; whether it be unpleasant tastes that need masking, protection from harsh environments/enzymes or simply a delivery vehicle. The core shell model provided by EmFG is therefore a potential candidate for delivering many of these components.

This chapter furthers the knowledge of WPI EmFG systems formulated in the previous chapter, by investigating the *in vitro* response to digestion. Having previously shown the potential of the micro-composites as multifunctional particles for rheology modification, their ability to deliver poorly soluble compounds is further probed. It is hypothesised that release of poorly soluble compounds will be mediated through emulsion failure, subsequently allowing absorption within the GI tract. The work therefore focuses on understanding oil release (emulsion failure), studying the digestion of the gelled layer as a route to targeted delivery.

## 6.2. Materials and Methods

### *6.2.1. Materials*

Whey protein isolate (WPI) was obtained from Kerry Ingredients, Listowel, Ireland (WPI, W994, S-493391) and used without further purification. WPI composition

as stated by the supplier was 91.0 % protein, moisture 4.0 %, fat 1.0 %, ash 3.5 % and lactose 0.5 %. Mineral content of the WPI was: Ca – 0.50, P – 0.65, Na – 0.10, K – 0.15, Mg – 0.02 and Cl - 0.02 %. High oleic sunflower oil was obtained from Cargill (Cargill Inc., BE). Silicone oil (10 cSt), paraffin oil (analytical grade - Ph. Eur., BP), sodium azide, hydrochloric acid, simulated gastric fluid (USP x8), simulated intestinal fluid (USP x8), pepsin (porcine) and pancreatin (porcine) were purchased from Sigma-Aldrich (Sigma-Aldrich, UK).

### *6.2.2. Preparation of EmFG particles*

Preparation of the WPI-oil composites was conducted as outlined by Moakes et al. (2015b) (see chapter 5.2.):

#### *6.2.2.1. Preparation of emulsions*

Whey protein stock solution (20 % (w/w), on a protein basis) was first prepared by dispersing WPI in deionised water. An anti-microbial, sodium azide (0.02 % (w/w)) was added to increase storage time. The solution was stirred overnight at ambient conditions until completely hydrated and subsequently stored at 5 °C until further usage.

Oil (high oleic sunflower, silicone or paraffin) was added to WPI primary solution to result in a 10 % (v/v) oil in water mixture. The system was mixed using a high shear mixer (Silverson, SL2T) at 4000 rpm for 10 mins. The resultant emulsion pH was slowly adjusted to pH 4.6 with concentrated hydrochloric acid (12 M) and aged for 48 hrs.

#### *6.2.2.2. Preparation of particles*

A jacketed vessel and overhead stirrer equipped with pitched blade impeller was used to prepare all emulsion fluid gels. Emulsions were added to the jacketed vessel set to 50 °C, controlled via a circulating water bath. Shear was applied through the stirrer and impeller at 450 rpm (±5 %). Once thermal equilibrium was obtained (*ca.* 10 minutes), emulsions were heated at a rate of 0.5 °C$min^{-1}$ to 80 °C, using a cover to avoid significant water loss. Suspensions were subsequently decanted and left to cool quiescently at ambient conditions. Cooled EmFG were further stored at 5 °C until tested.

### *6.2.3. Digestion and release*

#### *6.2.3.1. In vitro digestion*

*In vitro* studies were carried out using an orbital shaking incubator at 37 °C. Simulated gastric and intestinal fluids were prepared as follows:

*Simulated gastric and intestinal fluid preparation*

Simulated gastric fluid was prepared by diluting concentrated simulated gastric fluid (Sigma Aldrich - USP grade: 0.07 M NaCl, 0.1 M HCl) with deionised water, as per packaging instructions. Powdered pepsin was then added resulting in a final concentration of 0.32% (w/v) as described by Remondetto et al. (2004). The solution was allowed to equilibrate at 37 °C and decanted into smaller vessels for further digestion experiments.

Simulated intestinal fluid was prepared in a similar manner by diluting concentrated simulated intestinal fluid (Sigma Aldrich - USP grade: 0.6 g/L sodium

hydroxide, 6.8 g/L potassium phosphate monobasic) with deionised water, as per packaging instructions. Pancreatin was then added, resulting in a final concentration of 1.0% (w/v), again as described by Remondetto et al. (2004). The solution was allowed to equilibrate at 37 °C and decanted into smaller vessels for further digestion experiments, removing any sediment.

After simulated fluids had reached thermal equilibrium, EmFG alliquots were syringed into the separate conical flasks at a ratio of 20 ml: 80 ml (sample to digester) and warmed at 37 °C under agitation, using an orbital shaking incubator (Incu-shake, SciQuip, UK), until removed for the extraction process.

#### *6.2.3.2. Release determination*

Release was determined by first extracting the free oil within an organic solvent, hexane. Hexane (20 ml) was added to the digester, manually shaken and separated using a separating funnel under gravity. The aqueous phase was discarded and organic phase placed in a rotor evaporator until only high oleic/silicon or paraffin oil remained. A mass balance was then used to determine the degree of release within the system.

### *6.2.4. Static light scattering (SLS)*

A MS2000 Mastersizer with attached Hydro SM manual small volume dispersion unit (Malvern Instruments Ltd, UK) was used to obtain size distributions. Distributions are the average of three repeats. Particle size calculations were based upon the Mie theory; thus, particles were assumed to be homogenous spheres. For size measurements

during the dissolution the refractive index of the oil was used (high oleic = 1.47, paraffin oil = 1.48 and silicone oil = 1.4). (For further details see Appendix i)

### *6.2.5. Microscopy*

A Brunel SP300-fl (Brunel Microscopes Ltd, UK) optical light microscope fitted with an SLR camera (Cannon EOS Rebel XS, DS126 191) at 20 and 40x optical magnification was used to image the particles. Slides were prepared by addition of 50 μL of sample to a microscope slide (VWR, UK) and covered with a coverslip (Thickness no.1, VWR, UK).

### *6.2.6. Interfacial Tension Analysis*

Interfacial tension (IFT) measurements were obtained using a K100 Tensiometer (Kruss GmBH, Germany) equipped with a Wilhelmy plate set up. Dynamic surface tension measurements were obtained over 600 s for: paraffin, silicone and high oleic oils with/without the presence of WPI (20% w/v). Experiments were run in triplicate and error calculated as the 95% confidence range.

### *6.2.7. Rheological Analysis*

Rheometry was conducted using a Bohlin Gemini HR Nano stress-controlled Rheometer (Malvern Instruments Ltd, UK) equipped with serrated parallel plate (25 mm diameter) at 1 mm gap height. Experiments were undertaken at 25 °C using a silicon oil moisture trap. An equilibrium time of 5 minutes prior to testing, allowed for consistent loading conditions. Stress sweeps were conducted at 1 Hz from 0.1 to 400 Pa and frequency sweeps were obtained between 0.1 and 10 Hz at controlled stress. The stress

was determined by amplitude sweeps as a value within the linear viscoelastic region (LVR) for all EmFG tested. (For further details see Appendix i)

## 6.3. Results and Discussion

### *6.3.1. In vitro digestion of protein-oil composites*

Oil release was studied as a function of emulsion failure under both simulated gastric and intestinal conditions. Figure 6.1 shows release curves for WPI stabilised emulsions (open symbols) and EmFG suspensions (closed symbols). It was observed for simple emulsion systems, whereby the system had not undergone sheared gelation, failure of the emulsion - facilitated by stripping off of the emulsified layer allowing extraction into the organic solvent, occurred under both *in vitro* environments. It is expected that emulsifier breakdown follows a mechanism as outlined by Sarkar et al. (2009); whereby enzymatic hydrolysis leads to instability and eventual stripping off of the interfacial layer. WPI contains a mixture of several proteins, however, it primarily consists of β-lactogloblin (β-lg). Within its native globular 3-dimensional conformation, β-Lg exhibits a high level of resistance to proteolysis (Mandalari et al., 2009, Sarkar et al., 2009, Malaki Nik et al., 2010); as the binding sites needed for enzyme adsorption are inaccessible, buried within its globular structure (Reddy et al., 1988). Proteolysis here is achieved through partial denaturation of the protein, where unravelling at an interface exposes the cleavage sites needed for enzymatic action (Mackie and Macierzanka, 2010, Sarkar et al., 2009). The slow rate of release *ca.* 20-25% over 5 hrs, is therefore a function of the accessibility of the enzyme to the binding sites; where the rigid β-lg

structure inhibits digestion in comparison to much more flexible milk proteins such as caseins (Macierzanka et al., 2009).

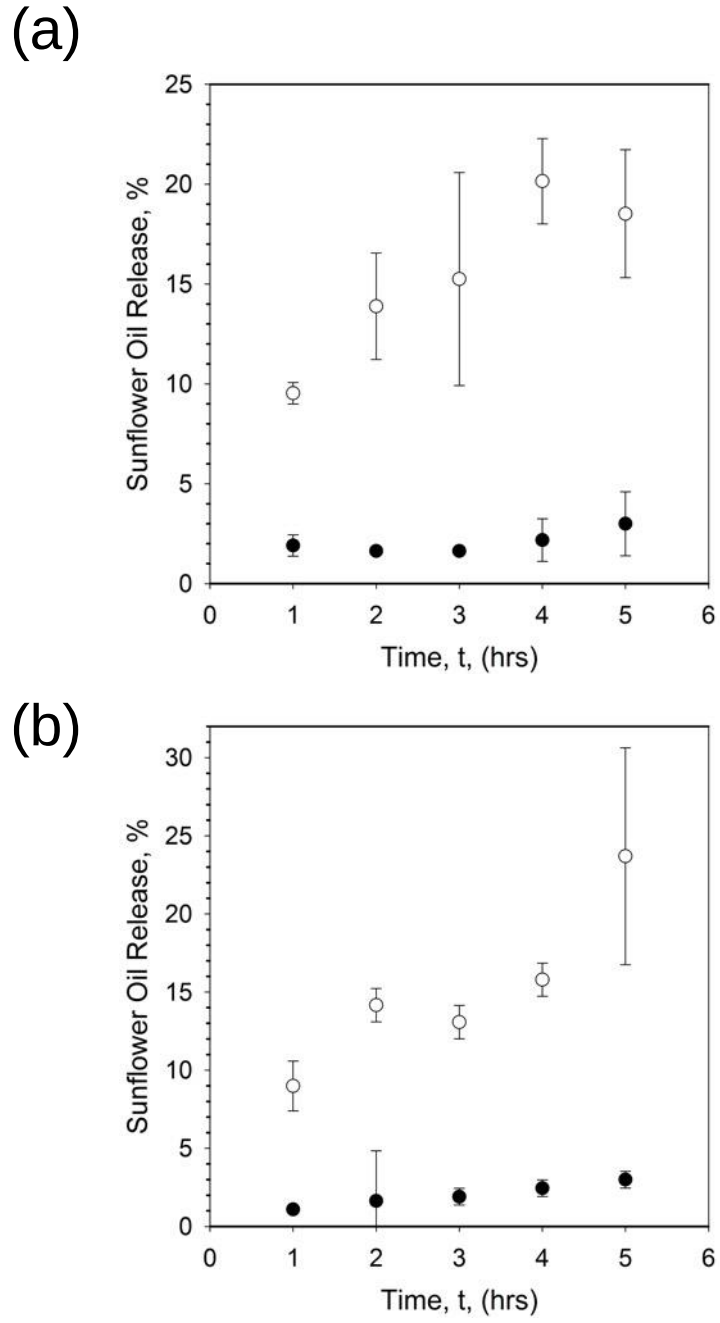


*Figure 6.1: Release profiles for: (a) gastric and (b) intestinal digestion of a simple WPI stabilised emulsion (○) and high oleic sunflower oil microgel composites (●).*

Release profiles for the core-shell particulate suspensions, prepared using a shear-gel process, have also been presented in Figure 6.1 (closed markers). Curves obtained for composite systems deviated from those shown for simple emulsions with low levels of release, ~3 % (vol), observed within both digestive environments. The low degree of release observed can be compared to the degree of entrapment during processing, reflecting the amount of oil which does not become coated within a gel layer (Chapter 5)(Moakes et al., 2015b). Therefore, the reduction in release is argued to be a function of the processing; where no gelation/protein shell is formed, droplet breakdown occurs similarly to that of simple emulsion systems. It is therefore suggested that proteolysis prevention is derived from a microstructural change, which occurs during thermal denaturation and growth stages at the substrate/water interface.

#### *6.3.1.1. Digestion studied via SLS*

EmFG suspension digestion was further studied as a function of droplet size, using a combination of light scattering and optical techniques. Sample aliquots were obtained and analysed immediately, as such enzyme deactivation was not needed. Figure 6.2a, b and c show optical micrographs obtained (x20 magnification) for EmFG systems after: 0, 1 and 6 hours respectively. At $t_0$ droplets appear darker with non-uniformed edges indicating the presence of WPI shells. Such shells can no longer be observed after 1 hr of digestion signifying that proteolysis of the gel coating occurs relatively early on in the study. Following microscopy, emulsion stability was probed as a function of coalescence, using a sizing technique (Figure 6.2, distributions). An initial shift in peak maxima originally centred over 20 μm at $t_0$ to 30 μm after $t_{1hr}$ can be seen,

with distributions showing good agreement with each other thereafter. Such changes can be explained through the digestion of small protein aggregates, which present a larger surface area for enzymatic attack (observed in Figure 6.2a), causing a shift in the distributions to centre over higher droplet sizes.

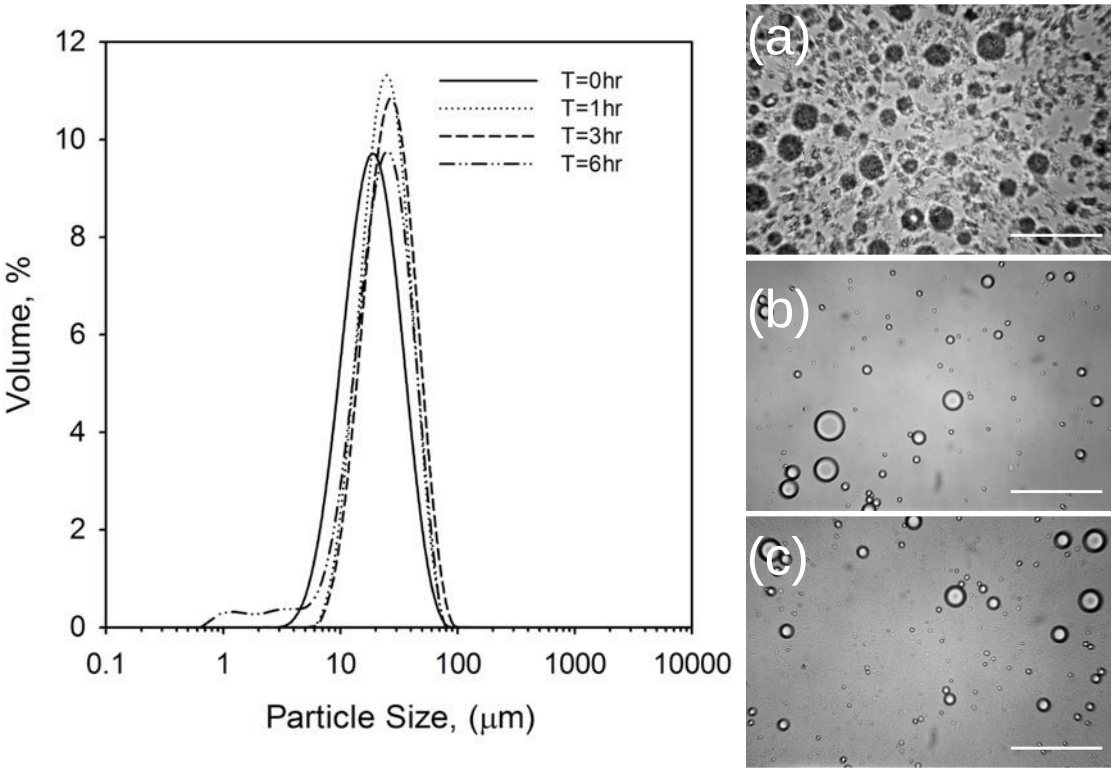


*Figure 6.2: Composite droplet size distributions as a function of digestion time (gastric conditions) and optical micrographs depicting typical images for composites undergoing digestion at time (a) 0 hours, (b) 1 hour and (c) 6 hours. Scale bars represent 100 μm.*

The lack of evidence for droplet coalescence over the whole digestion period suggests the formation of gastro-stable emulsions, where proteolysis becomes inhibited at the interfacial layer, separating the oil core and continuous medium. Such observations agree with the data presented for release via extraction, as the hydrophilic surfaces prevent transfer of the lipophilic core into the hydrophobic solvent. Therefore, the low

levels of release previously observed in Figure 6.1 cannot solely be a function of the gelled coating itself, as emulsion droplets remain stable even though the gelled layer has become digested.

#### *6.3.1.2. Proteolysis of the shell*

The time-scale for shell digestion was investigated using a hot-stage microscope. Simulated digestive solutions were added to EmFG (4:1) and pipetted on to a concave microscope slide at 37 °C. Micrographs were obtained every minute, with the first 5 mins presented in Figure 6.3. Rapid breakdown of the protein can clearly be seen, with shells visually disappearing by minute 3 (Figure 6.3c) and complete digestion of the WPI gel by minute 5 (Figure 6.3e). However, loss in image clarity was observed due to digestion of the gel coating, allowing migration of less dense oil droplets towards the top of the sample. As such, a slight reduction in the focusing was seen, shown by the broadening of the droplet "interface".

Previous studies have shown digestion kinetics dependent on the gel microstructure, with gels prepared far from the isoelectric point exhibiting a greater degree of proteolysis in comparison to those formed where no net charge results in high aggregation (Macierzanka et al., 2012). Additional work on iron release from bulk gels, again indicated that a particulate microstructure provides a greater resistance to breakdown, with enzymes only being able to attack proteins at the surface (Remondetto et al., 2004). The fast rate of digestion observed here is argued to be a function of the small particle sizes, due to the particulate nature of the system, presenting a large available surface area increases enzyme binding. Furthermore, gel layers surrounding the oil droplets were observed to be on the order of several microns, shown using CLSM

in Chapter 5, Figure 5.3. As such, enzyme diffusion within the gel matrix will be short, leading to a reduction in digestion time. Therefore, it is proposed that the combination of a large surface area and thin-gelled layers result in fast digestion kinetics, even though resistance to proteolysis might be expected for gels formed at this pH.

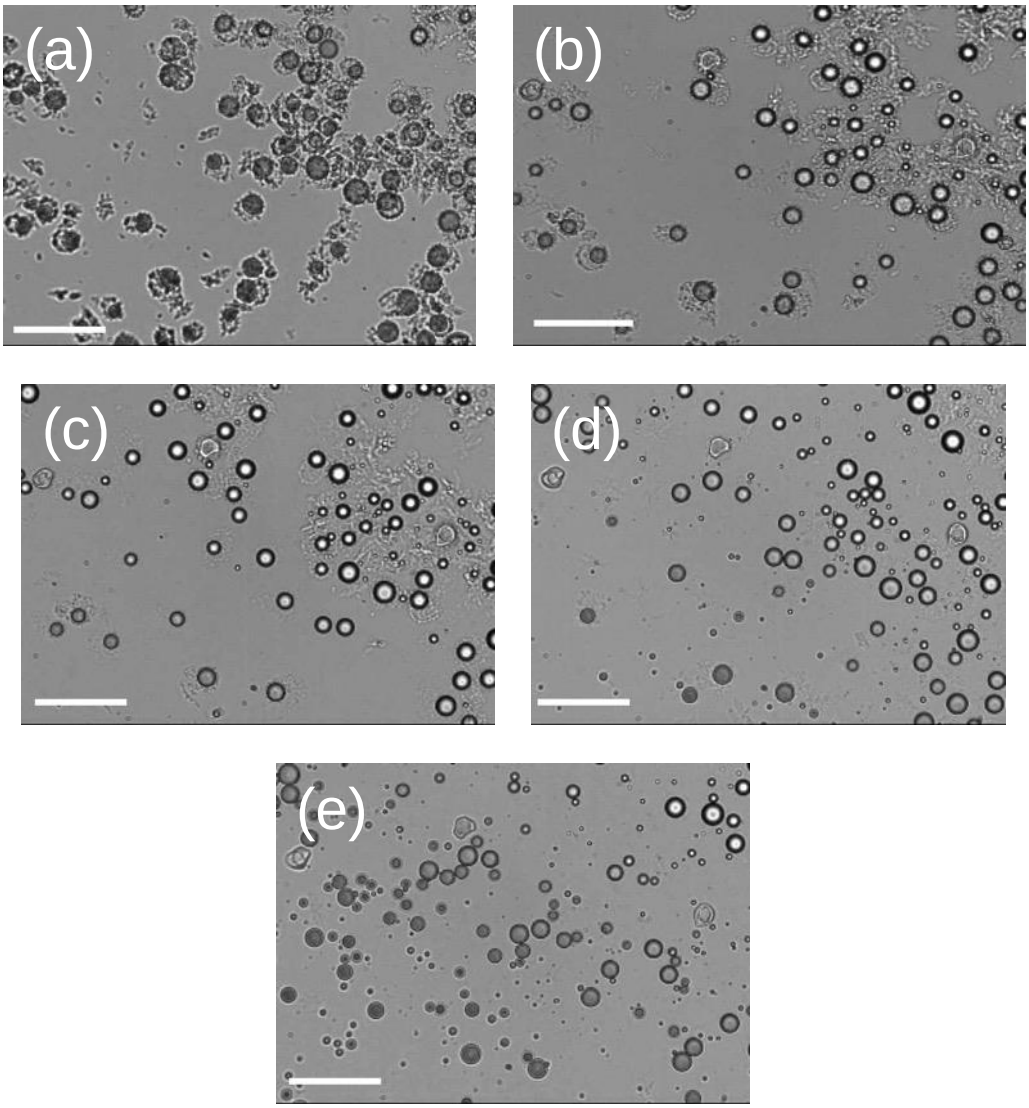


*Figure 6.3: Micrographs showing proteolysis of the gel layer under a gastric (4:1 digester to sample ratio) environment: (a) 1 min, (b) 2 mins, (c) 3 mins, (d) 4 mins and (e) 5 mins. Scale bar shows 100 μm.*

#### *6.3.1.3. Mechanism for emulsion stability*

As previously discussed (sections 6.3.1.1. and 6.3.1.2.) shell proteolysis occurs on such a short time-scale that emulsion stability must be a function of a stable interfacial layer. Protein conformation has a direct effect on droplet stability (Das and Kinsella, 1990). However, thermal interfacial cross-linking of protein via disulphide interactions has been previously shown to have little effect on digestion inhibition (Sandra et al., 2008). Therefore, the following mechanism is proposed for protein adsorption and protection, based on protein arrangement around the interface: Thermal treatment causes further re-arrangement of the protein at the interface, increasing surface hydrophobicity (Das and Kinsella, 1990), and creating points of nucleation for growth from the surrounding continuous phase. Partial denaturation of the protein within the continuous phase at lower temperatures results in proteins retaining the majority of their original structure, providing a greater resistance to proteolysis (Reddy et al., 1988). These proteins then diffuse to the interface providing a secondary interfacial layer, sterically burying enzymatic cleavage sites, shown by the schematic representation in Figure 6.4. Shell growth then continues via enrichment of denatured protein as the temperature increases. Where no further enrichment from the continuous phase has occurred, a greater degree of thermal crosslinking within the interfacial layer is expected, however, an insufficient degree of protein is available to hinder enzymatic attack.

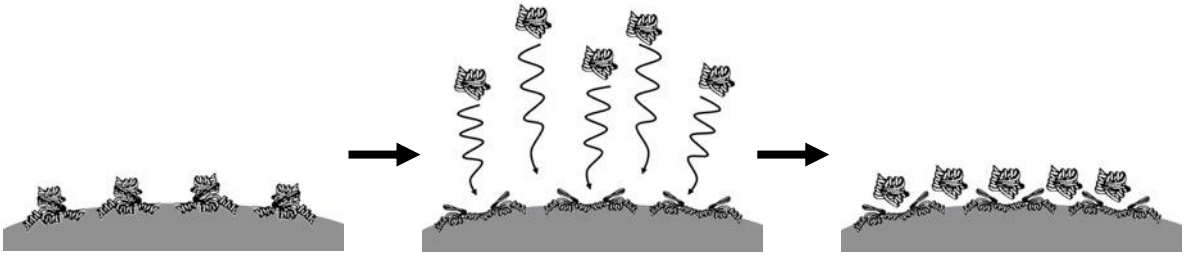

*Figure 6.4: Schematic showing the evolution of a secondary interfacial layer, resulting in the blockage of enzymatic cleavage sites. Proteins adapted from Wilde et al. (2004)*

### *6.3.2. Effect of oil polarity on emulsion failure (release) during digestion*

The proposed mechanism for emulsion stability under gastro-intestinal conditions was further probed as a function of oil substrate polarity. Previous work on protein stabilised emulsions has shown protein conformation adopted at an oil/water interface to change dependent on the polarity of the dispersed phase (Rampon et al., 2004). Thus, it was believed that through control of the WPI interfacial conformation and subsequent packing, a route to enzymatic attack and release within *in vitro* conditions could be achieved.

Figure 6.5 shows the interfacial tension (IFT) measurements obtained for all 3 oil substrates used; high oleic (circles), silicone (upwards triangles) and paraffin oil (downwards triangles), corresponding with literature presented for such systems (Fox et al., 1947, Jasper, 1972). A decrease in substrate polarity can be seen from the increase in IFT between the water and the oil phases. The change in polarity arises as a function of the oil chemical structure; where polar groups become increasing hidden within the polymer backbone for silicone oil, and absent within paraffin. The change in IFT can therefore be interpreted as an increase in hydrophobicity.

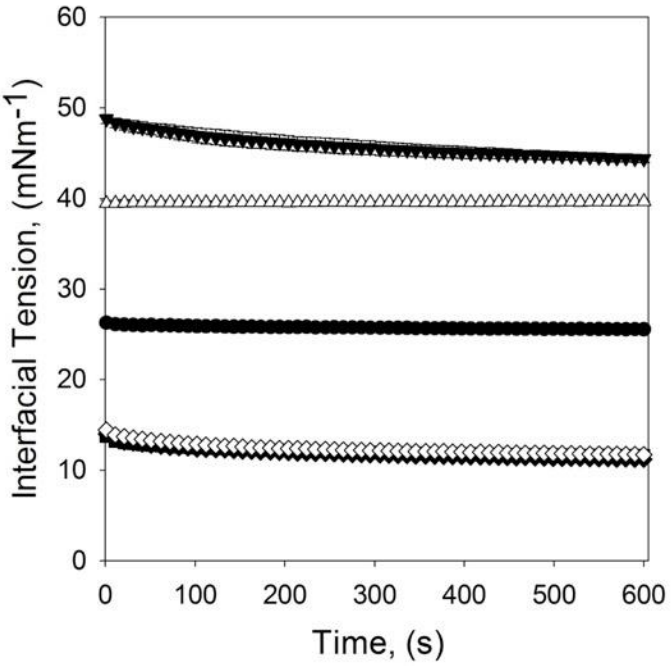


*Figure 6.5: Interfacial tension measurements showing decreasing tension for water and (▼) paraffin oil, (△) silicone oil, and (●) high oleic oil systems. Additionally, measurements for each oil system in the presence of WPI have been shown: (◆) paraffin oil, (◇) silicone oil, and (■) high oleic oil, overlapping ca. 14 mNm$^{-1}$. Data shows the average of 3 repeats, with error bars showing the 95% confidence interval (error bars are hidden by the data points, apart from paraffin only).*

In the presence of an emulsifier (WPI), however, all systems show the same IFT, with curves overlapping *ca.* 14 mNm$^{-1}$, again corresponding with the literature (Córdova and María, 2014, Kato and Nakai, 1980). Such observations suggest a similarity across the different oil-water and protein mixtures with proteins lowering the interfacial tension between the two fluids. EmFG were prepared using both paraffin and silicone oil to study the effect of substrate polarity on digestion and subsequent droplet failure. Figure 6.6a and b show typical micrographs obtained for silicone oil EmFG and paraffin oil EmFG systems respectively. The micrographs show high levels of entrapment for both systems, similar to systems prepared with high oleic oil.

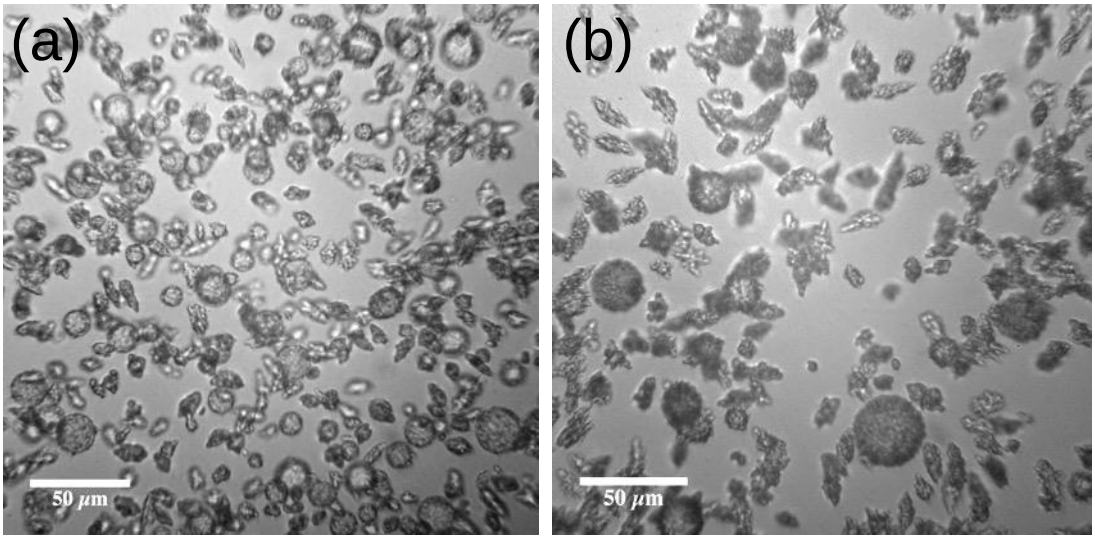


*Figure 6.6: Optical micrographs presenting typical images for (a) silicone oil EmFG and (b) paraffin oil EmFG.*

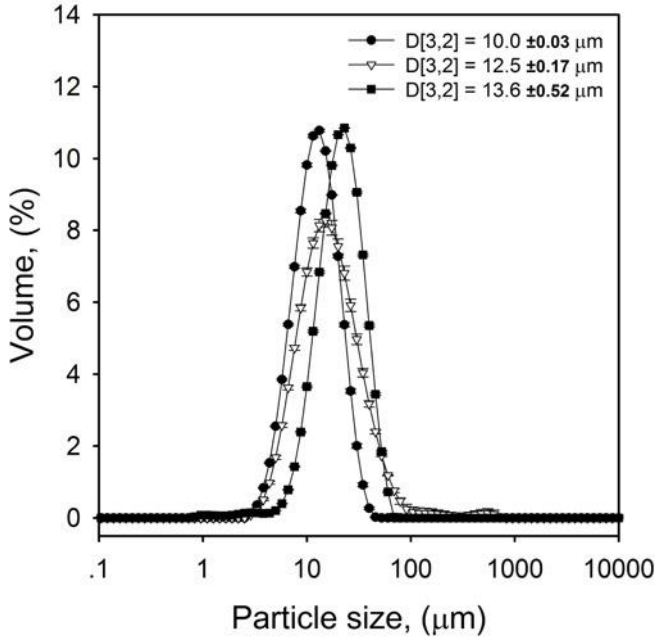


*Figure 6.7: Particle size distributions for: (●) silicone oil, (▽) paraffin oil, and (■) sunflower oil EmFG systems. The surface weighted mean ($D_{[3,2]}$) for each system has been presented in top right of the plot.*

Size distributions obtained for the same systems, Figure 6.7, are also very close to those obtained for high oleic sunflower oil; with surface weighted means within 3.6 μm

of each other. Similarity between surface volumes and particle morphology reinforced the assumption that changes in digestion would be a function of the gel/interfacial layer, and not effective area for enzymatic attack.

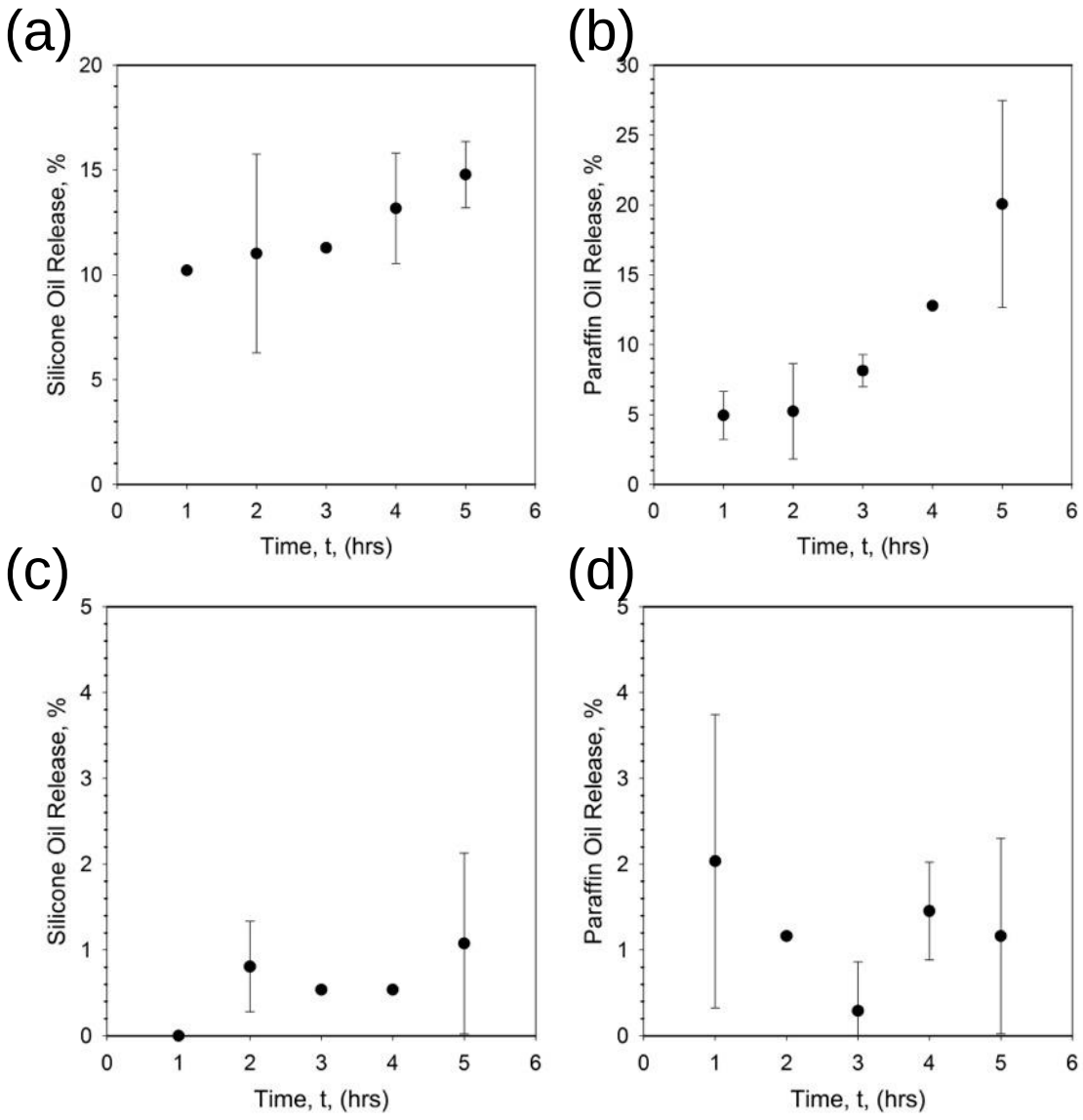


*Figure 6.8: Release plots for the gastric digestion of: (a) silicone, (b) paraffin oil and intestinal digestion (c) silicone, (d) paraffin oil micro-composites.* ***Note changes in y-axis scale****.*

The effect of polarity on release profiles under both gastric and intestinal environments has been presented in Figure 6.8. Release plots for gastric digestion show

both silicone oil (Figure 6.8a) and paraffin oil (Figure 6.8b), where extraction has been facilitated through enzymatic digestion of the protein layers. Increasing the hydrophobic nature of the oil droplet is suggested to have resulted in a change in the interfacial protein during thermal processing, in a similar way to work published by Rampon et al. (2004). It is proposed that the increased hydrophobicity causes a greater degree of unfolding and subsequent anchoring between the emulsified protein and the oil core, with stronger hydrophobic interactions (Maldonado-Valderrama et al., 2012). This reduces degree of re-arrangement during the heating stages, resulting in a more open secondary interfacial structure. Thus, enzymes are no longer sterically prevented from accessing the cleavage sites required for pepsin specific proteolysis.

A lower gradient can be observed when comparing the change in release over time for the silicone system compared to the paraffin oil EmFG. Again, such observations can be explained through the degree of packing around the interface, hindering access to the enzymatic cleavage sites. Move over, the data shows the presence of release from the two systems, signifying proteolysis and striping of the interfacial proteins. On comparison to the release curves shown for non-heat treated high oleic emulsions, the extent of release is the same when accounting for variation between samples (20 **±5**%) (Figure 6.1). Such data suggests a change in the microstructure present at the substrate interface, which is closer to that of an untreated oil in water emulsion. Again, such data suggests that the release is governed by the intrinsic properties of the interfacial layers, which in the case of high oleic oil EmFG become altered in the gelation process.

Intestinal dissolutions (Figure 6.8c and d) for both oils yielded similar release profiles to the sunflower oil EmFG systems. Again, like high oleic micro-composites, the extent of release is suggested to be more indicative of the entrapment efficiency during

processing. Therefore it is argued that increasing the hydrophobicity of the substrate leads to the exposure of residues that are more associated with pepsin proteolysis such as leucine and isoleucine (Fersht, 1999), than the major pancreatic enzymes: trypsin and chymotrypsin (Tomé and Debabbi, 1998). However, further study in this area is needed to investigate such arguments.

### *6.3.2. Effect of oil polarity on suspension properties*

Rheology was also used to probe any changes in particle microstructure as a function of the oil core.

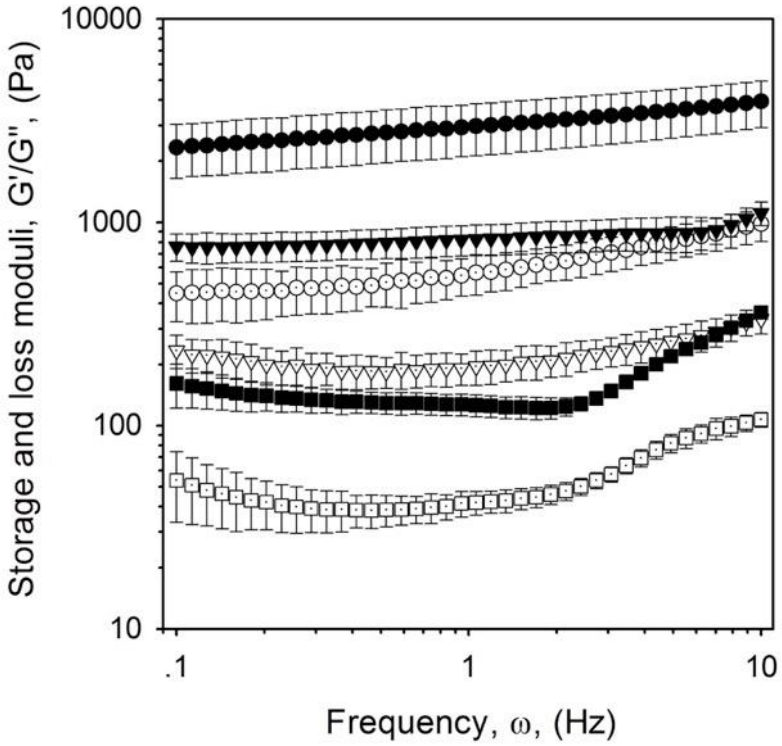


*Figure 6.9: Frequency sweeps obtained (1 Pa stress) for microgel composites prepared using (●/○) high oleic oil, (▼/▽) silicone oil and (■/□) paraffin oil as the oil substrate. Closed markers denote G' and open G".*

Figure 6.9 shows the mechanical spectra obtained for EmFG particles prepared high oleic oil (circles), silicone oil (downward triangles) and paraffin oil (squares). Gel-like behaviours were observed across all three systems, with G' dominating G'', typical of highly packed micro gel suspensions (Adams et al., 2004, Garrec and Norton, 2012, Norton et al., 1999, Moakes et al., 2015b). An elastic response can be seen to be dependent on the oil type, where decreasing moduli follow the same trend to substrate polarity. As oil volume faction and degree of gelation remain constant across all systems (assuming gelation to be solely dependent on the thermal history for all systems), changes in the elastic response are argued to be a function of the number of interactions occurring within the suspensions.

The interactions between particles were further studied using stress sweeps to probe system breakdown. Figure 6.10 demonstrates the same trend shown for frequency sweeps, with LVRs becoming shorter with increasing oil hydrophobicity. Here lower stresses are needed to induce flow, inferring a lesser degree of interactions between particles. It has long been known that the microstructure is key to system material properties. As such, it is argued that the observed differences in suspension moduli and "yielding" are a result of different degrees of interactions between particles, arising from a change in the gelation around the particles. It is suggested that the increased anchoring of protein to the more hydrophobic interfaces hinders further re-arrangement during heating, as previously described. This results in a more retained protein structure propagating throughout the final shell. Further studies using surface hydrophobicity and tryptophan analysis could help confirm this hypothesis, however, such changes would lead to the burying of sites needed for particle-particle bridging, describing the results shown.

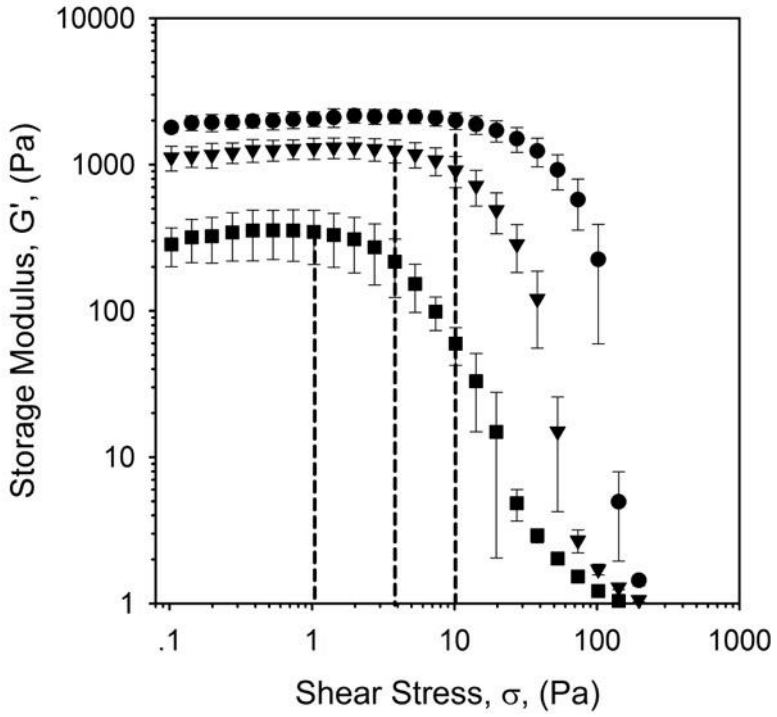


*Figure 6.10: Stress sweeps obtained at 1Hz for microgel composites prepared with (●) high oleic oil, (▼) silicone oil and (■) paraffin oil. Dashed lines are to guide the eye, highlighting the end of the LVR.*

## 6.4. Conclusions

This study has looked at the *in vitro* response of WPI oil-gel micro-composites to gastric and intestinal conditions. EmFG showed a high degree of resistance to proteolysis at both stages, with oil release comparable to the degree of oil non-gel coated droplets during processing. A combination of sizing and microscopy techniques revealed that proteolysis of the gel layer was achieved on a relatively short time scale, having completed within 5 mins of digestion. However, oil droplets remained stable for the remainder of the time studied. This suggested that oil release was not a function of the gel, but more closely linked to the intrinsic properties of the interfacial layers. Oil

polarity was used to probe such inferences; changing protein confirmation and packing at the interface. It was found that increasing the hydrophobicity of the oil phase facilitated release in gastric environments, however, within intestinal conditions droplets still remained stable. It has been suggested that the oil substrate plays an important role in the digestion stage, controlling protein packing and conformations during the heating stages of processing. As such, a mechanism was proposed postulating that a secondary interfacial layer is formed at lower temperatures during the sol-gel transition, which acts as a protecting layer. Changing oil hydrophobicity can manipulate the protein conformation and anchoring at the interface, therefore dictating the degree of openness within the secondary layer. This proves a route for enzymatic attack. Similar changes in the gel microstructure were also shown using mechanical testing. Suspension rheology correlated to changes in the oil core, highlighting a decrease G' and changes in yielding. Such observations represent a marked decrease in the number of interactions between particles as a function of the change in gel network.

Results obtained in this chapter have therefore highlighted the use of EmFG systems to deliver various oils, showing their potential to deliver essential oils or other potential lipophilic compounds. however, more work is needed to fully characterise the effects that such changes will have on the final release properties of the micro capsules.

# Chapter 7. *Conclusions and Future Recommendations*

## 7.1. Conclusions

The overarching objectives for this thesis were to further the knowledge surrounding micro-particulate suspensions known as sheared or fluid gels though the use of whey proteins as the gelling medium. Having identified design principles for such systems, the aim was to utilise the technology to investigate the whey protein systems as a potential multifunctional ingredient. Therefore, the project was split into three key areas:

- Investigating the effects of processing on the bulk suspension characteristics, arising from the resulting particle intrinsic properties.
- Utilising the knowledge base derived from processing fluid gel particles to formulate a system capable of both the structuring of liquids, and delivery.
- Understanding the behaviour of the particulates once consumed, within digestive conditions.

The key conclusions arising from these areas of study have been detailed under the following three headings:

***<u>Understanding WPI particle formation</u>***

- ***WPI particles were formed with the lowest particle sizes ca. 20 μm, via a shearing method, without the use of additives.***

Applying a separating shear force during the sol-gel transition of the WPI resulted in the formation of particles, with sizes dependent on both the shear and heating rate applied. Microscopy and sizing techniques suggested that primary aggregates were initially formed, subsequently aggregating to form final particles.

Resulting particle size was thus dictated by the degree of gelation between primary aggregates. Additionally, particles exhibited irregular morphologies, best described by a higher length to width ratio. Such observations are thought to be a function of the shear environment, where elongational flow allowed inline growth.

- ***Kinetics play a key role in particle formation, dictating the mechanism by which they are formed.***

The mechanism for particle formation was proposed as a function of the rate of gelation. Where gelation was fast, gelled structures rapidly form, becoming broken down within the shear flow. However, in the cases where gelation occurs more slowly, weak supramolecular interactions (predominantly hydrophobic), result in compact aggregates. Therefore, particles are formed within the shear flow, subsequently remaining much smaller.

- ***Suspensions showed elastic behaviours above a critical volume fraction, where system rheology was governed by the formation mechanism.***

Bulk suspension rheology was ultimately governed through particle-particle interactions once in close proximity. When highly packed, elastic behaviour becomes a function of the processing parameters, where gelling kinetics and subsequent formation mechanism promote or hinder the degree of inter-particle response. The viscosity was found to be a function of the reduced phase volume, with thixotropic effects arising through flocculation breakdown.

***Cold-set WPI suspension can be formed using a shearing method.***

The formation of particulate cold-set systems has been shown, via crosslinking of pre-treated protein under shear. Here processing under shear formed particles of the same size (*ca.* 10 μm), which underwent further aggregation post-shearing. This resulted in large final aggregates, with sizes dependent on both the salt concentration and shear imposed.

- ***The presence of a secondary dispersed phase, oil, can be used to control particle growth.***

In the presence of a secondary phase separated component, in this case oil, particle growth became hindered at higher volume fractions. As such the degree of aggregation becomes limited to the space unoccupied by the oil.

- ***Material response for cold-set particulate systems showed a close correlation to gelling kinetics, obtained from their quiescently formed counterparts.***

Increasing the rate of particle formation lowered the bulk elasticity of the suspension. This was described by gelation kinetics for quiescent gels, where fast gelation results in burying of sites needed for particle-particle bridging.

***<u>Formation of micro-composites</u>***

- ***The formation of microcapsules can be achieved by thermally gelling WPI around an emulsion core, using shear-gel technology.***

The oil substrate provides a point of hydrophobic interaction for proteins having undergone thermal denaturation. Subsequent enrichment of the gel layer from the

surrounding protein occurs resulting in a core-shell capsule. Thus, particle morphology can be determined by the core, forming spherical entities.

- ***Entrapment efficiency is closely linked to the gelling polymer concentration within the primary emulsion prior to thermal treatment.***

Droplet entrapment is dictated by mass transport of the denatured polymer to the oil interface. As protein concentrations increase above 20% (w/w) the protein chains have a much higher chance of interacting with each other, rather than the oil interface. This increases the formation protein-protein particles, reducing the amount of protein available to migrate to the oil interface

- ***Rheological properties of the final suspensions can be controlled through the degree of oil in the system.***

An effective increase in the volume occupied by the particles, through structuring of the continuous phase during gelation, results in the close packing of the composite particles. This causes particles to become kinetically trapped through steric confinement and weak bridges, resulting in a soft glass-like structure. Increasing the volume of oil within the system results in a plateauing in elastic response, as soft EmFG particles become squashed (jammed). As such, systems containing as little as 10% oil (v/v) showed rheologies that correlate closely to those for highly concentrated emulsions.

***Digestion of protein-oil micro-particles***

- ***EmFG particles show a high degree of resistance to digestive breakdown.***

EmFG particles prepared using thermal treatment showed a high degree of resistance to proteolysis during *in vitro* conditions, with the level of oil release correlating closely to the amount of uncoated droplets during-processing.

- ***Changing the polarity of the EmFG core facilitated release.***

Increasing the hydrophobicity of the oil substrate ultimately led to release under gastric digestion. However, within intestinal conditions droplets still remained stable. This highlighted a change in the protein at the interfacial level, where residues needed for pepsin proteolysis became exposed.

- ***Suspension rheology can be affected through the polarity of the substrate core.***

Changes in protein arrangement/conformation at the interface as a function of the oil polarity, was observed by release data, but also through material characterisation methods such as rheology. Controllable system rheology as a function of the oil core is proposed to arise through a change in the interfacial protein structure, permeating throughout the gel network. This effected the degree of particle-particle interactions within the bulk sample, as bridging sites become inaccessible through steric effects.

***Summary of conclusions***

The work presented here has found that gelation kinetics play an important role in the resultant suspension properties. As such, processing conditions can be

manipulated to achieve particulate systems with varying sets of properties, *e.g.* particle sizes, morphologies, elastic/flow behaviours, viscosities and yield stresses. Coupled with their thermo-stability, WPI particulate suspensions pose as a potential candidate within foods as potential rheological modifiers. Furthermore, systems were formulated containing oil droplets within the gel particles, providing an agent with the ability to deliver or protect poorly soluble compounds, whilst retaining the ability to structure in a defined manner. Finally, it was shown that by controlling the particle formulation, controlled delivery could be achieved. In conclusion, by understanding the scientific principles, a technology was prepared with the potential to increase ingredient value, through nutrition, structuring and delivery.

## 7.2. Future work

This section looks to address future studies that could be used to further the work carried out within each chapter, and also highlights possible studies that may be conducted as a progression from the project. As such, two sub sections have been highlighted, the first focuses on further work arising through chapter conclusions, and the second, new areas of research that could be conducted using the system.

***Future work***

***Chapter 3: WPI fluid gels: The effects of shear and thermal history***

- This chapter focused on two main variables: shear and thermal history. This highlighted kinetics as a major contributor to resulting particle intrinsic properties.

Therefore, other processing parameters such as, salt, salt concentration, polymer concentration, pH and solvent quality could be studied systematically, obtaining the data needed to present a rounded model for predicting resulting suspension properties.

- Evidence for inter-particle interactions has been presented, however the origins of the interactions have not been shown. Previous work on polysaccharide fluid gels has posed an argument where non-structured chains at the particle surface are able to interlock, resulting in a "Velcro" effect (Norton et al., 1999). For globular proteins, it is much more likely that interactions between particles arise through supramolecular chemistry, in particular electrostatic interactions between negatively charged hydroxyl groups found along the polymer backbone. One possible way to study such interactions would be through the addition of salts post-production and mechanical testing. Taking this a step forward, the use of blocking agents could be used, binding to specific sites, probing the origins of the interaction further.

***Chapter 4: Cold-set particulate suspensions***

- Gelation kinetics were obtained under static conditions. Recent studies investigating kinetics in relation to salt set fluid gels have looked at an *in situ* approach, whereby release of the crosslinking agent occurs over time from an inert mineral and changes in system viscosity monitored (Fernández Farrés and Norton, 2014). Therefore, development of a method to look at dynamic gelation of WPI would yield kinetics more closely correlating to a sheared system.

- Gelling kinetics obtained for cold-set WPI quiescent gels showed further hardening with large timescales. The process used within this experimental setup only allowed for a residence time of 10 mins within the shear field. Development of a method for increasing the residence time within the shear flow would allow further probing on the degree of structuring that occurs during processing, and the effects it has on the resulting suspension rheology.

***Chapter 5: Whey protein emulsion fluid gels***

- The work investigated within this chapter looks at the material response gained from trapping an oil phase within a gelled coating. However, a comparison in material response as a function of separate co-dispersed oil droplets and protein particles has not been studied. An investigation into how the systems structure (droplets entrapped inside to outside the particles) effects suspension behaviour, studying reduced volume effects against inter-droplet/particle interactions would be valuable.

- The work undertaken within this thesis focused on a range of oil fractions from 5 to 20% (w/v). It was shown that elastic behaviours were achieved at volume fractions below the maximum packing fraction for hard spheres. Further work investigating a wider range of oil fractions would strengthen the hypothesis that systems undergo a transition from soft glass, whereby particles are trapped through inter-particle interactions, through to jammed systems once highly packed.

***Chapter 6: EmFG: In vitro digestion***

- A greater understanding over the mechanism for proteolysis is needed. The research would benefit from further study into the available residues and conformational structures surrounding the oil droplet. Analytical techniques such as surface hydrophobicity and X-ray crystallography techniques could be employed to gain a more in-depth knowledge of the protein structures at the interface. In addition, using micro-rheology (dilatational rheology or using AFM (atomic force microscopy)) to probe the interfacial elasticity, may provide more information regarding the structure of the interfacial microstructures, acting as a comparative technique when changing the polarity of the oil phase.

- The research presented in this thesis has focused on the effects of changing the oil phase. However, the addition of particles/molecules (actives) to the oil core could also affect the oils' chemical properties. This would provide a second route to testing the arrangement of the protein around the core. Additionally, information could be gathered to understand the effects of additives within the oil, on the digestive properties of the EmFG systems.

- Lastly, a model for digestion that more closely mimics the GI tract should be investigated. Such a model would involve systems that better represent the biology within the body including: residence times, movement from gastric to intestinal environments and digestive chemicals (bile salts *etc.*). This would improve the understanding on how the EmFG system reacts throughout the various stages, allowing better application of the EmFGs ability to target delivery.

***New research areas***

- When considering possible fat mimetics, in mouth perception is an important factor (Norton and Norton, 2010). Links between the study of tribology and sensory application have previously been shown (Pradal and Stokes, Prakash et al., 2013, Stokes et al., 2013), highlighting the technique as a plausible route to predicting sensory response. Recent work surrounding polysaccharide fluid gels, in particular composite fluid gels, have managed to significantly reduce the friction coefficient through the inclusion of a small amount of oil (Hamilton and Norton, 2016). Therefore, within their application as a food ingredient, tribological studies of the systems are needed to understand their lubricating properties. Furthermore, linking sensory to both rheology and tribology may enhance our understanding on the palatability of such systems, providing a model for prediction.

- The complexity of food is such that removing/changing a single component can have adverse effects on the final structure of the product. As one intended use for the work carried out in this thesis is to incorporate it into food products, knowledge regarding the structural behaviour of the final matrix is required. One method of characterising and understanding food behaviours is large amplitude oscillatory shear rheology (LAOS) (Melito et al., 2013). The use of such a technique on the original product, product without oil and newly formulated product with the EmFG particles, would allow the formation of a model that could be used to predict consumer response. It will also provide information on the amount of replacer needed to form structure within the food and lead to a better understanding on the interactions occurring within the complex systems.

- From an industrial point of view, removing the water to ship the systems would be greatly advantageous. Therefore, studying the effects drying has on the particulate suspensions and subsequent rehydration would have huge industrial implications.

# Appendices

# Appendix. i

## *i.1. Rheometry*

Amongst other techniques, the rotational rheometer can be used to study the rheology of systems. Rheology, by definition, is the study of both a materials flow and deformational properties; predominantly used to characterise material behaviours, however, is becoming more commonly used to probe system interactions and microstructures. A rotational rheometer primarily works, by applying a known force to a sample situated between two surfaces (one stationary and one rotating) at a specified rate and measuring the resistance. Figure 8.1 shows schematics for three common measuring systems: cone and plate, parallel plate and couette.

### ***Cone and plate***

The cone and plate geometry as seen in Figure 8.1a changes in gap height across the radius of the plate, resulting in a shear profile that remains constant across the system. As such, the gradient of the cone is necessary for calculating the strain applied for the system, found in Table 8.1. Although uniform in shear, the geometry becomes limited by the majority of suspension systems, where particles are in the micron scale. In order to study bulk properties gap height ($h$) needs to be in the order of 10 times the size of the particles. The fixed gap height needed to produce uniform shear prevents bulk response from confidently being reported. Therefore, a parallel system can be used.

### ***Parallel plates***

Although shear is not uniform across the radius of the parallel geometry (Figure 8.1b), an offset can be applied to the data, compensating for the change in shear profile.

In addition to being suited to particulate systems, a constant gap height across the system allows the surfaces to be adapted in a controlled manner, through the addition of roughness or serrations. Such changes aid in the prevention of wall-slip, protruding into the analyte preventing the continuous medium from creating a lubricating layer at the surface. Limitations to both the cone and parallel plate set-ups are expulsion of material from the gap at higher shear rates. Couette geometries have therefore been proposed.

***Couette***

Couette geometries (Figure 8.1c) use a cup system, whereby the measuring device is lowered into the sample. As such, the gap is created by the annulus between the two parts, resulting in a fixed height (distance). Apart from preventing expulsion from the gap, the large surface area allows lower shear rates/viscosities to be probed. In addition, different shapes, such as the vane can be used in order to lower effects such as slip. Within the research presented here, a cup and vane system was used to prepare gel particles on a rheometer. This particular setup was used as the vane most closely represented the pin stirrer, and larger sample volumes allowed testing of suspensions post-production.

***Summary***

Table 8.1 shows equations for shear stress and strains for the corresponding measurement systems presented in Figure 8.1. Once the stress and strain constants have been determined, the rheometer can be used to determine system viscosity ($\eta$), complex modulus ($G^*$) and phase angle ($\delta$), used to characterise material behaviour.

*Table 0.1: Table of shear stress and strain equations for common rheological geometries: where Γ is the torque (Nm), u is the displacement, θ is the angle of the cone, h is the height at a given radius, r (m), and L is the length (m).*

| Geometry | Shear stress | Shear strain |
|---|---|---|
| Cone and plate | $\tau = \frac{3\Gamma}{2\pi r^3}$ | $\gamma = \frac{u}{tan\theta}$ |
| Parallel plate | $\tau = \frac{2\Gamma}{\pi r^3}$ | $\gamma = \frac{(r).u}{h}$ |
| Couette | $\tau = \frac{\Gamma}{2\pi r^2 L}$ | $\gamma = \frac{r'.u}{r'' - r'}$<br>$u = 2\pi N$<br>($N$ = rotational speed (rps)) |

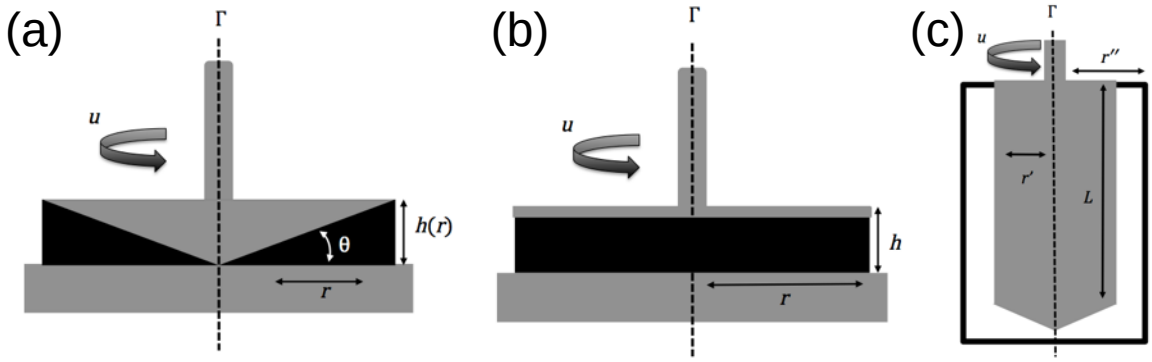


*Figure 0.1: Schematic representations of: (a) cone and plate, (b) parallel plates, and (c) couette measuring systems: where Γ is the torque (Nm), u is the displacement, θ is the angle of the cone, h is the height at a given radius, r (m), and L is the length (m).*

## Determining material properties

*Viscosity*

A system's viscosity is the direct measure of resistance a material exhibits against flow. As such, it can easily be calculated as the ratio of force applied (shear stress) to shear rate, Equation A. 1[1], where the shear rate is a function of the materials displacement over a given time scale (Equation 8.1[2]).

$$\eta = \frac{\tau}{\dot{\gamma}} \quad [1]$$

$$\dot{\gamma} = \frac{d\gamma}{dt} \quad [2]$$

*Equation A. 1: [1] equation for viscosity ($\eta$) as a function of the shear stress ($\tau$) and shear rate ($\dot{\gamma}$). [2] Derivation of the shear rate using the change in shear strain ($\gamma$) with time.*

Where $\eta$ is the viscosity as a function of the shear stress ($\tau$), shear rate ($\dot{\gamma}$) (derived by the change in shear strain ($\gamma$) with time ($t$)).

*Oscillatory rheology*

In addition to understanding system flow, oscillatory rheology can be used to probe a material's properties under "static" conditions. Here, the measuring system is resonated back and forth at a known frequency. Generally, a strain within the LVR (linear visco-elastic region) is used; preventing any permanent deformation of the material (structural breakdown). The ratio of stress to strain is again measured as a function of frequency, shown as the complex modulus (G*) of the system (Equation A. 2[1]). In addition, the lag time between instrumental action and material response, also

known as the phase angle, shows the degree of viscous to elastic behaviour in the analyte. Therefore, the phase angle can be used to separate the complex modulus into its two forms, storage (or elastic, G') and loss (or viscous, G'') moduli, Equations A. 2[2] and [3] respectively.

$$G^* = \frac{\tau}{\gamma} \quad [1]$$

$$G' = G^*.\cos(\delta) \quad [2]$$

$$G'' = G^*.\sin(\delta) \quad [3]$$

*Equation A. 2: [1] relationship between complex modulus ($G^*$), shear stress ($\tau$) and shear strain ($\gamma$). [2] Derivation of the storage modulus (G') using the complex modulus and phase angle ($\delta$). [3] Derivation of the loss modulus (G'') using the complex modulus and phase angle.*

Where G* is the complex modulus, $\tau$ is the shear stress $\gamma$ is the shear strain, G' is the storage modulus, $\delta$ is the phase angle and G'' is the loss modulus.

### *i.2. Confocal microscopy*

***<u>The technique</u>***

Confocal microscopy or confocal laser scanning microscopy (CLSM) is a branch of optical microscopy that uses an electromagnetic source to visualise a sample under fluorescence. A simplified schematic of a confocal microscope has been shown in Figure 8.2. The figure shows the use of a laser as the light source, where the wavelength of the beam can be controlled. The laser is deflected on to the sample using scanning mirrors through a lens objective. The emitted fluorescence returns using the same light path, where it is split and focused through a pinhole. Photomultipliers tubes (PMT) are used

to amplify the signal observed by the detector. The use of scanning mirrors allows the image to be obtained by scanning the sample with a focused beam. This means the image is built up point by point and can be focused at any point throughout the sample. As such, images can be obtained layer-by-layer, allowing slicing or stacking of the sample, resulting in a 3-dimentional image being obtained.

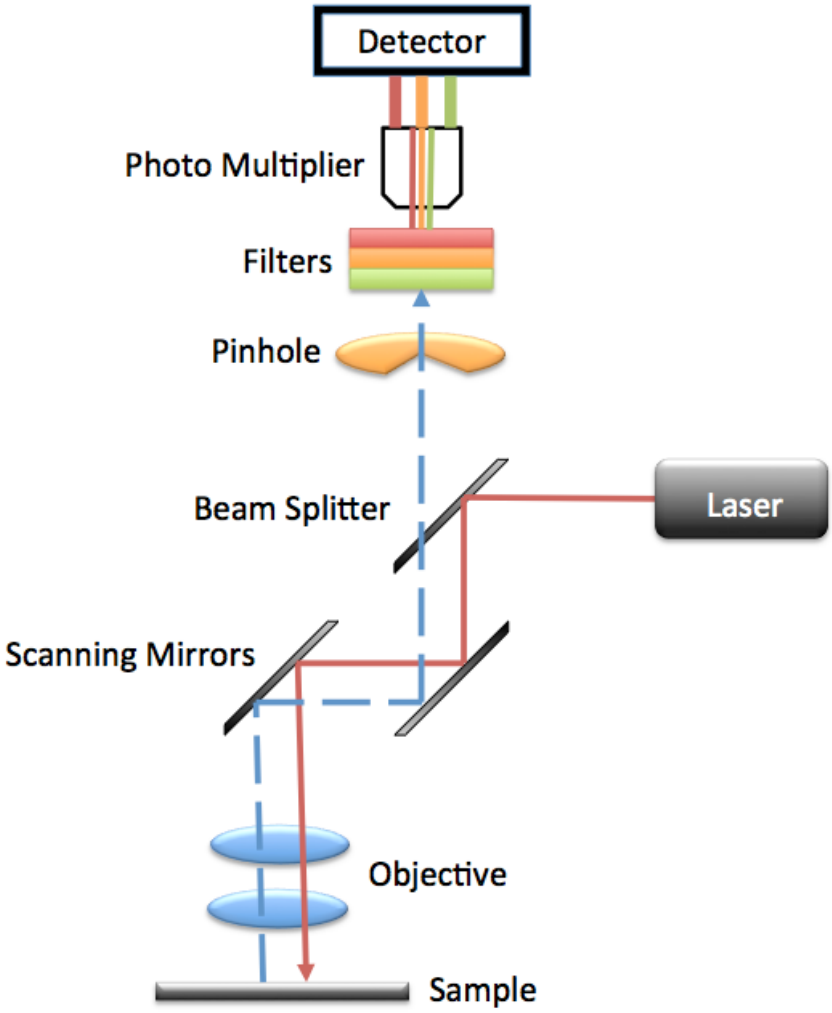


*Figure 0.2: Schematic representation of a confocal microscope setup.*

***Limitations to the technique***

Confocal microscopy however has its limitations; primarily the sample must contain a fluorophore. Many protein systems contain self-fluorescing properties, due to the many cyclic structures found along their backbones, however, in many cases their emittance is too low or excitation wavelengths too low for the light source. In these cases, dyes and stains are needed to provide the fluorescence needed.

The use of stains is often unfavourable, as their large molecular size can often affect the microstructure of the sample. In conjunction, the effects of processing, storage and environmental effects such as pH and solvent type *etc.* can also change the fluorescing properties of the dye used; leading to either quenching of the sample, or shifting its excitation or emittance wavelengths. This is of more concern in the presence of multiple dyes, where different stains are being used to highlight different components within the system. Therefore, it is important to use molecules that emit at different wavelengths, so deconvolution of the components can be achieved.

***Fluorophores***

Fluorophores are chemical compounds or structures that emit photons upon excitation. Typically, fluorophores consist of highly conjugated cyclic structures; an example has been shown in Figure 8.3, for Rhodamine B. The alternating double bonds lead to delocalised electrons surrounding the pi orbitals. The energy supplied by the laser results in temporary excitation of the electrons into a higher energy state. On returning to their ground energies, a photon is released in the form of fluorescence.

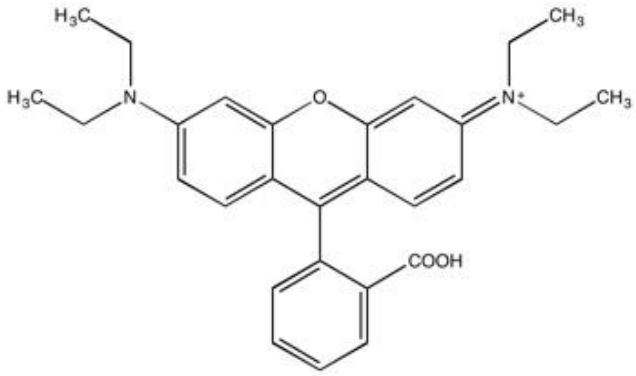


*Figure 0.3: Rhodamine B, showing its highly-conjugated ring structure.*

### *i.3. Particle sizing (light scattering techniques)*

Two light scattering techniques have been used within this thesis: the first, static light scattering (SLS) used for particle size measurements, and the second, dynamic light scattering (DLS) used for zeta potential experiments.

#### ***Static light scattering***

Static light scattering is an optical technique that measures the scattering of an electromagnetic wave as it comes into contact with a suspended particle. The schematic in Figure 8.4 shows a representative working of a general SLS apparatus. Here, particles are dispersed and flowed through the laser beam. The light becomes scattered as a function of the particle size, and angle/intensities detected. The Mie theory then becomes key in determining particle sizes, and distributions obtained.

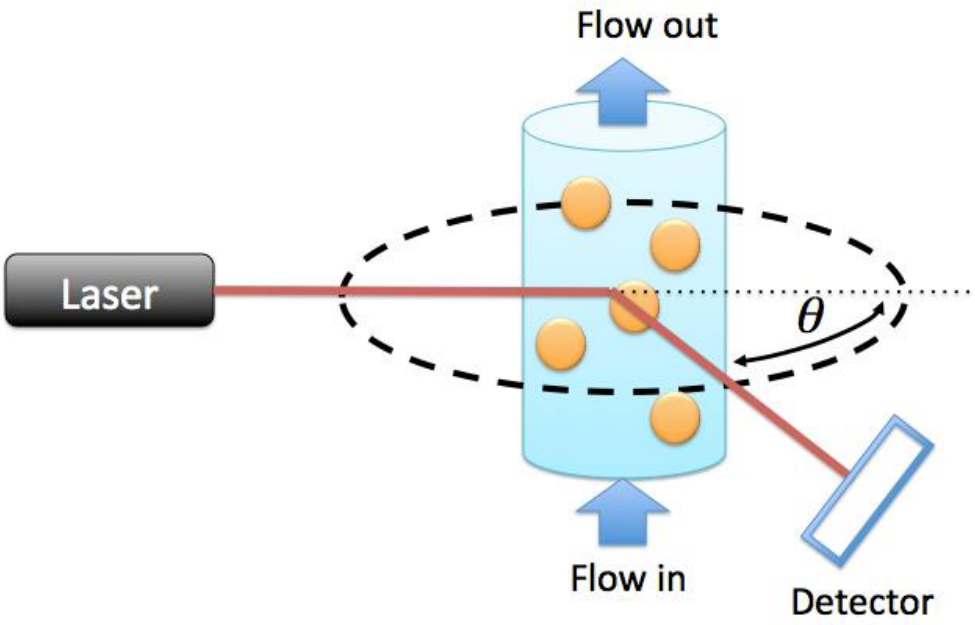


*Figure 0.4: Schematic of a static light scattering (SLS) setup.*

*Mie theory*

The Mie theory provides an exact solution to the Maxwell field equations, describing the interaction between a plane wave and spherical object, by encompassing both Rayleigh and the Fraunhofer theory. However, for the Mie theory to hold, several requirements must be met (Mie, 1908, Wriedt, 2012):

1. Both the incident and scattered rays must be of the same wavelength.
2. Particles must be sufficiently separated within the path of the incident rays.
3. Separation of the particles is such that they create discreet scattering patterns.
4. All particles share the same optical properties.
5. Particles must be spherical and isotropic.

Such requirements are attained by three main methods: a) design of the equipment, c) preparation of the suspension and c) particle formulation. Primarily the wavelength of

the incident ray can be controlled through the equipment, by use of a monochromator. However, separation is generally achieved through both dilution of the suspension and flowing of particles, aiding dispersion. The other requirements must be sufficed as a function of the suspended particle properties, as anisotropy results in random scattering paths, which can no longer be predicted.

***Dynamic light scattering***

Dynamic light scattering works in a similar way to static, whereby scattering of a laser source is used to size particles. However, in DLS the change in scatter patterns as particles diffuse through space is used to determine their displacement. Particle diffusion as a function of time and viscosity of the continuous medium can then be used to determine particle size. As such, the technique relies on diffusion through Brownian motion, thus particles must be within the sub-micron to nano scale to avoid external influences. In addition, very low concentrations are required to prevent multiple scattering within the system.

Zeta-potentials can also be calculated using this technique. Here a charge is applied across the system. Particle diffusion towards the anode/cathode is then detected and rate of movement used to approximate surface charge (potential at the stern layer, which approximates the charge at the surface).

# Appendix. ii

## *ii.1. EmFG formulation design process*

The formulation design process for EmFG was undertaken in five key steps:

- Initial preparation at native pH:

  *Systems were formulated using the same processing conditions as previously used for the preparation of WPI particles in chapter 3.*

- Preparation at native pH with slower heating rates:

  *Lower heating rates were applied to the system to try and control the degree of protein denaturation, promoting diffusion of the polymer to the substrate interface.*

- Addition of ionic salts:

  *The addition of varying ions was studied in an attempt to promote polymer bridging around the substrate interface.*

- Lowering the pH closer to the pI:

  *Reducing the pH of the system towards the isoelectric point in order to achieve no net repulsion between polymers. Again, to increasing the likelihood of gelation at the oil/water interface.*

- The effects of emulsion ageing:

  *Allowing an ageing step before gelling the system to provide maturation (changes in adsorbed protein conformations), at the oil droplet interface to providing a site of nucleation for further polymer growth.*

***Preparation of EmFG at native pH***

The initial stages in the formulation design process used a similar process presented in chapter 3, to heat gel protein around the interface of oil droplets. A pre-emulsion was formed using the WPI (5 to 30% w/w) as the emulsifier. Following this the excess protein after emulsification was used as the growth medium for the secondary gelation step. Gelation was undertaken using a controlled heating rate of 3 °Cmin$^{-1}$ at pH 6.4 whist applying mixing using an impeller set to 450 rpm.

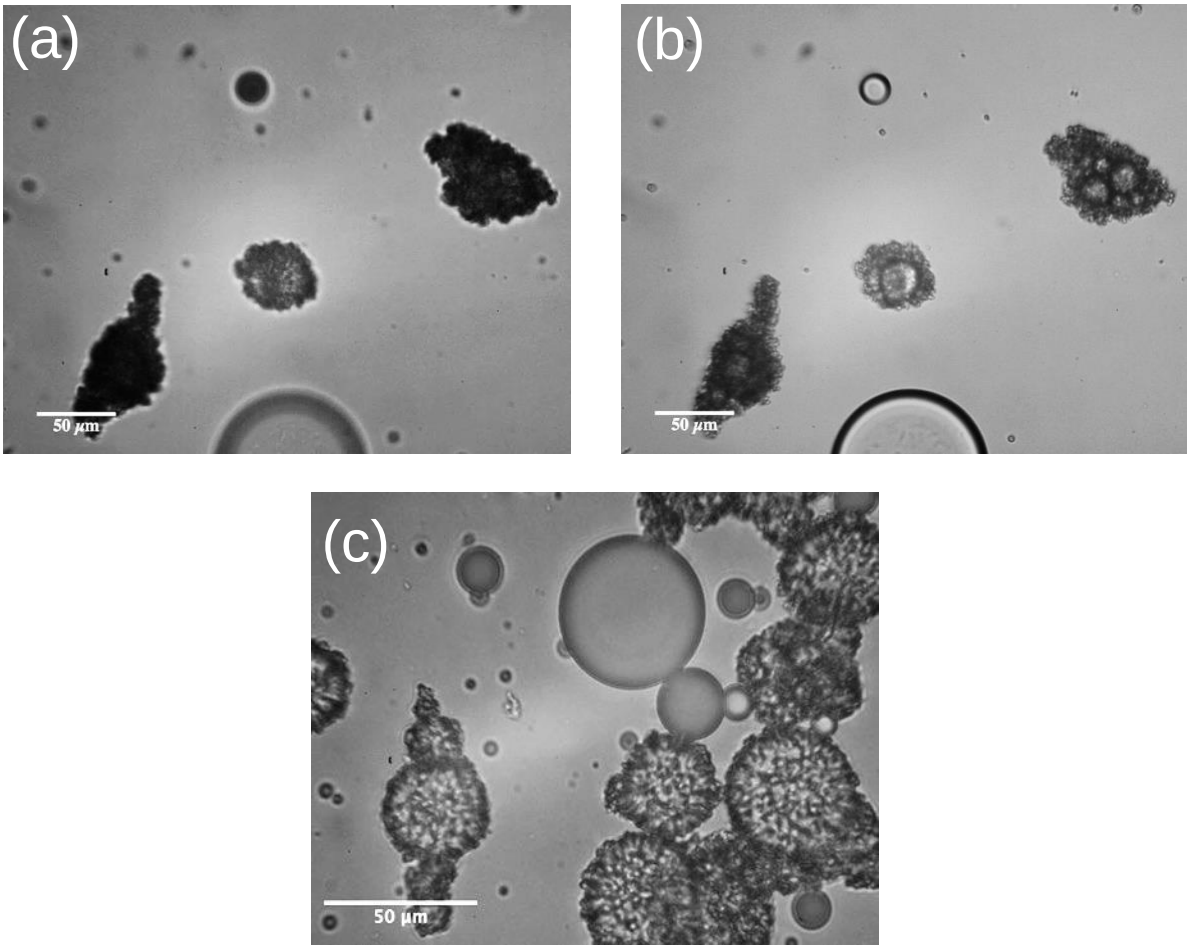


*Figure 0.5: Micrographs showing initial EmFG particles prepared at 3 °Cmin$^{-1}$ (pH 6.4): (a) and (b) show the same image at different focus heights and (c) shows a typical image taken from the same slide, but different area. Scale bar represents 50 μm.*

Micrographs presented in Figure 8.5 show examples of the particles prepared at this stage. It was observed that the oil substrate acted as a point for gel growth, resembling a template for the preparation of spherical particles. In addition, the formation of anisotropic particles was also seen, shown in Figure 8.5a. Through careful focusing of the microscope, it was possible to probe varying planes of the particles, highlighting multiple oil droplets becoming trapped within (shown in Figure 8.5b). Micrographs also visually highlighted poor entrapment of the oil droplets, with numerous droplets observed without a distinctive gel layer. It was hypothesised that the heating rate used (3 °Cmin$^{-1}$) quickly denatured the protein without allowing diffusion to an oil interface, resulting in the formation of polymer-polymer aggregates.

***Effect of a reduced heating rate on EmFG formation***

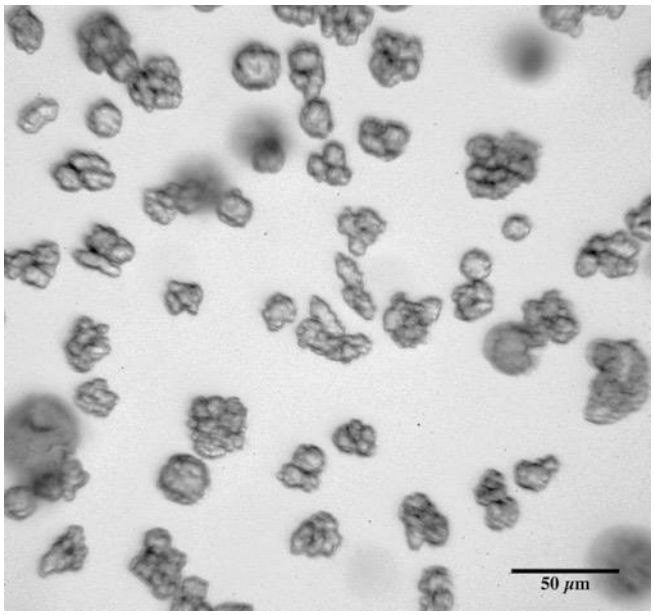


*Figure 0.6: EmFG suspension prepared at pH 6.4, 0.5 °Cmin$^{-1}$, showing a change in microstructure from smaller to larger protein aggregates. Scale bar represents 50 μm.*

A lower heating rate of 0.5 °Cmin$^{-1}$ was therefore applied. Visually, a rise in the amount of oil entrapment was observed. However, the microstructure of the gel layer was also effected, as shown in Figure 8.6. A shift from small globules to much smoother surfaces was observed; this was to be expected, as heating rate has previously been shown to change the globular nature of WPI gels (Bromley et al., 2006).

***Effect of electrostatic interactions***

The use of salt: Iron (ii) Sulphate, Potassium Chloride and Calcium Chloride (Table 8.2) to promote gelation at the water/oil interface was initially studied to increase entrapment efficiencies at the native pH.

*Table 0.2: Table of salts and corresponding concentrations used within EmFG formulation studies.*

| **$Fe^{2+}$** | **$Ca^{2+}$** | **$K^{+}$** |
|---|---|---|
| 0.05 M | 0.05 M | 0.1 M |
| 0.25 M | 0.25 M | 0.5 M |
| 0.4 M | 0.4 M | 0.8 M |
| 0.5 M | 0.5 M | 1 M |

It was observed that the addition of a cross-linker resulted in a lowering of the oil entrapment, again visually observed (example micrographs presented in Figure 8.7), for all salts and concentrations studied. The reduction in entrapment is suggested to arise similarly to systems prepared at higher heating rates, where an increased rate of

gelation due to the addition of a cross-linker (Ako et al., 2010) promotes the likelihood of polymer-polymer interactions over polymer-oil interactions.

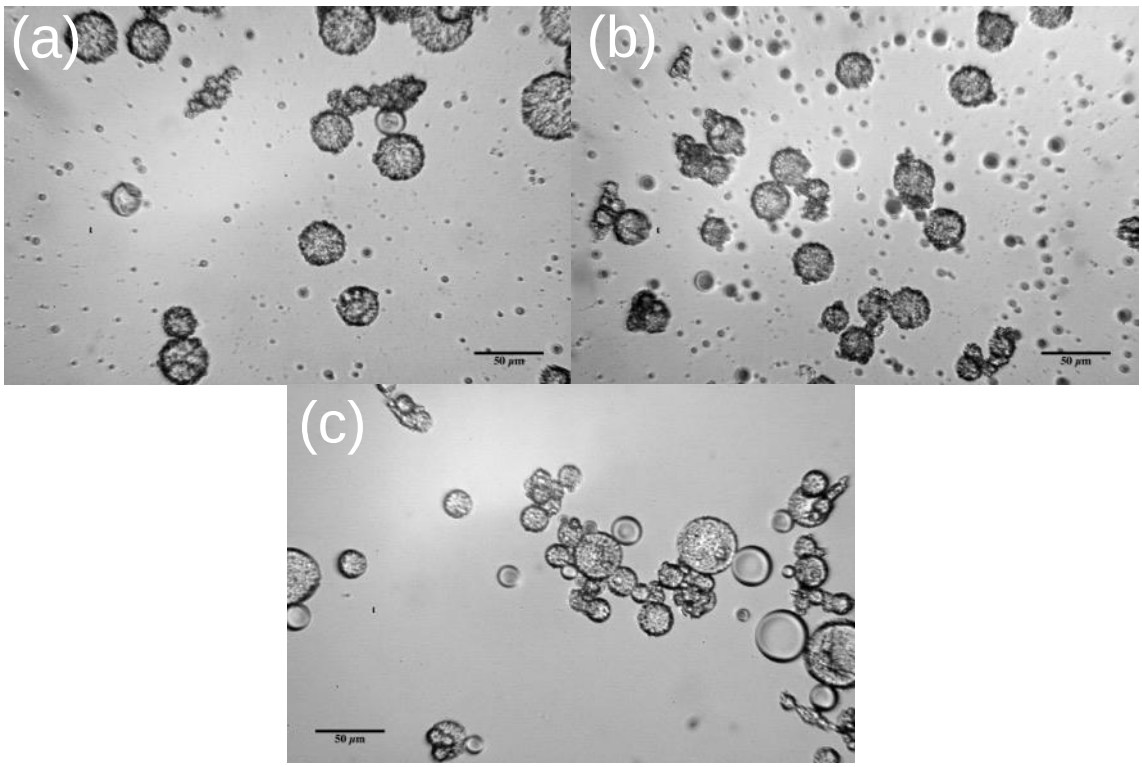


*Figure 0.7: Representative optical micrographs obtained for EmFG systems prepared using (a) $Fe^{2+}$ (0.5 M), (b) $K^{+}$ (1 M) and (c) $Ca^{2+}$ (0.5M) salts. Scale bar represents 50 μm.*

In addition to bridging negatively charged protein polymer, the pH of the systems was adjusted to 4.6, the isoelectric point (pI) (Chapter 4, Figure 4.5). At this pH the protein exhibit no net charge, removing any repulsion between the biopolymers once denatured. Once again, changes to environmental pH resulted in a change in the gel microstructure, pushing it back towards a globular morphology observed at higher heating rates, Figure 8.8. However, this was accompanied by an increase in entrapment efficiency; increasing to *ca.* 85 %.

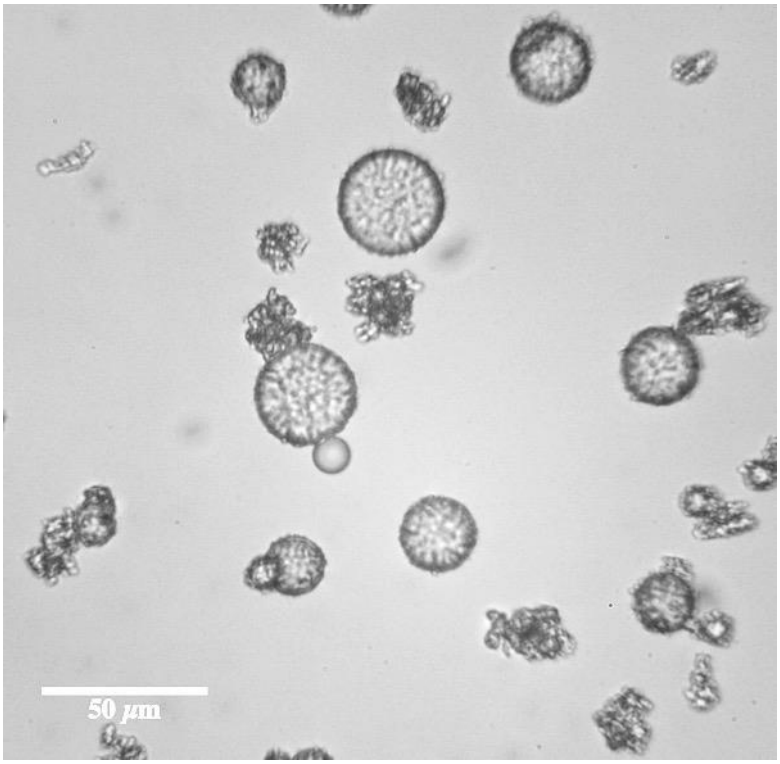


*Figure 0.8: Typical image of WPI EmFG capsules having been prepared at pH 4.6 and 0.5 °Cmin$^{-1}$. Scale bar represents 50 μm. Also presented in Chapter 5, Figure 5.1.*

***Ageing of the emulsion pre-gelation***

The last stage in the formulation/processing design stage incorporated a holding period, allowing the emulsion to undergo an ageing process before gelation. In Figure 8.9 the entrapment data obtained for EmFG prepared directly post-emulsification and 48 hrs, highlighted higher levels of entrapment with ageing. It is believed slow conformational changes at the interface over time lead to an increase in the surface hydrophobicity (Das and Kinsella, 1990), promoting a degree of polymerisation (Dickinson and Matsumura, 1991, Chen and Dickinson, 1993, Chen and Dickinson,

1999). This results in points for nucleation and further growth during the sol-gel transition.

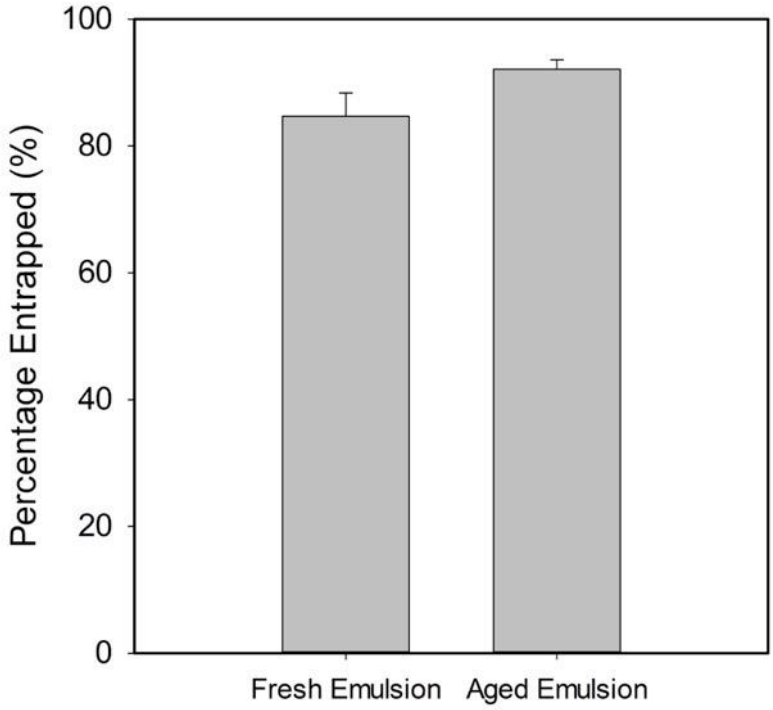


*Figure 0.9: Entrapment efficiency as a function of emulsion ageing time (0 and 48 hrs).*

The effect of applied shear during gelation was also investigated at this stage, as a function of the oil droplet entrapment. Figure 8.10 shows the percent of oil entrapped as a function of the stirring rate. Increasing the mixing from 250 rpm to 450 rpm had little effect on the entrapment of the included oil phase (within error). Further increasing the applied mixing however, showed a reduction in the trend with large variations of entrapment (shown by the large error bars in Figure 8.10). This reduction is most likely the result of a higher degree of turbulence and subsequent eddies within the vessel, resulting in localised gradients of polymer and oil. As such, 800 rpm was not used further. Additionally, visually observed viscosities (quantified data not obtained) for

systems produced at 250 rpm were higher than those prepared at 450 rpm. Therefore, 450 rpm was used thereafter, as the lower viscosity provided easier handling of the hot systems.

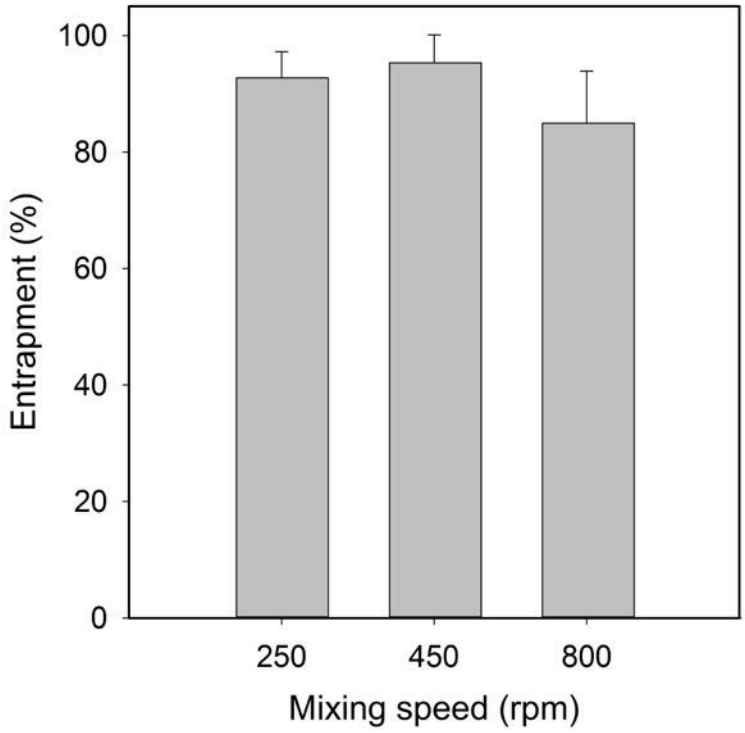


*Figure 0.10: WPI-Oil composites entrapment as a function of the preparation at pH4.6. Prepared at 0.5 °Cmin$^{-1}$ with varying mixing rates: 250, 450 and 800 rpm stirrer speed.*

### *ii.2. Summary of processing conditions*

The following two tables: Table 8.3 and 8.4 show a summary of the variables and processes changed during the development process, and the final processing parameters used to prepare EmFG throughout Chapter 5 respectively.

*Table 0.3: Summary table highlighting the various parameters changed in the development of EmFG systems. (+) shows increased entrapment and (-) decreased. "*" denotes systems that were prepared in the same way.*

| Parameter | Variable | Visual entrapment | |
|---|---|---|---|
| Heating Rate | 0.5 °Cmin$^{-1}$ | **+*** | *Slower rate of denaturation allowed diffusion of the protein to the substrate interface, instead of quickly bonding to a neighbouring denatured protein.* |
| | 3 °Cmin$^{-1}$ | **-** | |
| pH | 4.6 | **++** | *Lowering the pH close to the isoelectric point removed net repulsive forces between protein polymers, resulting in increased polymerisation at the oil interface.* |
| | 6.4 | **+*** | |
| Salt Addition | $Fe^{2+}$ | **- -** | *The addition of salts as cross-linkers lowered entrapment considerably, due to the increase in gelation also seen for higher heating rates.* |
| | $Ca^{2+}$ | **- -** | |
| | $K^{+}$ | **- -** | |
| Emulsion Ageing Process | 0 hrs | **+**** | *Ageing the emulsion for a 48hr period further increased entrapment, most likely due to increased surface hydrophobicity leading to polymerisation and points for further growth.* |
| | 48 hrs | **+++**** | |
| Mixing Rate | 250 rpm | **+++** | *Both 250 and 450 rpm mixing speeds resulted in the same degree of entrapment, however, further increasing to 800 rpm lowered the final amount of coated oil droplets. This is a function of the mixing where a larger degree of turbulence prevented diffusion of polymer to the substrate* |
| | 450 rpm | **+++**** | |
| | 800 rpm | **-** | |

*Table 0.4: Table summarising the processing parameters and values used to prepare the final EmFG systems.*

| Parameter | Value |
|---|---|
| Heating Rate | 0.5 °Cmin$^{-1}$ |
| Mixing Rate | 450 rpm |
| pH | 4.6 (48 hr ageing period pre-gelation) |

### *ii.3. Coating thickness determination*

Particle sizing was used as a technique to estimate the average coating thickness of the EmFG particles. Size distributions were obtained prior to and post-gelation, and shift in peak measured (represented in Figure 8.11a). The change in distributions are assumed to arise as a function of the gelling, thus the difference between peak maxima indicates gel growth across the diameter of the droplets. As such, half the shift in peak maxima has been assumed to be the thickness of the gel structure.

Figure 8.11b shows gel thicknesses as a function of both equivalent ionic strength, and salt type. Data obtained showed a decrease in the thickness of the shell with increasing the salt concentrations. It is suggested that the increase in charge density promotes a greater degree of charge screening, effectively shifting the zeta-potential towards to the pI; resulting in smaller, more tightly formed gel networks with an increased number of small gel only aggregates. However, the composite nature of the system inherently provides multiple refractive indices. Therefore, gel thicknesses have been regarded as semi-qualitative data.

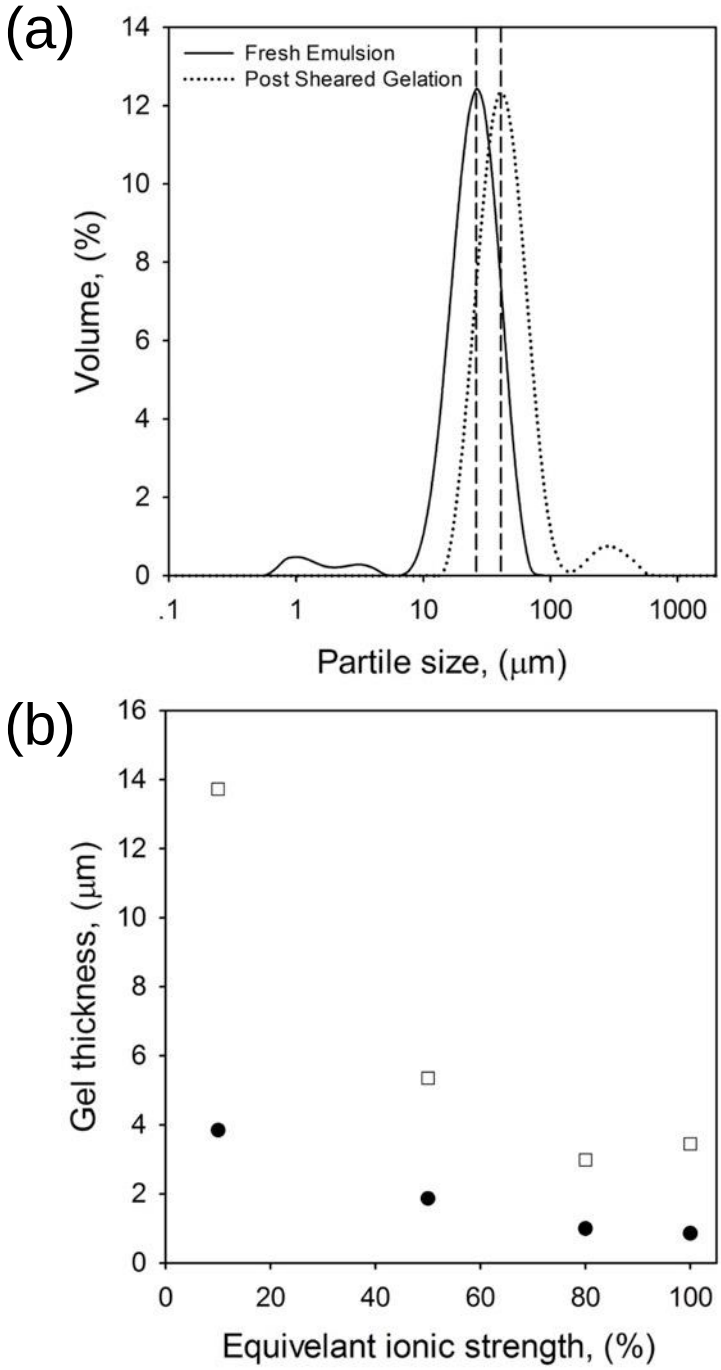


*Figure 0.11: Determination of coating thickness using a light scattering technique; (a) shows typical size distribution for emulsions both pre- and post-processing, highlighting a shift to higher particle sizes with gelation (system shown here is prepared using 0.5 M $CaCl_2$). (b) shows half the shift observed from the distributions, as a function of the cation type and concentration (□) $Ca^{2+}$ and (●) $K^{+}$.*

## Appendix. iii

### *iii.1. Initial digestion study and method design*

Understanding the route to emulsion failure under GI conditions is important in the design of a food delivery system; as such a digestive protocol was designed. Images for the preliminary release studies have been shown in Figure 8.12 and 8.13.

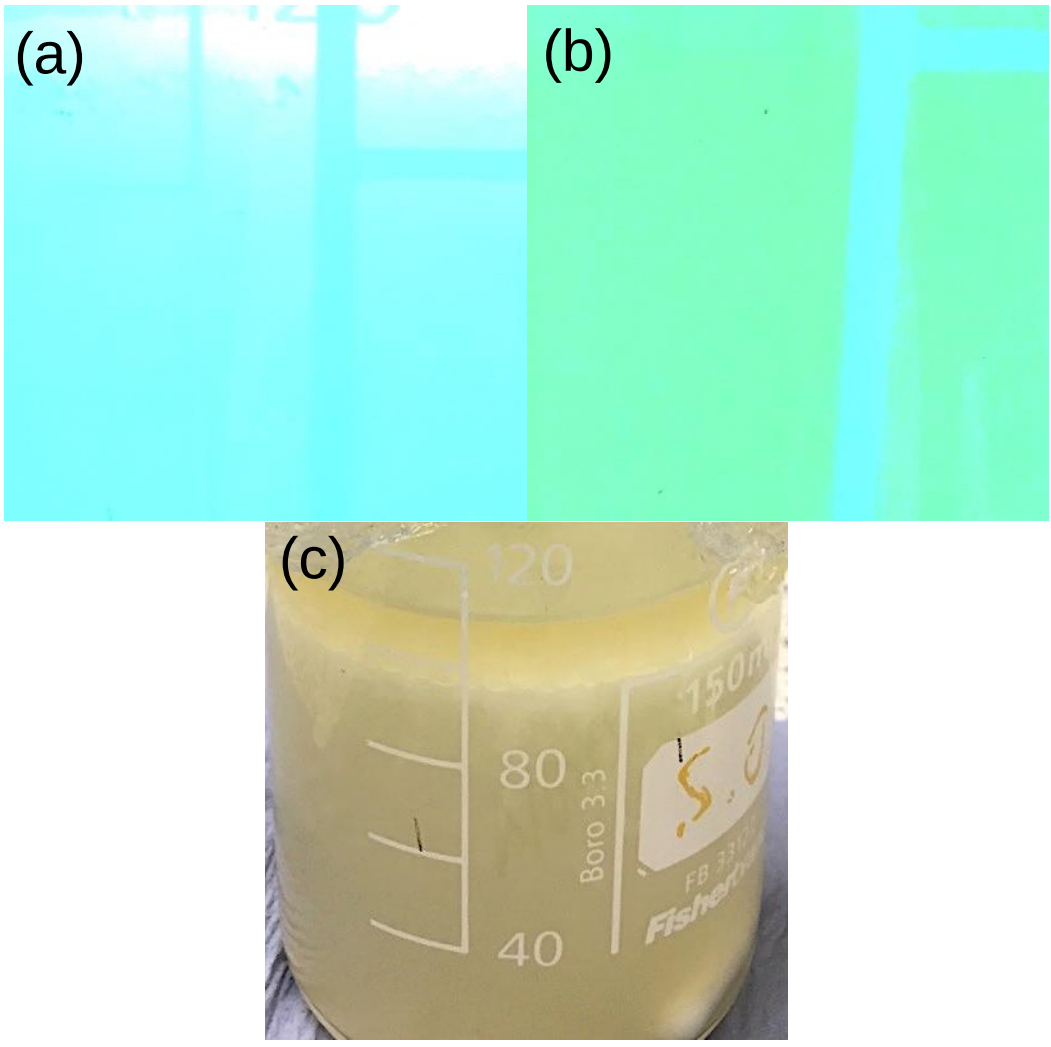


*Figure 0.12: Oil release under intestinal conditions for simple WPI emulsion systems. Images show stirred systems at (a) t=0, (b) t=24 hrs and (c) t=24 hrs after separation (static conditions). Images a and b have had the contrast enhanced to highlight the change in colour due to the reduction of droplet number scattering the light (less white more yellow).*

The initial stages in the method development process incorporated a water bath to heat the digester, and applied mixing via magnetic stirrer to prevent concentration gradients and creaming. It was observed that emulsion failure was accompanied by a change in suspension colour, becoming more yellow, shown in Figures 8.12a and b. Thus, two methods to determine release were probed: 1) using a colour change calibration, and 2) measurement of the oil phase once separated (Figure 8.13).

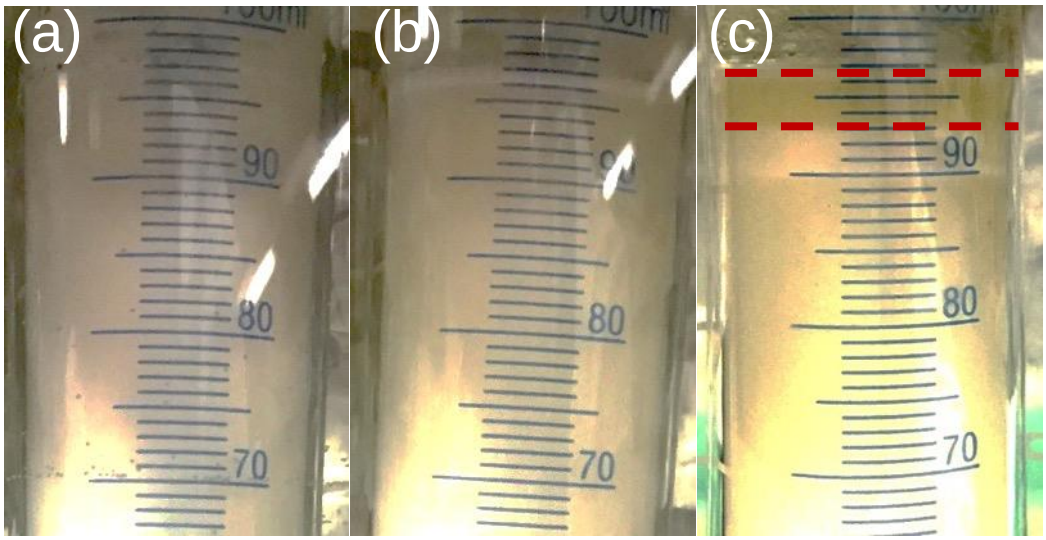


*Figure 0.13: Intestinal digestion of EmFG after a 10 min static resting period: (a) 0 hrs, (b) 20 hrs and (c) 44 hrs digestion time. Dotted red lines show phase separated (released) oil. Total oil content within the system was 10 mL.*

Colour change as a quantification technique presented several problems yielding poor reproducibility and low sensitivity. As such was discluded from further study. However, allowing the system to phase separate yielded better results, allowing release plots to be obtained (Figure 8.14). EmFG failure measured in this way showed very slow release kinetics, with no release-taking place within the first 20 hrs. Subsequent release over the following 28 hours showed a linear profile, resulting in close to 90% failure. At

this point digestion times were reduced in correspondence to work published by Minekus et al. (2014) focusing on the first 5-6 hours of digestion, as such no repeats of this experiment were undertaken.

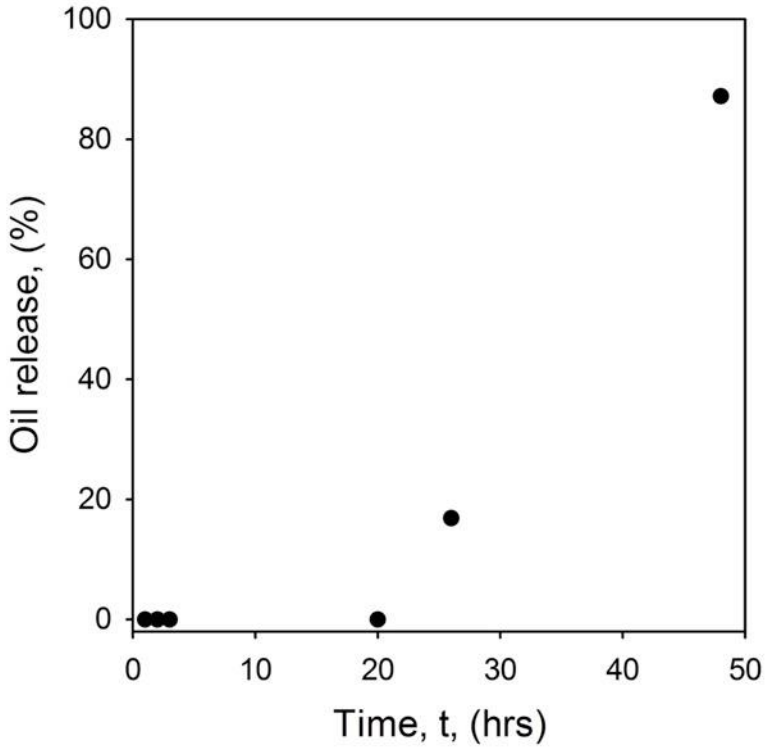


*Figure 0.14: Oil release under intestinal conditions over 48hrs. No error bars are present due to data showing a single experiment.*

Phase separation as a technique to visually identify emulsion failure inherently has it's limitations: high sensitivity as a result of small measuring cylinders does not allow the system to be stirred, large amounts of sample are needed and the time taken for the system to fully separate does not allow for accurate time points to be taken. Therefore, a third method was studied, whereby an organic solvent (hexane) was used to extract the unemulsified oil. The extract was then heated to remove the solvent and mass balance used to determine release. Solubility experiments were undertaken to

study the effect of oil extraction into the organic solvent, showing solubility levels sufficient to remove the maximum amount of oil within the systems, 0.1 ml/ml. Data obtained for both fresh emulsions and EmFG systems over the 5 hours, in the absence of digester (only solvent) showed no extraction of oil. Therefore, oil removal for digested systems was believed to show release as a function of proteolysis. In addition, the high degree of sensitivity, ease and more accurate time points confirmed this method as the candidate taken forward to undertake the release study presented in Chapter 6.

### *iii.2. Formulation effects on EmFG particles*

**changing the emulsifier type**

A preliminary study to probe the mechanism for droplet failure was probed by changing the emulsifier for a more flexible protein (Macierzanka et al., 2009). EmFG were prepared by first emulsifying oil (10% (v/v)) using sodium caseinate (NaCas) (1% (w/v)). WPI was subsequently added to the mixture increasing total protein content to (20% (w/v)), pH adjusted to 4.6 and aged (48 hrs) before gelling under shear. Release profiles for both GI stages have been presented in Figure 8.15. Results presented do not show repeats as the preliminary work was not taken to a full study. Therefore, the reproducibility of the data is questionable, however, it was observed that both stages of digestion produced very similar release curves. In both cases a maximum release close to 10 % was achieved over the 5 hours studied. It is unclear at this point whether the observed EmFG failure was a function of the emulsifier type. It is believed migration of the protein at the interface has occurred during the ageing period, causing a percentage of the caseinate to become displaced by the WPI. Thus, during digestion only the droplets that remained stabilised via the caseinate were susceptible to proteolysis. As

such, more work within this field is needed, concentrating on entrapment efficiencies and determining the microstructure of the two protein polymers.

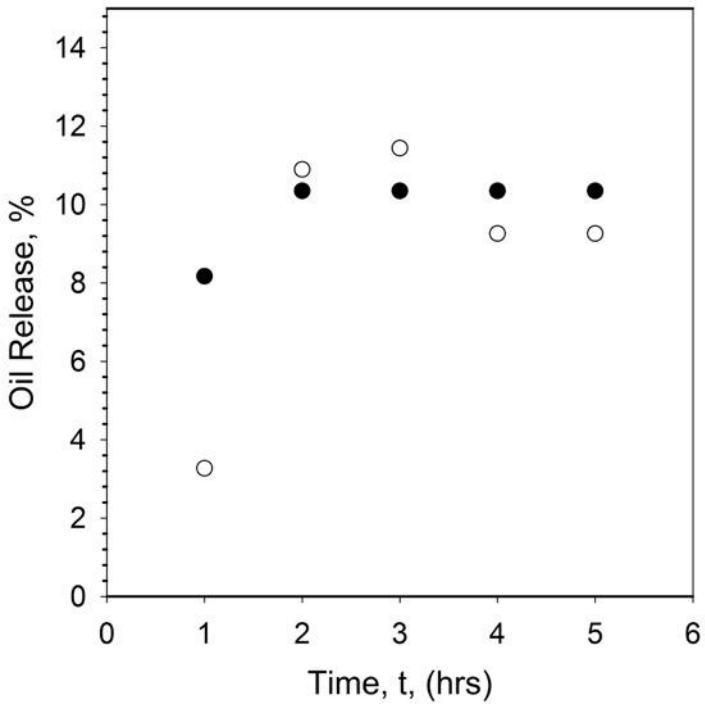


*Figure 0.15: (●) Gastric and (○) intestinal release plots (n=1) for WPI EmFG having undergone the primary emulsification stage stabilised using NaCas.*

### *iii.3. Preliminary active release studies*

Preliminary release measurements were obtained for model actives from both within the composite particles and within the inter-particle network formed post processing.

**β-Carotene release**

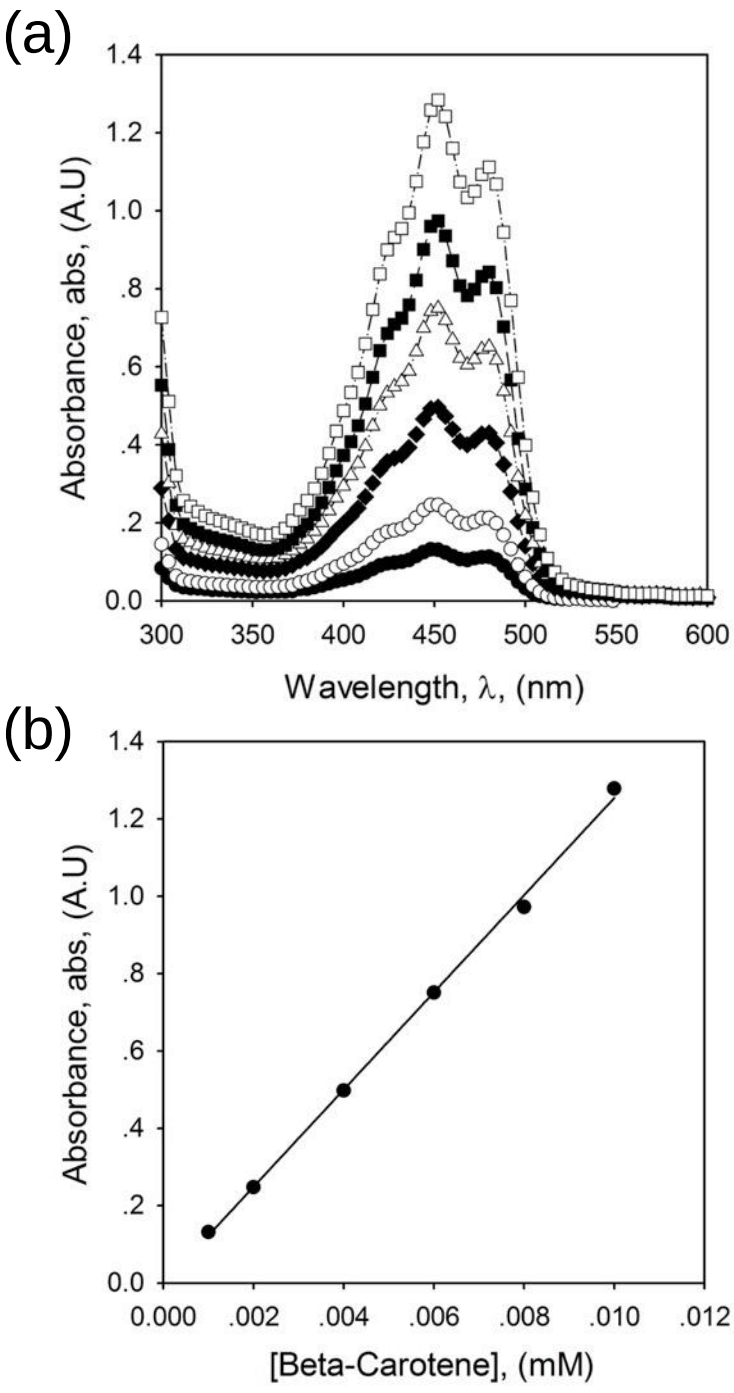


*Figure 0.16: (a) UV/Vis spectra obtained for β-carotene in hexane at concentrations of: (●) 1 mM, (○) 2 mM, (◆) 4 mM, (△) 6 mM, (■) 8 mM and (□) 10 mM. (b) Calibration curve taken at 450 nm, equation of the line is y=125.72x -0.0027.*

β-carotene loaded EmFG (βcEmFG; 20% WPI 10% high oleic oil) were formed through the addition of the carotenoid (0.1 mM) to the oil phase prior to the emulsification step outlined in chapter 5.2.2. Release was studied by the same means as presented in chapter 6, whereby simulated gastric and intestinal phases were used to digest the WPI shell, and oil/active removed using an organic solvent extraction. Once extracted, UV/Vis was used to determine the concentration of active released.

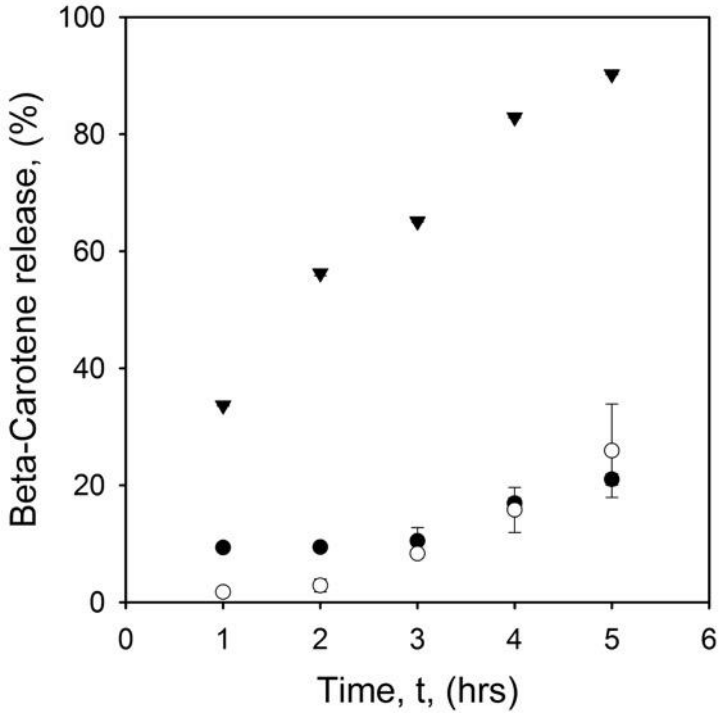


*Figure 0.17: β-Carotene release plots for: (●) gastric conditions, (○) intestinal conditions, and (▼) intestinal conditions in the presence of bile salts (0.5% (w/v)) (error bars masked by points).*

β-Carotene concentrations were calculated using a calibration curve (Figure 8.16). Standards were prepared by firstly forming a primary solution of β-carotene (0.1 mM) in high oleic oil. The primary solution was subsequently serial diluted in hexane

resulting in standards ranging from 0.001 to 0.01 mM. Release profiles obtained for βcEmFG systems showed a degree of release (Figure 8.17), corresponding closely to data obtained for fresh emulsion systems (chapter 6.3.1). It has been initially proposed that addition of the active into the oil phase resulted in a rearrangement of protein at the interface, facilitating release as described in chapter 6.3.1.3 (interfacial tension measurements presented in Chapter 7.2).

Carotenoid release was studied in the presence and absence of bile salts (0.5% (w/v)), (bile salts shown using triangles) in Figure 8.17. The addition of bile salts increased the rate and extent of β-carotene release, with close to all the active having been extracted after 5 hours. The incorporation of the naturally occurring surfactants within the digester resulted in displacement of the interfacial protein (Maldonado-Valderrama et al., 2011). Subsequently forming a new interfacial layer with a greater affinity for the organic solvent, facilitating active extraction. Preliminary results obtained for β-carotene release without bile salts reported yields of up to 60% release over the 5 hours studied (Figure 8.17). From the early results, it was suggested that the addition of a model active changed the intrinsic properties of the oil; shown is Figure 8.18 through a reduction in interfacial tension between the water and oil phases. This highlights a new area of study looking at the effects of actives and particles on the rate and extent of release.

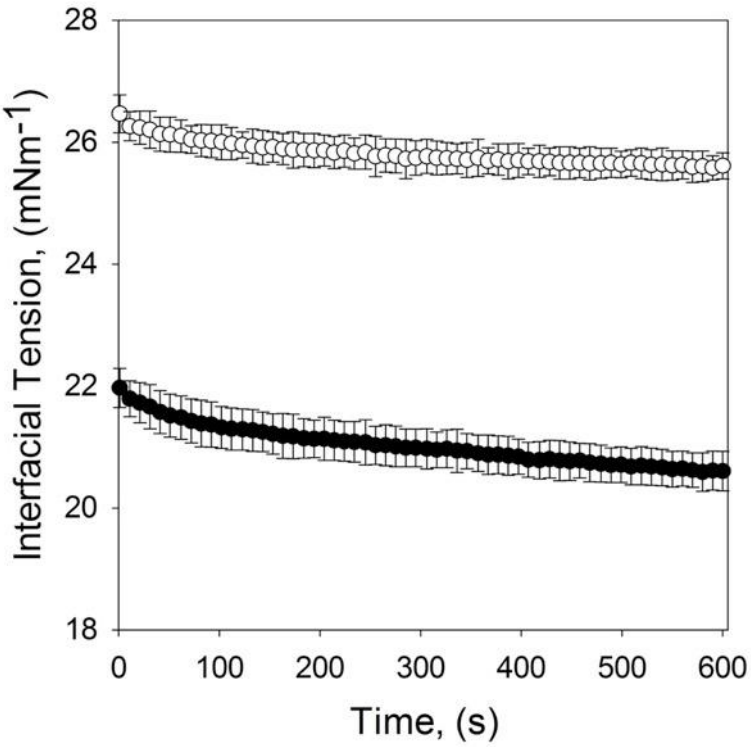


*Figure 0.18: Plot showing the decrease in interfacial tension for water/oil systems with β-carotene (closed) and without β-carotene (open). No protein present.*

**Fluorescein release**

For fluorescein delivery, EmFG were firstly prepared as detailed in chapter 5.2.2. Once left to cool, crystalline fluorescein salts were added to the suspensions and mixed until homogenously dissolved. Samples were added to dialysis tubing, sealed and allowed to rest at 5 °C for 24 hrs before dialysing. Release was determined using conductivity over 360 mins, using water as the continuous medium, results have been shown in Figure 8.19. Again, data presented only depicts a single experiment; as such reproducibility is questioned, however, release kinetics show first-order release typical of diffusion-based systems from a matrix. As such release is argued to be concentration

driven, with rates dependent on the amount of active and diffusibility through the flocculated network.

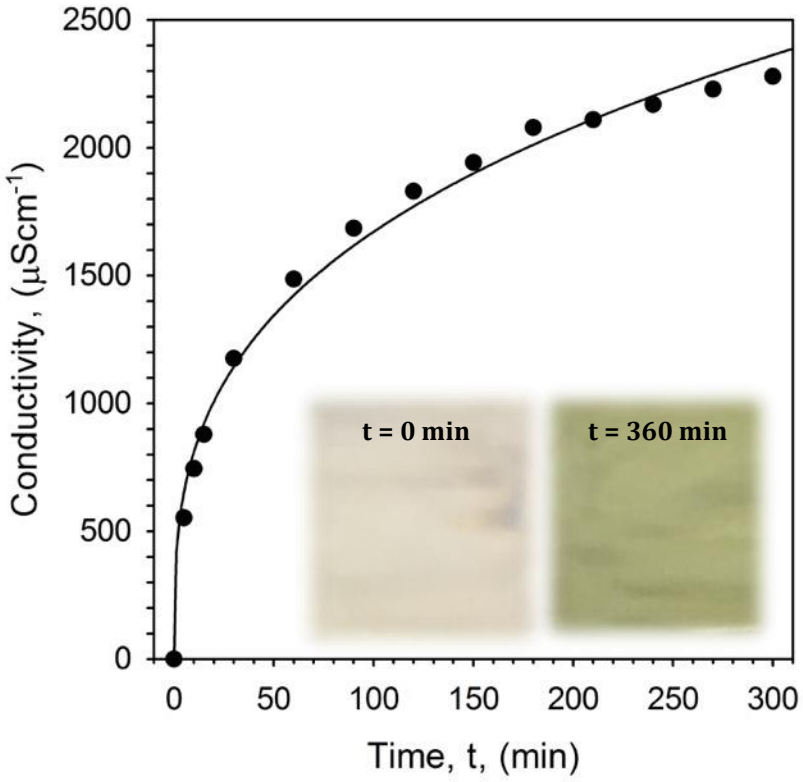


*Figure 0.19: Fluorescein release profile (n=1), obtained using a dialysis technique and conductivity measurements in water. Inserts show the change in water-colour over the dissolution period.*

This work therefore presents the starting blocks towards future study, investigating controlled release through manipulation over three key areas: volume fraction/packing, degree of interactions (flocculation), and addition of counter ions within particle shells.

# *References*

"FUNCTIONAL-FOODS" 2016. Functional Foods Market Analysis By Product (Carotenoids, Dietary Fibers, Fatty Acids, Minerals, Prebiotics & Probiotics, Vitamins), By Application, By End-Use (Sports Nutrition, Weight Management, Immunity, Digestive Health) And Segment Forecasts, 2014 To 2024. *Functional Foods Market Size, Growth & Trends, Industry Report, 2024.* Nutraceuticals and functional Foods: Grand View Research.

"WORLD-OBESITY-DAY". 2015. *World Obesity Day: Global Graphs and Maps* [Online]. Obesity Federation. Available: http://www.worldobesity.org/ [Accessed].

ADAMS, S., FRITH, W. J. & STOKES, J. R. 2004. Influence of particle modulus on the rheological properties of agar microgel suspensions. *Journal of Rheology,* 48**,** 1195.

AKHTAR, M. & DICKINSON, E. 2003. Emulsifying properties of whey protein–dextran conjugates at low pH and different salt concentrations. *Colloids and Surfaces B: Biointerfaces,* 31**,** 125-132.

AKO, K., NICOLAI, T. & DURAND, D. 2010. Salt-Induced Gelation of Globular Protein Aggregates: Structure and Kinetics. *Biomacromolecules,* 11**,** 864-871.

ALTING, A. C., DE JONGH, H. H. J., VISSCHERS, R. W. & SIMONS, J.-W. F. A. 2002. Physical and Chemical Interactions in Cold Gelation of Food Proteins. *Journal of Agricultural and Food Chemistry,* 50**,** 4682-4689.

ALTMANN, N., COOPER-WHITE, J. J., DUNSTAN, D. E. & STOKES, J. R. 2004. Strong through to weak 'sheared' gels. *Journal of Non-Newtonian Fluid Mechanics,* 124**,** 129-136.

ANDRÉS, S. C., ZARITZKY, N. E. & CALIFANO, A. N. 2008. Stress relaxation characteristics of low-fat chicken sausages made in Argentina. *Meat Science,* 79**,** 589-594.

BARBUT, S. & FOEGEDING, E. A. 1993. Ca2+-Induced Gelation of Pre-heated Whey Protein Isolate. *Journal of Food Science,* 58**,** 867-871.

BARNES, H. A. 1994. Rheology of emulsions — a review. *Colloids and Surfaces A: Physicochemical and Engineering Aspects,* 91**,** 89-95.

BARNES, H. A. 2000. *A Handbook of Elementary Rheology*, University of Wales, Institute of Non-Newtonian Fluid Mechanics.

BARNES, H. A. & CARNALI, J. O. 1990. The vane‐in‐cup as a novel rheometer geometry for shear thinning and thixotropic materials. *Journal of Rheology,* 34**,** 841-866.

BARNES, H. A. & NGUYEN, Q. D. 2001. Rotating vane rheometry — a review. *Journal of Non-Newtonian Fluid Mechanics,* 98**,** 1-14.

BAUER, R., HANSEN, S. & ØGENDAL, L. 1998. Detection of intermediate oligomers, important for the formation of heat aggregates of β-lactoglobulin. *International Dairy Journal,* 8**,** 105-112.

BENICHOU, A., ASERIN, A. & GARTI, N. 2007. W/O/W double emulsions stabilized with WPI–polysaccharide complexes. *Colloids and Surfaces A: Physicochemical and Engineering Aspects,* 294**,** 20-32.

BERLI, C. L. A., DEIBER, J. A. & AÑÓN, M. C. 1999. Heat-Induced Phenomena in Soy Protein Suspensions. Rheometric Data and Theoretical Interpretation. *Journal of Agricultural and Food Chemistry,* 47**,** 893-900.

BERLI, C. L. A. & QUEMADA, D. 2000. Rheological Modeling of Microgel Suspensions Involving Solid−Liquid Transition. *Langmuir,* 16**,** 7968-7974.

BHATTACHARJEE, C., SAHA, S., BISWAS, A., KUNDU, M., GHOSH, L. & DAS, K. P. 2005. Structural Changes of Beta-Lactoglobulin during Thermal Unfolding and Refolding - An FT-IR and Circular Dichroism Study. *The Protein Journal,* 24**,** 27-35.

BINKS, B. P. 1998. *Modern aspects of emulsion science*, Royal Society of Chemistry.

BOLDER, S. G., VASBINDER, A. J., SAGIS, L. M. C. & VAN DER LINDEN, E. 2007. Heat-induced whey protein isolate fibrils: Conversion, hydrolysis, and disulphide bond formation. *International Dairy Journal,* 17**,** 846-853.

BOUKANY, P. E., WANG, S.-Q. & WANG, X. 2009. Universal scaling behavior in startup shear of entangled linear polymer melts. *Journal of Rheology,* 53**,** 617-629.

BRADY, J. F. 1993. Brownian motion, hydrodynamics, and the osmotic pressure. *The Journal of Chemical Physics,* 98**,** 3335-3341.

BRANDELLI, A., DAROIT, D. J. & CORRÊA, A. P. F. 2015. Whey as a source of peptides with remarkable biological activities. *Food Research International,* 73**,** 149-161.

BREW, K., VANAMAN, T. C. & HILL, R. L. 1968. The role of alpha-lactalbumin and the A protein in lactose synthetase: a unique mechanism for the control of a biological reaction. *Proceedings of the National Academy of Sciences,* 59**,** 491-497.

BRODKORB, A., CROGUENNEC, T., BOUHALLAB, S. & KEHOE, J. J. 2016. Heat-Induced Denaturation, Aggregation and Gelation of Whey Proteins. *In:* MCSWEENEY, H. P. L. & O'MAHONY, A. J. (eds.) *Advanced Dairy Chemistry: Volume 1B: Proteins: Applied Aspects.* New York, NY: Springer New York.

BROMLEY, E. H., KREBS, M. R. & DONALD, A. M. 2006. Mechanisms of structure formation in particulate gels of beta-lactoglobulin formed near the isoelectric point. *The European Physical Journal E,* 21**,** 145-152.

BROWNLOW, S., CABRAL, J. H. M., COOPER, R., FLOWER, D. R., YEWDALL, S. J., POLIKARPOV, I., NORTH, A. C. T. & SAWYER, L. 1997. Bovine beta-lactoglobulin at 1.8 Å resolution - still an enigmatic lipocalin. *Structure,* 5**,** 481-495.

BRYANT, C. M. & MCCLEMENTS, D. J. 1998. Molecular basis of protein functionality with special consideration of cold-set gels derived from heat-denatured whey. *Trends in Food Science & Technology,* 9**,** 143-151.

BRYANT, C. M. & MCCLEMENTS, D. J. 2000. Influence of NaCl and CaCl2 on Cold-Set Gelation of Heat-denatured Whey Protein. *Journal of Food Science,* 65**,** 801-804.

BU, Z., COOK, J. & CALLAWAY, D. J. E. 2001. Dynamic regimes and correlated structural dynamics in native and denatured alpha-lactalbumin1. *Journal of Molecular Biology,* 312**,** 865-873.

BULDO, P., BENFELDT, C., FOLKENBERG, D. M., JENSEN, H. B., AMIGO, J. M., SIEUWERTS, S., THYGESEN, K., VAN DEN BERG, F. & IPSEN, R. 2016. The role of exopolysaccharide-producing cultures and whey protein ingredients in yoghurt. *LWT - Food Science and Technology,* 72**,** 189-198.

BUSCALL, R., MILLS, P. D. A., STEWART, R. F., SUTTON, D., WHITE, L. R. & YATES, G. E. 1987. The rheology of strongly-flocculated suspensions. *Journal of Non-Newtonian Fluid Mechanics,* 24**,** 183-202.

CAIROLI, S., LAMETTI, S. & BONOMI, F. 1994. Reversible and irreversible modifications of β-lactoglobulin upon exposure to heat. *Journal of Protein Chemistry,* 13**,** 347-354.

CHEANG, B. & ZYDNEY, A. L. 2003. Separation of α-lactalbumin and β-lactoglobulin using membrane ultrafiltration. *Biotechnol. Bioeng.,* 83**,** 201-209.

CHEN, J. & DICKINSON, E. 1993. Time-dependent competitive adsorption of milk proteins and surfactants in oil-in-water emulsions. *Journal of the Science of Food and Agriculture,* 62**,** 283-289.

CHEN, J. & DICKINSON, E. 1999. Interfacial ageing effect on the rheology of a heat-set protein emulsion gel. *Food Hydrocolloids,* 13**,** 363-369.

CHEN, J., DICKINSON, E., LANGTON, M. & HERMANSSON, A.-M. 2000. Mechanical Properties and Microstructure of Heat-set Whey Protein Emulsion Gels: Effect of Emulsifiers. *LWT - Food Science and Technology,* 33**,** 299-307.

CHOTHIA, C. 1976. The nature of the accessible and buried surfaces in proteins. *Journal of Molecular Biology,* 105**,** 1-12.

CHUNG, C., DEGNER, B., DECKER, E. A. & MCCLEMENTS, D. J. 2013. Oil-filled hydrogel particles for reduced-fat food applications: Fabrication, characterization, and properties. *Innovative Food Science & Emerging Technologies,* 20**,** 324-334.

CHUNG, C., DEGNER, B. & MCCLEMENTS, D. J. 2014. Development of Reduced-calorie foods: Microparticulated whey proteins as fat mimetics in semi-solid food emulsions. *Food Research International,* 56**,** 136-145.

CÓRDOVA, R. & MARÍA, A. 2014. *Interfacial rheology and behaviour of chemically modified whey proteins.* Wageningen/Wageningen University & Research Centre/2014.

CORRÊA, A. P. F., DAROIT, D. J., FONTOURA, R., MEIRA, S. M. M., SEGALIN, J. & BRANDELLI, A. 2014. Hydrolysates of sheep cheese whey as a source of bioactive

peptides with antioxidant and angiotensin-converting enzyme inhibitory activities. *Peptides,* 61**,** 48-55.

CROGUENNEC, T., O'KENNEDY, B. T. & MEHRA, R. 2004. Heat-induced denaturation/aggregation of β-lactoglobulin A and B: kinetics of the first intermediates formed. *International Dairy Journal,* 14**,** 399-409.

DAMODARAN, S. 2005. Protein Stabilization of Emulsions and Foams. *Journal of Food Science,* 70**,** R54-R66.

DAS, K. P. & KINSELLA, J. E. 1990. Effect of heat denaturation on the adsorption of β-lactoglobulin at the oil/water interface and on coalescence stability of emulsions. *Journal of Colloid and Interface Science,* 139**,** 551-560.

DERKACH, S. R. 2009. Rheology of emulsions. *Advances in Colloid and Interface Science,* 151**,** 1-23.

DICKINSON, E. 1998. Proteins at interfaces and in emulsions Stability, rheology and interactions. *Journal of the Chemical Society, Faraday Transactions,* 94**,** 1657-1669.

DICKINSON, E. 2001. Milk protein interfacial layers and the relationship to emulsion stability and rheology. *Colloids and Surfaces B: Biointerfaces,* 20**,** 197-210.

DICKINSON, E. 2010. Food emulsions and foams: Stabilization by particles. *Current Opinion in Colloid & Interface Science,* 15**,** 40-49.

DICKINSON, E. 2016. Biopolymer-based particles as stabilizing agents for emulsions and foams. *Food Hydrocolloids*.

DICKINSON, E. & CHEN, J. 1999. Heat-set whey protein emulsion gels: role of active and inactive filler particles. *Journal of Dispersion Science and Technology,* 20**,** 197-213.

DICKINSON, E., GOLLER, M. I. & WEDLOCK, D. J. 1993. Creaming and rheology of emulsions containing polysaccharide and non-ionic or anionic surfactants. *Colloids and Surfaces A: Physicochemical and Engineering Aspects,* 75**,** 195-201.

DICKINSON, E. & MATSUMURA, Y. 1991. Time-dependent polymerization of β-lactoglobulin through disulphide bonds at the oil-water interface in emulsions. *International Journal of Biological Macromolecules,* 13**,** 26-30.

DISSANAYAKE, M., KELLY, A. L. & VASILJEVIC, T. 2010. Gelling properties of microparticulated whey proteins. *Journal of Agricultural and Food Chemistry,* 58**,** 6825-6832.

DONOHUE, J. 1953. Hydrogen Bonded Helical Configurations of the Polypeptide Chain. *Proceedings of the National Academy of Sciences of the United States of America,* 39**,** 470-478.

EL-MAGOLI, S. B., LAROIA, S. & HANSEN, P. M. T. 1996. Flavor and texture characteristics of low fat ground beef patties formulated with whey protein concentrate. *Meat Science,* 42**,** 179-193.

ETZEL, M. R. 2004. Manufacture and Use of Dairy Protein Fractions. *The Journal of Nutrition,* 134**,** 996S-1002S.

FERNÁNDEZ FARRÉS, I., DOUAIRE, M. & NORTON, I. T. 2013. Rheology and tribological properties of Ca-alginate fluid gels produced by diffusion-controlled method. *Food Hydrocolloids,* 32**,** 115-122.

FERNÁNDEZ FARRÉS, I., MOAKES, R. J. A. & NORTON, I. T. 2014. Designing biopolymer fluid gels: A microstructural approach. *Food Hydrocolloids,* 42, Part 3**,** 362-372.

FERNÁNDEZ FARRÉS, I. & NORTON, I. T. 2014. Formation kinetics and rheology of alginate fluid gels produced by in-situ calcium release. *Food Hydrocolloids,* 40**,** 76-84.

FERSHT, A. 1999. *Stucture and mechanism in protein science: a guide to enzyme catalysis and protein folding*, W. H. Freeman and Co.

FISCHER, P. & WINDHAB, E. J. 2011. Rheology of food materials. *Current Opinion in Colloid & Interface Science,* 16**,** 36-40.

FITZSIMONS, S. M., MULVIHILL, D. M. & MORRIS, E. R. 2007. Denaturation and aggregation processes in thermal gelation of whey proteins resolved by differential scanning calorimetry. *Food Hydrocolloids,* 21**,** 638-644.

FOEGEDING, E. A., DAVIS, J. P., DOUCET, D. & MCGUFFEY, M. K. 2002. Advances in modifying and understanding whey protein functionality. *Trends in Food Science & Technology,* 13**,** 151-159.

FOEGEDING, E. A., LUCK, P. J. & DAVIS, J. P. 2006. Factors determining the physical properties of protein foams. *Food Hydrocolloids,* 20**,** 284-292.

FOLTZ, M., MALJAARS, J., SCHURING, E. A., VAN DER WAL, R. J., BOER, T., DUCHATEAU, G. S., PETERS, H. P., STELLAARD, F. & MASCLEE, A. A. 2009. Intragastric layering of lipids delays lipid absorption and increases plasma CCK but has minor effects on gastric emptying and appetite. *American Journal of Physiology-Gastrointestinal and Liver Physiology,* 296**,** G982-G991.

FOX, H., TAYLOR, P. & ZISMAN, W. 1947. Polyorganosiloxanes...Surface Active Properties. *Industrial & Engineering Chemistry,* 39**,** 1401-1409.

FRIEDMAN, M. I., RAMIREZ, I. & TORDOFF, M. G. 1996. Gastric emptying of ingested fat emulsion in rats: implications for studies of fat-induced satiety. *American Journal of Physiology - Regulatory, Integrative and Comparative Physiology,* 270**,** R688.

GABRIELE, A., SPYROPOULOS, F. & NORTON, I. T. 2009. Kinetic study of fluid gel formation and viscoelastic response with kappa-carrageenan. *Food Hydrocolloids,* 23**,** 2054-2061.

GABRIELE, A., SPYROPOULOS, F. & NORTON, I. T. 2010. A conceptual model for fluid gel lubrication. *Soft Matter,* 6**,** 4205-4213.

GARREC, D. A. 2013. *Understanding fluid gels and hydrocolloid tribology.* Eng.D, University of Birmingham.

GARREC, D. A., GUTHRIE, B. & NORTON, I. T. 2013. Kappa carrageenan fluid gel material properties. Part 1: Rheology. *Food Hydrocolloids,* 33**,** 151-159.

GARREC, D. A. & NORTON, I. T. 2012. Understanding fluid gel formation and properties. *Journal of Food Engineering,* 112**,** 175-182.

GENOVESE, D. B. 2012. Shear rheology of hard-sphere, dispersed, and aggregated suspensions, and filler-matrix composites. *Advanced Colloid and Interface Science,* 171-172**,** 1-16.

GEREMIAS-ANDRADE, I. M., SOUKI, N. P., MORAES, I. C. & PINHO, S. C. 2016. Rheology of Emulsion-Filled Gels Applied to the Development of Food Materials. *Gels,* 2**,** 22.

GOLDING, M. & WOOSTER, T. J. 2010. The influence of emulsion structure and stability on lipid digestion. *Current Opinion in Colloid & Interface Science,* 15**,** 90-101.

GOLDING, M., WOOSTER, T. J., DAY, L., XU, M., LUNDIN, L., KEOGH, J. & CLIFTON, P. 2011. Impact of gastric structuring on the lipolysis of emulsified lipids. *Soft matter,* 7**,** 3513-3523.

GOODWIN, J. W. & REYNOLDS, P. A. 1998. The rheology of flocculated suspensions. *Current Opinion in Colloid and Interface Science,* 3**,** 401-407.

GUNASEKARAN, S., KO, S. & XIAO, L. 2007. Use of whey proteins for encapsulation and controlled delivery applications. *Journal of Food Engineering,* 83**,** 31-40.

GUNASEKARAN, S., XIAO, L. & OULD ELEYA, M. M. 2006. Whey protein concentrate hydrogels as bioactive carriers. *Journal of Applied Polymer Science,* 99**,** 2470-2476.

GUZEY, D. & MCCLEMENTS, D. J. 2006. Formation, stability and properties of multilayer emulsions for application in the food industry. *Advances in Colloid and Interface Science,* 128–130**,** 227-248.

HA, E. & ZEMEL, M. B. 2003. Functional properties of whey, whey components, and essential amino acids: mechanisms underlying health benefits for active people (review). *The Journal of Nutritional Biochemistry,* 14**,** 251-258.

HAMILTON, I. E. & NORTON, I. T. 2016. Modification to the lubrication properties of xanthan gum fluid gels as a result of sunflower oil and triglyceride stabilised water in oil emulsion addition. *Food Hydrocolloids,* 55**,** 220-227.

HAUG, A., HØSTMARK, A. T. & HARSTAD, O. M. 2007. Bovine milk in human nutrition – a review. *Lipids in Health and Disease,* 6**,** 1-16.

HERMANSSON, A. M. 1975. Functional properties of proteins for foods-flow properties *Journal of Texture Studies,* 5**,** 425-439.

HILLIER, R. M., LYSTE, R. L. J. & CHEESEMAN, G. C. 1980. Gelation of reconstituted whey powders by heat. *Journal of the Science of Food and Agriculture,* 31**,** 1152-1157.

HOFFMANN, M. A. M., ROEFS, S. P. F. M., VERHEUL, M., VAN MIL, P. J. J. M. & DE KRUIF, C. G. 1996. Aggregation of beta-lactoglobulin studied by in situ light scattering. *Journal of Dairy Research,* 63**,** 423-440.

HONGSPRABHAS, P. & BARBUT, S. 1996. Ca2+ -induced gelation of whey protein isolate: effects of pre-heating. *Food Research International,* 29**,** 135-139.

HONGSPRABHAS, P. & BARBUT, S. 1997a. Ca2+-Induced cold gelation of whey protein isolate: effect of two-stage gelation. *Food Research International,* 30**,** 523-527.

HONGSPRABHAS, P. & BARBUT, S. 1997b. Protein and Salt Effects on Ca2+-Induced Cold Gelation of Whey Protein Isolate. *Journal of Food Science,* 62**,** 382-385.

HONGSPRABHAS, P., BARBUT, S. & MARANGONI, A. G. 1999. The Structure of Cold-Set Whey Protein Isolate Gels Prepared With Ca++. *LWT - Food Science and Technology,* 32**,** 196-202.

HORNE, D. S. & LEAVER, J. 1995. Milk proteins on surfaces. *Food Hydrocolloids,* 9**,** 91-95.

JASPER, J. J. 1972. The Surface Tension of Pure Liquid Compounds. *Journal of Physical and Chemical Reference Data,* 1**,** 841-1010.

KABALNOV, A. S. 2007. Coalescence in Emulsions. *In:* BINKS, B. P. (ed.) *Modern Aspects of Emulsion Science.* Technology and Engineering: RSC.

KALOGERIS, T. J., REIDELBERGER, R. D. & MENDEL, V. E. 1983. Effect of nutrient density and composition of liquid meals on gastric emptying in feeding rats. *American Journal of Physiology-Regulatory, Integrative and Comparative Physiology,* 244**,** R865-R871.

KAPOOR, R. & METZGER, L. E. 2004. Evaluation of Salt Whey as an Ingredient in Processed Cheese. *Journal of Dairy Science,* 87**,** 1143-1150.

KATO, A. & NAKAI, S. 1980. Hydrophobicity determined by a fluorescence probe method and its correlation with surface properties of proteins. *Biochimica et Biophysica Acta (BBA) - Protein Structure,* 624**,** 13-20.

KERRY 2015. Kerry Group Corporate History. *In:* PLC, K. G. (ed.).

KORHONEN, H. & PIHLANTO, A. 2003. Food-derived Bioactive Peptides - Opportunities for Designing Future Foods. *Current Pharmaceutical Design,* 9**,** 1297-1308.

KORHONEN, H. & PIHLANTO, A. 2006. Bioactive peptides: Production and functionality. *International Dairy Journal,* 16**,** 945-960.

KOUMAKIS, N., PAMVOUXOGLOU, A., POULOS, A. S. & PETEKIDIS, G. 2012. Direct comparison of the rheology of model hard and soft particle glasses. *Soft Matter,* 8**,** 4271-4284.

KRIEGER, I. M. & DOUGHERTY, T. J. 1959. A Mechanism for Non-Newtonian Flow in Suspensions of Rigid Spheres. *Journal of Rheology,* 3**,** 137-152.

KUHN, K. R., CAVALLIERI, Â. L. F. & DA CUNHA, R. L. 2010. Cold-set whey protein gels induced by calcium or sodium salt addition. *International Journal of Food Science & Technology,* 45**,** 348-357.

KURUKJI, D., NORTON, I. & SPYROPOULOS, F. 2016. Fabrication of sub-micron protein-chitosan electrostatic complexes for encapsulation and pH-Modulated delivery of model hydrophilic active compounds. *Food Hydrocolloids,* 53**,** 249-260.

LAZIDIS, A., HANCOCKS, R. D., SPYROPOULOS, F., KREUS, M., BERROCAL, R. & NORTON, I. T. 2016. Whey protein fluid gels for the stabilisation of foams. *Food Hydrocolloids,* 53**,** 209-217.

LE BON, C., NICOLAI, T. & DURAND, D. 1999. Growth and structure of aggregates of heat-denatured beta-Lactoglobulin. *International Journal of Food Science and Technology,* 34**,** 451-465.

LE GRAND, A. P., G. 2008. Effects of particle softness on the rheology and yielding of colloidal glasses. *Rheologica Acta,* 47**,** 579-590.

LEE, L. & NORTON, I. T. 2013. Comparing droplet breakup for a high-pressure valve homogeniser and a Microfluidizer for the potential production of food-grade nanoemulsions. *Journal of Food Engineering,* 114**,** 158-163.

LEFÈVRE, T. & SUBIRADE, M. 2000. Molecular differences in the formation and structure of fine-stranded and particulate beta-lactoglobulin gels. *Biopolymers,* 54**,** 578-586.

LI, D. H. & GANCZARCZYK, J. 1989. Fractal geometry of particle aggregates generated in water and wastewater treatment processes. *Environmental Science & Technology,* 23**,** 1385-1389.

LIANG, L., LEUNG SOK LINE, V., REMONDETTO, G. E. & SUBIRADE, M. 2010. In vitro release of α-tocopherol from emulsion-loaded β-lactoglobulin gels. *International Dairy Journal,* 20**,** 176-181.

LIU, X., JIANG, D. & PETERSON, D. G. 2014. Identification of Bitter Peptides in Whey Protein Hydrolysate. *Journal of Agricultural and Food Chemistry,* 62**,** 5719-5725.

LIVNEY, Y. D. 2010. Milk proteins as vehicles for bioactives. *Current Opinion in Colloid & Interface Science,* 15**,** 73-83.

LLOYD, D. M. 2016. *Mechanistic understanding of the rotating membrane emulsification process towards the development of design and scale-up theory.* University of Birmingham.

LÓPEZ-RUBIO, A. & LAGARON, J. M. 2012. Whey protein capsules obtained through electrospraying for the encapsulation of bioactives. *Innovative Food Science and Emerging Technologies,* 13**,** 200-206.

LOVEDAY, S. M., WANG, X. L., RAO, M. A., ANEMA, S. G., CREAMER, L. K. & SINGH, H. 2010. Tuning the properties of β-lactoglobulin nanofibrils with pH, NaCl and CaCl2. *International Dairy Journal,* 20**,** 571-579.

LOVEDAY, S. M., WANG, X. L., RAO, M. A., ANEMA, S. G. & SINGH, H. 2012. β-Lactoglobulin nanofibrils: Effect of temperature on fibril formation kinetics, fibril morphology and the rheological properties of fibril dispersions. *Food Hydrocolloids,* 27**,** 242-249.

LUHOVYY, B. L., AKHAVAN, T. & ANDERSON, G. H. 2007. Whey Proteins in the Regulation of Food Intake and Satiety. *Journal of the American College of Nutrition,* 26**,** 704S-712S.

LUNDIN, L., GOLDING, M. & WOOSTER, T. J. 2008. Understanding food structure and function in developing food for appetite control. *Nutrition & Dietetics,* 65**,** S79-S85.

MACIERZANKA, A., BOTTGER, F., LANSONNEUR, L., GROIZARD, R., JEAN, A. S., RIGBY, N. M., CROSS, K., WELLNER, N. & MACKIE, A. R. 2012. The effect of gel structure on the kinetics of simulated gastrointestinal digestion of bovine beta-lactoglobulin. *Food Chemistry,* 134**,** 2156-2163.

MACIERZANKA, A., SANCHO, A. I., MILLS, E. N. C., RIGBY, N. M. & MACKIE, A. R. 2009. Emulsification alters simulated gastrointestinal proteolysis of beta-casein and beta-lactoglobulin. *Soft Matter,* 5**,** 538-550.

MACKIE, A. & MACIERZANKA, A. 2010. Colloidal aspects of protein digestion. *Current Opinion in Colloid & Interface Science,* 15**,** 102-108.

MACRITCHIE, F. 1978. Proteins at Interfaces. *In:* C.B. ANFINSEN, J. T. E. & FREDERIC, M. R. (eds.) *Advances in Protein Chemistry.* Academic Press.

MADUREIRA, A. R., PEREIRA, C. I., GOMES, A. M. P., PINTADO, M. E. & XAVIER MALCATA, F. 2007. Bovine whey proteins – Overview on their main biological properties. *Food Research International,* 40**,** 1197-1211.

MALAKI NIK, A., WRIGHT, A. J. & CORREDIG, M. 2010. Surface adsorption alters the susceptibility of whey proteins to pepsin-digestion. *Journal of Colloid and Interface Science,* 344**,** 372-381.

MALDONADO-VALDERRAMA, J., WILDE, P., MACIERZANKA, A. & MACKIE, A. 2011. The role of bile salts in digestion. *Advances in Colloid and Interface Science,* 165**,** 36-46.

MALDONADO-VALDERRAMA, J., WILDE, P. J., MULHOLLAND, F. & MORRIS, V. J. 2012. Protein unfolding at fluid interfaces and its effect on proteolysis in the stomach. *Soft Matter,* 8**,** 4402-4414.

MALKIN, A. Y., MASALOVA, I., SLATTER, P. & WILSON, K. 2004. Effect of droplet size on the rheological properties of highly-concentrated w/o emulsions. *Rheologica Acta,* 43**,** 584-591.

MANDALARI, G., MACKIE, A. M., RIGBY, N. M., WICKHAM, M. S. J. & MILLS, E. N. C. 2009. Physiological phosphatidylcholine protects bovine β-lactoglobulin from simulated gastrointestinal proteolysis. *Molecular Nutrition & Food Research,* 53**,** S131-S139.

MANNINEN, A. H. 2004. Protein Hydrolysates in Sports and Exercise: A Brief Review. *Journal of Sports Science & Medicine,* 3**,** 60-63.

MAO, L., ROOS, Y. H. & MIAO, S. 2014. Study on the Rheological Properties and Volatile Release of Cold-Set Emulsion-Filled Protein Gels. *Journal of Agricultural and Food Chemistry,* 62**,** 11420-11428.

MARANGONI, A. G., BARBUT, S., MCGAULEY, S. E., MARCONE, M. & NARINE, S. S. 2000. On the structure of particulate gels—the case of salt-induced cold gelation of heat-denatured whey protein isolate. *Food Hydrocolloids,* 14**,** 61-74.

MARCIANI, L., WICKHAM, M., SINGH, G., BUSH, D., PICK, B., COX, E., FILLERY-TRAVIS, A., FAULKS, R., MARSDEN, C., GOWLAND, P. A. & SPILLER, R. C. 2007. Enhancement of intragastric acid stability of a fat emulsion meal delays gastric emptying and increases cholecystokinin release and gallbladder contraction. *American Journal of Physiology - Gastrointestinal and Liver Physiology,* 292**,** G1607.

MARCIANI, L., WICKHAM, M. S. J., BUSH, D., FAULKS, R., WRIGHT, J., FILLERY-TRAVIS, A. J., SPILLER, R. C. & GOWLAND, P. A. 2006. Magnetic resonance imaging of the behaviour of oil-in-water emulsions in the gastric lumen of man. *British Journal of Nutrition,* 95**,** 331-339.

MASON, T., LACASSE, M.-D., GREST, G. S., LEVINE, D., BIBETTE, J. & WEITZ, D. 1997. Osmotic pressure and viscoelastic shear moduli of concentrated emulsions. *Physical Review E,* 56**,** 3150.

MASON, T. G., BIBETTE, J. & WEITZ, D. A. 1995. Elasticity of Compressed Emulsions. *Physical Review Letters,* 75**,** 2051-2054.

MASON, T. G., BIBETTE, J. & WEITZ, D. A. 1996. Yielding and Flow of Monodisperse Emulsions. *Journal of Colloid and Interface Science,* 179**,** 439-448.

MATALANIS, A. & MCCLEMENTS, D. J. 2013. Hydrogel microspheres for encapsulation of lipophilic components: Optimization of fabrication & performance. *Food Hydrocolloids,* 31**,** 15-25.

MCCLEMENTS, D. J. 2005. *Food Emulsions Principles, Practices, and Techniques*, CRC Press.

MCCLEMENTS, D. J. 2015. Encapsulation, protection, and release of hydrophilic active components: Potential and limitations of colloidal delivery systems. *Advances in Colloid and Interface Science,* 219**,** 27-53.

MCINTOSH, G. H., ROYLE, P. J., LE LEU, R. K., REGESTER, G. O., JOHNSON, M. A., GRINSTED, R. L., KENWARD, R. S. & SMITHERS, G. W. 1998. Whey Proteins as Functional Food Ingredients? *International Dairy Journal,* 8**,** 425-434.

MEAKIN, P. 1983. Formation of Fractal Clusters and Networks by Irreversible Diffusion-Limited Aggregation. *Physical Review Letters,* 51**,** 1119-1122.

MELITO, H. S., DAUBERT, C. R. & FOEGEDING, E. A. 2013. Relating large amplitude oscillatory shear and food behavior: Correlation of nonlinear viscoelastic, rheological, sensory and oral processing behavior of whey protein isolate/κ-carrageenan gels. *Journal of Food Process Engineering,* 36**,** 521-534.

MENDICHI, R., ŠOLTÉS, L. & GIACOMETTI SCHIERONI, A. 2003. Evaluation of Radius of Gyration and Intrinsic Viscosity Molar Mass Dependence and Stiffness of Hyaluronan. *Biomacromolecules,* 4**,** 1805-1810.

MIE, G. 1908. Beiträge zur Optik trüber Medien, speziell kolloidaler Metallösungen. *Annalen der Physik,* 330**,** 377-445.

MINEKUS, M., ALMINGER, M., ALVITO, P., BALLANCE, S., BOHN, T., BOURLIEU, C., CARRIERE, F., BOUTROU, R., CORREDIG, M., DUPONT, D., DUFOUR, C., EGGER, L., GOLDING, M., KARAKAYA, S., KIRKHUS, B., LE FEUNTEUN, S., LESMES, U., MACIERZANKA, A., MACKIE, A., MARZE, S., MCCLEMENTS, D. J., MENARD, O., RECIO, I., SANTOS, C. N., SINGH, R. P., VEGARUD, G. E., WICKHAM, M. S. J., WEITSCHIES, W. & BRODKORB, A. 2014. A standardised static in vitro digestion method suitable for food - an international consensus. *Food & Function,* 5**,** 1113-1124.

MISHRA, R., SÖRGJERD, K., NYSTRÖM, S., NORDIGÅRDEN, A., YU, Y.-C. & HAMMARSTRÖM, P. 2007. Lysozyme Amyloidogenesis Is Accelerated by Specific Nicking and Fragmentation but Decelerated by Intact Protein Binding and Conversion. *Journal of Molecular Biology,* 366**,** 1029-1044.

MOAKES, R. J. A., SULLO, A. & NORTON, I. T. 2015a. Preparation and characterisation of whey protein fluid gels: The effects of shear and thermal history. *Food Hydrocolloids,* 45**,** 227-235.

MOAKES, R. J. A., SULLO, A. & NORTON, I. T. 2015b. Preparation and rheological properties of whey protein emulsion fluid gels. *RSC Advances,* 5**,** 60786-60795.

MORR, C. V. & HA, E. Y. W. 1993. Whey protein concentrates and isolates: Processing and functional properties. *Critical Reviews in Food Science and Nutrition,* 33**,** 431-476.

MORRIS, A. M., WATZKY, M. A. & FINKE, R. G. 2009. Protein aggregation kinetics, mechanism, and curve-fitting: a review of the literature. *Biochimica et Biophysica Acta,* 1794**,** 375-397.

MUDGAL, P., DAUBERT, C. R., CLARE, D. A. & FOEGEDING, E. A. 2011a. Effect of disulfide interactions and hydrolysis on the thermal aggregation of beta-lactoglobulin. *Journal of Agricutural and Food Chemistry,* 59**,** 1491-1497.

MUDGAL, P., DAUBERT, C. R. & FOEGEDING, E. A. 2009. Cold-set thickening mechanism of β-lactoglobulin at low pH: Concentration effects. *Food Hydrocolloids,* 23**,** 1762-1770.

MUDGAL, P., DAUBERT, C. R. & FOEGEDING, E. A. 2011b. Kinetic study of β-lactoglobulin thermal aggregation at low pH. *Journal of Food Engineering,* 106**,** 159-165.

MURRAY, B. S. 2002. Interfacial rheology of food emulsifiers and proteins. *Current Opinion in Colloid & Interface Science,* 7**,** 426-431.

MURRAY, B. S. 2007. Stabilization of bubbles and foams. *Current Opinion in Colloid & Interface Science,* 12**,** 232-241.

MURRAY, B. S. & ETTELAIE, R. 2004. Foam stability: proteins and nanoparticles. *Current Opinion in Colloid & Interface Science,* 9**,** 314-320.

NEIRYNCK, N., VAN DER MEEREN, P., BAYARRI GORBE, S., DIERCKX, S. & DEWETTINCK, K. 2004. Improved emulsion stabilizing properties of whey protein isolate by conjugation with pectins. *Food Hydrocolloids,* 18**,** 949-957.

NELSON, D. L., NELSON, D. L., LEHNINGER, A. L. & COX, M. M. 2008. *Lehninger principles of biochemistry,* New York, W.H. Freeman.

NI, Y., WEN, L., WANG, L., DANG, Y., ZHOU, P. & LIANG, L. 2015. Effect of temperature, calcium and protein concentration on aggregation of whey protein isolate: Formation of gel-like micro-particles. *International Dairy Journal,* 51**,** 8-15.

NICOLAI, T. 2016. Formation and functionality of self-assembled whey protein microgels. *Colloids and Surfaces B: Biointerfaces,* 137**,** 32-38.

NISHINARI, K., ZHANG, H. & IKEDA, S. 2000. Hydrocolloid gels of polysaccharides and proteins. *Current Opinion in Colloid and Interface Science,* 5**,** 195-201.

NORTON, I., FRYER, P. & MOORE, S. 2006a. Product/Process integration in food manufacture: Engineering sustained health. *AIChE Journal,* 52**,** 1632-1640.

NORTON, I., MOORE, S. & FRYER, P. 2007. Understanding food structuring and breakdown: engineering approaches to obesity. *Obesity Reviews,* 8**,** 83-88.

NORTON, I. T. & FRITH, W. J. 2001. Microstructure design in mixed biopolymer composites. *Food Hydrocolloids,* 15**,** 543-553.

NORTON, I. T., FRITH, W. J. & ABLETT, S. 2006b. Fluid gels, mixed fluid gels and satiety. *Food Hydrocolloids,* 20**,** 229-239.

NORTON, I. T., GOODALL, D. M., AUSTEN, K. R. J., MORRIS, E. R. & REES, D. A. 1986. Dynamics of molecular organization in agarose sulphate. *Biopolymers,* 25**,** 1009-1029.

NORTON, I. T., JARVIS, D. A. & FOSTER, T. J. 1999. A molecular model for the formation and properties of fluid gels. *International Journal of Biological Macromolecules,* 26**,** 255-261.

NORTON, J. E., GONZALEZ ESPINOSA, Y., WATSON, R. L., SPYROPOULOS, F. & NORTON, I. T. 2015. Functional food microstructures for macronutrient release and delivery. *Food & Function,* 6**,** 663-678.

NORTON, J. E. & NORTON, I. T. 2010. Designer colloids—towards healthy everyday foods? *Soft Matter,* 6**,** 3735-3742.

NÚÑEZ, G. A., BRICEÑO, M., MATA, C., RIVAS, H. & JOSEPH, D. D. 1996. Flow characteristics of concentrated emulsions of very viscous oil in water. *Journal of Rheology,* 40**,** 405-423.

O'SULLIVAN, J. & NORTON, I. 2016. Novel Ultrasonic Emulsification Technologies. *Gums and Stabilisers for the Food Industry 18: Hydrocolloid Functionality for Affordable and Sustainable Global Food Solutions,* 18**,** 89.

OLIVER, L., SCHOLTEN, E. & VAN AKEN, G. A. 2015. Effect of fat hardness on large deformation rheology of emulsion-filled gels. *Food Hydrocolloids,* 43**,** 299-310.

ONSEKIZOGLU, P. B. & GUNASEKARAN, S. 2016. Iron-encapsulated cold-set whey protein isolate gel powder - Part 2: Effect of iron fortification on sensory and storage qualities of Yoghurt. *International Journal of Dairy Technology*.

OTSUBO, Y. & PRUD'HOMME, R. K. 1994. Rheology of oil-in-water emulsions. *Rheologica Acta,* 33**,** 29-37.

PAL, R. 1996. Effect of droplet size on the rheology of emulsions. *AIChE Journal,* 42**,** 3181-3190.

PAL, R. & RHODES, E. 1989. Viscosity/Concentration Relationships for Emulsions. *Journal of Rheology,* 33**,** 1021-1045.

PAULING, L., COREY, R. B. & BRANSON, H. R. 1951. The Structure of Proteins: Two Hydrogen-Bonded Helical Configurations of the Polypeptide Chain. *Proceedings of the National Academy of Sciences of the United States of America,* 37**,** 205-211.

PEÑA-RAMOS, E. A. & XIONG, Y. L. 2003. Whey and soy protein hydrolysates inhibit lipid oxidation in cooked pork patties. *Meat Science,* 64**,** 259-263.

PÉREZ, M. D. & CALVO, M. 1995. Interaction of β-Lactoglobulin with Retinol and Fatty Acids and Its Role as a Possible Biological Function for This Protein: A Review. *Journal of Dairy Science,* 78**,** 978-988.

PERMYAKOV, E. A. & BERLINER, L. J. 2000. α-Lactalbumin: structure and function. *FEBS Letters,* 473**,** 269-274.

PICOT, A. & LACROIX, C. 2004. Encapsulation of bifidobacteria in whey protein-based microcapsules and survival in simulated gastrointestinal conditions and in yoghurt. *International Dairy Journal,* 14**,** 505-515.

PIHLANTO-LEPPÄLÄ, A. 2000. Bioactive peptides derived from bovine whey proteins: opioid and ace-inhibitory peptides. *Trends in Food Science & Technology,* 11**,** 347-356.

PRADAL, C. & STOKES, J. R. Oral Tribology: Bridging the gap between physical measurements and sensory experience. *Current Opinion in Food Science*.

PRAKASH, S., TAN, D. D. Y. & CHEN, J. 2013. Applications of tribology in studying food oral processing and texture perception. *Food Research International,* 54**,** 1627-1635.

PRESTIDGE, C. & TADROS, T. F. 1988. Viscoelastic properties of aqueous concentrated polystyrene latex dispersions containing grafted poly(ethylene oxide) chains. *Journal of Colloid and Interface Science,* 124**,** 660-665.

QUEMADA, D. 1998. Rheological modelling of complex fluids. I. The concept of effective volume fraction revisited. *The European Physical Journal of Applied Physics,* 1**,** 119-127.

RAMPON, V., BROSSARD, C., MOUHOUS-RIOU, N., BOUSSEAU, B. T., LLAMAS, G. & GENOT, C. 2004. The nature of the apolar phase influences the structure of the protein emulsifier in oil-in-water emulsions stabilized by bovine serum albumin.: A front-surface fluorescence study. *Advances in Colloid and Interface Science,* 108–109**,** 87-94.

RAVINDRANATH, S. & WANG, S.-Q. 2008. Universal scaling characteristics of stress overshoot in startup shear of entangled polymer solutions. *Journal of Rheology,* 52**,** 681-695.

REDDY, I. M., KELLA, N. K. D. & KINSELLA, J. E. 1988. Structural and conformational basis of the resistance of .beta.-lactoglobulin to peptic and chymotryptic digestion. *Journal of Agricultural and Food Chemistry,* 36**,** 737-741.

REMONDETTO, G. E., BEYSSAC, E. & SUBIRADE, M. 2004. Iron availability from whey protein hydrogels: an in vitro study. *Journal of Agricutural and Food Chemistry,* 52**,** 8137-8143.

RICCI-CABELLO, I., OLALLA HERRERA, M. & ARTACHO, R. 2012. Possible role of milk-derived bioactive peptides in the treatment and prevention of metabolic syndrome. *Nutrition Reviews,* 70**,** 241-255.

RON, N., ZIMET, P., BARGARUM, J. & LIVNEY, Y. D. 2010. Beta-lactoglobulin–polysaccharide complexes as nanovehicles for hydrophobic nutraceuticals in non-fat foods and clear beverages. *International Dairy Journal,* 20**,** 686-693.

ROSS-MURPHY, S. B. 1994. Rheological characterization of polymer gels and networks. *Polymer Gels and Networks,* 2**,** 229-237.

SAĞLAM, D., VENEMA, P., DE VRIES, R., SAGIS, L. M. C. & VAN DER LINDEN, E. 2011. Preparation of high protein micro-particles using two-step emulsification. *Food Hydrocolloids,* 25**,** 1139-1148.

SAĞLAM, D., VENEMA, P., DE VRIES, R., VAN AELST, A. & VAN DER LINDEN, E. 2012. Relation between gelation conditions and the physical properties of whey protein particles. *Langmuir,* 28**,** 6551-6560.

SANDRA, S., DECKER, E. A. & MCCLEMENTS, D. J. 2008. Effect of Interfacial Protein Cross-Linking on the in Vitro Digestibility of Emulsified Corn Oil by Pancreatic Lipase. *Journal of Agricultural and Food Chemistry,* 56**,** 7488-7494.

SANTANGELO, A., PERACCHI, M., CONTE, D., FRAQUELLI, M. & PORRINI, M. 1998. Physical state of meal affects gastric emptying, cholecystokinin release and satiety. *British Journal of Nutrition,* 80**,** 521-527.

SARKAR, A., GOH, K. K. T., SINGH, R. P. & SINGH, H. 2009. Behaviour of an oil-in-water emulsion stabilized by β-lactoglobulin in an in vitro gastric model. *Food Hydrocolloids,* 23**,** 1563-1569.

SAVAGE, S. B. & JEFFREY, D. J. 2006. The stress tensor in a granular flow at high shear rates. *Journal of Fluid Mechanics,* 110**,** 255-272.

SAWYER, W. H. 1968. Heat Denaturation of Bovine β-Lactoglobulins and Relevance of Disulfide Aggregation. *Journal of Dairy Science,* 51**,** 323-329.

SCHAEFER, D. W., MARTIN, J. E., WILTZIUS, P. & CANNELL, D. S. 1984. Fractal Geometry of Colloidal Aggregates. *Physical Review Letters,* 52**,** 2371-2374.

SCHEUBLE, N., GEUE, T., WINDHAB, E. J. & FISCHER, P. 2014. Tailored Interfacial Rheology for Gastric Stable Adsorption Layers. *Biomacromolecules,* 15**,** 3139-3145.

SCHMITT, C., BOVAY, C., VUILLIOMENET, A.-M., ROUVET, M. & BOVETTO, L. 2011. Influence of protein and mineral composition on the formation of whey protein heat-induced microgels. *Food Hydrocolloids,* 25**,** 558-567.

SCHUSTER, D. 1996. *Encyclopedia of emulsion technology*, CRC Press.

SETHURAMAN, A., VEDANTHAM, G., IMOTO, T., PRZYBYCIEN, T. & BELFORT, G. 2004. Protein unfolding at interfaces: Slow dynamics of α-helix to β-sheet transition. *Proteins: Structure, Function, and Bioinformatics,* 56**,** 669-678.

SHEA, A. P., CROFCHECK, C. L., PAYNE, F. A. & XIONG, Y. L. 2009. Foam fractionation of α-lactalbumin and β-lactoglobulin from a whey solution. *Asia-Pacific Journal of Chemical Engineering,* 4**,** 191-203.

SHERWOOD, J. D. 2008. Transient flow of viscoelastic, thixotropic fluid in a vane rheometer or infinite slot. *Journal of Non-Newtonian Fluid Mechanics,* 154**,** 109-119.

SINGER, N. S., YAMAMOTO, S. & LATELLA, J. 1988. *Protein product base*.

SINGH, V. P., PATHAK, V., NAYAK, N. K. & BHARTI, S. K. 2015. Development of cost effective soya extended whey incorporated chicken meat nuggets. *Nutrition & Food Science,* 45**,** 350-356.

SINHA, R., RADHA, C., PRAKASH, J. & KAUL, P. 2007. Whey protein hydrolysate: Functional properties, nutritional quality and utilization in beverage formulation. *Food Chemistry,* 101**,** 1484-1491.

SMITHERS, G. W. 2008. Whey and whey proteins—From 'gutter-to-gold'. *International Dairy Journal,* 18**,** 695-704.

SOK LINE, V. L., REMONDETTO, G. E. & SUBIRADE, M. 2005. Cold gelation of β-lactoglobulin oil-in-water emulsions. *Food Hydrocolloids,* 19**,** 269-278.

STADING, M. & HERMANSSON, A.-M. 1990. Viscoelastic behaviour of β-lactoglobulin gel structures. *Food Hydrocolloids,* 4**,** 121-135.

STOKES, J. R., BOEHM, M. W. & BAIER, S. K. 2013. Oral processing, texture and mouthfeel: From rheology to tribology and beyond. *Current Opinion in Colloid & Interface Science,* 18**,** 349-359.

STUART, M. A. C. 1991. Adsorbed Polymers in Colloidal Systems: from Statics to Dynamics. *Polym J,* 23**,** 669-682.

SULLO, A., WATSON, R. L. & NORTON, I. T. 2014. Design of Colloidal Foods for Healthier Diets. *Gums and Stabilisers for the Food Industry 17: The Changing Face of Food Manufacture: The Role of Hydrocolloids.* The Royal Society of Chemistry.

TADROS, T. F. 1994. Fundamental principles of emulsion rheology and their applications. *Colloids and Surfaces A: Physicochemical and Engineering Aspects,* 91**,** 39-55.

TAYLOR, S. M. & FRYER, P. J. 1994. The effect of temperature/shear history on the thermal gelation of whey protein concentrates. *Food Hydrocolloids,* 8**,** 45-61.

TOMÉ, D. & DEBABBI, H. 1998. Physiological Effects of Milk Protein Components. *International Dairy Journal,* 8**,** 383-392.

TOTOSAUS, A., MONTEJANO, J. G., SALAZAR, J. A. & GUERRERO, I. 2002. A review of physical and chemical protein-gel induction. *International Journal of Food Science & Technology,* 37**,** 589-601.

TOVAR, X. J., ARANA, A. C., TÉLLEZ, A. J., ABREU, A. C. & MURO, C. R. U. 2012. Traditional Methods for Whey Protein Isolation and Concentration: Effects on Nutritional Properties and Biological Activity. *Journal of the Mexican Chemical Society,* 56**,** 369-377.

VAN AKEN, G. A., BOMHOF, E., ZOET, F. D., VERBEEK, M. & OOSTERVELD, A. 2011. Differences in in vitro gastric behaviour between homogenized milk and emulsions stabilised by Tween 80, whey protein, or whey protein and caseinate. *Food Hydrocolloids,* 25**,** 781-788.

VAN DEN BERG, L., ROSENBERG, Y., VAN BOEKEL, M. A. J. S., ROSENBERG, M. & VAN DE VELDE, F. 2009. Microstructural features of composite whey

protein/polysaccharide gels characterized at different length scales. *Food Hydrocolloids,* 23**,** 1288-1298.

VIGNATI, E., PIAZZA, R. & LOCKHART, T. P. 2003. Pickering Emulsions: Interfacial Tension, Colloidal Layer Morphology, and Trapped-Particle Motion. *Langmuir,* 19**,** 6650-6656.

VOORHEES, P. W. 1985. The Theory of Ostwald Ripening. *Journal of Statistical Physics,* 38**,** 231-252.

WALKENSTROM, P., WINDHAB, E. & HERMANSSON, A.-M. 1998. Shear-induced structuring of particulate whey protein gels. *Food Hydrocolloids,* 12**,** 459-468.

WALSTRA, P. 1993. Principles of emulsion formation. *Chemical Engineering Science,* 48**,** 333-349.

WANG, W., DE KEE, D. & KHISMATULLIN, D. 2011. Numerical simulation of power law and yield stress fluid flows in double concentric cylinder with slotted rotor and vane geometries. *Journal of Non-Newtonian Fluid Mechanics,* 166**,** 734-744.

WHO 2015. European food and nutrition action plan 2015-2020. *In:* ORGANISATION, W. H. (ed.) http://www.euro.who.int/en/health-topics/noncommunicable-diseases/obesity/publications/2015/european-food-and-nutrition-action-plan-20152020. http://www.euro.who.int/en: World Heath Organisation.

WILDE, P., MACKIE, A., HUSBAND, F., GUNNING, P. & MORRIS, V. 2004. Proteins and emulsifiers at liquid interfaces. *Advances in Colloid and Interface Science,* 108–109**,** 63-71.

WOLF, B., FRITH, W. J., SINGLETON, S., TASSIERI, M. & NORTON, I. T. 2001. Shear behaviour of biopolymer suspensions with spheroidal and cylindrical particles. *Rheologica Acta,* 40**,** 238-247.

WOLF, B., SCIROCCO, R., FRITH, W. J. & NORTON, I. T. 2000. Shear-induced anisotropic microstructure in phase-separated biopolymer mixtures. *Food Hydrocolloids,* 14**,** 217-225.

WRIEDT, T. 2012. Mie Theory: A Review. *In:* HERGERT, W. & WRIEDT, T. (eds.) *The Mie Theory: Basics and Applications.* Berlin, Heidelberg: Springer Berlin Heidelberg.

YANG, Y., FANG, Z., CHEN, X., ZHANG, W., XIE, Y., CHEN, Y., LIU, Z. & YUAN, W. 2017. An Overview of Pickering Emulsions: Solid-Particle Materials, Classification, Morphology, and Applications. *Frontiers in Pharmacology,* 8**,** 287.

YE, A. & TAYLOR, S. 2009. Characterization of cold-set gels produced from heated emulsions stabilized by whey protein. *International Dairy Journal,* 19**,** 721-727.

YOON, E.-S., SINGH, R. A., OH, H.-J. & KONG, H. 2005. The effect of contact area on nano/micro-scale friction. *Wear,* 259**,** 1424-1431.

ZHANG, Z., ZHANG, R., DECKER, E. A. & MCCLEMENTS, D. J. 2015. Development of food-grade filled hydrogels for oral delivery of lipophilic active ingredients: pH-triggered release. *Food Hydrocolloids,* 44**,** 345-352.

ZHU, D., DAMODARAN, S. & LUCEY, J. A. 2008. Formation of Whey Protein Isolate (WPI)−Dextran Conjugates in Aqueous Solutions. *Journal of Agricultural and Food Chemistry,* 56**,** 7113-7118.

ZIMET, P. & LIVNEY, Y. D. 2009. Beta-lactoglobulin and its nanocomplexes with pectin as vehicles for ω-3 polyunsaturated fatty acids. *Food Hydrocolloids,* 23**,** 1120-1126.